Titre: Title:	Highly Structured and Surface Modified Poly (e-Caprolactone) Scaffolds Derived from Co-Continuous Polymer Blends for Bone Tissue Engineering
Auteur: Author:	Nima Ghavidel Mehr
Date:	2014
Type:	Mémoire ou thèse / Dissertation or Thesis
Référence: Citation:	Ghavidel Mehr, N. (2014). Highly Structured and Surface Modified Poly (e-Caprolactone) Scaffolds Derived from Co-Continuous Polymer Blends for Bone Tissue Engineering [Thèse de doctorat, École Polytechnique de Montréal]. PolyPublie. https://publications.polymtl.ca/1484/

URL de PolyPublie: PolyPublie URL:	https://publications.polymtl.ca/1484/
Directeurs de recherche: Advisors:	Basil D. Favis, & Caroline D. Hoemann
Programme: Program:	Génie chimique

UNIVERSITÉ DE MONTRÉAL

HIGHLY STRUCTURED AND SURFACE MODIFIED POLY(ε-CAPROLACTONE) SCAFFOLDS DERIVED FROM CO-CONTINUOUS POLYMER BLENDS FOR BONE TISSUE ENGINEERING

NIMA GHAVIDEL MEHR

DÉPARTEMENT DE GÉNIE CHIMIQUE

ÉCOLE POLYTECHNIQUE DE MONTRÉAL

THÉSE PRÉSENTÉE EN VUE DE L’OBTENTION

DU DIPLÔME DE PHILOSOPHIAE DOCTOR

(GÉNIE CHIMIQUE)

AOÛT 2014

UNIVERSITÉ DE MONTRÉAL

ÉCOLE POLYTECHNIQUE DE MONTRÉAL

Cette thèse intitulée:

HIGHLY STRUCTURED AND SURFACE MODIFIED POLY(ε-CAPROLACTONE) SCAFFOLDS DERIVED FROM CO-CONTINUOUS POLYMER BLENDS FOR BONE TISSUE ENGINEERING

présentée par : GHAVIDEL MEHR Nima

en vue de l'obtention du diplôme de : PHILOSOPHIAE DOCTOR

a été dûment acceptée par le jury d'examen constitué de :

Mme HEUZEY Marie Claude, Ph.D., présidente

M. FAVIS Basil, Ph.D., membre et directeur de recherche

Mme HOEMANN Caroline, Ph.D., membre et codirectrice de recherche

M. DUBOIS Charles, Ph.D., membre

Mme FAUCHEUX Nathalie, Ph.D., membre

DEDICATIONS

To my supportive family

ACKNOWLEDGEMENTS

I would like to convey my sincere and heartfelt gratitude to my Ph.D research supervisor, Professor Basil D. Favis for giving me an exceptional support and assistance in the course of this challenging multidisciplinary project. I am honored to have had the opportunity to work as a Ph.D candidate under his supervision at École Polytechnique de Montréal. Not only has he been a great mentor and a role model to me as a professional to overcome many difficulties that I encountered during this thesis, he has also helped me through difficult times when my father deceased as well as periods of painful medical problems. I will never forget his patience, enthusiasm, motivation and accurate scientific attitude.

I would also like to thank my research co-supervisor, Professor Caroline D. Hoemann whose full support, vast knowledge and professionalism, helped me to fully succeed in this project. I am blessed to have worked in one of the most equipped bioengineering laboratories in North America under her direction and I am extremely lucky to have learnt from her through her continuous professional assistance during this research project. Professor Hoemann has always been there for me whenever I needed help both personally and professionally.

I would also like to acknowledge Dr Xian Li and Dr Marianne B. Ariganello who have greatly contributed to the accomplishment of this work. Precious contributions of these two professionals have surely paved the way to the accomplishment of this research project.

I would also like to thank Professor Mike Buschmann for generously allowing me to have access to the BCL lab equipments. My thanks also go to other professors and technical staff of the chemical and biomedical engineering as well as engineering physics departments especially Suzie Poulin and Josianne Lefebvre at École Polytechnique de Montréal for providing the best possible assistance in this interesting project.

My deep gratitude goes to my friends and colleagues at École Polytechnique de Montréal, Charles-Hubert, David, Jessica, Elias, Mohsen, Ashkan, Sepehr, Ebrahim, Marie, Josianne, Nicholas, Vincent, Daniel and many more whose names I might have forgotten to mention, who helped me in various aspects during this Ph.D thesis.

At the end, I would like to thank my parents who have always supported me to continue my studies; my mother who took care of us three brothers when we had no one and my supporting father whose devastating loss almost destroyed the dream of finishing this Ph.D thesis. Finally, I would like to thank my wife for her love, patience, and encouragement and having faith in me when I was down and pushing me to stand up and continue.

RÉSUMÉ

L'utilisation d’échafaudages tridimensionnels poreux ensemencés avec des cellules ostéoprogénitrices, telles que les cellules souches mésenchymateuses humaines (CSM) pour la régénération des os, est devenue un outil prometteur pour l’ingénierie tissulaire osseuse. Les échafaudages dans l’ingénierie tissulaire osseuse agissent à titre de structure facilitant l'attachement, la migration, et la distribution des cellules hôtes impliquées dans le processus de réparation osseuse. Ces structures poreuses doivent être biocompatibles, biodégradables et doivent idéalement avoir une chimie de surface favorable, un niveau élevé d’interconnectivité des pores, des pores au diamètre favorable et finalement une distribution étroite de la taille des pores. Parmi une panoplie de matériaux synthétiques et naturels proposés pour l’ingénierie tissulaire osseuse, le poly(ε-caprolactone) (PCL) a été largement utilisé à cette fin grâce à sa biocompatibilité, sa basse immunogénicité, sa lente biodégradation et sa stabilité mécanique allant jusqu'à trois ans *in vivo*. Différentes techniques de fabrication ont été utilisées afin de produire des échafaudages pour l’ingénierie tissulaire osseuse, telles que le frittage, la coulée avec un solvant suivi du lessivage des particules, le moussage, et le prototypage rapide. Ces méthodes présentent habituellement de nombreux inconvénients comme l'utilisation de solvants toxiques, les limitations imposées par la forme de la phase de l’agent porogène, le niveau faible d'interconnectivité des pores, la température élevée du procédé, la large distribution de la taille des pores et les coûts élevés du traitement. Jusqu’à présent, une recherche complète sur les échafaudages utilisés en génie tissulaire ayant des pores de taille significativement différente et contrôlée de manière précise au niveau microscopique tout en considérant l'infiltration de l'échafaudage comme un paramètre déterminant n'a pas encore été faite.

Des échafaudages en PCL ayant les propriétés mentionnées précédemment ont été fabriqués par un mélange à l'état fondu avec du poly(oxyde d'éthylène) (PEO) choisi comme phase porogène. La composition du mélange a été choisie pour avoir une morphologie co-continue. Un recuit statique et une extraction sélective du PEO, qui est hydrosoluble, ont été effectués sur les mélanges ainsi obtenus. Les pores générés par cette méthode se sont avérés être entièrement interconnectés une propriété qui n'a pas été perturbée par le recuit. Le niveau d'interconnectivité des pores a été mesuré indirectement en déterminant le pourcentage de continuité de la phase porogène suite à l’extraction. Afin d'étudier l'effet de la taille des pores sur l'infiltration dans

l'échafaudage, des structures en PCL ayant des diamètres moyens de pores de 84, 116, 141, et 162 micromètres ont été produits en faisant varier la durée du recuit. Pour cela, une nouvelle analyse *in vitro* a été utilisée pour comparer l'infiltration à travers l'échafaudage par des billes de polystyrène de 10 micromètres de diamètre ayant la même taille que les cellules souches mésenchymateuses (CSM) humaines et celle par des CSMs humaines. Le niveau de pénétration des billes à travers l’échafaudage a montré une augmentation linéaire avec la hausse de la taille de pores, tandis que les CSMs ne se sont infiltrées que dans les pores ayant une taille de 141 et 162 micromètres. Pour les tailles de pores inférieures, les cellules se sont agrégées et ont adhéré près de la zone d’ensemencement avec une basse infiltration dans la structure poreuse. Utiliser des billes sphériques non réactives a permis d’obtenir un point de référence pour les systèmes non-agrégés qui pourraient être considérés comme le scénario idéal pour l'infiltration. Ces résultats ont indiqué que les billes imitent étroitement les cellules pour des tailles de pores égales ou supérieures à 141 micromètres. Les tests de cytotoxicité utilisant des fibroblastes de souris L929 ont démontré que les échafaudages ne sont pas cytotoxiques et qu’ils n’induisent pas de nécrose lors du contact avec les cellules. Cependant, une légère diminution de l'activité métabolique des cellules a été observée, elle peut être attribuée à la surface hydrophobe du PCL. Par conséquent, la modification de la surface des échafaudages en PCL avec un agent cytocompatible et hydrophile peut fortement augmenter l’adhésion, la propagation et la différenciation des CSMs en ostéoblastes.

Le chitosane, un composant important de la famille de polysaccharides, a été utilisé pour modifier la chimie des échafaudages de PCL en apportant l’hydrophilicité sur la surface. Le dépôt d'une couche homogène de chitosane sur la surface des échafaudages de PCL a été effectué à l'aide d'un autoassemblage couche-par-couche (LbL) de poly(chlorure de dialyldemethylammunium) (PDADMAC) comme polyélectrolyte cationique et de poly(styrenesulfonate de sodium 4) (PSS) comme polyélectrolyte anionique. La dernière couche de PSS négativement chargée permet l'addition du chitosane positivement chargé comme couche externe. Les mesures gravimétriques ont indiqué qu’une addition allant jusqu'à 3 couches a abouti à la formation de chaînes interpénétrées de polyélectrolyte qui ne permettent pas la formation de couches distinctes de charges positives ou négatives clairement définies. En augmentant le nombre de couches de polyélectrolytes chargés alternativement, des couches distinctes et mieux définies ont été formées. Les analyses détaillées des rapports d'O/C, de N/C et de S/C par la spectroscopie de photoélectrons induits par rayons X (XPS), ont confirmé la présence dominante de la molécule de PSS à la surface, étant la dernière couche de polyélectrolyte déposée et en plus grand nombre de dépôts (n=8), qui pourra être plus tard la surface de déposition du chitosane. Il a alors été montré que la méthode de dépôt LbL a conduit à l'obtention d'une couche homogène de chitosane pour toutes les profondeurs de cavités dans les échafaudages. Cela confirme que la méthode de dépôt LbL est une meilleure stratégie que la méthode de revêtement par immersion. L'analyse au microscope électronique à balayage (MEB) a montré une surface rugueuse de chitosane sur les substrats 2D de PCL, dont l'épaisseur totale s'étend de 550-700 nanomètres. Ces résultats ont permis de vérifier que l'utilisation de l'autoassemblage couche-par-couche de polyélectrolytes suivie de l'addition de chitosane comme couche externe, a conduit à une modification stable et bien homogène de la surface. De plus, cette méthode a le potentiel de transformer un matériel classique en polymère synthétique avec des pores complètement interconnectés en un matériel ayant des caractéristiques de surface identiques à celles du chitosane.

Le potentiel ostéogénique des échafaudages de PCL avec un traitement de surface par chitosane utilisant la méthode de dépôt LbL n'a jamais été évalué. Cette partie de la thèse considère l'hypothèse que l'ostéogenèse *in vitro* pourrait être réalisée dans les échafaudages 3D de PCL avec des pores interconnectés ayant un diamètre moyen de 84 et 141 micromètres, et que la biominéralisation pourrait être améliorée quand les pores sont revêtus avec du chitosane par l'approche LbL. Afin de réduire au minimum les erreurs provenant des inefficacités de l'infiltration cellulaire, le protocole le plus performant d'ensemencement des cellules a du être établi. Parmi l'ensemencement classique des cellules à 37 °C, l'ensemencement en deux étapes à 37°C, et l'ensemencement à froid à 4°C, dans un milieu contenant 2% de FBS (Fetal Bovine Serum), le dernier a montré la plus grande population de CSMs fraîchement trypsinisées dans toutes les profondeurs des échafaudages de 1 mm d'épaisseur. Les CSMs ensemencées dans des échafaudages de PCL, avec ou sans revêtement de chitosane par LbL, ont tout d'abord été mis en culture dans un milieu de prolifération pendant 10 jours, puis cultivées 21 jours dans un milieu ostéogénique. Au jour 2, les CSMs ont formé des monocouches creuses avec des morphologies cellulaires arrondies ayant de minces filopodes ancrés à la surface non modifiée du PCL, contrairement aux cellules étalées sur la surface des pores de PCL revêtue avec le chitosane. Au jour 10, les cellules ont proliféré formant une couche externe sur PCL et ont migré sur les réseaux

de collagène sécrétés qui remplissent les espaces entre les pores dans tous les échafaudages, par contre, elles n’adhèrent qu’à des surfaces de pores revêtues par le chitosane. Au jour 31, des quantités équivalentes de tissu ont été observées dans les échafaudages avec et sans chitosane, cependant les dépôts de tissu ont été plus importants dans les pores externes que dans les pores internes. En outre, une plus grande quantité de matrice biominéralisée a été observée dans les pores internes des échantillons de 84 micromètres ayant un revêtement de chitosane. Dans les échantillons de PCL pur, le dépôt de minéraux a été observé de façon aléatoire dans les sections supérieures très colonisées et dans les pores internes de 141 micromètres de diamètre. Les CSMs cultivées sur la surface de contrôle 2D avec un revêtement de chitosane ont montré une coloration plus prononcée de la phosphatase alcaline, demeurant une minéralisation négligeable. Cette étude prouve que les CSMs survivent, se prolifèrent, et adhérent plutôt à la matrice fibreuse qu’à la surface non-modifiée des pores du PCL. De plus, les échafaudages revêtus par LbL-chitosane présentent plus de biominéralisation en 3D dans les pores internes de 84 micromètres; une réponse cellulaire qui peut être liée à la courbure de la surface ainsi qu’à l’amélioration de l'hydrophilicité de la surface.

ABSTRACT

The application of porous three-dimensional scaffolds seeded with osteoprogenitor cells such as human mesenchymal stem cells (hBMSC) for bone regeneration has become a promising tool for *in vitro* bone tissue engineering. Scaffolds in bone tissue engineering act as a supportive bridge that facilitates the migration, attachment and distribution of the host cells involved in bone ingrowth. These porous structures should be biocompatible, biodegradable and ideally exhibit a favorable surface chemistry, controlled interconnected pores, pore sizes and narrow pore size distributions. Among a variety of synthetic and natural materials suggested for bone tissue engineering, poly(ε-caprolactone) (PCL) has been widely used for this purpose, owing to its biocompatibility, low immunogenicity, slow biodegradation and mechanical stability for up to three years *in vivo*. Various fabrication techniques have been used for the production of bone tissue engineering scaffolds, such as sintering, solvent casting and particulate leaching, gas foaming and rapid prototyping. These methods are normally associated with numerous drawbacks such as the use of toxic solvents, limitations imposed by the shape of the porogen phase, low levels of pore interconnectivity, high processing temperatures, large pore size distributions and high processing costs. To date, a thorough investigation of tissue engineering scaffolds of significantly different and highly controlled pore sizes at the microscopic level including scaffold infiltration as a crucial parameter has not been done.

PCL scaffolds with the features mentioned above have been fabricated by melt blending of PCL with poly(ethylene oxide) (PEO) at co-continuous composition followed by static annealing of the blends and selective extraction of water soluble PEO as the porogen phase. The pores generated by this method were proved to be fully interconnected- a property which was not disrupted by annealing. The level of pore interconnectivity was measured indirectly by determining the continuity % of the porogen phase post-extraction. PCL scaffolds with 84, 116, 141, and 162 μm average diameter pore sizes have been generated by varying the annealing time to investigate the effect of pore size on the scaffold infiltration. For this purpose, a novel *in vitro* assay was used to compare scaffold infiltration by 10-micron diameter polystyrene beads and trypsinized human bone marrow stromal cells (hBMSCs). Beads showed a linear increase in the extent of scaffold infiltration with increasing pore size. BMSCs infiltrated the 162 and 141 μm pore samples, below which the cells aggregated and adhered near the seeding area with low

infiltration into the porous device. Using non-interacting spherical beads provides a base-line for non-aggregated systems which could be considered as the ideal infiltration scenario. These results revealed that the beads closely mimic the cells at pore sizes equal and higher than 141 μm. Cytotoxicity studies using L929 mouse fibroblasts demonstrated that the scaffolds are not cytotoxic and do not induce necrosis upon contact with the cells. However, a slight decrease in the metabolic activity of the cells was observed which was attributed to the hydrophobic surface of PCL. Hence, the surface modification of PCL scaffolds with a hydrophilic cytocompatible agent could potentially enhance cell attachment, spreading and differentiation of hBMSCs into osteoblasts.

Chitosan, an important member of the polysaccharide family was used to alter the chemistry of PCL scaffolds and bring hydrophilicity to the surface. The deposition of a homogeneous chitosan layer on the surface of the PCL scaffolds was carried out using a Layer-by-Layer (LbL) self-assembly of poly(dialyldemethylammunium chloride) (PDADMAC) as cationic and poly(sodium 4-styrenesulfonate) (PSS) as anionic polyelectrolytes. The final negatively charged PSS layer allows for the addition of the positively charged chitosan as the outermost layer. Gravimetric measurements revealed that the addition of up to 3 layers leads to the formation of interdiffusing polyelectrolyte layers which do not allow for the formation of defined positive or negative charges. By increasing the number of polyelectrolyte layers with alternating charges, more well-defined layers are formed. Detailed analyses of O/C, N/C and S/C ratios by X-ray photoelectron spectroscopy (XPS) show that the PSS molecule dominates the surface as the last deposited polyelectrolyte layer at higher number of depositions (n=8), which can later be the surface for the deposition of chitosan. The LbL deposition of the chitosan layer on the LbL coating was then shown to be locally homogeneous at different depths within the scaffolds which also clarified that the LbL method is superior to the dip coating strategy. SEM analysis showed that there is a rough chitosan surface on the 2D solid PCL constructs whose thickness ranges from 550-700 nanometers. These results demonstrate that the application of LbL self-assembly of polyelectrolytes followed by the addition of chitosan as the outermost layer provides a route towards stable and homogeneous surface modification and has the potential to transform a classic fully interconnected porous synthetic polymer material to one with essentially complete chitosan-like surface characteristics.

The osteogenic potential of PCL scaffolds with a chitosan coating using Layer-by-Layer (LbL) surface modification has never been evaluated before. This part of the study tests the hypothesis that *in vitro* osteogenesis can be achieved in 3D PCL scaffolds with fully interconnected pores of 84 μm or 141 μm average diameter and biomineralization can be enhanced when pore surfaces are coated with chitosan adsorbed to LbL deposited polyelectrolytes. In order to reduce the errors originating from cell infiltration inefficiencies, the most competent cell seeding protocol has to be defined. Among classical cell seeding at 37°C, 2-step seeding at 37°C and cold seeding at 4°C in a medium containing 2% FBS, the last strategy proved to yield the best population of freshly trypsinized hBMSCs at all depths of the 1mm-thick scaffolds. hBMSCs cold-seeded in PCL scaffolds with or without an LbL-chitosan coating were cultured for 10 days in proliferation medium, followed by 21 days in osteogenic medium. At day 2, MSCs formed sparse monolayers with rounded cell morphologies with thin filopodia anchored to the unmodified PCL, as compared to more spread cells on chitosan-coated pore surfaces. At day 10, cells proliferated as an external layer, and migrated onto secreted collagen networks that filled the interpore spaces of all scaffolds, but only adhered to chitosan-coated pore surfaces. At day 31, similar levels of tissue formed in scaffolds with and without chitosan, but more tissue was deposited in the outer pores than the inner pores. Furthermore, more biomineralized matrix was observed in the inner 84 μm chitosan-coated pores ($p<0.05$). In the PCL-only samples, haphazard mineral deposits were observed in highly colonized outer layers and in the inner 141 μm pores. MSCs cultured on chitosan-coated 2D control surfaces show higher alkaline phosphatase staining but negligible mineralization. This study showed that hBMSCs survive, proliferate, and attach to fibrotic matrix rather than the PCL-only scaffold pore surfaces. LbL-chitosan-coated scaffolds showed more biomineralization in 3D inner 84 μm pores, a cell response that may be related to surface curvature in addition to improved surface hydrophilicity.

TABLE OF CONTENTS

LIST OF TABLES

Appendices

LIST OF FIGURES

Appendices

LIST OF APPENDICES

NOMENCLATURE

English Letters

A	Area
a	Area of one adsorbed nitrogen molecule
c	Dimensionless coefficient
d	Average pore diameter
ff	Form factor
G’	Storage modulus
k	Dimensionless coefficient
M_w	Weight average molecular weight
M_n	Number average molecular weight
N	Avogadro’s number
P	Perimeter of the domains
p	Droplet viscosity/matrix viscosity (Tomotika)
R	Ideal gas constant
r	Pore radius
R_0	Initial thread radius
T	Temperature
T_g	Glass transition temperature
t	Time
V_A	Molar volume of component A
V	Pore volume
V_m	Volume of the gas required for monolayer adsorption
W	Weight

Greek letters

ΔG_{mix}	Gibbs free energy of mixing
ΔH_{mix}	Enthalpy of mixing
$\Delta Smix$	Entropy change by mixing
α	Deviation from homogeneity
α_0	Initial distortion amplitude
γ	Interfacial tension of the blend components
δ_A	Solubility parameter of component A
η_A	Viscosity of component A
θ	Contact angle of mercury
γ	Interfacial tension of the blend components
δ_A	Solubility parameter of component A
η_A	Viscosity of component A
θ	Contact angle of mercury
λ	Viscosity ratio
σ	Surface tension
φ_A	Volume fraction of phase A
χ_{AB}	Interaction parameter between phase A and B
ω	Weight fraction

Abbreviations

ALP	Alkaline phosphatase
AR	Alizarin Red
ASC	Ascorbic acid

BET	Brunauer–Emmett–Teller Apparatus
BMP-2	Bone Morphogenic Protein-2
BMSC	Bone Mesenchymal Stem Cells
CCM	Complete culture medium
CT	Computer tomography
DDA	Degree of deacetylation
Dex	Dexamethasone
ECM	Extracellular Matrix
FBS	Fetal bovine serum
FEG-SEM	Field emission gun scanning electron microscope
GP	β-glycerophosphate
HA	Hydroxyapatite
hBMSC	Human Bone Mesenchymal Stem Cell
LbL	Layer-by-Layer
MIP	Mercury intrusion porosimetry
PAA	Poly(acrylic acid)
PAH	Poly(allylamine) hydrochloride
PBS	Phosphate buffer saline
PCL	Poly(ε-caprolactone)
PDADMAC	Poly(diallyl dimethyl ammonium chloride)
PEG	Poly(ethylene glycol)
PEO	Poly(ethylene oxide)
PGA	Poly(glycolic acid)
PLGA	Poly(lactic-co-glycolic acid)

PLLA	Poly(L-lactic acid)
PMMA	Poly(methyl methacrylate)
PS	Polystyrene
PSS	Poly(sodium 4-styrenesulfonate) (PSS)
PVA	Polyvinyl alcohol
RGD	Arg-Gly-Asp tripeptide
RITC	Rhodamine isothiocyanate
SEBS	Styrene ethylene butylene styrene block copolymer
SEM	Scanning electron microscopy
TCP	Tricalcium phosphate
TGF-β	Transforming growth factor beta
TIPS	Thermally-induced phase separation
ToF-SIMS	Time of flight secondary ion mass spectrometry
XPS	X-ray photoelectron spectroscopy

CHAPTER 1 INTRODUCTION AND OBJECTIVES

1.1 Introduction

Broken bone is one of the most painful medical conditions that people are commonly suffering from every day. Even the seemingly simple bone fractures could potentially cause recurring pain through a lifetime and may eventually require physical therapy or surgery as the last measure. According to the most recent data, over 717,000 Canadians aged 12 or older suffered from broken or fractured bones in the years 2009 and 2010, which is approximately 2% of the whole population (Canadian Community Health Survey, 2009-2010). Although sport accidents seem to be the most common cause for fractured bones, an average Canadian suffers from a broken bone triggered by road accidents, falls and animal attacks. Among all mentioned causes, fall accidents are the main unintentional reason for the initiation of a fracture or eventually breaking a bone. Only in the years 2009 and 2010, over 1,714,000 fall accidents were reported which mostly led to injuries in the hands and the spine (Canadian Community Health Survey, 2009-2010).

Most of the bone fractures heal naturally through a cascade of overlapping events comprised of three major phases: inflammation, repair and remodeling (Remedios, 1999). However, depending on the type of the fracture, fracture stability, and fracture gap some variations in these healing phases might occur, which are not the focus of this thesis study. Although most fractures heal naturally through all or a portion of the aforementioned classical bone healing steps, certain complications do exist.

Delayed and nonunion fracture healings across species are defined as follows. By definition, when a bone fracture is not repaired in an expected time frame, yet signs of healing still exist, a delayed fracture healing is occurring (Taylor, 1992). On the other hand, when the normal healing process is permanently ceased without attaining completion, it is perceived that a nonunion fracture healing has taken place (Taylor, 1992). A considerable percentage of 5-10% of bone fractures end up as delayed or nonunion fractures, which accounts for 35,850-71,700 Canadians in 2009-2010 (Canadian Community Health Survey, 2009-2010). Figure 1.1 illustrates a nonunion fracture at the proximal fifth metatarsal bone.

There are two main factors that contribute to the formation of delayed and nonunion fractures: insufficient fracture stability and inadequate biologic environment. The existence of either or the combination of both these adverse parameters increases the chance of such bone healing abnormalities. Other factors include inadequate vascularity, lack of nutrition, large fracture gaps, interposition of soft tissue between the fracture gaps, unfavorable metabolism, patient’s age, infection and administration of drugs that can interfere with the healing process (such as anticoagulants) (Bartels, 1987; DeAngelis, 1975; Hoefle, 1993).

Figure 1.1: Radiograph of a patient with a nonunion stress fracture of the proximal fifth metatarsal (demonstrated by an arrow) (Rosenberg & Sferra, 2000)

In some cases, these complications occur because of the excessive extraction of bone during surgery, which leads to degenerative abnormalities with very little bone mineralization at the site of the injury. Figure 1.2 demonstrates the posteroanterior skull radiograph of a young female with microsomia (i.e. abnormal smallness of body parts) who had undergone distraction of the mandible.

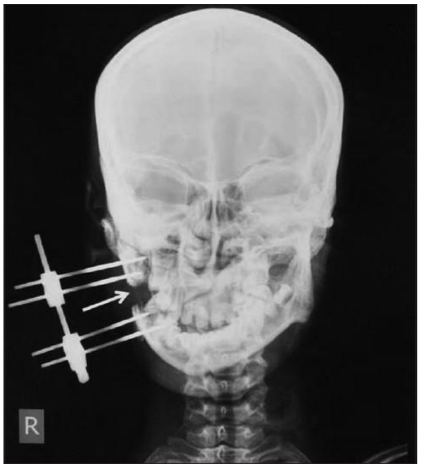

Figure 1.2: Microsomia due to a distraction of the mandible, leading to nonunion bone defect (Agarwal, 2013)

The exact approach taken to treat fracture nonunion depends on many parameters such as existence of infection, surrounding tissue damage, and the fracture condition (Chao & Inoue, 2003). However, a long and complicated orthopedic surgery is usually needed to repair the nonunion site. Additionally, although a variety of biological, mechanical and physical approaches have been investigated, there is still a need for a treatment that will consistently assist in the repair of non-healing or delayed healing of bone fractures and also provide convincing evidence that the healing of a fracture can be enhanced (Einhorn, 1995). One promising approach is the use of bone tissue engineering scaffolds to guide local bone regeneration and repair.

Bone tissue engineering also has the potential to be used in order to avoid delayed or nonunion fracture healing for the bones that are more susceptible to poor healing conditions. These sites include upper thigh bone (femur head and neck) and small wrist bones (scaphoid) which have limited vascularity and therefore are more prone to destruction, should an impact occur. Also, moderate blood supply exists in some bones like tibia and might be sufficient for fracture repair, but a severe trauma or injury can destroy internal or external vascular network and therefore natural healing would be compromised. Another example is the fifth metatarsal fractures (i.e., Jones fracture) which usually end up in delayed and nonunion healings despite surgical treatments (Nunley, 2001). Should there be a fracture in the mentioned sites, tissue engineering approaches could be applied to repair the bone and further avoid surgical complications. Furthermore, large defects in load bearing bones with the aforementioned limitations always need graft interventions for providing the best healing conditions (Banes et al., 2001; Khan et al., 2008).

1.2 Research Hypothesis

We hypothesize that PCL scaffolds with controlled pore sizes, fabricated by the melt blending of co-continuous immiscible polymers and surface modified by chitosan, can enhance 3D *in vitro* osteogenesis of hBMSCs and lead to biomineralization.

1.3 Objectives

The main objective of this thesis is to fabricate a fully functional porous polymeric poly(ε-caprolactone) (PCL) scaffold which can satisfy all features required for *in vitro* bone tissue engineering (discussed in Section 2.2.3), in order for it to be clinically used as grafts to repair bone fracture nonunions. There are an important number of parameters that have to be considered simultaneously for the design and application of these scaffolds as bone grafts, such as scaffold infiltration behavior, porous microstructure and surface chemistry. The specific objectives of this thesis are thus defined as the following:

1. To fabricate and thoroughly characterize (pore size, pore size distribution, pore interconnectivity, surface chemistry) PCL scaffolds derived by a melt blending approach of PCL/Poly(ethylene oxide) (PEO) followed by static annealing and selective extraction
2. To examine the scaffold infiltration by human bone mesenchymal stem cells (hBMSCs) by establishing the pore size and cell seeding protocol requirements that yield the most homogeneous cell distribution inside the 3D constructs
3. To systematically modify the hydrophobic surface of PCL by chitosan as a hydrophilic compound and evaluate the uniformity of such surface treatment at all positions inside the 3D scaffolds with considerable and comparable spatial dimensions
4. To determine the effect of pore size and chitosan coating on the *in vitro* matrix mineralization behaviour of human bone mesenchymal stem cells (hBMSCs) seeded inside 3D porous scaffolds, and elicit matrix calcification through cell-biomaterial interactions

CHAPTER 2 LITERATURE REVIEW

What is tissue engineering and why is it needed? What are the strategies in tissue engineering in general and how do they relate to bone tissue engineering? What are the roles and requirements for bone tissue engineering scaffolds? How are they produced and how can melt blending of polymer blends serve bone tissue engineering? This chapter seeks help from the existing scientific works in literature to answer these questions along with many others.

2.1 Tissue engineering overview

The research into tissues and organs dates back to 3000 B.C. The most ancient and well-known example of creating living creatures from living or non-living specimens is the biblical tale of the creation of Eve from Adam's rib which triggered the curiosity of men of ancient ages to strive to discover such concepts according to social, cultural and scientific backgrounds of the people in those times. As a result of such curiosities, Theophrastus von Hohenheinm (Paracelsus) tried to find a recipe to create human life by mixing chemical substances in a confined environment, whose efforts of course failed.

Although similar research activities went on for centuries in ancient history, the term "Tissue Engineering" was coined for the first time by Skalak and Fox in 1988 and defined as follows: "Tissue engineering is the application of principles and methods of engineering and life sciences toward the fundamental understanding of structure-function relationships in normal and pathological mammalian tissues and the development of biological substitutes to restore, maintain, or improve tissue functions" (Skalak & Fox, 1988). Therefore, the concept of tissue engineering can be considered mostly as a therapeutic action whose aim is to replace, remove, repair or reconstruct a lost or damaged tissue.

In general, two main parameters are required for tissue engineering: cells and matrix also known as scaffold. These two fundamental elements will be discussed further in detail in this chapter. There are several strategies in tissue regeneration: first strategy involves the implantation of a biomaterial matrix inside the injured region, in order to fill the gaps produced by the defect and let the body repair the defect by growing tissue on the implanted matrix. However, a typical *in-*

vitro tissue regeneration process involves the incorporation of cells into the matrix followed by *in vitro* cultivation and maturation over a certain period of time, and eventually its implantation into the target body (Figure 2.1). The advantage of this technique is that less cellular migration from the host body to the damaged region is needed, since the already present cells in the scaffold have initiated the deposition of extracellular matrix which accelerates the healing process (Mano et al., 2002). Bone tissue engineering strategies will be discussed in further detail in section 2.2.1.

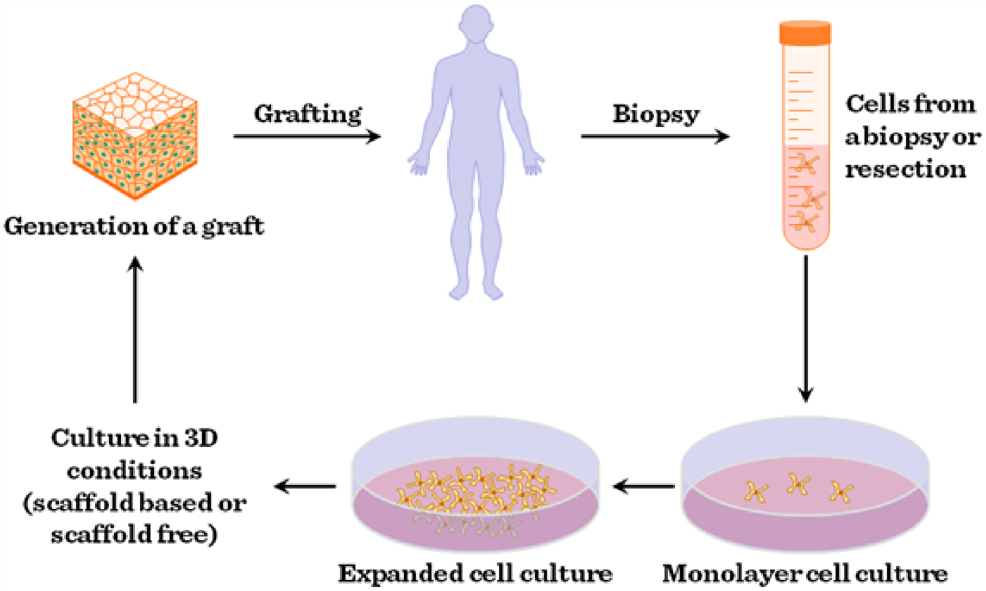

Figure 2.1: Representative tissue engineering process involving *in vitro* expansion of healthy autologous cells (Bartis, 2011)

2.2 Bone tissue engineering

Even though an estimation on total bone grafting procedures performed in Canada does not yet exist, this value for the United States is predicted to be approximately half a million per year (AATB, September 2010). It is a known fact that there is a critical shortage of musculoskeletal tissue donors who are crucial to these procedures. Figure 2.2 depicts the evolution of the number of musculoskeletal tissue donors before the year 2007 (AATB, September 2010). The number of donors of these types of tissues account for only 5% of the total required grafting procedures. As a result of such shortage in donor supplies, the sales for bone grafts and graft substitutes have increased substantially from $300 million in 1999 and reached a value of $1.5 billion over a period of 10 years (Orthopedics Network News, 2011).

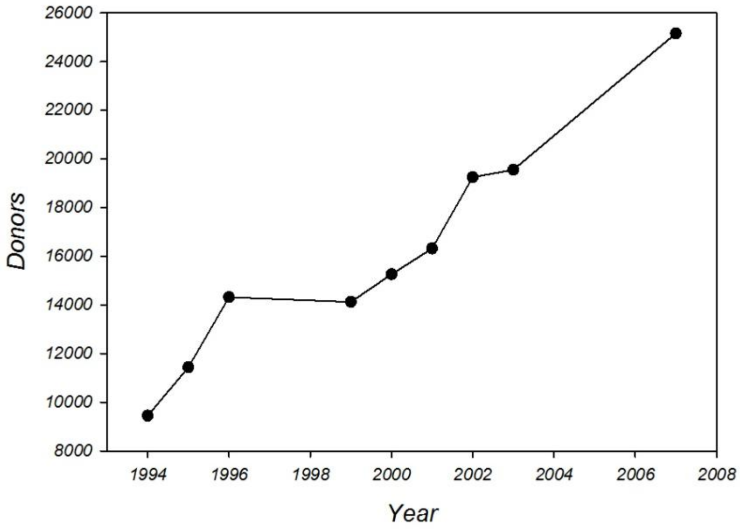

Figure 2.2: Musculoskeletal tissue donors over the years in the US (AATB, September 2010)

2.2.1 Bone tissue engineering strategies

2.2.1.1 Osteoconduction

In the Osteoconduction strategy, as the oldest approach used in bone regeneration (Keating & McQueen, 2001), bone graft (scaffold) acts as a supportive “bridge” which due to its specific microstructure facilitates the migration, attachment and distribution of the host cells involved in vascular bone ingrowth and healing (Bauer & Muschler, 2000; Fleming et al., 2000; Keating & McQueen, 2001). For instance, hydroxyapatite (HA) grafts have proved to possess osteoconductive properties as new bone was shown to form around and inside the implant (Figure 2.3) (Scaglione et al., 2012). Since the scaffolds are not pre-seeded with cells in the osteoconductive approach, the efficiency of bone formation in the healing process is mostly dependent upon the three-dimensional (3D) micro-architecture, porosity, surface chemistry and *in vivo* degradation time of the scaffold. After implantation, the surrounding soft tissue of the host migrates through the porous network and into the voids of the scaffold, which gives a rise to the formation of new fibrovascular tissue and new blood vessels. These newly formed blood vessels could again drive more bone-forming cells to the damage site and accelerate the healing process

(Fleming et al., 2000). Although bone itself is the most osteoconductive material, other synthetic biomaterials such as HA whose properties mimic those of the mineral phase of the bone have been extensively studied. As another option, bioactive proteins can be impregnated inside the scaffolds and be delivered to the grafted site in order to enhance bone regeneration (Fleming et al., 2000).

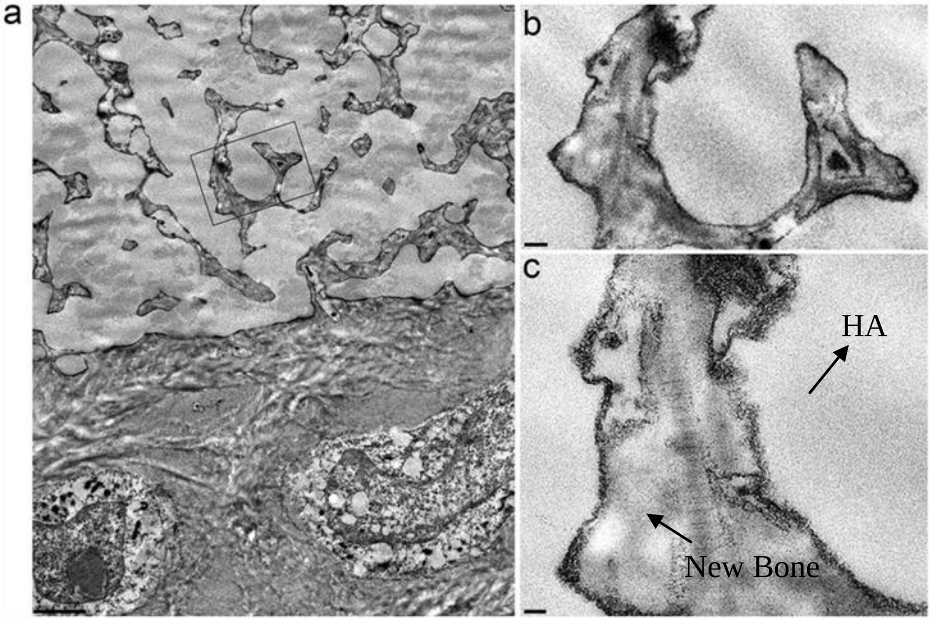

Figure 2.3: (a) the interface between the new bone and HA scaffolds, 2 months post-implantation. (b) and (c) are high magnifications of (a) (adapted from (Scaglione et al., 2012))

2.2.1.2 Osteoinduction

Osteoinduction is the ability of a biomaterial scaffold to induce migration and differentiation of osteogenic precursor cells in the surrounding host tissue (Ladd & Pliam, 1999; Weigel, 1993). Although by definition osteoinductivity is an intrinsic behaviour of the graft material, synthetic biomaterials are not capable of such feature without the incorporation of functional bioactive molecules. These biomolecules include epidermal growth factor (EGF), platelet-derived growth factors (PDGFs), fibroblast growth factor (FGF), transforming growth factor beta (TGF-β) superfamily, and parathyroid hormone (PTH) (Muschler & Midura, 2002). Among these bio-agents, bone morphogenetic proteins (BMPs) are the most investigated osteoinductive stimuli (Klokkevold 2003).

2.2.1.3 Osteogenesis

Osteogenesis as a strategy is the process of bone formation by pre-seeded cells in the presence or absence of growth factors inside the scaffold. In this approach, all the effort is focused on the maintenance of cells such as multipotent precursor cells (such as BMSCs), osteocytes and osteoblasts, together with matrix proteins which are synthesized during the osteogenesis period. These cells are accompanied by other diffusing cells from the tissue fluids in the vicinity of the graft and are therefore maintained or compensated via further vascularisation inside the graft (Attawia, 2003). For instance, new bone was formed within porous bioglass scaffolds pre-seeded with primary rat BMSCs after 4 weeks post-implantation in rat cortical bone defects (Livingston et al., 2002) (Figure 2.4). Also, when poly(lactic-co-glycolic acid) (PLGA) scaffolds were seeded with rabbit BMSCs and implanted into rabbit mandible defect models, considerable amount of new bone was detected at the defect at 4 and 8 weeks post-implantation (Liu et al., 2014).

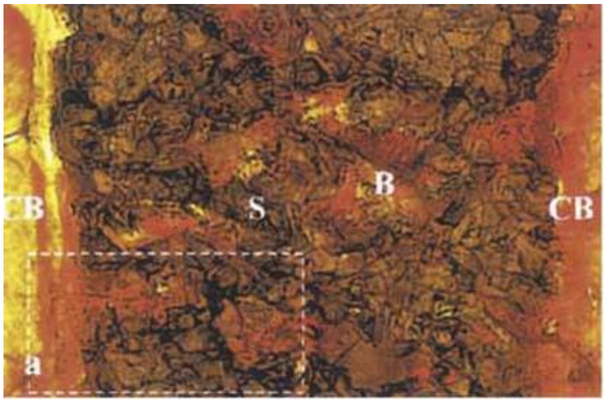

Figure 2.4: Histological micrograph of a bioglass scaffolds pre-seeded and cultured in alpha essential medium (αMEM) with primary rat bone marrow stromal cells, and implanted in rat cortical bone defects for 4 weeks. Stevenel's Blue as the stain and Van Gieson's Picro-Fuchsin was used as counterstain (SVG stain). S, B and CB are scaffold, new bone and host cortical bone (adapted from (Livingston et al., 2002))

These strategies have been separately exercised in the past. Yet, in order to achieve the most successful integration of the bone implant and the surrounding tissue at the damaged site, a combination of osteoconduction, osteoinduction and/or osteogenesis should be used (Betz, 2002; Fox, 1984; Keating & McQueen, 2001).

In this thesis, we aim to generate bone tissue engineering scaffolds that are presumed to satisfy a combination of osteoconductive and osteogenic strategies for potential future *in vivo* applications. Since this study does not include the use of bioactive agents, osteoinductive strategy is not considered. Moreover, since we only evaluate the *in vitro* osteogenesis, the term “scaffold” has been mostly used instead of “bone graft”.

2.2.2 Cells used in bone tissue engineering

Several cell types have been commonly used in bone tissue engineering such as mesenchymal stem cells isolated from various tissues (bone marrow, periosteum, human umbilical cord blood) and mature osteoblasts including primary cells from trabecular bone derived during iliac crest biopsies (Barralet et al., 2005; Batorsky et al., 2005; Chiu et al., 2006; Hattori et al., 2005; Hillsley & Frangos, 1994; Jayakumar & Di Silvio, 2010; Khan et al., 2008; Pietrzak & Woodell-May, 2005). Among the aforementioned cells, bone mesenchymal stem cells mainly derived from bone marrow and periosteum are the most frequent cell type used in bone tissue engineering (Seong et al., 2010). As their name implies, mesenchymal stem cells are progenitor cells that contribute to the generation or regeneration of mesenchymal tissues such as bone, cartilage, muscle, tendons, ligaments, and other connective tissues as shown in Figure 2.5 (Caplan, 2005).

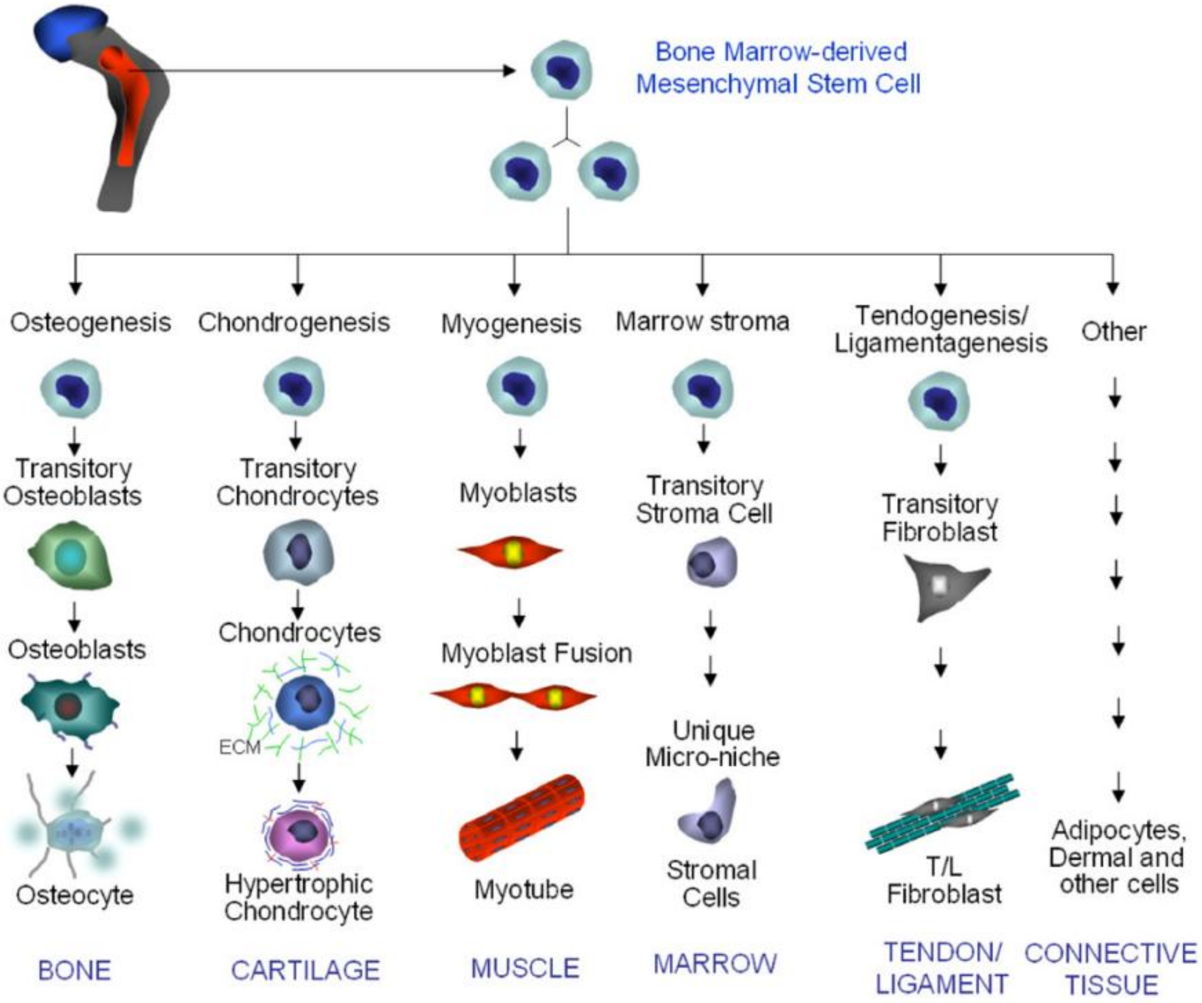

Figure 2.5: Differentiation strategies of BMSCs (adapted from (Seong et al., 2010))

2.2.2.1 Bone marrow-derived mesenchymal stem cells (BMSCs)

Mesenchymal stem cells derived from bone marrow have been extensively cultured *in vitro* and shown to be able to differentiate into multiple cell lineages depending on the culture conditions. Upon addition of certain exogenous supplements such as β-glycerophosphate (GP), ascorbic acid (ASC) and dexamethasone (Dex) or their derivatives, these cells differentiate into colonies composed of cuboidal osteoblastic cells which can finally form mineralized bone nodules (Costa-Pinto et al., 2009). Table 2.1 summarizes the most common culture conditions (cell culture media and supplements) for the osteogenesis of BMSCs.

Table 2-1: Cell culture supplements for the osteogenesis of BMSCs. Abbreviations used are Dulbecco’s modified Eagle’s medium (DMEM), alpha-modified minimum essential Eagle’s medium (αMEM), fetal bovine serum (FBS) and fetal calf serum (FCS)

Media	Serum	Ascorbic Acid or Derivative	Dexamethasone or Derivative	β-glycerophosphate or Derivative	Reference
DMEM	10% FBS	50 µmol/L	10^{-7} mol/L	10 mmol/L	(Bosnakovski et al., 2005)
	10% FBS	50 µmol/L	10^{-8} mol/L	10 mmol/L	(Costa-Pinto et al., 2009)
αMEM	10% FBS	200 µmol/L	10^{-8} mol/L	10 mmol/L	(Sugiura et al., 2004)
	10% FCS	100 µmol/L	10^{-8} mol/L	10 mmol/L	(Gronthos et al., 1994)

Apart from the supplements added to the culture, other exogenous osteoinductive factors (as mentioned in section 2.2.1.2) such as recombinant human BMP-2 (rhBMP-2) and parathyroid hormone (PTH)-related peptide have been reported to accelerate osteogenesis of BMSCs in *in vitro* and *in vivo* investigations (Miao et al., 2001; Yamagiwa et al., 2001). Also, it has been shown that low passage number as opposed to high passage number cells and culture in alpha-modified minimum essential Eagle’s medium (αMEM) as opposed to Dulbecco’s modified Eagle’s medium (DMEM) lead to higher expression of osteogenic markers and mineralization (Coelho et al., 2000; Sugiura et al., 2004).

2.2.2.2 Osteogenesis of BMSCs and marker expressions

The bone tissue currently produced by today’s osteogenic strategies is not sufficiently stiff to endure high load-bearing functions (Dawson & Oreffo, 2008). Therefore, bone tissue engineering scientists are now facing specific challenges for the development of new bone regeneration approaches to produce fully functional bone constructs in clinical applications. These challenges could not be tackled without a proper knowledge about the molecular and cellular mechanisms involved in the process of osteogenesis. Insights into specific mechanisms controlling osteogenesis are made possible by *in vitro* cell culture assays, and the ability to detect various components or “markers” of different stages of osteogenesis. Some bone tissue engineering approaches analyze the interaction between a new material and primary osteoblasts or osteoblast cell lines that are already committed to forming a mineralized matrix. It could be said that to better reflect processes occurring in clinical bone repair, a scaffold should be seeded with primary cells that normally participate in bone repair, with human cells, and primary cells as opposed to immortalized cells that require artificial conditions to arrest proliferation and differentiate. Bone marrow stromal cells (BMSCs) from adult bone marrow aspirates are such a cell source.

BMSCs are multipotent adult progenitors capable of differentiating into osteoblasts, chondrocytes, adipocytes, or fibroblasts depending on the culture medium (Yoo & Johnstone, 1998). In the osteogenesis assay, BMSCs are seeded at low density as monolayers, allowed to become confluent, then a medium containing osteogenic factors is added. In osteogenic medium, dexamethasone is an additive that suppresses inflammatory factor secretion by BMSCs, which allows cells to stop proliferating and differentiate to osteoblasts (Guzmán-Morales et al., 2009). Other factors including beta-glycerol phosphate and ascorbate are added to supply phosphate for hydroxyapatite mineral formation and for appropriate collagen type I fibril assembly. With the addition of the osteogenic medium to a culture of BMSCs, these cells increase expression of alkaline phosphatase, a marker expressed by the osteoblasts or bone making cells and the initiation of osteogenesis is hence confirmed. Other markers such as osteonectin, osteopontin, and osteocalcin may also be induced. According to Huang et al. the osteogenic differentiation of BMSCs to osteoblasts occurs in three principal stages (Huang et al., 2007). The first stage takes place in the first four days and it denotes a peak in the number of cells. The early osteogenic marker alkaline phosphatase (ALP) protein is transcribed and expressed in the days 5 to 14 whose expression is known to decline afterwards (Aubin, 2001). The expression of collagen type I could also be detected in these early stages of osteogenesis (Quarles et al., 1992). The final stage of the osteogenesis occurs from the days 14 to 28 when high levels of osteocalcin and osteopontin marker expression are observed, especially in rodent cultures, together with the deposition of calcium and phosphate minerals in the assembled collagen type I matrix (Hoemann et al., 2009). As also explained in the previous section, the existence of osteogenic factors such as dexamethasone, ascorbic acid and β-glycerol phosphate is known to stimulate the osteogenesis of BMSCs (Vater et al., 2011).

When differentiating into osteoblasts, the morphology of the BMSCs transforms from a fibroblastic to a cuboidal shape (Vater et al., 2011). Also, an extracellular matrix mainly composed of collagen type I is secreted from the cells at this and later stages of the osteogenesis which can ultimately form mineral nodules in rodent cultures that can be detected by alizarin red (AR) and/or Von Kossa (VK) staining (Vater et al., 2011). In osteogenic cultures of human primary BMSCs that have been amplified by 3 to 6 passages, a more diffuse mineral stain is normally observed (Guzmán-Morales et al., 2009). It should be noted that both fibroblasts and osteoblasts express collagen type I, and that undifferentiated BMSCs can sporadically express alkaline phosphatase (Hoemann et al., 2009). Therefore, more than 1 marker is usually needed to convincingly demonstrate successful osteoblast differentiation and end-stage functional bone deposition. The two most frequently employed markers of osteogenesis are alkaline phosphatase (an enzyme reflecting osteoblast commitment and competence to hydrolyze β-glycerol phosphate to free phosphate), and a histological stain for hydroxyapatite mineral deposition. Alizarin red stain for calcium is often used because the dye can be further extracted from monolayer cultures and quantified using standard spectroscopic absorbance for statistical hypothesis testing.

2.2.2.3 In vitro osteogenesis of BMSCs in 3D constructs

Whether the *in vitro* system is two or three-dimensional can be very determining for the osteogenic outcome from the cells. As an example, higher levels of osteogenic differentiation of rat BMSCs were observed in 3D as compared to 2D systems (Hosseinkhani et al., 2006). Also, increased absolute expression of osteogenic markers such as alkaline phosphatase, osteonectin, osteopontin and Collagen type I of human adipose-derived stem cells was observed in 3D as opposed to 2D substrates (Gabbay et al., 2006). Moreover, in 3D culture, an increase was observed in the differentiation of primary human osteoblasts (bone-forming cells) into osteocytes (bone cells) as compared to the classic 2D-culture (Boukhechba et al., 2009). Therefore, obtaining fully functional mineralizing matrix in a 3D environment becomes crucial as bone tissue regeneration almost never occurs on a 2D substrate.

Fischer et al. demonstrated that hybrid injectable microparticles of HA impregnated with BMSCs could exhibit osteogenic potential in a 3D environment (Fischer et al., 2003). In another work, BMP-2 Gene transfection (process of introducing genes into a cell) performed on BMSCs led to the endogenous secretion of BMP-2 which highly improved osteogenic differentiation of the cells seeded in 3D porous silk fibroin sponge-like scaffolds (Meinel et al., 2006). Moreover, following the procedure scheme in Figure 2.1, BMSCs harvested from a patient's body, cultured *in vitro* and directed toward differentiation and mineralization inside three-dimensional HA ceramic scaffolds, were implanted back into the original patient and proved to have osteogenic potential with no side effects (Morishita et al., 2006). Table 2.2 summarizes some of the recent works that investigated 3D osteogenesis involving BMSCs. In this table, abbreviations GP, ASC and Dex, represent pure or chemical derivatives of β-glycerophosphate, ascorbic acid and dexamethasone.

Table 2-2: Recent developments in 3D-osteogenesis by BMSCs

BMSC source	Osteogenic media/culture time	3D scaffold (details)	Seeding density	Reference
Rat	α MEM, 10% FBS, 10 mM b-GP, 50 µg/ml ASC, (No Dex)	PCL and HA composite scaffold by fiber deposition and LbL assembly Shape: 5×5×2 mm^3	5×10^4 cells on each scaffold	(Hong et al., 2009)
Rat	DMEM, 15% FBS, 10 mM GP, 0.28 mM ASC, 10^{-8} M Dex Culture Time: 14 days	HA and starch–polycaprolactone (SPCL) Scaffolds by sintering and melt spinning Shape: discs of 5 mm in diameter and 4 mm thickness	5×10^2, 1×10^3, 5×10^3 and 1×10^4 cells on each scaffold (low seeding densities)	(Oliveira et al., 2009)
Rat	DMEM, 15% FBS, 10 mM GP, 50 µg/ml ASC, 10nM Dex Culture time: 21 days	Poly(L-lactic acid) (PLLA) and nano-HA by phase separation Shape: 5×5×2 mm	5×10^5 cells in 50µl DMEM on each scaffold	(Eslaminejad et al., 2011)
Rat	DMEM, 10% FBS, 10nmol/L GP, 50 µmol/L ASC, 10 nmol/L Dex, 10 nmol/L 1α,25-dihydroxyvitamin D_3 Culture time: 1,2 and 4 weeks	PHBV-based Scaffold by electrospinning	10 000 cells/cm^2	(Lü et al., 2012)
Rat	α MEM, 10% FBS, 10 mM GP, 50 µg/mL ASC, 10 nM Dex Culture time: 14 days	PLA scaffold by phase separation Shape: discs of 16 mm in diameter and 1 mm thickness	4×10^4 cells on each scaffold	(Lee et al., 2012)
Rat	DMEM, 10% FBS, 10 mM GP, 50 µg/mL ASC, 0.1 µM Dex, 10	PCL, PLGA by CO_2 dense phase sintering	552,000 cells in 55.2uL on	(Bhamidipati et al., 2013)

	nM 1α,25 dihydroxyvitamin D_3, 50 ng/mL BMP-2 Culture time: 6 weeks	Shape: discs of 7.8 ± 0.2 mm in diameter and 1.7 ± 0.7 mm in thickness	each scaffold	
Rabbit	DMEM, 10% FBS, 10 mM GP, 50 mM ASC, 1 μM Dex Culture time: 10 days	pearl/PLGA by low-temperature deposition manufacturing (LDM) Shape: $10 \times 10 \times 3$ mm^3	2×10^6 cells on each scaffold	(Xu et al., 2010b)
Human	DMEM, 10% FBS, 3.5 mM GP, 0.05 mM ASC, 10^{-7}M Dex Culture time: 28 days	Mineralized collagen by freeze drying followed by chemical crosslinking with collagen Shape: discs of 10mm diameter and 5mm height	2×10^5 cells in 60μL of medium on each scaffold	(Bernhardt et al., 2009)
Human	DMEM, 10% FBS, 10mM GP, 50mg/mL ASC, 100 nM Dex, Culture time: 45 days	3D woven PCL Shape: discs of 7mm diameter and 1.3mm thickness	1×10^6 cells mixed with 30μL of 0.6% (w/v) collagen type I gel	(Abrahamsson et al., 2010)
Human	α MEM, 10% FBS, 10 mM GP, 0.05 mM ASC, 100 nM Dex, Culture time: 6 weeks	Silk/HA Scaffolds by direct write assembly Shape: $8 \times 8 \times \sim 1.2$ mm^3	1×10^5 cells in 100 μl of medium	(Sun et al., 2012)

2.2.3 Requirements for bone tissue engineering scaffolds

Apart from the previously mentioned parameters, the 3D scaffold should also possess certain specific properties. The key function of the scaffold is the direction and guidance of the cell growth, either migrating from the surrounding tissues (for *in vivo*) into or those pre-seeded onto the scaffold (*in vitro* or *in vivo*). The scaffold acts as a mechanical support for the cell growth, differentiation, proliferation, and other cellular functions. Moreover, it should possess appropriate mechanical structure for the transport of nutrient, waste and extracellular matrix (ECM) material. In this section, essential properties of the scaffolds (bone grafts) are discussed.

2.2.3.1 Biocompatibility

Biocompatibility is the most significant factor in the rapid and successful integration of the scaffold with the host tissue. The parameters that reflect the biocompatibility of a material are the absence of cytotoxicity, low or no immunogenicity and the presence or absence of carcinogenic effects. BIO-OSS (deproteinized bovine bone mineral), for example, is an efficient biocompatible bone substitutes that has been used for bone damage repair in a scaffold-assisted bone regeneration process for quite some time (Carmagnola et al., 2003). On the other hand, implantation of a bio-incompatible scaffold at the injury site often leads to the induction of inflammatory responses as the body attempts to contain, neutralize and protect the damaged bone and the cells inside (Ratner, 2005) . Incompatibility of the foreign matrix with the biological environment of the defect could also lead to the secretion of toxic compounds, which might further trigger inflammatory responses of the body as well as infection (Athanasiou et al., 1996). Biocompatibility of the scaffold material is closely related to its biodegradation. Some scaffold materials like poly(lactic acid) release acidic by-products which are trapped at the damaged site and are lethal to osteogenic cells (Guo et al., 2004).

Figure 2.6 illustrates how subcutaneously implanted polyethylene scaffolds in mice are encapsulated with layers of fibrous tissue as a foreign body inflammatory reaction to a bio-incompatible material (Ehashi et al., 2014).

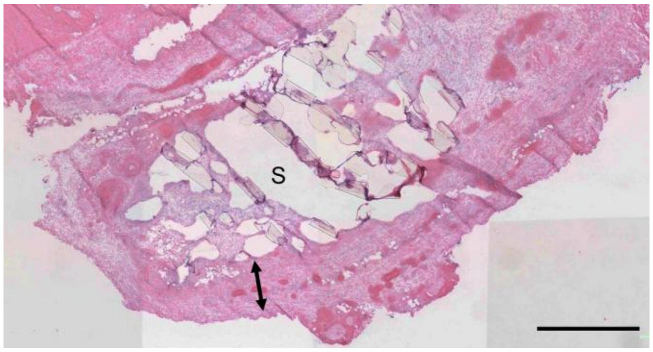

Figure 2.6: Foreign body reaction by disordered tissue formation (arrow) to bio-incompatible polyethylene material. The scaffold is represented by the letter S (Ehashi et al., 2014)

2.2.3.2 Biodegradation

In most cases, the implanted scaffold should degrade and leave the host's physiological system. In the case of metals, as bone grafts, a surgery is required to extract the foreign material from the body. In bone tissue engineering where mechanical strength is provided by the scaffold especially at the early stages of bone healing, the degradation rate of the material must be tailored in such a way that it comply with the growth rate of the new forming tissue (Wang et al., 2010). Ideally, the entire scaffold should be degraded by the time that the damaged tissue is totally renewed. Figure 2.7 illustrates the degradation behavior of biodegradable scaffolds made of porcine small intestinal submucosa implanted into the subcutaneous pocket of axilla (arm-pit) in mice (Kim et al., 2013). While tissue ingrowth is taking place, the scaffold is degrading after 28 days. It is clear that the rate of material degradation higher than that of the bone tissue formation leads to the collapse of the scaffold sooner than the bone tissue becomes self-supporting.

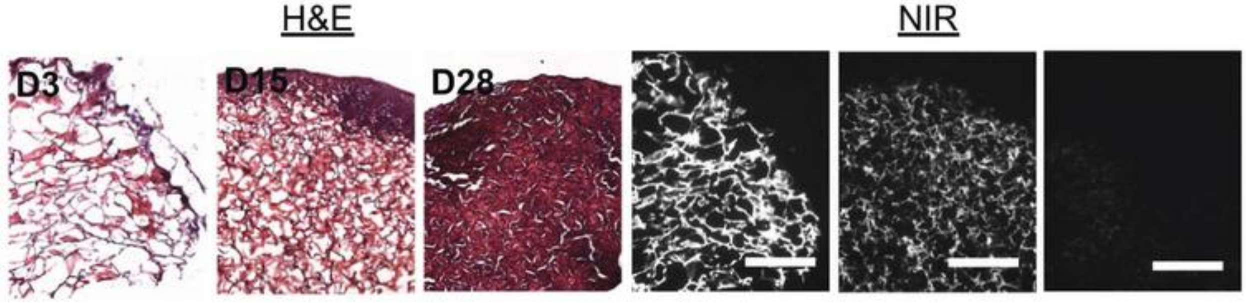

Figure 2.7: Tissue ingrowth by hematoxylin and eosin (H&E) staining and *in vivo* degradation of the scaffold by near-infrared fluorescence (NIR) imaging (adapted from (Kim et al., 2013))

2.2.3.3 Porosity, pore size and level of pore interconnectivity

In order to provide the cells with nutrients and evacuate the waste products present from the defect site, the bone tissue needs to be highly vascularized. As explained in section 2.2.1.1, vascularization at the damaged zone also promotes the flow of neutrophils, macrophages, osteoblasts, mesenchymal cells and bioactive molecules to the site of injury which leads to the callus formation. In order to maintain high levels of vascularization, the scaffold should possess high levels of porosity and pore interconnectivity (Salgado et al., 2004). Also, porosity leads to an enhanced mechanical interlocking between the scaffold and the bone environment of the host tissue (Story et al., 1998). An example of the mechanical interlocking is illustrated in Figure 2.8 where the osseointegration of the new bone into the porous titanium implant is evident (De Vasconcellos, 2012). High porosity which can also provide a high surface-to-volume ratio can optimize the interactions between the cells and the polymeric scaffolds by affecting the cellular adhesion. Low levels of pore interconnectivity, on the other hand, limits the formation of blood vessels *in vivo*, whereas extremely open networks might affect the cell seeding efficiency and cellular adhesion (Bai et al., 2010).

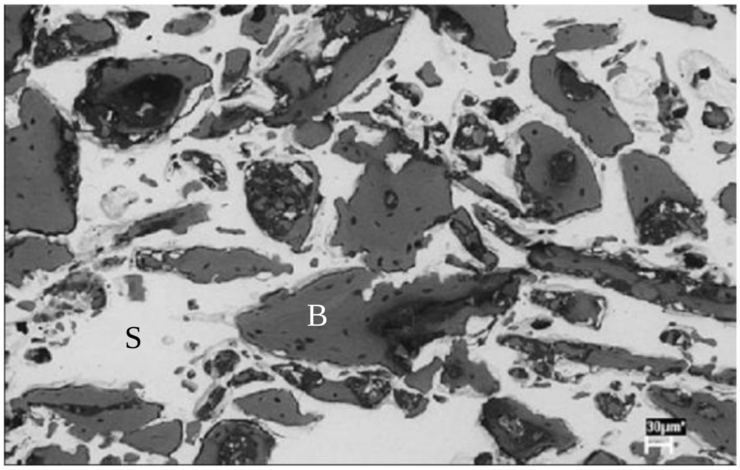

Figure 2.8: Mechanical interlocking of the new bone into porous titanium scaffolds. The scaffold and new bone are represented by the letters S and B respectively (adapted from (De Vasconcellos, 2012))

There is a rule of thumb which establishes 90% porosity as the minimum porosity required for growing cells inside a scaffold. The main reason for this limit is that achieving high pore interconnectivities with porosities less than 90% is very difficult. As a matter of fact, this appears to be the case when conventional scaffold fabrication methods like the solvent casting and particulate leaching are used. There have been a lot of works in the literature that attempted to establish the optimal porosity and pore size for tissue engineering applications. Nonetheless, these porosity/pore size limits are undoubtedly different from an application to another (tissue type). By increasing the porosity, the mechanical properties of the scaffolds which are of utmost importance in bone regeneration fall drastically. Therefore, many attempts have been made in the past to maintain the pore interconnectivity at high levels while keeping the mechanical integrity of the scaffold together with its load-bearing features (Karageorgiou & Kaplan, 2005).

Depending on the materials and processing techniques used, bone ingrowth has been observed with porosities as low as 47% to 74% (Whang et al., 1999). Additionally, pore sizes ranging from 50-710 μm are proposed for bone regeneration (Li et al., 2002b; Lu & Mikos, 1996). The effect of porosity and pore size on the efficiency of osteogenesis will be discussed in further detail in the next subsection.

2.2.3.3.1 Effect of porosity on osteogenesis

The effect of porosity on bone formation has been studied for both *in vitro* and *in vivo* experiments, and will be discussed in this section.

2.2.3.3.1.1 In vitro

The effect of porosity on the *in vitro* osteogenesis has been investigated for both osteoblasts and undifferentiated mesenchymal stem cells. However, while some studies showed that porosity does not affect bone formation, others argued otherwise. To begin with, regarding cellular proliferation, composites of apatite and collagen seeded with MC3T3-E1 preosteoblasts did not exhibit any improvements with increasing porosities from 49 to 79% (Itoh et al., 2004). Contrarily, rat BMSCs seeded in non-woven fibers made of polyethylene terephthalate (PET) exhibited an increase in cellular proliferation with an increase in the scaffold porosity from 93 to 97%, which was attributed to a rise in the transport of oxygen and nutrients at higher porosities (Takahashi & Tabata, 2004). On the other hand, lower porosities (~93%) led to a higher expression of ALP and osteocalcin, which are markers for osteoblasts activities after 4 weeks of culture in normal and bone differentiation medium containing DMEM supplemented with 15%

FCS, 10 nM dexamethasone, 50 μg/ml ascorbic acid and 10 mM β-glycerophosphate (Figure 2.9). The black bars in this figure denote high porosity samples and bear lower levels of ALP and osteocalcin than the low porosity samples (grey bars). This effect was attributed to the fact that in lower porosities, cell aggregation occurs which could stimulate the expression of these markers (Takahashi & Tabata, 2004).

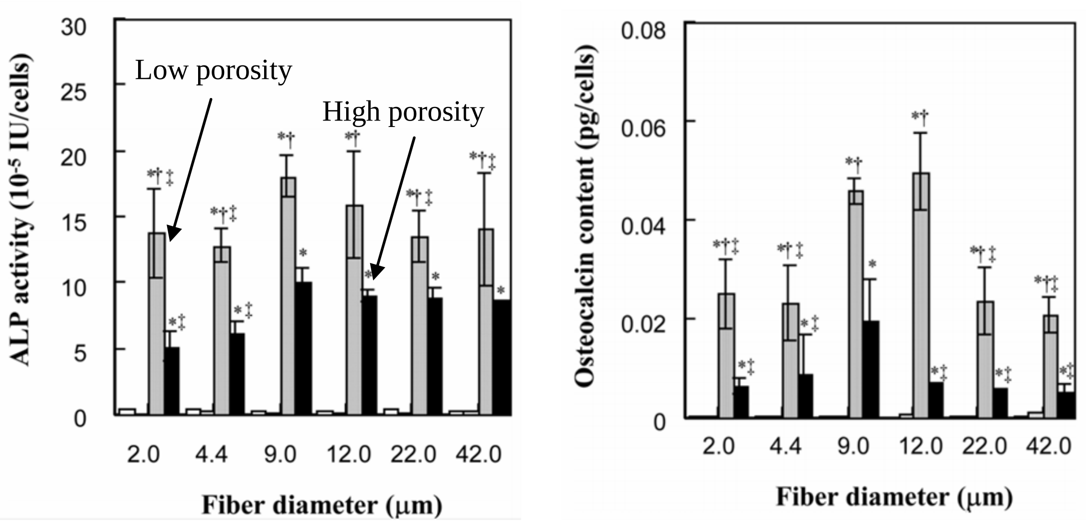

Figure 2.9: ALP and osteocalcin activity of mesenchymal stem cells in low porosity (grey) vs. high porosity (black) PET fibers. Small bars correspond to culture in non-osteogenic medium (Takahashi & Tabata, 2004)

2.2.3.3.1.2 In vivo

As discussed in this thesis, the scaffold-assisted *in vivo* osteogenesis involves the recruitment and penetration of cells and other agents from the neighboring tissue into the porous scaffold. Therefore, higher levels of porosity are expected to favor the osteogenesis process. Scaffolds fabricated by a poly(L-lactide-co-D,L-lactide) containing 20wt% β-tricalcium phosphate (TCP) with porosities ranging from 80-88% were implanted for the repair of rabbit craniums, and it was shown that higher tissue ingrowth occurred at higher scaffold porosities (Figure 2.10) (Roy et al., 2003).

Higher porosities in HA/TCP scaffolds also led to higher ALP activities of skeletal stem cells after 28 days post-implantation in mice (Figure 2.11) (Aarvold et al., 2013). In another study, soluble calcium filler salts were incorporated with poly(propylene fumarate) to produce porosity in the scaffolds, More salt particles led to higher porosities, and in this case induced greater and deeper bone ingrowth for rat tibia repair (Lewandrowski et al., 2000). Also, the higher porosity (48% as opposed to 44%) in dental implant coatings by porous titanium led to a higher tissue ingrowth in canine mandible defects (Story et al., 1998).

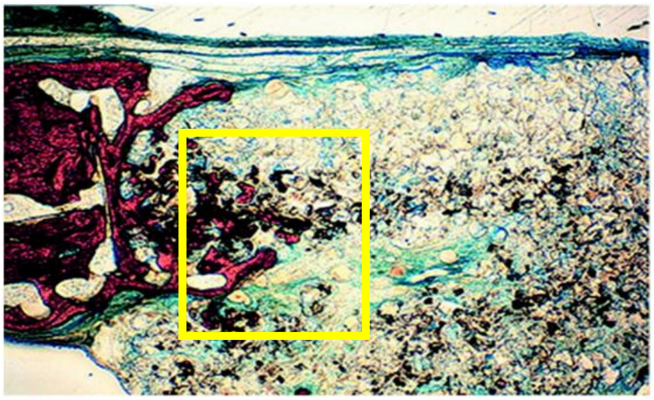

Figure 2.10: More new bone formation inside PLGA Scaffolds evidenced by SVG stain at 8 weeks post-surgery in rabbit cranial defects with an increase in porosity towards the center of the scaffold (yellow rectangle). (adapted from (Roy et al., 2003))

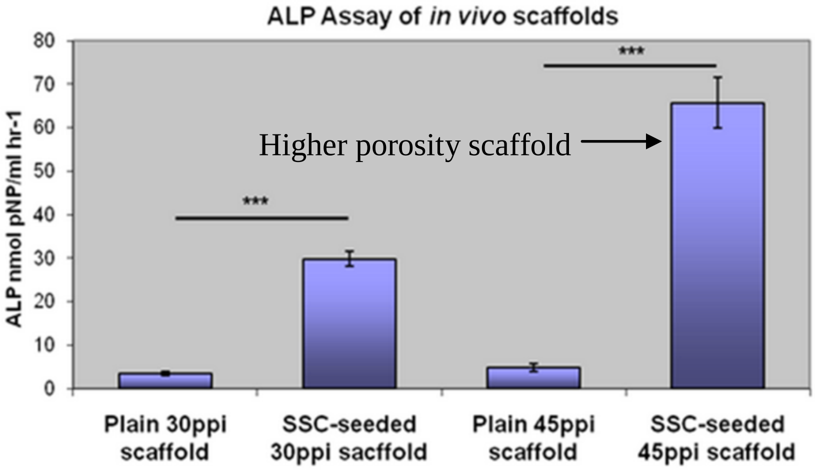

Figure 2.11: Higher porosity in HA/TCP scaffolds leads to higher ALP activity (better differentiation of preseeded MSCs) (Aarvold et al., 2013)

Most of the works in the literature have shown that the porosity has a positive effect on new bone formation *in vivo*. However, Amemiya et al reported that the increase in the porosity has a neutral effect on tissue formation (Amemiya et al., 2012).

2.2.3.3.2 Effect of pore size on osteogenesis

2.2.3.3.2.1 In vitro

As compared to *in vivo* investigations, the effect of pore size on *in vitro* osteogenesis has seen very little attention in the literature and there is good potential for further research in this field. In addition, the pore dimensions investigated in these few efforts are significantly smaller than the minimum pore size requirements for *in vivo* osteogenesis. Moreover, the results obtained from these studies are quite contradictory. For example, it was shown that while the surface modification of PolyHIPE polymer (PHP) scaffolds with HA has a considerable impact on biomineralization by primary rat osteoblasts after 28 and 35 days, the pore size increase from 40 µm to 100 µm has no such effect (Figure 2.12) (Akay et al., 2004).

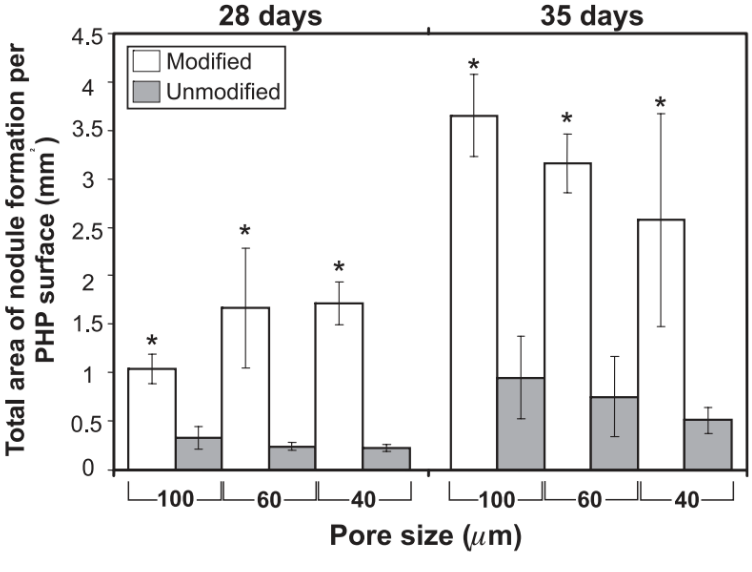

Figure 2.12: Neutral effect of pore size on mineral nodule formation (Akay et al., 2004)

Contrarily, a recent work by Huri et al. demonstrated that PCL scaffolds with pore sizes ranging from (0.5-1.5 mm) seeded with adipose derived stem cells (ASCs) showed higher levels of mineral deposition via VK staining at larger pore sizes (Figure 2.13) (Huri et al., 2014). The reason for these inconsistencies in the literature might be due to different behaviors of undifferentiated stem cells and differentiated osteoblastic cells. Due to these controversial results, it is difficult to explain the effect of pore size for *in vitro* osteogenesis.

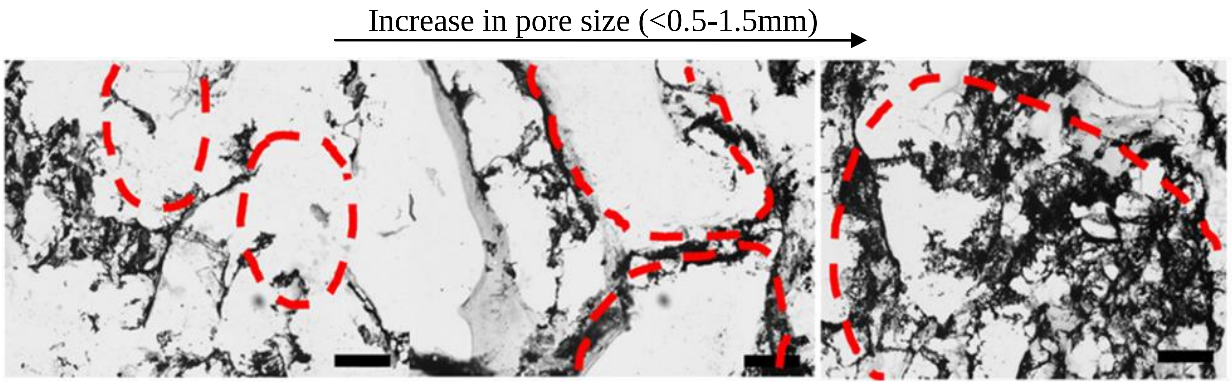

Figure 2.13: Positive impact of the increase in pore size in the amounts of mineral deposits detected (adapted from (Huri et al., 2014))

In Chapter 6 of this thesis, we also try to investigate the effect of pore size on cellular adhesion, proliferation and biomineralization.

2.2.3.3.2.2 In vivo

Apart from the pioneer work by Hulbert et al who determined a minimum pore size of 100 µm for *in vivo* bone formation (Hulbert et al., 1970), other groups have determined higher values as optimum pore dimensions. For instance, a range of 300-600 µm was considered sufficient by Kuboki et al. for new bone formation as well as for observing high levels of ALP and osteocalcin expression (Kuboki et al., 2001). While these studies associated high levels of bone ingrowth with higher pore sizes than the initially proposed 100 µm, some controversial results demonstrated that the increase in the pore size can have no or negative effects on bone ingrowth and vascularization (Ayers et al., 1999; Bai et al., 2011).

Karageorgiou et al concluded that the pore sizes of over 300 µm are able to promote vascularization (Karageorgiou & Kaplan, 2005). Lower values of pore size lead to hypoxic conditions that favor fibrosis or callus formation instead of osteogenesis. Also, such small pore sizes might not be adequate for cell migration and nutrient/waste transport inside the construct (Kuboki et al., 2001). Larger pore sizes, in contrast, promote the mass transport and cell migrations in the scaffold and are preferred due to their abilities to support the formation of capillaries (Kuboki et al., 2001; Tsuruga et al., 1997). However, large pore sizes are always associated with higher risks of mechanical failure due to an excess of void volume.

2.2.3.4 Surface chemistry

Cellular functions are highly dependent on the interaction between the cells and the surface of the scaffold material. Such interactions are primarily a function of the scaffold surface chemistry (hydrophilicity, surface charge) and topology (roughness) (Graziano et al., 2008; Luthen et al., 2005). For instance, hydrophobicity of polymers like poly(lactic acid) and poly(glycolic acid) complicates the cell seeding procedures, since the cells tend to poorly adhere to these polymeric materials. Therefore, surface modification techniques are normally employed to enhance the surface chemistry of these scaffolds. One example of such surface modifications is blending these polymers with hydrophilic poly(vinyl alcohol) (PVA) (Oh et al., 2003). Chitosan has also been used in the past for improving the PLA cytocompatibility (Cui et al., 2003; Xiao et al., 2008). Figure 2.14 demonstrates the positive impact of surface modification of PLA discs by chitosan (white bars) on the viability of L929 (MTT method) as compared to the pure PLA (light grey) and tricalcium phosphate (TCP) discs as positive controls. $^*P < 0.05$ (compared to cell density on PLA disks on the respective day), $^{**}P < 0.01$ (compared to cell density on PLA disks on the respective day).

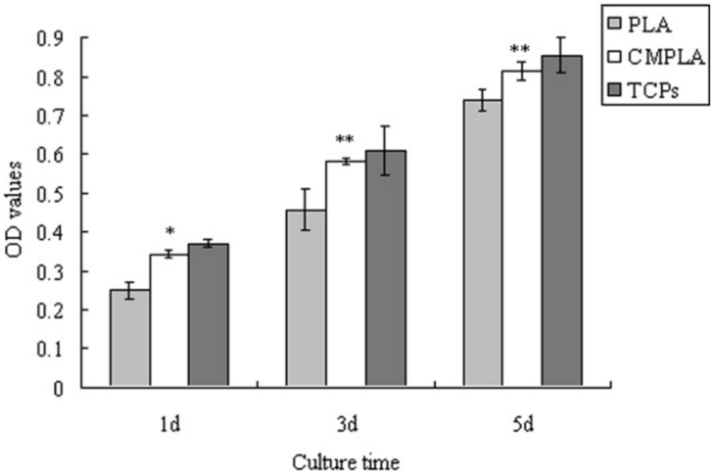

Figure 2.14: MTT assay showing the positive effect of chitosan modification after on the L929 cell viability after 1, 3 and 5 days of culture as compared to pure PLA (Xiao et al., 2008)

In Chapter 5, we also address an issue of poor surface chemistry in our material of interest (PCL) and we seek to modify the surface by using chitosan via a method of layer-by-layer self-assembly of polyelectrolytes.

2.2.3.5 Mechanical properties

Bone repair often requires a structural immobilization at early stages of healing, which is provided by a graft or scaffold. Clearly, there should be a good correlation between the mechanical properties of the scaffold and those of the tissue which is about to be produced. According to the mechanotransduction mechanisms by which cells convert mechanical stimulus into chemical activity, both high and low mechanical properties of a scaffold may affect the growth and integration of new tissue (Hing, 2004). The properties lower than a critical limit leads to the scaffold breakdown under normal or severe conditions, which would lead to tissue growth defects such as deformed tissue shapes or formation of no tissue at all. Moreover, mechanical properties higher than a specific threshold might inhibit the flexibility of the *in vivo* conditions required for the cell growth.

According to mechanotransduction processes, the bone tissue uses stress as an indication to produce more bone cells. As a result, if the mechanical properties of the scaffold are much higher than those of the surrounding bone, low levels of stress exerted on the bone itself prevents new bone formation and leads to a decrease in the density of the surrounding bone. This phenomenon is called "stress-shielding" (Chanlalit et al., 2012). Figure 2.15 illustrates how bone resorption (low bone density areas shown with arrows) might occur in the presence of bone implants due to the stress shielding phenomenon.

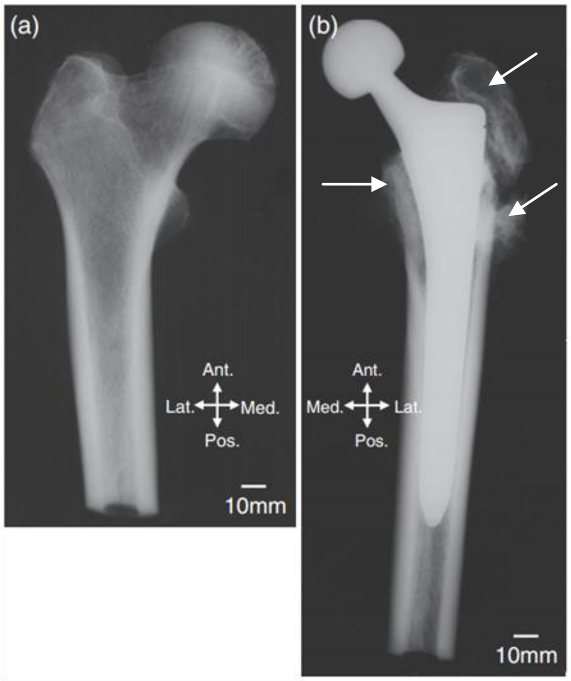

Figure 2.15: X-ray radiographs of a human femur (a) without and (b) with an artificial hip joint (adapted from (Niinomi & Nakai, 2011))

2.2.4 Biomaterials of interest

In this section of the dissertation, we only discuss the biomaterials of our interest in this thesis. However, for more detailed information on other materials used in bone tissue engineering and their contribution to this growing field, please refer to Appendix 1 of this report. During the current study, the following synthetic and natural polymers have been used:

2.2.4.1 Poly(ε-caprolactone)

PCL is also an aliphatic polyester which has recently received a lot of attention in bone and cartilage tissue engineering (Li et al., 2005; Yoshimoto et al., 2003). The chemical structure of

PCL is illustrated in Figure 2.16.

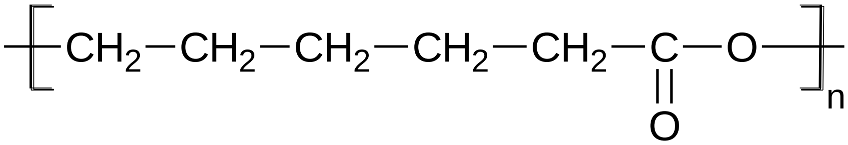

$$-\!\!\left[CH_2-CH_2-CH_2-CH_2-CH_2-\underset{\underset{O}{\|}}{C}-O- \right]_n$$

Figure 2.16: Chemical structure of polycaprolactone

This chemical structure can be degraded by several mechanisms which makes it suitable for use in biomedical applications. PCL can be degraded by microorganisms, bulk hydrolysis under physiological conditions and finally by enzymatic surface erosion (Pitt et al., 1981). The degradation reaction of PCL involves a 2 step process: first, the amorphous region of the polymer degrades after hydration and newly mobilized low molecular weight amorphous chains start to recrystallize, and finally the breakup of the crystalline region occurs (Chu, 1981). The recrystallization step becomes the rate limiting step in the degradation process of PCL and makes it degrade in a period of more than two years. For example, an *in vitro* study in water demonstrated that only 27% of the PCL particle mass was degraded after 33 months (Pitt et al., 1981). A rabbit calvarial defect *in vivo* model showed that molecular weight of the PCL scaffold dropped by 63% after 2 years implantation (Lam et al., 2009). Therefore, it is one of the most suitable biodegradable polymers that can be used for long-term implantable systems such as bone tissue engineering.

Among aliphatic polyesters, PCL shows some unusual characteristics; its glass transition temperature and melting temperature are -72°C and 58°C, respectively (Mark, 2009). Due to its low glass transition temperature, PCL is a semi-crystalline polymer in its rubbery form at room temperature. Therefore, for increasing its mechanical strength and at the same time accelerating the process of degradation, blending or copolymerization of PCL and PLA can be done (Middleton & Tipton, 2000). PCL also has an unusually high decomposition temperature among aliphatic polyesters (which are normally decomposed in the range of 235-255 °C) which is 350°C. This feature of PCL makes it an ideal polymer for its processing at high temperature. In our research, we use this intrinsic characteristic of PCL to increase the temperature far higher than its melting temperature in the annealing process.

With regard to mechanical properties, PCL is considered as a tough polymer with tensile modulus of 0.21-0.44 GPa, which are values between those of low density polyethylene (LDPE) and high density polyethylene (HDPE). The winning mechanical property of PCL is its elongation at break ε_b(%) which is reported to be more than 400% (Labet & Thielemans, 2009).

Since the PCL is the building block material in the scaffolds fabricated in this study, its application in bone tissue regeneration is discussed further in this section. The application of PCL and its composites in bone tissue engineering has been studied since the year 2000 and a variety of PCL products have been investigated including PCL-only scaffolds (generated by Fused Deposition Modeling (FDM) (Choong et al., 2004), electrospun PCL (Yoshimoto et al., 2003), or solvent-extracted PCL (Ciapetti et al., 2003)), loaded PCL scaffolds (scaffolds containing transforming growth factor beta-1 (TGFβ-1) (Huang et al., 2002) or BMPs (Savarino et al., 2007; Williams et al., 2005)) as well as PCL composites (PCL combined with PLLA (Landis et al., 2005), tricalcium phosphate (TCP) (Shao et al., 2006; Yeo et al., 2010), or collagen (Srouji et al., 2008)). Yeo et al. demonstrated the potential of PCL-TCP composite scaffolds for bone regeneration in rabbit calvaria defects, as the scaffold is surrounded by new bone after 4 weeks post-surgery (Figure 2.17) (Yeo et al., 2010).

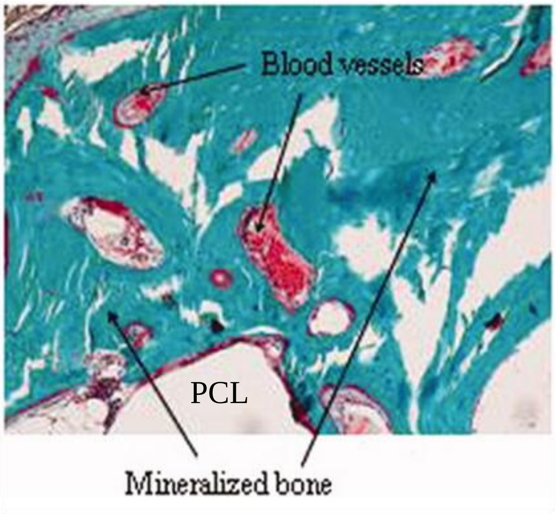

Figure 2.17: Goldner's trichrome staining (mineralized tissue = green; osteoid (unmineralized) = red) reveals newly formed mineralized bone after 4 weeks post-implantation (adapted from (Yeo et al., 2010))

In vitro studies with cell-seeded PCL have shown osteogenic potential through the expression of ALP and mineral deposition (Ciapetti et al., 2003). However, conclusive results for the stimulation of osteogenesis in 3D scaffolds have not yet been produced. While most of the efforts for investigating the PCL polymer are concentrated on *in vivo* experiments, there is still lack of knowledge on whether PCL can systematically induce *in vitro* osteogenesis by primary bone stem cells. In Chapter 6 of this thesis dissertation we investigate the role of PCL to independently induce cell differentiation of BMSCs and biomineralization.

In vivo studies have shown that PCL scaffolds exhibit osteoconductive, osteoinductive or osteogenic potential (when seeded with MSCs) in a variety of animal models (periosteal implant, trabecular bone defects, phalanges or calvarial defects) (Huang et al., 2002; Landis et al., 2005; Schantz et al., 2006; Schantz et al., 2003; Srouji et al., 2008; Williams et al., 2005; Yeo et al., 2010)[8, 9, 11, 13-16], When seeded with MSCs, *in vivo* results were promising as they led to good tissue integration with the implant and sufficient vascularization (Srouji et al., 2008). However, none of these scaffolds has yet achieved clinical use for fracture repair, potentially due to lack of mechanical integrity and/or lack of structural requirements due to the limitations in the fabrication techniques as shown in a previous work (Sarazin et al., 2004).

Because of the lack of functional groups in the backbone of PCL, this biomaterial is intrinsically hydrophobic, which makes its surface relatively non-adherent to cells and therefore is unfavorable for cell growth (Figure 2.18) (Sudarmadji et al., 2011).

The water contact angle of pure PCL surfaces has been reported to be approximately 82°, which is considered to be fairly hydrophobic (Ma et al., 2007). Previous results showed that L929 mouse fibroblasts tend to form spherical morphologies on electrospun PCL scaffolds (Mattanavee et al., 2009). Therefore, the surface of PCL should be modified in order to enhance the cytocompatibility of PCL through hydrophilic interactions. However, it is now a proven fact that both extremes of surface hydrophilicity and hydrophobicity are not suitable for cell attachments and rather moderate hydrophilicity is required for protein adsorption and positive cell response (Tziampazis et al., 2000).

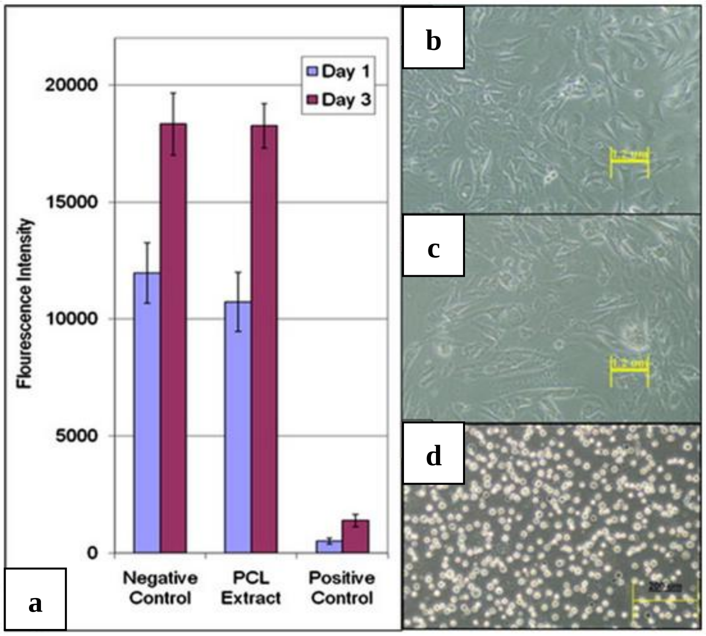

Figure 2.18: Cytotoxicity assay of PCL by the extract dilution method: (a) Cell viability of osteoblasts by Picogreen assay; cells in (b) negative control (fresh culture medium); (c) PCL extract; (d) positive control (extract from latex rubber gloves) (adapted from (Sudarmadji et al., 2011))

2.2.4.2 Poly(ethylene glycol) (PEG) and PEG-based materials

Poly(ethylene oxide) (PEO) also known as poly(ethylene glycol) (PEG) is one of the most studied biomaterials in biomedical applications due to its biocompatibility and hydrophilicity. This polymer with molecular weights lower than 100 kDa is usually termed PEG, while a higher molecular weight polymer is classified as PEO. PEG is able to form hydrogels using chemical or physical crosslinking which can further be used as scaffolds or drug carriers (Anseth et al., 2002). Due to its low mechanical strength, PEG hydrogels have only been used in cartilage repair in orthopedics (Bryant & Anseth, 2001). However, for using PEG in osteogenic applications, it should be reinforced by its blending with other biomaterials. For example, a blend of PEG and PLGA was used with bovine periosteal cells in order to generate osteochondral composites *in vitro* (Schaefer et al., 2000). In order to overcome its low barrier properties, PEG is functionalized through various approaches to make PEG-based materials such as PEG-diacrylate

(PEG-DA) and PEG-dimethacrylate (PEG-DM) which can make the base for the synthesis of PEG-based hydrogels (Williams et al., 2003). These hydrogels cannot degrade as easily as PEG itself and therefore should be blended or copolymerized with other polymers like PLA and be applied to the cartilage repair (Fisher et al., 2004).

2.2.4.3 Chitosan

Chitosan is a positively charged polysaccharide obtained by the deacetylation of chitin; another polysaccharide that can be extracted from the crustacean exoskeleton or by fungal fermentation processes (Wu et al., 2005). The chemical structure of chitosan is depicted in Figure 2.19. Chitosan is degraded *in vivo* by the lysozyme (enzyme that hydrolyzes glycosidic bonds), and the rate of degradation depends on the amount of residual acetyl content (Pachence, 1997). Moreover, the degradation products of chitosan are non-toxic. Since chitosan is a significant substance for this thesis dissertation and acts as a key player in Chapter 5 and Chapter 6, this section elaborates this material in detail.

Chitosan is also demonstrated to support the attachment and proliferation of rat calvarial osteoblasts as well as mineral depositions *in vitro* (Seol et al., 2004). On the other hand, Guzman et al. showed that chitosan microparticles inhibit mineralization of hBMSCs (Guzmán-Morales et al., 2009). In this work, the cells were believed to actively pull and dislodge and internalize chitosan particles from the surface. Very recent study by Amir et al. contrarily demonstrated that chitosan particles permit biomineralization of macaque dental pulp stromal cells (Amir et al., 2014). These controversial results have potential to be studied in more detail.

One of the most interesting properties of chitosan is the flexibility of modifications that it can go through in order to produce diverse derivatives with different chemical and mechanical properties; it can be combined with a variety of materials including ceramics and polymers to yield composite scaffolds with superior mechanical and biological properties. These modified chitosan scaffolds have also been proved osteoconductive *in vivo* in surgically created bone defects in sheep femoral condyle and mouse calvarial defects (Jin et al., 2012; Muzzarelli et al., 1994).

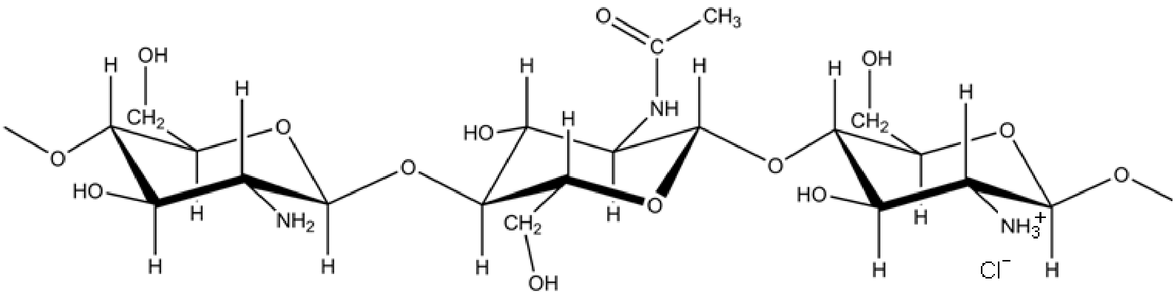

Figure 2.19: Chemical structure of chitosan (Hoemann et al., 2013)

Pure chitosan scaffolds are not generally regarded as a suitable material for bone regeneration application due to its poor mechanical strength. Moreover, the fabrication of pure chitosan scaffolds is not a straightforward process. Thermally-induced phase separation (Phase separation and lyophilization) is one of the most frequently used methods for the production of chitosan scaffolds. In this process, a dilute chitosan solution is made in acetic acid, introduced into a mold of interest and subjected to freezing. Ice crystals are formed in the freezing step and separated from the acetate salts of chitosan through sublimation in the freeze-drying step, which leads to a porous structure (Seol et al., 2004). Lower freezing temperatures and higher chitosan concentrations in this process are known to reduce the pore size (Jana et al., 2012; Madihally & Matthew, 1999). Nonuniform porosity, formation of surface skin and low levels of pore interconnectivity are the major drawbacks of this technique (Dalton et al., 2009). Moreover, it is very difficult to prepare chitosan solutions in acetic acid with a chitosan concentration above 4 wt% due to the high solution viscosity which is a constant problem in all chitosan solution based techniques. Thermally-induced phase separation technique and its characteristics are discussed in detail in Appendix 2 in this thesis dissertation.

2.2.5 Bone scaffold fabrication techniques

Having selected the best biomaterials for the scaffold or implant, this material must be processed to generate an ideal three-dimensional porous network with interconnected pores to be able to physically and biologically support bone ingrowth according to the requirements mentioned in section 2.2.3. Some of the common scaffold fabrication techniques for the generation of porous polymer scaffolds are listed in Figure 2.20 along with their pros and cons (Dalton et al., 2009). The most common fabrication techniques are discussed in further detail in Appendix 2.

The method used for the generation of three-dimensional scaffolds most importantly depends on the biomaterials used. For example, almost all processes used for the fabrication of ceramic scaffolds involve sintering. Other fabrication techniques commonly employed for the production of bone scaffolds include solvent casting and particulate leaching, gas foaming, phase separation and freeze-drying. Nonetheless, other techniques such as melt molding/particulate leaching and electrospinning have also been used. Modern rapid-prototyping methods like 3D printing (3DP), selective laser sintering (SLS) and fusion deposition modeling (FDM) have also been developed for the production of scaffolds.

Table 2.3 summarizes the use of various fabrication techniques, the materials used, generated pore size and their application in bone tissue engineering.

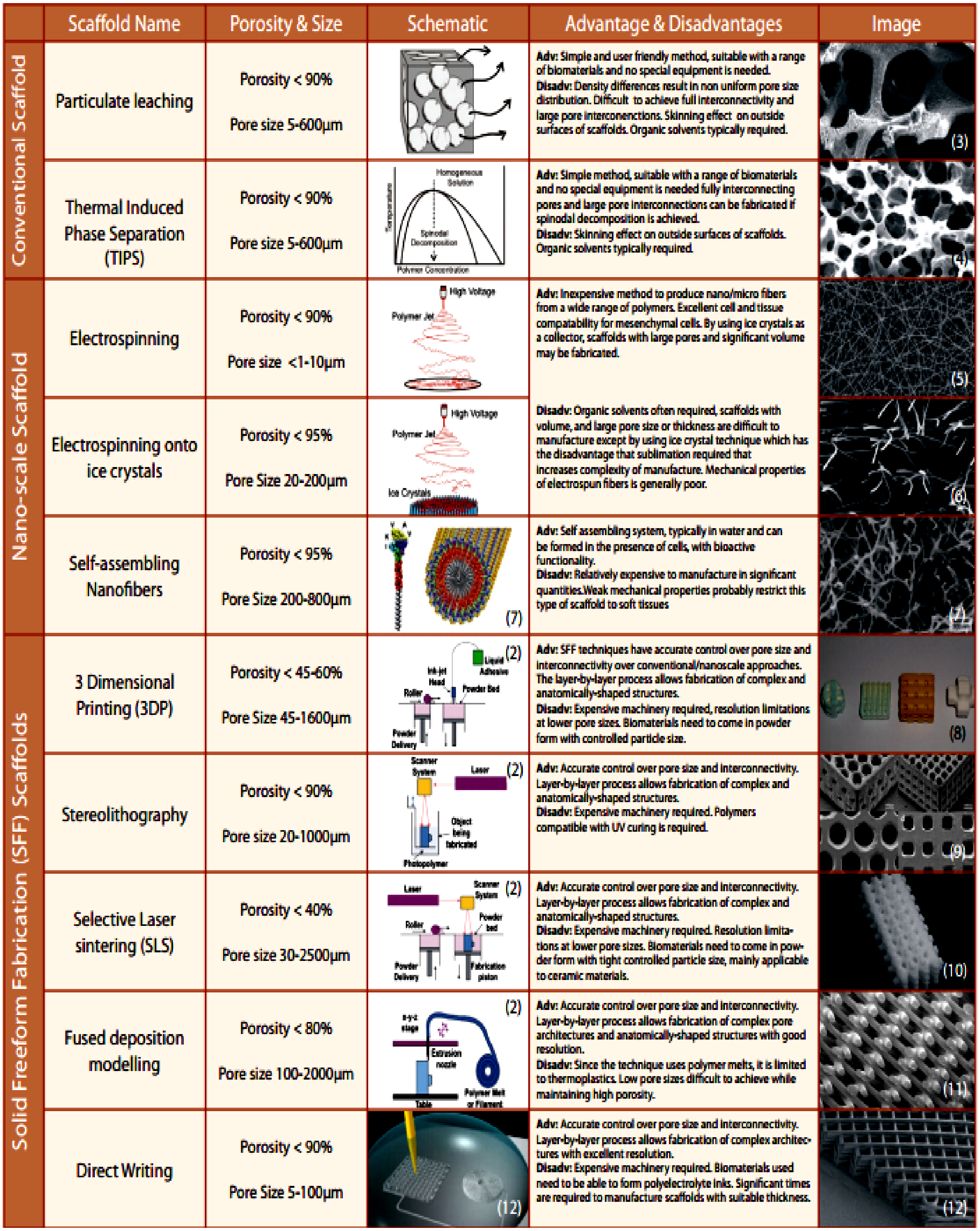

	Scaffold Name	Porosity & Size	Schematic	Advantage & Disadvantages	Image
Conventional Scaffold	Particulate leaching	Porosity < 90% Pore size 5-600μm		**Adv:** Simple and user friendly method, suitable with a range of biomaterials and no special equipment is needed. **Disadv:** Density differences result in non uniform pore size distribution. Difficult to achieve full interconnectivity and large pore interconenctions. Skinning effect on outside surfaces of scaffolds. Organic solvents typically required.	(3)
	Thermal Induced Phase Separation (TIPS)	Porosity < 90% Pore size 5-600μm		**Adv:** Simple method, suitable with a range of biomaterials and no special equipment is needed fully interconnecting pores and large pore interconnections can be fabricated if spinodal decomposition is achieved. **Disadv:** Skinning effect on outside surfaces of scaffolds. Organic solvents typically required.	(4)
Nano-scale Scaffold	Electrospinning	Porosity < 90% Pore size <1-10μm		**Adv:** Inexpensive method to produce nano/micro fibers from a wide range of polymers. Excellent cell and tissue compatability for mesenchymal cells. By using ice crystals as a collector, scaffolds with large pores and significant volume may be fabricated. **Disadv:** Organic solvents often required, scaffolds with volume, and large pore size or thickness are difficult to manufacture except by using ice crystal technique which has the disadvantage that sublimation required that increases complexity of manufacture. Mechanical properties of electrospun fibers is generally poor.	(5)
	Electrospinning onto ice crystals	Porosity < 95% Pore Size 20-200μm			(6)
	Self-assembling Nanofibers	Porosity < 95% Pore Size 200-800μm	(7)	**Adv:** Self assembling system, typically in water and can be formed in the presence of cells, with bioactive functionality. **Disadv:** Relatively expensive to manufacture in significant quantities.Weak mechanical properties probably restrict this type of scaffold to soft tissues	(7)
Solid Freeform Fabrication (SFF) Scaffolds	3 Dimensional Printing (3DP)	Porosity < 45-60% Pore Size 45-1600μm	(2)	**Adv:** SFF techniques have accurate control over pore size and interconnectivity over conventional/nanoscale approaches. The layer-by-layer process allows fabrication of complex and anatomically-shaped structures. **Disadv:** Expensive machinery required, resolution limitations at lower pore sizes. Biomaterials need to come in powder form with controlled particle size.	(8)
	Stereolithography	Porosity < 90% Pore size 20-1000μm	(2)	**Adv:** Accurate control over pore size and interconnectivity. Layer-by-layer process allows fabrication of complex and anatomically-shaped structures. **Disadv:** Expensive machinery required. Polymers compatible with UV curing is required.	(9)
	Selective Laser sintering (SLS)	Porosity < 40% Pore size 30-2500μm	(2)	**Adv:** Accurate control over pore size and interconnectivity. Layer-by-layer process allows fabrication of complex and anatomically-shaped structures. **Disadv:** Expensive machinery required. Resolution limitations at lower pore sizes. Biomaterials need to come in powder form with tight controlled particle size, mainly applicable to ceramic materials.	(10)
	Fused deposition modelling	Porosity < 80% Pore size 100-2000μm	(2)	**Adv:** Accurate control over pore size and interconnectivity. Layer-by-layer process allows fabrication of complex pore architectures and anatomically-shaped structures with good resolution. **Disadv:** Since the technique uses polymer melts, it is limited to thermoplastics. Low pore sizes difficult to achieve while maintaining high porosity.	(11)
	Direct Writing	Porosity < 90% Pore Size 5-100μm	(12)	**Adv:** Accurate control over pore size and interconnectivity. Layer-by-layer process allows fabrication of complex architectures with excellent resolution. **Disadv:** Expensive machinery required. Biomaterials used need to be able to form polyelectrolyte inks. Significant times are required to manufacture scaffolds with suitable thickness.	(12)

Figure 2.20: Fabrication techniques for the production of polymer scaffolds (Dalton et al., 2009)

Table 2-3: Summary of the fabrications techniques, materials used and porous network generated for bone tissue engineering

Fabrication Technique	**Material(s)**	**Pore Size (μm)**	**Porosity (%)**	**Reference**
Sintering	HA	400, 800	60, 70	(Kruyt et al., 2003)
	Natural coral	150-200	36	(Chen et al., 2002)
Solvent casting and particulate leaching	Hyaluronic acid	100–600	80-90	(Kim & Valentini, 2002)
	Poly(ε-caprolactone)	< 500-1500	65	(Huri et al., 2014)
Gas foaming	Biphasic calcium phosphate (HA)	300-800	75-85	(Kim et al., 2012)
	Poly(propylene fumarate)	70	51	(Lewandrowski et al., 2003)
Thermally-induced phase separation (TIPS)	Biphasic calcium phosphate /polyamide 6	100-900	77-89	(Shen et al., 2010)
	Poly(l-lactide-co-glycolide)	75-400	84-90	(Yang et al., 2008)
Freeze drying	Collagen/HA	30-100	85	(Lickorish et al., 2004)
	Collagen and elastin	130, 340	90-98	(Buttafoco et al., 2006)
Electrospinning	Poly(lactide-co-glycolide)	2-465	92	(Li et al., 2002b)
Rapid prototyping	Poly(ε-caprolactone)	1750-2500	63-79	(Williams et al., 2005)

2.3 Melt blending of polymers

2.3.1 Fundamentals

Section 2.2.5 elaborated the most common scaffold fabrication techniques. By knowing their characteristics and their major drawbacks, newer methods could be devised so that polymer scaffolds of more suitable properties could be produced and applied in bone tissue engineering. Most common disadvantages of the mentioned techniques include the use of toxic solvents, limitations imposed by the use of a third party agent (shape of the porogen phase in the case of solvent casting/particulate leaching), low levels of pore interconnectivity, high processing temperatures, large pore size distributions and high processing costs. These negative points guided the scientists towards developing the approach of melt blending of polymers in order to fabricate scaffolds that also has potential to be applied to osteogenic applications.

The requirements for polymeric materials have become continuously stricter in order to meet specific and targeted applications. A quick response for the production of polymers with the imposed specific requirements is polymer synthesis. Nevertheless, due to strenuous intricacies and high production costs of the polymer synthesis, other alternatives such as melt blending of polymers have been developed to produce an array of optimal requirements such as physicochemical, mechanical and electrical properties in the final product by employing the intrinsic characteristics of the individual homopolymers used. For instance, osteoconductive properties of polymeric scaffolds could be considerably enhanced by blending hydroxyapatite-based ceramics with polymers. At the same time, biodegradation and mechanical property adjustments could be provided by the polymer phase. Sometimes, however, the idea of blending comes into play in order to facilitate the production of a particular morphology as required by the final application of the product. For example, major physical requirements needed in bone tissue engineering scaffolds include porosity and pore interconnectivity which could be provided by the blending technique as will be demonstrated in this dissertation. In this part of this dissertation, the basics of the melt blending technique are going to be discussed.

There are two thermodynamically different types of polymer blends: miscible and immiscible. A miscible polymer blend is defined as a system which is homogeneous down to the molecular level and form a single phase structure. On the other hand, immiscible polymer blends are systems which are phase separated due to the independent existence of the individual blend ingredients. This type of polymer blends is known to be the most populous group. These definitions can be translated thermodynamically by use of the equation of Gibbs free energy of mixing:

$$\Delta G_{mix} = \Delta H_{mix} - T\Delta S_{mix} \quad (1)$$

Where ΔG_{mix} is the Gibbs free energy of mixing, ΔH_{mix} is the enthalpy of mixing, T is the mixing temperature, and ΔS_{mix} is the entropy change by mixing.

Like any mixing system, a negative Gibbs free energy for polymer blends represents miscibility and the formation of a single phase.

$$\Delta G_{miscible} = \Delta H_{mix} - T\Delta S_{mix} < 0 \;\; \Rightarrow \; \Delta H_{mix} < T\Delta S_{mix} \quad (2)$$

The term $\mathrm{T\Delta S_{mix}}$ is always positive due to an increase in the entropy of the system by mixing. Thus, for low molecular weight materials, increasing the temperature leads to a negative contribution of $\mathrm{T\Delta S_{mix}}$ to the $\mathrm{\Delta G_{mix}}$ and therefore increasing the miscibility. However, considering the lattice theory of Flory-Huggins, by increasing the molecular weight and reaching the range corresponding to that of macromolecules, this increase in the entropy becomes negligible and its contribution in the equation above becomes minimal (Sperling, 2005). Therefore, for macromolecular chains, the term ΔG_{mix} will only depend on the enthalpy of mixing. For most of the polymer blends, the enthalpy of mixing is a positive value. In this case, by considering the Flory-Huggins solution theory and Hildebrand-Scatchard-van Laar equation:

$$\Delta G_{mix} = RTV\left\{\frac{\varphi_A ln\varphi_A}{\widehat{V_A}} + \frac{(1-\varphi_A)\ln(1-\varphi_A)}{\widehat{V_B}} + \chi_{AB}\varphi_A(1-\varphi_A)\right\} \quad (3)$$

$$\Delta H_{mix} = V_{mix}(\delta_A - \delta_B)^2\varphi_A(1-\varphi_A) \quad (4)$$

Where φ_A is the volume fraction of phase A, $\widehat{V_A}$ is the molar volume of phase A, χ_{AB} is the interaction parameter between phase A and B, V_{mix} is the volume of the mixture, R is the ideal gas constant and δ_A is the solubility parameter of component A of the blend. It is concluded that the term χ_{AB} is closely related to ΔH_{mix} which is closely related to the differences in the solubility parameters of the components A and B. The closer the solubility parameters of the blend components, the smaller the interaction parameters between them and therefore the more compatible or miscible they become.

Consequently, unless there are specific interactions between the blend components such as attractive forces like dipole-dipole, hydrogen bonding and acceptor-donor interactions, spontaneous miscibility cannot be obtained. Therefore, a negative enthalpy of mixing is a necessary requirement for miscibility. However, this is not the case for most of the polymer pairs and that is why most of the polymer blend systems are immiscible.

Although negative ΔG_{mix} is a necessary requirement for miscibility of polymers, the sufficient criterion for miscibility is that the second derivative of the Gibbs free energy with respect to composition, at constant temperature and pressure must be positive:

$$(\frac{\partial^2 \Delta G_{mix}}{\partial {\varphi_i}^2})_{T,P} > 0 \quad (5)$$

Similarly, the sufficient requirement for a polymer blend to be immiscible is that this second derivative of the free energy becomes negative, even if ΔG_{mix} might remain negative. This means that in a window of volume fraction of component i where this second derivative becomes negative, a phase separation occurs into phases with both of the blend components but rich in one of them.

It should be noted that among all investigated polymer pairs, a small percentage of them were determined to be miscible. Some examples of these polymers include polystyrene/poly(phenylene oxide), poly(ethylene terephthalate)/ poly(butylene terephthalate) and poly(methyl methacrylate)/ poly(vinylidene fluoride).

2.3.2 Immiscible polymer blends

As explained by the Gibbs free energy in the previous section, most of the polymer pairs are immiscible, and although obtaining miscible polymer blends might be considered as an achievement over immiscible blends in the production of materials with enhanced properties due to the lack of weak component interfaces, immiscibility is sometimes the only choice for the fabrication of a highly specific morphology. In the case of producing porous morphologies, for instance, miscible polymer blends cannot be of any use since there is no possibility for the formation of the pores, whereas melt blending of immiscible polymer pairs can lead to the production of sophisticated morphologies with interconnected pores as required by the specific bone tissue engineering application.

Melt blending of the immiscible polymers are commonly exercised in an internal mixer, where the two polymers are homogeneously mixed with each other in a confined chamber through strong shearing forces provided by two counter-rotating blades, as demonstrated in Figure 2.21.

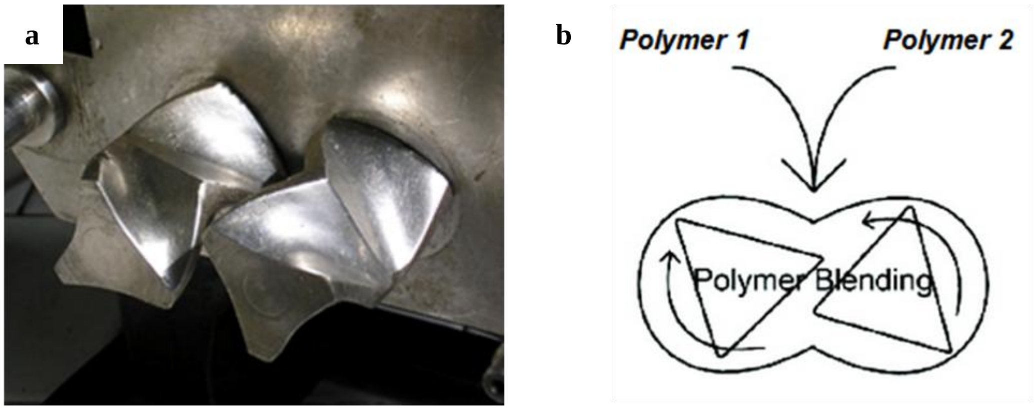

Figure 2.21: (a) Rotor-blades of an internal mixer (ISMAC); and (b) Schematic of internal mixing (adapted from (Xiang et al., 2009))

In order to achieve the desired morphological structure, the intrinsic properties of the system such as molecular weight and the chain nanostructure of the polymers, as well as the processing conditions like mixing temperature and shear rate are of ultimate importance. All these key factors come down to two key parameters: kinetic and thermodynamic. Kinetic parameters include mixing conditions such as mixing temperature and shear rate and rheological properties of the blend components such as viscosity and elasticity. As its name suggests, the latter type of morphology-controlling parameters involves the thermodynamic properties of the blend system such as the interfacial characteristics of the blend materials (Reignier & Favis, 2000). By modifying these parameters in the melt blending process, a wide range of phase (pore) sizes from the nanometer scale up to hundreds of microns together with various shapes (cylindrical, spherical, ellipsoidal, ribbon-like, subinclusion and cocontinuous type morphologies) can be obtained (Utracki, 2002). There are two basic processes in the droplet scale that make up the final morphology in the product: deformation/breakup and coalescence. Although these processes are the building blocks of the melt-blending approach, their details are out of the scope of this thesis. Among all the morphologies named above, cocontinuous structures are the way to go for the production of porous scaffolds with interconnected pores. As a matter of fact, the level of pore interconnectivity in the porous construct is closely related to that of co-continuity.

In immiscible polymer blends, there are basically two main types of morphologies: dispersed droplet and co-continuous morphology. Figure 2.22 demonstrates the scanning electron microscopy images for poly(L-lactide)/polystyrene (PLLA/PS) blends at 80/20 and 60/40 v% compositions.

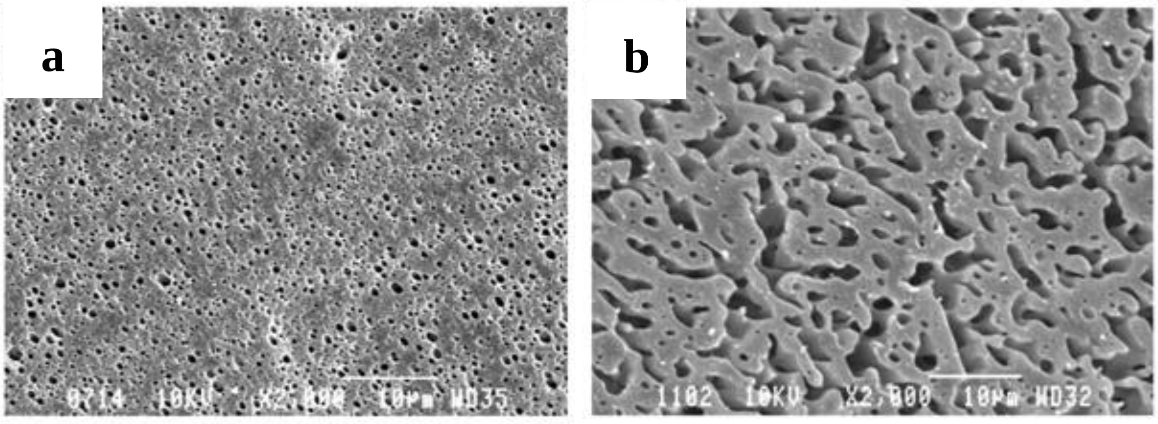

Figure 2.22 : SEM micrographs of PLLA/PS binary blend at a) 80/20 and b) 60/40 v% (adapted from (Sarazin & Favis, 2003))

The figure above clearly demonstrates that by a slight change in the composition of the components, completely different morphologies can be obtained: in micrograph (a) clearly droplets of PS are dispersed in a matrix of PLLA and in micrograph (b) by a 20% increase in the composition of PS, the droplets of polystyrene coalesce and form a network. This type of microstructure in which the distinction of the droplets and matrix phase becomes almost impossible is called co-continuous morphology.

This phenomenon can also be observed by transmission electron microscopy images from poly(methyl methacrylate) PMMA/PS blends illustrated in Figure 2.23.

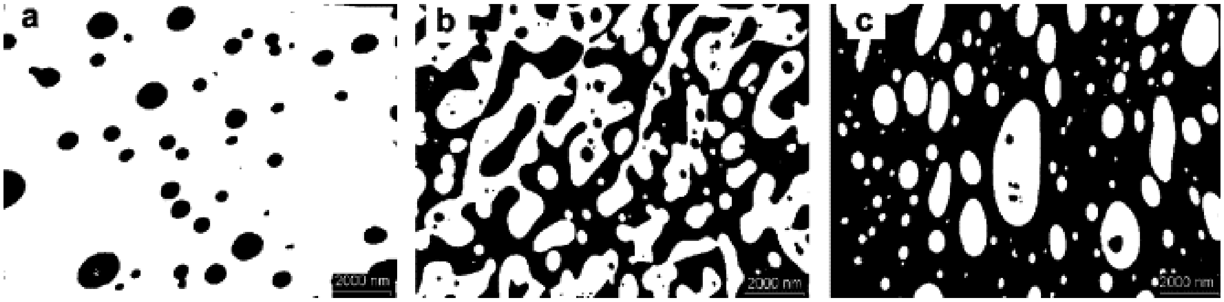

Figure 2.23: Transmission electron micrographs for PMMA/PS blends at different blend compositions: (a) 90/10, (b) 50/50, (c) 30/70 (Steinmann et al., 2001)

According to this figure, by increasing the concentration of the droplet phase in a binary blend, a phase inversion takes place which replaces the droplets and matrix positions. This window of composition is called the phase inversion region. The phase inversion region is defined as the composition at which the blend phases switch their role, i.e. the dispersed phase droplets combine to form the matrix and the matrix breaks up to form droplets. In the proximity of the phase inversion concentration, the other morphology of the immiscible polymer blends is achieved which is called co-continuity region. In the co-continuous region, none of the phases can be considered as droplets or the matrix. The two phases interpenetrate in a manner that can only be described as two continuous pathways.

In order to achieve porosity at cocontinuous composition, one of the two continuous phases should be selectively extracted. Given the blends are prepared at co-continuous compositions, the pores formed are completely interconnected due to nature of co-continuity. In Figure 2.24, a binary blend of A and B at the cocontinuous composition is demonstrated, where the extraction of any of the phases leads to the generation of an interconnected porous network of the extracted component (porogen).

By adding other components to a binary blend (to make ternary or quaternary blends) other interesting morphologies can also be obtained. For instance, subinclusions or composite droplet (droplet in droplet) morphologies have also been studied in this research group. PMMA droplets located inside a thin shell of PS while dispersed inside a matrix of high density polyethylene (HDPE) are an example to these relatively complex morphologies (Reignier & Favis, 2003; Virgilio et al., 2005).

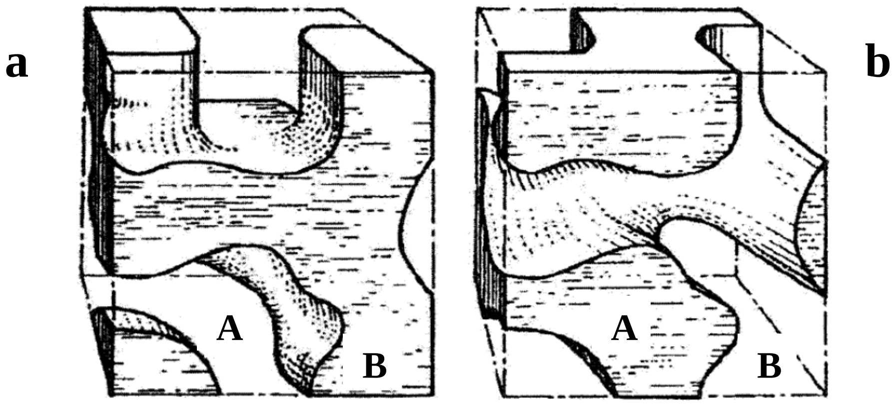

Figure 2.24: Schematics of a co-continuous structure in the binary blend A/B: (a) phase A is extracted, (b) phase B is extracted (adapted from (Gergen W.P., 1996))

2.3.3 Co-continuity in polymer blends

Thus far, we have established that in order to be able to use polymer blends as the means to fabricate bone tissue engineering scaffolds, the formation of a highly interconnected porous network is required. Therefore, the phenomenon of co-continuity or dual phase continuity, as described in the previous section, can be employed to achieve such requirement. Consequently, the aforementioned objective requires a more specific and detailed understanding of the development of co-continuity in polymer blends, i.e. how it is characterized and how it can be controlled to serve our mission.

2.3.3.1 Percolation theory and the development of co-continuity

Since the concept of co-continuity lies on the concept of phase inversion for which the former droplets become the matrix and the former matrix becomes the droplets, the development of co-continuous structures can to some extent be explained by the percolation theory.

Percolation theory divides a system including a polymer inside a solvent or another polymer in the case of polymer blends, into a number of lattices with a defined shape. “p” is designated to the fraction of lattices that randomly contain at least one building block of the polymer. By increasing the amount of the polymer in the system, the probability of finding these occupied lattices also increases and clusters are formed by adjacent occupied lattices. Above a critical number of lattices (p_c) containing the polymer building blocks (monomers), an infinite continuity of the occupied lattices will occur. This limit is called the percolation threshold (Hsu & Wu, 1993).

The concept of percolation threshold can also be applied to the development of co-continuity. By increasing the composition of the droplet phase in a binary blend, the level of interconnection of occupied lattices and formed clusters also increases and the system ultimately reaches the percolation threshold which is in fact the onset of co-continuity and the beginning of phase inversion. The percolation concept has also been applied to investigate the mechanical properties of the blends in the phase inversion region as a function of the morphology. Such attempts showed that the percolation theory could be readily applied for explaining the phase inversion phenomenon (Arends, 1992; Hsu & Wu, 1993). The transition process from a dispersed droplet morphology to a co-continuous morphology according to the percolation theory is illustrated in Figure 2.25.

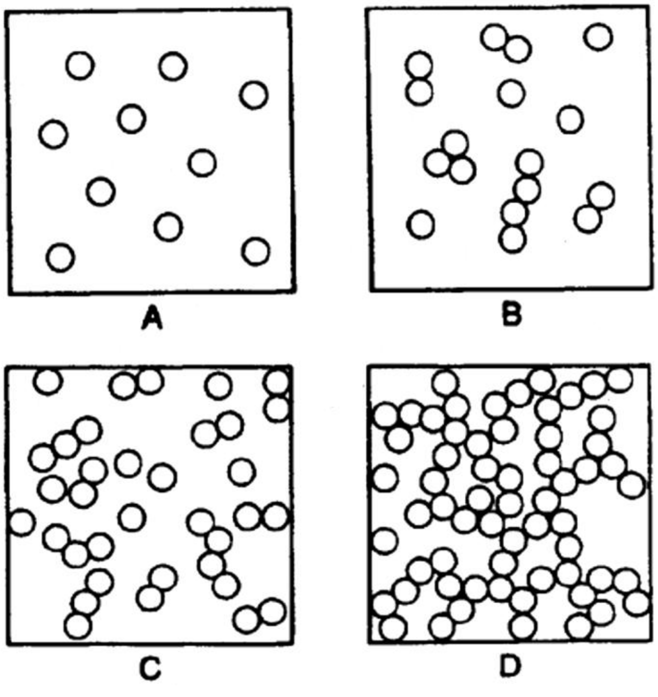

Figure 2.25: Co-continuity explained by the percolation theory (Hsu & Wu, 1993)

The percolation threshold or the onset for co-continuity varies from one system to another. Also, the width of the region in which phases are co-continuous depends on many parameters such as the viscosity ratio and the interfacial tension of the blend components. As an example, by use of the percolation theory, Lyngaae-Jorgensen et al. demonstrated that the onset of the co-continuity region occurs at the volume fraction of 0.19 ± 0.09 (Lyngaae-Jørgensen & Utracki, 1991).

2.3.3.2 Characterization of co-continuity or pore interconnectivity

Co-continuous structures can generally be characterized by using imaging techniques such as SEM, transmission electron microscopy (TEM) and atomic force microscopy (AFM). However, dual phase continuity is not a two-dimensional concept, as the phases form completely intertwining and irregular three-dimensional structures which cannot be fully characterized by photomicrographs. As a result, the aforementioned approaches are normally combined with fairly new statistical quantitative tools to support the two-dimensional images.

2.3.3.2.1 Image analysis

SEM is the classical approach for phase size and phase size distribution measurements. However, the polymer domains in a co-continuous structure are not well defined for the SEM approach to be able to analyze them. Therefore, the use of SEM for the evaluation of the co-continuous structure becomes strenuous if not impossible (Arns et al., 1999). For resolving this issue, other statistical techniques such as form factors and interfacial area could aid SEM to characterize the co-continuous morphology.

Form factor (ff) is a measure of the deviation of a finite shape from circularity (sphericity in 3D). This parameter can be very useful in determining the co-continuous region, as the structure completely deviates from the spherical droplets within the matrix. The form factor is defined as follows:

$$ff = 4\pi \frac{A}{P^2} \quad (6)$$

Where A is the area and P is the perimeter of the domains. Since for a circle, there is no deviation from circularity, the ff becomes 1 and more irregular domains deviate from unity and for infinitely irregular shapes, where the perimeter tends to infinity the form factor becomes 0.

This approach has been used to characterize the co-continuous morphology and to determine the cocontinuous composition for a blend of PMMA/PS (Steinmann et al., 2001; Weis et al., 1998). The SEM images used for the analysis showed that at all ranges of composition, circularity with ff_c close to unity existed, as well as irregular domains with different sizes. Therefore, the form factor for these latter domains ff_{irr} were calculated separately and the region where the most deviation from unity was observed was considered as the region of dual phase continuity as demonstrated in Figure 2.26.

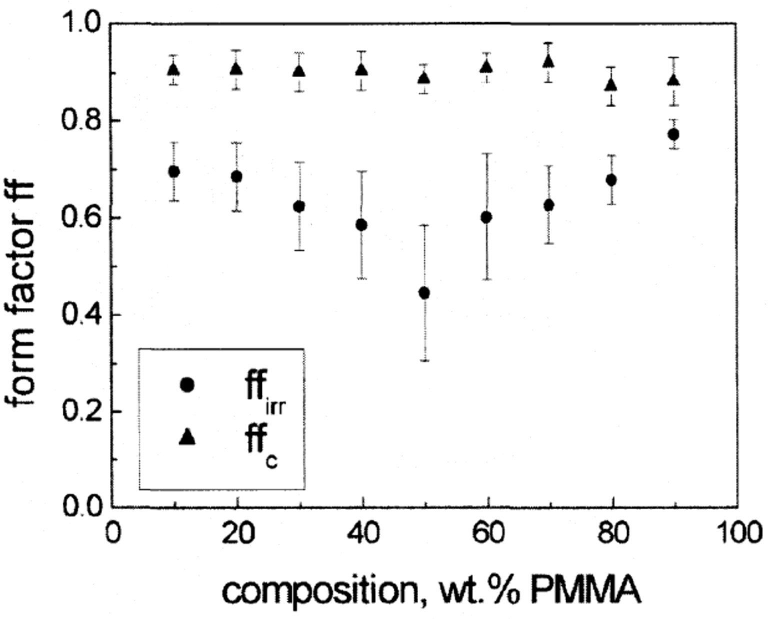

Figure 2.26: Mean form factors for both circular and irregular domains of PMMA/PS blends as a function of composition (Steinmann et al., 2001)

Galloway and Macosko presented another image analysis technique which measured the amount of interfacial area per unit volume for a blend of PS/PEO, and they showed that this value exhibits two maxima (35 and 65 wt%) for blend compositions at the extremes of the cocontinuous region (Figure 2.27) (Galloway & Macosko, 2004).

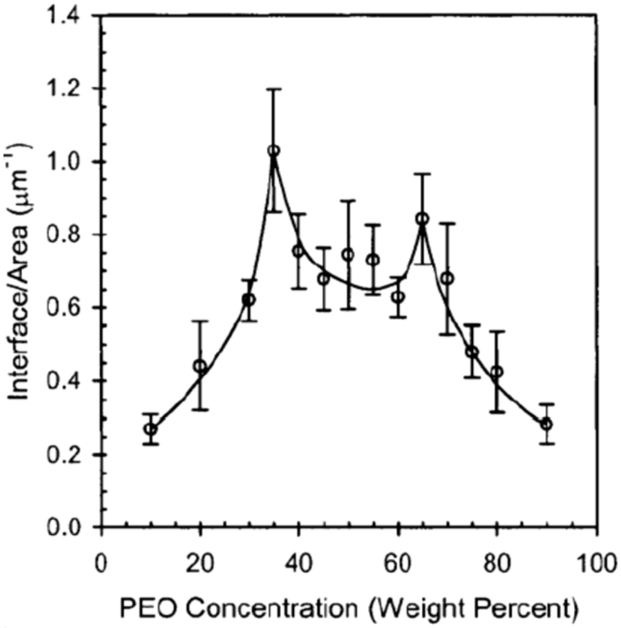

Figure 2.27: Interfacial area per unit volume of the blends as a function of composition in PS/PEO blends. The composition range of 35-65% is considered co-continuous (Galloway & Macosko, 2004)

2.3.3.2.2 BET and mercury intrusion porosimetry (MIP)

BET (Brunauer, Emmet and Teller) nitrogen adsorption and the mercury intrusion porosimetry has also been employed for the analysis of co-continuous morphologies (Li & Favis, 2001). For both of these techniques, one of the binary blend components should be selectively extracted in its specific solvent to give a porous construct.

In the BET technique, nitrogen gas passes through the porous construct, after which it is quenched down by liquid nitrogen. This rapid quenching causes the nitrogen gas to condense and adsorb on the internal porous structure of the sample. By measuring the volume of the adsorbed nitrogen on the surface and assuming that only one layer of nitrogen molecule is adsorbed on the surface, the surface area of the construct is calculated by using the following equation:

$$S = \frac{V_m . N . a}{V_M} \quad (7)$$

Where S is the surface area of the sample, V_m is the volume of the gas required for monolayer adsorption, N is the Avogadro's number, a is the area of one adsorbed nitrogen molecule which is

$16.2 \times 10^{-20}\ m^2$ and V_M is the molar volume of the gas.

By assuming that the pores are interconnected cylinders and that the volume of the pores (V) is equal to that of the extracted phase, the average pore diameter (d) can be calculated according to the following equation:

$$d = 4\frac{V}{S} \quad (8)$$

Mercury intrusion porosimetry is based on the capillary law governing the penetration of mercury as a non-wetting liquid into the small pores. In this method, dry porous samples are exposed to mercury under vacuum, after which pressure is applied to the mercury for it to penetrate into the pores of the construct. Mercury porosimetry uses the Washburn equation to describe the relation between the porous structure dimensions and the pressure applied to the mercury (Washburn, 1921).

$$P.r = -2\sigma Cos\theta \quad (9)$$

Where P is the applied pressure, r is the radius of the pores, σ is the surface tension (480 mN/m) and θ is the contact angle of mercury (140°).

The fact that these two methods do not involve two-dimensional micrographs as a representation of a three-dimensional sample is an advantageous factor for these two techniques.

2.3.3.2.3 Gravimetric measurements

Gravimetric measurement is the simplest and the most common approach for the determining the co-continuous region. This method is based on the weight of the sample before and after selective extraction of one of the phases (porogen). The quantitative parameter calculated in this approach is % continuity.

$$\%\ Continuity = \frac{W(porogen_{init}) - W(porogen_{final})}{W(porogen_{init})} \quad (10)$$

The only challenge in calculating the % continuity is to find the initial weight of the porogen phase, since $W(porogen_{init}) - W(porogen_{final})$ is in fact the difference between the weight of the whole sample, before and after the extraction, assuming the solvent selectively extracts only the porogen phase. The initial weight of the porogen phase can be estimated by multiplying the initial weight of the whole sample by the weight fraction of the porogen phase. Therefore, Equation 10 simplifies to the following equation:

$$\%Continuity = \frac{W(sample_{init}) - W(sample_{final})}{W(sample_{init}) \times \omega(porogen_{init})} \quad (10)$$

Where $\omega(porogen_{init})$ is the weight fraction of the porogen phase.

Although this approach is quite classical and simple, many researchers have recently used this method for characterizing co-continuity (Antunes et al., 2011; Filippone et al., 2010; Kucharczyk et al., 2012).

Co-continuity is reported to have synergistic effects on the properties like high modulus or high impact strength in commercial blends. Co-continuity also provides high rigidity during deformation (elongation), good barrier and conduction properties. Poly(ethylene terephthalate) (PET)/ polycarbonate (PC), Poly(butylene terephthalate) (PBT)/PC, Acrylonitrile butadiene styrene (ABS)/PC and ABS/ polyamide (PA) are examples of commercial co-continuous blends.

In this thesis, the concept of co-continuity is going to be used for the fabrication of a highly porous scaffold with high levels of pore interconnectivity for tissue engineering applications. Our research group has previously developed a novel melt blending technique for the formation of co-continuous structures (Sarazin & Favis, 2003; Sarazin et al., 2004; Yuan & Favis, 2005). Former studies have also investigated various parameters that can control the morphology of the co-continuous system reflecting the porosity and pore diameter of the final porous structure. Composition, components viscosity, viscosity ratio, interfacial tension and interfacial modification via compatibilizers and annealing are the factors that affect the morphology of a co-continuous blend. The following section elaborates the parameters that are in the scope of this study.

2.3.3.3 Parameters affecting the co-continuous morphology

In order to generate an apt porous material for orthopedic applications, a high level of control over the porous network is considered a powerful tool. In the case of immiscible polymer blends, this level of control can be precisely achieved at a submicron scale. As mentioned in section 2.3.2, there are many parameters (kinetic or thermodynamic) that can affect the morphology of a polymer blend, some of which are discussed in further detail in this section.

2.3.3.3.1 Composition and viscosity ratio of the blend components

Composition is the most important parameter for the formation of the co-continuous morphology. As discussed above, the increase in the composition of the minor phase is the main reason for the transformation of the morphology from the droplet/matrix system to the co-continuous system. Favis and Chalifoux (1988) investigated a blend of PC dispersed in the polypropylene (PP) matrix, and by increasing the composition, they witnessed an increase in the phase size of PC droplets. However, it is believed that the change in the composition does not independently influence the phase (pore) size in the co-continuous region (Favis & Chalifoux, 1988).

Significant efforts have been done in the past to determine the composition where the phase inversion occurs. However, the idea of finding this specific composition could only be valid for high interfacial tension systems. For other types of systems, a wider window of compositions exists rather than a single point of phase inversion. Some mathematical-experimental methods have been suggested to estimate the co-continuous composition either based on the viscosity ratio or elasticity ratio. Generally, viscosity ratio-based models place the low viscosity component in the matrix, while elasticity ratio-based models reserve the matrix position for highly elastic materials.

In 1976, the co-continuous composition was related to the viscosity ratio of the blend components by Avgeropoulos et al (Avgeropoulos et al., 1976). Such correlation was later generalized empirically by Paul and Barlow and was put in the form of Equation 11 for determining the phase inversion composition (Paul & Barlow, 1980). Equation 11 was later extended for the viscosities calculated at the shear rate of mixing (Miles & Zurek, 1988).

$$\frac{\varphi_1}{\varphi_2} = \frac{\eta_1}{\eta_2} \quad (11)$$

Where φ_i is the volume fraction of component i at phase inversion, and η_i is the viscosity of component i.

Also, based on Tomotika's theory of capillary instabilities, the ratio of volume fractions at phase inversion was related to the viscosity ratio according to Equations 12 and 13 (Metelkin & Blekht, 1984).

$$\varphi_2 = \frac{1}{1 + F(\lambda)\lambda} \quad (12)$$

$$F(\lambda) = 1 + 2.25\, Log\, \lambda + 1.81\, (Log\, \lambda)^2 \quad (13)$$

Where $\lambda = \frac{\eta_1}{\eta_2}$ and η_i is the viscosity of component i at the shear rate of mixing.

The models above can give fairly precise values for the phase inversion composition when the viscosity ratio (λ) approaches unity. However, by increasing the value of the viscosity ratio, these equations demonstrate a rapid change in the value of φ_2.

There are many other models that could be used for the estimation of the phase inversion composition such as that of Krieger and Dougherty's model for highly viscous systems, semi-empirical model of Willemse et al., model of Steinman et al, and elasticity dependent model of Van Oene and that of Bourry and Favis (Bourry & Favis, 1998; Krieger & Dougherty, 1959; Steinmann et al., 2002; Vanoene, 1972; Willemse et al., 1998). Nevertheless, none of the aforementioned equations can precisely predict the composition of phase inversion or the composition window over which co-continuity exists and consequently experimental methods have to be employed.

2.3.3.3.2 Interfacial tension and interfacial modification

The interfacial tension between the two blend components has a major effect on the morphology. In order to understand the effect of interfacial tension on the morphology of polymer blends, Li et al. investigated three distinct systems with regards to their interfacial tension: I) low interfacial tension system like high density polyethylene (HDPE)/styrene-ethylene-butylene-styrene (SEBS), II) high interfacial tension system like HDPE/PS and finally III) compatibilized (or interfacially modified) system such as that of type II compatibilized with SEBS (Li et al., 2002a).

First, the mechanisms associated to type I, II and III blend systems were reported to be fiber-fiber coalescence, droplet-droplet coalescence and hindered droplet-droplet coalescence, respectively. As illustrated in Figure 2.28a, a low onset and a wide range of co-continuity with invariant domain sizes were observed for type I systems. In the case of the high interfacial tension system, where droplet-droplet coalescence mechanism is governing in the formation of the co-continuous morphology, a higher onset yet a smaller range of phase inversion was evident. Moreover, an increase in the composition led to a higher phase size (Figure 2.28b). Type III system which is a hindered type II system demonstrated an even higher percolation threshold and even a narrower co-continuity region. It must be noted that partial miscibility of the polymer blend components can push the phase inversion to occur at higher compositions of the minor phase. This was investigated by Marin et al. for the case of partially miscible poly(methyl methacrylate) (PMMA)/PC blends (Marin & Favis, 2002).

Interfacial modifiers or compatibilizers are known to reduce the interfacial tension and prevent the coarsening phenomena. Regarding the dispersed droplet/matrix structure, the most noteworthy observation is that the phase size decreases with the increase of the interfacial modifier composition. Willis and Favis studied the polyamide/polyolefin (PA/PO) blends, and the trend of phase size with the addition of an ionomer as the interfacial modifier can be best described as a rapid decrease followed by a plateau (Willis et al., 1991; Willis & Favis, 1988). Also, Matos et al, in a comprehensive study, investigated the interfacial modification of PS/PE-PP rubber (Matos et al., 1995).

The effect of interfacial modification is different for co-continuous morphologies. In this case, interfacial modification reduces the interfacial tension between the blend components which is favorable for the formation and the stability of the co-continuous structure. On the other hand, interfacial modification suppresses the coarsening phenomenon or coalescence. This can hinder the formation of co-continuous morphology. However, once the co-continuous morphology is formed, such reduction in the coarsening actually leads to the stability of the morphology. Adding interfacial modifiers to the system also reduces the phase sizes in the co-continuous system. The reduction of the interfacial tension or the increase of the interfacial adhesion strengthens the interface and as a result a finer morphology is achieved.

The interfacial modifiers or compatibilizers are normally block (diblock, triblock or branched) or grafted copolymers with sections containing each of the immiscible homopolymers of the blend. Therefore, each section of these copolymers has affinity toward one of the phases of the blend. Diblock copolymer was used by Elemans et al. in the introduction of the breaking thread method and it was found that the addition of the diblock copolymer leads to the decrease of the interfacial tension by a factor of 4, and therefore the stabilization of the melt was clearly observed as the break-up lasted for a longer time (Elemans et al., 1990).

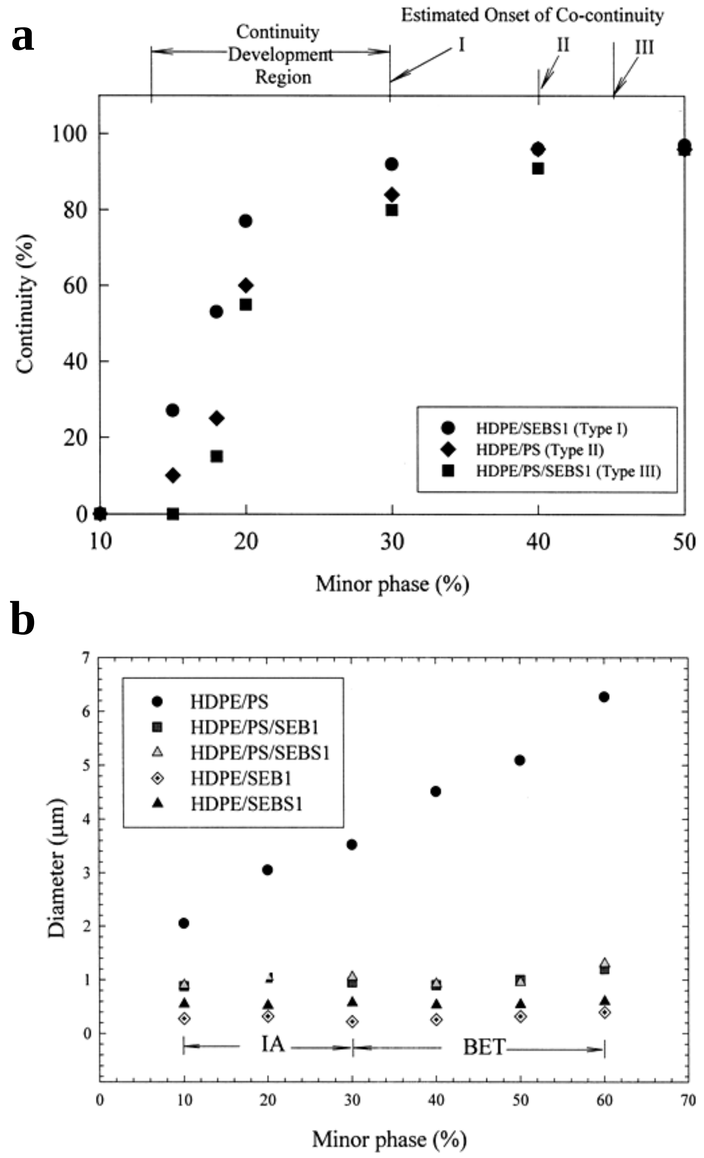

Figure 2.28: Effect of interfacial tension for different blend systems on (a) Continuity development, (b) Pore size as a function of minor phase composition (Li et al., 2002a)

Mekhilef and coworkers investigated the interfacial modification of the PS/PE blends and they also observed a reduction in the dispersed phase size by the addition of the modifier (SEBS, a triblock copolymer). The co-continuous region was also considered in this work, as they also observed the inhibition of coalescence, which was attributed to the steric stabilization of the morphology with the addition of the modifier (Mekhilef et al., 1997). Figure 2.29 demonstrates the impact of the addition of the copolymer on the PE particle size. The reduction in the phase size by the addition of the interfacial modifier to the system was also shown by a work by Li and Favis (Li & Favis, 2002).

The addition of a copolymer could also have potential to transform the co-continuous morphology into the dispersed phase morphology. However, the time needed for such transformation depends on the concentration of the interfacial modifier (Dedecker et al., 1998).

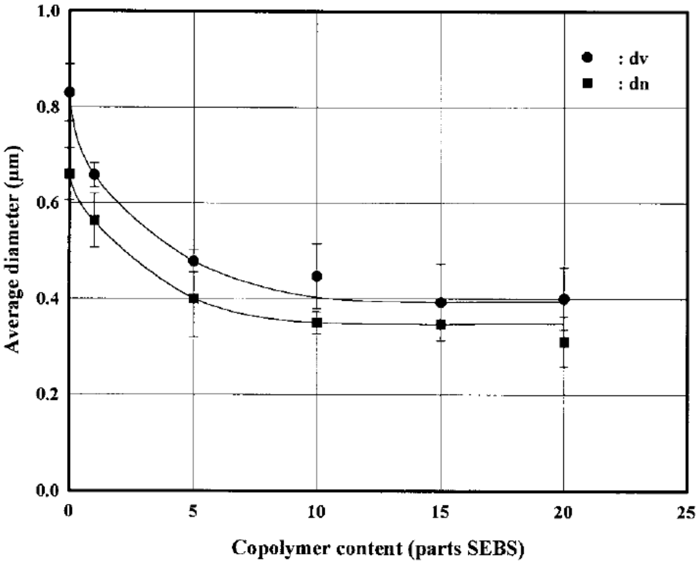

Figure 2.29: The effect of copolymer content on the average size of PE in a PS90/PE10 blend (Mekhilef et al., 1997)

2.3.3.3.3 Annealing

The concept of annealing was first introduced to immiscible polymer blends by Xie et al in 1992. They investigated the morphology of a dispersed droplet/matrix system of poly(propylene) (PP)/ ethylene vinyl acetate copolymer (EVAc), and they noticed an increase in the droplet size with increasing the annealing time (Xie et al., 1992). Like interfacial modification, the annealing process has different effects for dispersed droplets and co-continuous morphologies.

According to Yang et al, the annealing process increases the domain size and broadens the phase size distribution. Moreover, it was shown that annealing at higher temperatures leads to faster phase growth and coalescence (Yang & Han, 1996).

Nevertheless, many studies report a breakup in the co-continuous morphology and its transformation to a dispersed droplet system while static annealing took place, which suggests that the annealing process effectively reduces the composition window over which the morphology is co-continuous (Mekhilef et al., 1997; Willemse et al., 1999). However, Willemse et al. demonstrated that such breakup into the dispersed droplet morphology only occurs when the composition is below a critical limit ($\phi_{cc,stable}$) (Willemse, 1999). Above this critical concentration, the co-continuous morphology becomes stable and the coarsening phenomenon will become effective as the phases can readily grow while maintaining their continuity.

The coarsening rate in the annealing process was investigated by Veenstra et al. and it was shown that the phase growth (dr/dt) is directly proportional to the interfacial tension and inversely proportional to the viscosity (Veenstra et al., 2000). This is shown in Equation 14:

$$\frac{dr}{dt} = c\frac{\gamma}{\eta_e} \quad (14)$$

Where r is the average pore radius, c is a dimensionless coefficient specific to the blend system, γ is the interfacial tension of the blend components and η_e is the effective viscosity which is the weighted average viscosity at zero shear rate of the blend components. This equation proves that the coarsening phenomenon is driven by the interfacial tension but hindered by the viscous nature of the polymers.

By using the principles above, Yuan and Favis studied the effect of static annealing on the co-continuous system of PS/PLLA for the generation of micro-porous structures with pore sizes varying from 1 to hundreds of microns due to the effects of annealing time and temperature (Yuan & Favis, 2004). In another study, they proposed a mechanism for the coarsening phenomenon during the quiescent annealing process by use of a conceptual model of co-continuity based on thin and thick rods. They demonstrated that the driving force for the coarsening phenomenon is the difference between the capillary pressure, which leads to the merging of thin parts (rods) into thick ones (Yuan & Favis, 2005). In this theory, the thick rods cannot break up due to the existence of thin rods that merge into them. By taking thick rods as threads, the Tomotika's breaking thread principles were also applied for estimating the coarsening rate dr/dt (Equation 15).

$$\frac{dr}{dt} = \frac{\alpha_0}{R_0} \times \frac{\gamma\Omega(\lambda, p)}{2\eta_c} \quad (15)$$

Where α_0 is the initial distortion amplitude, R_0 is the initial thread radius, γ is the interfacial tension, $\Omega(\lambda, p)$ is the complex function (distortion function) from the Tomotika equation, and η_c is the zero shear viscosity of the continuous phase. As a result, the easier the domains break, the readier they can grow and coarsen during the static annealing.

It has also been reported that for the co-continuous regions occurring far from the asymmetric compositions, the annealing process might push the system from the co-continuous morphology towards the dispersed droplet/matrix structure. Contrarily, symmetric co-continuous compositions are reported to be more stable and comprising of a wider range of co-continuity. Figures 2.30 and 2.31 demonstrate the effect of annealing time and annealing temperature on the phase growth of the domains (pores).

In this thesis, the polymer blends derived from the two immiscible biomaterials of interest PCL and PEO previously discussed in section 2.2.4 will be investigated. The blends of PCL and PEO are going to be prepared at the cocontinuous composition, and consequently annealed for achieving the desired pore size. Since PEO is a water soluble polymer, it can be used as the porogen phase and be selectively extracted from the blend system after annealing. This will provide the PCL scaffolds with precisely controlled morphology and highly interconnected porous structure.

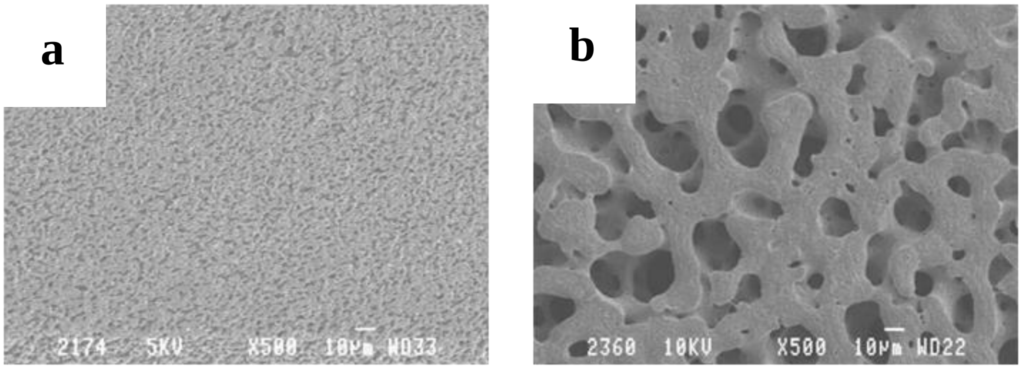

Figure 2.30: Effect of annealing time on the pore size in a blend of PLLA/PCL at 50/50 % (a) no annealing, and (b) 2h annealing (adapted from (Sarazin et al., 2004))

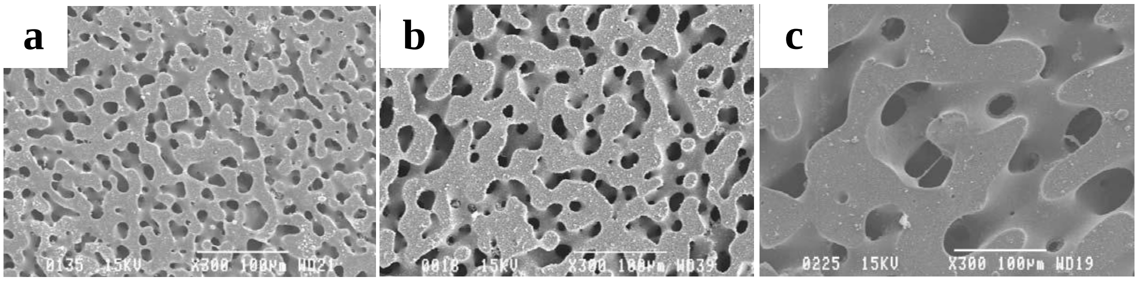

Figure 2.31: Effect of annealing temperature for on the pore size in a blend of PLLA/PS (a) 190°C, (b) 200°C, and (c) 220°C (adapted from (Yuan & Favis, 2004)). All the blends have been annealed for t = 1h.

2.4 Surface modification of polymers

Since porous PCL scaffolds derived from the melt blending approach are going to be used in *in vitro* osteogenic assays (Chapter 6 in this dissertation), the hydrophobic nature of PCL (as discussed in section 2.2.4.1) can negatively interfere with the cell adhesion and hence other cellular functions. Therefore, it will be established that the surface modification of PCL with a hydrophilic material becomes inevitable for culturing fibroblasts and BMSCs. The hydrophilic material which is going to be used for the surface modification of PCL is chitosan whose properties are elaborated in section 2.2.4.3. Therefore, this section is dedicated to the methods used for the surface modification of polymers and specifically PCL.

There are many structural materials that possess favorable physical and chemical characteristics which make them attractive candidates for clinical biomedical applications. However, in many cases, the clinical use of these materials becomes highly limited due to unfavorable parameters such as undesirable (non-specific) adsorption as well as conformational changes of proteins on the surface of these biomaterials (Groth et al., 1994). Surface modification of polymers is a booming approach that can provide the exact required characteristics according to specific tissue engineering applications. Since the biomaterials are in intimate contact with the cells and the biological environment, the appropriate surface chemistry (such as hydrophilicity) is believed to be only required in a scale of a few nanometers to a micrometer underneath the external surface (Groth et al., 2010).

There have been lots of efforts in the past to bring hydrophilicity to the surface of polymers. Plasma treatment is considered as a convenient measure for this purpose. In this technique, polarized functional groups such as hydroxyl, carboxyl, amino and sulfate groups can be introduced to the surface of polymer surfaces in general by using various reactive gases such as oxygen (Ma et al., 2007). Another common method used for surface modification is to graft hydrophilic polymers through copolymerization on the polymer substrate of interest. For this method, like any other polymerization reaction the existence of initiators is crucial. The initiators (such as radicals) should be incorporated to the substrate by other methods such as plasma treatment (as a separate step), ozone oxidation, γ-ray, electron beam and laser treatment (Abbasi et al., 2002; Poncin-Epaillard et al., 1994; Shim et al., 2001; Steffens et al., 2002).

2.4.1 Methods for the surface modification of polymers

There are generally two categories for surface treatments of polymers: physical methods and chemical methods. As their name implies, physical approaches involve the formation of physical bonds such as electrostatic, van der Waals, hydrogen bonding, and hydrophobic interactions, and they include surface self-assembly (Croll et al., 2006), coating (Vonarbourg et al., 2006) and vapor deposition (Klee et al., 2003). Chemical approaches mainly involve the addition of functional groups to the surface of the polymer through covalent bonds such as surface grafting or surface etching methods (Guo et al., 2008). Chemical surface modification techniques include plasma treatment, UV-induced or ozone grafting polymerization, and aminolysis (Groth et al., 2010). These methods have been put to use in order to incorporate hydrophilic components specifically on the surface of our polymer of interest PCL (Darain et al., 2010; Domingos et al., 2013; Siri et al., 2010; Zhu et al., 2002a; Zhu et al., 2002b). The hydrophilic groups that are used for surface modification of PCL are mostly extracellular matrix components such as collagen or small peptide sequence molecules containing RGD (Arg-Gly-Asp).

There has always been competition between the physical and chemical approaches for modifying polymeric surfaces. While physical approaches provide simplicity and cost-efficiency, low stability of the modified surface due to the physical nature of the bonds has constantly been an issue. Chemical surface modification techniques, on the other hand, can use various functional compounds to alter the surface, but complications exist due to the intrinsic limitation of the number of functional groups per surface area (Zajac & Chakrabarti, 1995). Given that the polymer surface in chemical surface modifications is a reaction site, other limitations do exist, such as lack of initiators and their improper surface concentrations, steric hindrance leading to non-uniform grafting, and finally side reactions which lead to nonspecific surface bonds (Edmondson et al., 2004; Fukuda et al., 2000).

In this thesis, a physical approach of Layer-by-Layer (LbL) deposition of electrolytes has been used to homogeneously modify the surface of PCL, and therefore will be discussed in further detail in the next section.

2.4.2 Layer-by-Layer deposition of polyelectrolytes

Originally introduced by Decher et al. in 1992, Layer-by-Layer (LbL) deposition of polymers (polyelectrolytes) is an exceptionally simple and cost-effective technique which has become a powerful tool for the production of molecularly controlled ultrathin multilayer films. This method involves the sequential adsorption of oppositely charged polyelectrolytes on a charged planar substrate (Decher et al., 1992). The charged species inside the solution can be kinetically trapped on the substrate and generate a film assembly whose thickness can be precisely controlled from a few angstroms to a couple of microns (Decher, 1997). Adsorption of each polyelectrolyte on the substrate inverses the surface charge promoting the addition of the next layer. Electrostatic interactions between the polyelectrolyte pairs (polycations and polyanions) are the most studied driving forces for making film assemblies on substrates. LbL approach has been vastly used to produce thin films as corrosion protectors, antibacterial layers, sensors and antistatic coatings (Decher et al., 1992; Farhat & Schlenoff, 2002; Graul & Schlenoff, 1999; Rudra et al., 2006).

The key players in the LbL technique are the polyelectrolytes. These materials have both characteristics of polymers and electrolytes, i.e. they produce viscous charged solutions while in aqueous media. The LbL technique involves subsequent submersion of the substrate into an oppositely charged polyelectrolyte solution, followed by a rinsing step to remove the unbound material, until the desired thickness or charge is obtained. The thickness of each deposited layer is dependent upon the polyelectrolyte chain geometry (Decher, 1997). The schematic of the LbL technique is illustrated in Figure 2.32.

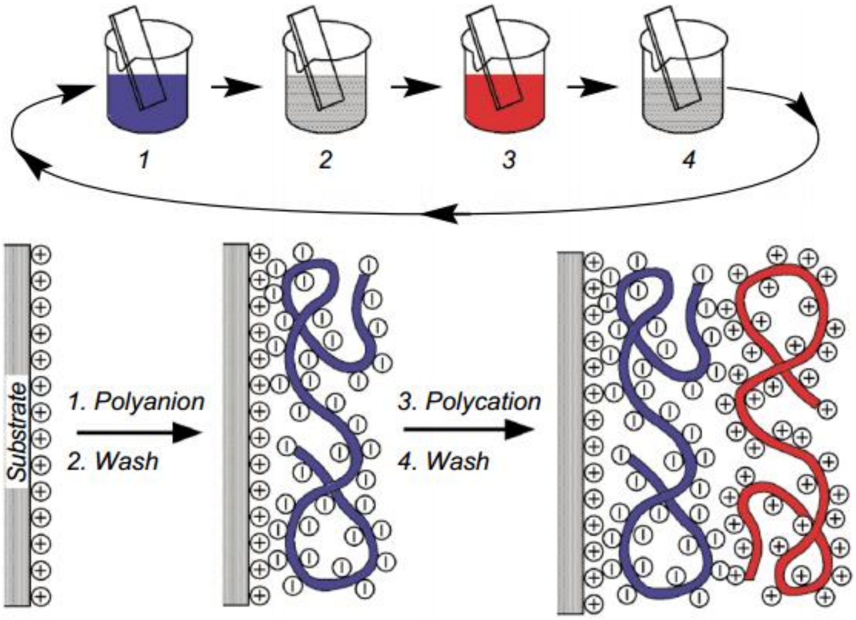

Figure 2.32: Schematic of the Layer-by-Layer (LbL) deposition technique. The substrate is positively charged in this case (adapted from (Decher, 1997))

The characterization of the multilayer assemblies could be done by several techniques such as gravimetric analysis, UV-VIS adsorption, quartz crystal microbalance (QCM), and ellipsometry (Adusumilli & Bruening, 2009; Ravati & Favis, 2011; Richert et al., 2003). The reproducibility of the adsorption process from layer to layer was demonstrated by Ferreira et al. by using UV-Vis adsorption measurements (Ferreira & Rubner, 1995). The permeability and stability of polyelectrolyte multilayer films along with the effect of pH on the layer thickness were investigated using in-situ ellipsometry by Harris and Bruening (Harris & Bruening, 1999).

2.4.2.1 Mechanism of LbL deposition of polyelectrolytes

The main driving force for the formation of polyelectrolyte multilayer films on a substrate is known to be charge overcompensation, i.e. the adsorption of the subsequent polyelectrolyte layers reverses the charge on the substrate by over-compensating the charge so that the next polyelectrolyte layer can be adsorbed on the surface (Schlenoff & Dubas, 2001; Schlenoff et al., 1998). The formation of the precursor layer is very important since the polyelectrolyte can be added via electrostatic or hydrophilic forces and therefore can or cannot be strong enough to support the multilayer assembly of the next attaching polyelectrolyte layers.

The thickness of the formed multilayer assembly usually increases linearly with the number of adsorbed polyelectrolyte layer (Caruso et al., 1997; Ramsden et al., 1995; Ruths et al., 2000). However, in cases where a high level of polyelectrolyte interdiffusion into the entire assembly occurs, an exponential growth of layer thickness has been recorded (Hübsch et al., 2004).

2.4.2.2 Determining parameters in LbL deposition of polyelectrolytes

The formation of a desired assembly of layers on a substrate depends on several parameters such as the nature of the polyelectrolytes, polyelectrolyte concentration and molecular weight, pH of the polyelectrolyte solutions, presence or absence of salt and adsorption time. In this section, some of these determining parameters and their effects are discussed.

2.4.2.2.1 Effect of salt concentration

Salt can act as a supporting electrolyte in an LbL system. In the absence of salt, the polyelectrolytes extend their chains on the substrate in such a way that the distance between the charges on their backbone is maximized. As a result, the established layer on the substrate becomes ultrathin and the charge overcompensation becomes minimal (Schwarz & Schönhoff, 2002). As an example, the thickness of 20 layers of poly(sodium 4-styrenesulfonate) (PSS) / poly(diallyl dimethyl ammonium chloride) (PDADMAC) film in the absence of salt is about 60 Å, which establishes an average thickness per layer of only 3 Å (Dubas & Schlenoff, 1999). The addition of salt to the LbL system, on the other hand, leads to a thousand times this value. In this case, salt particles locate themselves between the polyelectrolyte repeating units and therefore stabilizing the coil-structure, and inhibit rod-like adsorptions on the substrate (Lvov et al., 1993; Schwarz & Schönhoff, 2002). Figure 2.33 demonstrates the effect of salt on the adsorption behavior of the polyelectrolytes.

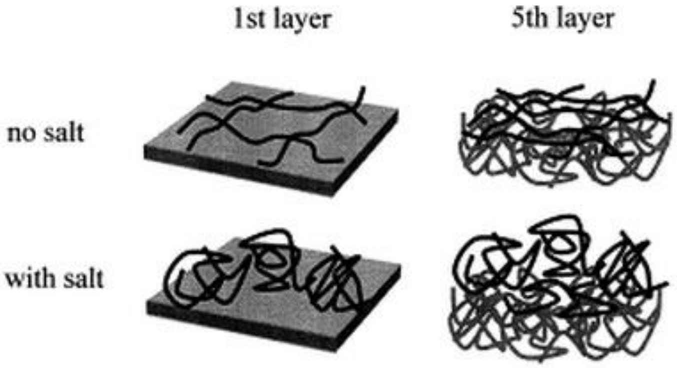

Figure 2.33: Effect of the addition of salt on the adsorption behavior of polyelectrolytes (Schwarz & Schönhoff, 2002)

Many studies have shown the effect of salt concentration on the thickness of the polyelectrolyte multilayer assembly (Dubas & Schlenoff, 1999; Guzman et al., 2009). Dubas et al, in a comprehensive study, demonstrated that there is a linear increase in the layer thickness with the salt concentration (Dubas & Schlenoff, 1999). Figure 2.34 demonstrates the evolution of the thickness of 10-bilayers of PSS/PDADMAC with an increase in the salt concentration. Apart from salt concentration, many studies also investigated the effect of salt type (El Haitami et al., 2009; Salomäki et al., 2004), which are not going to be discussed here.

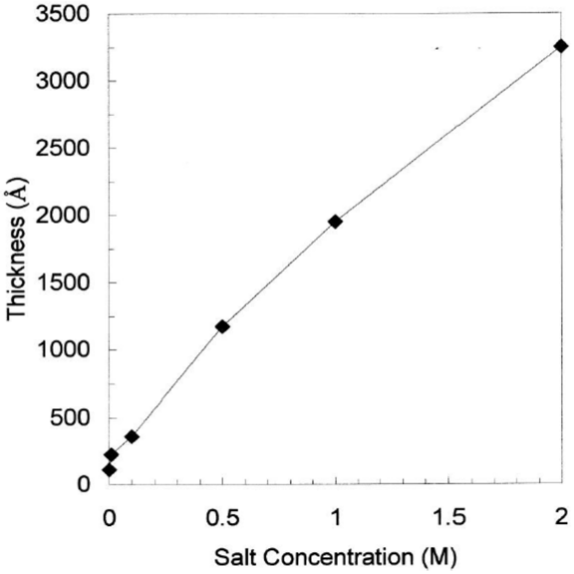

Figure 2.34: Thicknesses of LbL $(PSS/PDADMAC)_{10}$ films deposited on silicon wafers using a series of NaCl concentrations (Dubas & Schlenoff, 1999)

2.4.2.2.2 Effect of polyelectrolyte type

The polyelectrolyte type is of crucial significance in the quality of multilayer films formed on a substrate. Strong polyelectrolyte pairs such as PSS/ poly(allylamine) hydrochloride (PAH) form distinct layer assemblies whose thickness varies linearly with the number of depositions (Caruso et al., 1997). On the other hand, PGA/poly(L-lysine) (PLL), PGA/PAH, and HA/chitosan form assemblies with thicknesses exponentially growing with the addition of layers (Boulmedais et al., 2002; Kujawa et al., 2005; Lavalle et al., 2003). For a PDADMAC/PSS LbL system also used in this thesis, a linear variation of assembly thickness with the number of added bilayers was observed after the addition of 3 bilayers (McAloney et al., 2001), as illustrated in Figure 2.35.

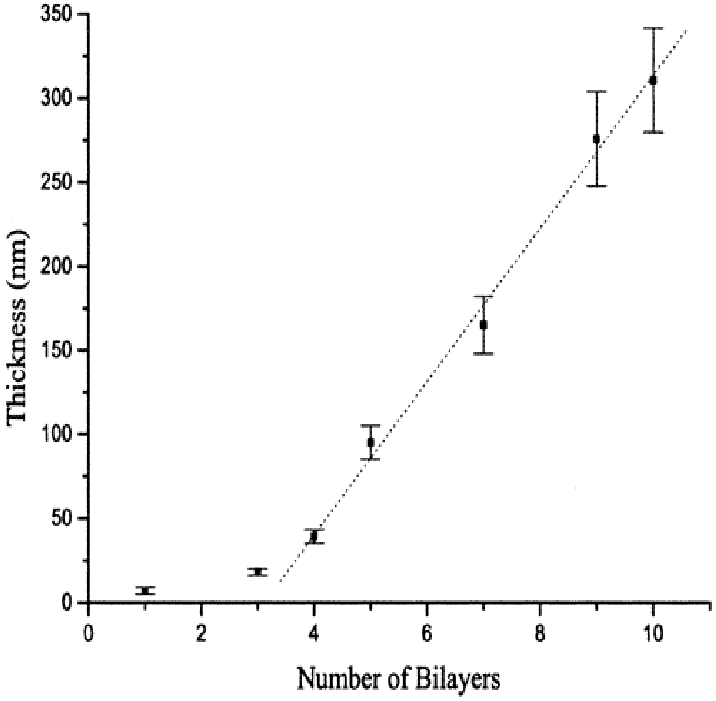

Figure 2.35: Thickness of a (PDADMAC/PSS)$_n$ multilayer film deposited from a 1.0 M NaCl salt solution versus the number of bilayers (McAloney et al., 2001)

The effect of molecular weight on the thickness is not very straightforward. While some reports showed that the thickness of the assembly is independent of the molecular weight (Lösche et al., 1998; Porcel et al., 2004), others have discussed variable trends of thickness with a change in the molecular weight (Porcel et al., 2007; Richert et al., 2003).

2.4.2.2.3 Effect of polyelectrolyte concentration

One of the main parameters that can affect the deposition of polyelectrolyte multilayer films is the concentration of the polymers in the solution. Many scientific groups reported that there is an increase in the amount of adsorbed polyelectrolyte with increasing the polyelectrolyte concentration (Dubas & Schlenoff, 1999; Wang et al., 1999). Figure 2.36 demonstrates that there is approximately 150 Å of increase in the thickness of 5 bilayers of PSS/PDADMAC on silicon wafers with an increase of polyelectrolyte concentration from 2mM up to 50mM (Dubas & Schlenoff, 1999). It should be noted however that the effect of polymer concentration is not as significant as that of the addition of salt (See Figure 2.34)

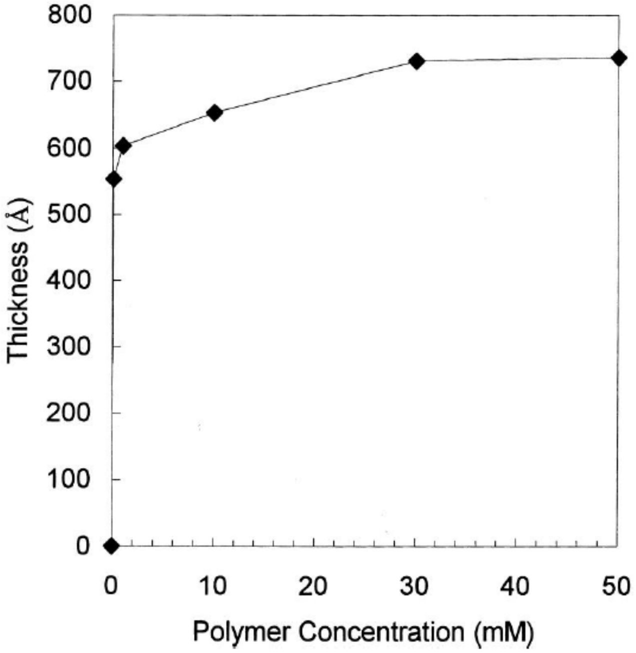

Figure 2.36: Thickness of (PSS/PDADMAC)$_5$ films as a function of polyelectrolyte concentration (NaCl salt concentration of 1M) (Dubas & Schlenoff, 1999)

The reason for such increasing trend of thickness with concentration is explained as follows: at high polyelectrolyte concentrations, many polymer chains can adhere to few available binding sites on the surface leading to thick films, whereas, at low concentrations, few polymer chains find many available binding sites and therefore can form thin films by rod-like depositions (Fleer, 1993).

2.4.2.2.4 Effect of deposition pH (degree of ionization of polyelectrolytes)

The thickness, permeability and morphology of multilayer thin films also depend on the degree of ionization of the polyelectrolytes used in the LbL process, which depends on the pH of the deposition solution. Strong polyelectrolytes such as PAH/PSS and PDADMAC/PSS pairs are fully ionized for a wide ranges of pH. However, in the case of weak polyelectrolytes, the charge density on the polymer backbone is highly dependent upon the ionization of groups such as amines and carboxylic acids which vary considerably with the pH (Aulin et al., 2008; Lulevich & Vinogradova, 2004).

In a system of PAH/ poly(acrylic acid) (PAA), when the pH of both electrolytes changed from 2.5 to 4.5, the thickness of an assembly of 30 bilayers changed from 120 to 210 nm, which is due to the fact that the fraction of ionic carboxylates also increases from 30 to 70% (Yoo et al., 1998). The same system was again studied at a wide range of pH and it was determined that each PAH and PAA layer can vary in thickness from 5 up to 80 Å depending on the pH (Shiratori & Rubner, 2000).

2.4.2.2.5 Effect of deposition time

Several studies in the literature have investigated the effect of deposition time on the thickness of multilayer films (Angelatos et al., 2008; Dubas & Schlenoff, 1999; M. Lvov et al., 1998). The differences in the molecular weights, chemical structures and deposition pH of each polyelectrolyte in a pair, necessitate short or high times of deposition. One main reason for longer deposition times is the limitations that exist in the mass transport of the polyelectrolyte from the solution to the surface of the polymer. These limitations could be overcome by using efficient methods like spin-coating, and hence the rate of layer formation could be enhanced (Cho et al., 2001; Dubas & Schlenoff, 1999). It is known that most of the deposition (95%) occurs in the first minute of exposure to the polyelectrolyte deposition (Garg et al., 2008). However, longer times are needed for polyelectrolyte rearrangements and complete depositions on the surface of the substrate (Garg et al., 2008). It is evident that performing the LbL process on a 3D substrate (like in the case of our study) rather than 2D also could require longer periods of deposition due to penetration limitations inside a 3D sample.

Surface modification of PCL by the LbL technique has seen little attention in the literature. Moreover, none of the works done in this field aimed to modify the surface of a virtually three-dimensional PCL construct, i.e. a substrate whose third dimension is in the same order of magnitude of the other two, such as cubic or large irregular structures. A qualitative study has investigated the LbL surface deposition on PCL nanofiber films (Dubas et al., 2009). Also, due to the fact that the PCL film is only weakly charged at the surface, this study lacks solid proof of the efficiency of the depositions. In another work, PCL films were coated by the LbL technique using chitosan and heparin as polyelectrolytes (Lv et al., 2008). However, due to the fact that both heparin and chitosan are weak polyelectrolytes, the uniformity of the layers formed is still an issue.

CHAPTER 3 ORGANIZATION OF THE ARTICLES

This section is dedicated to the scientific contribution of this thesis in the form of three original journal articles.

The first part of the study involves the fabrication and characterization of the PCL scaffolds. The article is entitled "Poly(ε-caprolactone) Scaffolds of Highly Controlled Porosity and Interconnectivity Derived from Co-Continuous Polymer Blends: Model Bead and Cell Infiltration Behavior". In this paper, the melt blending of the immiscible polymers PCL and PEO followed by controlled static annealing and selective extraction is used for the generation of porous 3D PCL constructs with 100% pore interconnectivity with pore sizes ranging from 41-212 μm. Although scaffold infiltration by cells is of ultimate importance in the quality of the final tissue formed *in vitro* and *in vivo*, this parameter has seen very little attention specifically for *in vitro* studies. In this paper, a novel assay is presented to compare scaffold infiltration by trypsinized hBMSCs and that of model polystyrene beads of the same size. Through this assay, a threshold for the pore size will be determined beyond which the cells behave more like the beads as they homogeneously populate the scaffold. Finally, the cytotoxicity of the PCL scaffolds is going to be studied. The results obtained from the cytotoxicity assay guides this thesis toward modifying the PCL surface. This paper has been published in the "Journal of Materials Science: Materials in Medicine" (Ghavidel Mehr et al., 2014b).

The second article entitled "Chitosan Surface Modification of Fully Interconnected 3D Porous Poly(ε-caprolactone) by the LbL Approach" investigates the surface wettability modification of the intrinsically hydrophobic PCL by hydrophilic chitosan according. By comparing the common dip-coating strategy and the controlled LbL self-assembly of polyelectrolytes via surface characterization techniques, this original paper presents a thorough investigation of chitosan coating on porous PCL constructs via the LbL technique for the first time. The minimum number of required polyelectrolyte layers is determined by surface elemental analysis by X-ray photoelectron spectroscopy, in order to obtain well defined polyelectrolyte layers and a more uniform chitosan deposition. Furthermore, the deposition of chitosan is going to be examined on and in the depth of a 3D cubic construct whose three spatial dimensions are of considerable and comparable values. Finally, the morphology, surface roughness and thickness of the multilayer assembly will be determined. This work will establish the foundation for our third and last paper in which the effect of such homogeneous chitosan coating in a 3D structure will be studied and the contribution of our PCL constructs to scaffold-assisted bone tissue engineering will be discussed. This article has been submitted to the journal of “ACS Applied Materials & Interfaces” (Ghavidel Mehr et al., 2014a).

Having generated the PCL scaffolds with appropriate characteristics for bone tissue engineering and brought hydrophilicity to the PCL surface with chitosan, we can finally test our hypothesis that *in vitro* osteogenesis by hBMSCs is achieved in our 3D PCL scaffolds and enhanced when pore surfaces are coated with chitosan via the LbL techniques. Therefore, two principal parameters are going to be thoroughly discussed in this last paper: 1) The effect of pore size (84 μm and 141 μm); and 2) The effect of chitosan surface modification. However, the novel beads assay in the first paper of this thesis showed that the pore size can highly affect the infiltration behavior of hBMSCs. Therefore, in order to faithfully examine the effect of pore size and that of chitosan coating, the cell seeding protocol should reflect the maximum possible homogeneity of cell distribution at various depths inside the scaffold. Thus, the optimal seeding protocol with the most uniform cell distribution is going to be suggested and applied to the three-week hBMSC osteogenic assay in the scaffolds. The main parameters to be investigated in this work are the following: cell morphology and surface attachments, cell-biomaterial interactions in the presence or absence of the chitosan coating, ECM formation and finally mineral deposition in the outer and inner pores. This original paper entitled “Osteogenic mesenchymal stem cells populate 3D poly(ε-caprolactone) scaffolds with interconnected pores and preferentially mineralize LbL chitosan-coated surfaces” has been submitted to the journal of “Tissue Engineering Part A” (Ghavidel Mehr et al., 2014c).

CHAPTER 4 ARTICLE 1: POLY(E-CAPROLACTONE) SCAFFOLDS OF HIGHLY CONTROLLED POROSITY AND INTERCONNECTIVITY DERIVED FROM CO-CONTINUOUS POLYMER BLENDS: MODEL BEAD AND CELL INFILTRATION BEHAVIOR

The objective of this study is to fabricate and fully characterize bone tissue engineering scaffolds made of PCL. The requirements that are going to be assessed in this chapter are pore interconnectivity, pore size, cytocompatibility (i.e. surface chemistry) and infiltration properties. In this section, we seek to generate a range of highly controlled, fully interconnected, porous PCL constructs based on the melt blending of co-continuous immiscible polymers. Many scientific groups have investigated various *in vitro* tissue engineering studies. Yet, we believe that little attention has been given to an efficient seeding protocol that can lead to a homogeneous cell distribution within 3D scaffolds. These lacking studies become crucial due to the scarcity and high cost of bone-derived mesenchymal stem cells (BMSCs). Therefore, in this chapter, we present a novel *in vitro* approach using non-interacting model bead infiltration to mimic BMSCs which allows evaluating the potential of the interconnected pathways in the scaffolds to retain cells. We will later investigate how the cells are distributed inside the scaffolds as a function of their pore size, and we compare this distribution with that of the model beads. The topic of cell infiltration and efficient seeding protocol will be further studied in Chapter 6.

This article has been published in the "*Journal of Materials Science: Materials in Medicine"*.

Poly(ε-caprolactone) Scaffolds of Highly Controlled Porosity and Interconnectivity Derived from Co-Continuous Polymer Blends: Model Bead and Cell Infiltration Behavior

Nima Ghavidel Mehr[a,b], Xian Li[a,c], Marianne B. Ariganello[a], Caroline D. Hoemann[a,c] and Basil D. Favis [a,b,1]

[a] Department of Chemical Engineering, École Polytechnique, Montreal, QC, H3C 3A7 Canada

[b] Centre de Recherche sur les Systèmes Polymères et Composites à Haute Performance (CREPEC), École Polytechnique, Montréal, QC, H3C 3A7 Canada

[c] Institute of Biomedical Engineering, and Groupe de Recherches Sciences et Technologies (GRSTB), École Polytechnique, Montréal, QC, H3C 3A7 Canada

Contribution of co-authors:

Xian Li: Assistance in the verification of the beads experiments with hBMSCs

Marianne B. Ariganello: Assistance in the beads experiments and cytotoxicity assays

Caroline D. Hoemann: Co-director of this research study

Basil D. Favis: Director of this research study

---

[1] Corresponding author. Tel.: + 1 514 340 4711x4527; fax: + 1 514 340 4159.

E-mail address: basil.favis@polymtl.ca (B.D. Favis).

Abstract

Porous structures destined for tissue engineering applications should ideally show controlled and narrow pore size distributions with fully interconnected pores. This study focuses on the development of novel poly(ε-caprolactone) (PCL) structures with fully connected pores of 84, 116, 141, and 162 micron average diameter, from melt blending of PCL with poly(ethylene oxide) (PEO) at the co-continuous composition, followed by static annealing and selective extraction of PEO. Our results demonstrate a low onset concentration for PEO continuity and a broad region of phase inversion. A novel *in vitro* assay was used to compare scaffold infiltration by 10-micron diameter polystyrene beads intended to mimic trypsinized human bone marrow stromal cells (hBMSCs). Beads showed a linear increase in the extent of scaffold infiltration with increasing pore size, whereas BMSCs infiltrated 162 and 141 micron pores, below which the cells aggregated and adhered near the seeding area with low infiltration into the porous device. While providing a baseline for non-aggregated systems, the beads closely mimic trypsinized cells at pore sizes equal to or larger than 141 microns, where optimal retention and distribution of hBMSCs are detected. A cytotoxicity assay using L929 cells showed that these scaffolds were cytocompatible and no cell necrosis was detected. This study shows that a melt blending approach produces porous PCL scaffolds of highly controlled pore size, narrow size distribution and complete interconnectivity, while the bead model system reveals the baseline potential for a homogeneous, non-aggregated distribution of hBMSCs at all penetration depths.

Keywords: scaffold, co-continuous morphology, pore size, interconnectivity, cell infiltration, model bead

4.1 Introduction

A variety of synthetic or natural polymers have been proposed for the preparation of three-dimensional porous scaffolds for tissue engineering [1]. Among them, poly(ε-caprolactone) (PCL) has been widely used as the material of choice in tissue engineering and drug delivery owing to its favorable mechanical and biodegradable properties. Mechanical stability of PCL scaffolds facilitates to withstand early functional loads as crucial criteria suggested by Hutmacher [2]; PCL degrades at a slow rate with results showing that it can persist *in vivo* for up to two years [3]. Even if the mechanical properties of PCL are similar to trabecular bone, these properties can be easily enhanced and tailored by incorporating micro and nanoparticles into the PCL matrix [4, 5]. PCL scaffolds have been characterized by their biocompatibility, low immunogenicity, processability and long degradation time and considered as a promising candidate for various tissue engineering applications including bone regeneration [6-11].

The success of tissue engineering scaffolds highly depends on their infiltration capacity which is greatly affected by cell/pore size and pore size distribution [12]. A small pore size resulting from a dense network hinders cell infiltration and ultimately reduces their use in replacing large tissues that require ample vascularization and nutrient diffusion [13]. A large pore size might promote angiogenic ingrowth into the scaffold, however, cell seeding of scaffolds with large pore sizes run the risk of poor cell retention during *in vitro* cell seeding, and biomechanical failure due to excess void volume [14].

Melt blending of immiscible polymers at co-continuous compositions followed by static annealing and selective extraction, among various methods for fabricating porous scaffolds, could be a robust approach specifically for the production of porous constructs for tissue engineering purposes. The region of co-continuity, a notion used in the fabrication method in this study, is defined as the zone in which neither dispersed nor matrix phase in a binary blend can be distinguished. The morphology in immiscible binary blends depends on the interfacial properties and the composition of the components. Co-continuous polymer blend structures have been examined in the past and show the potential for the production of highly controlled structures [15-17], however, very few works have investigated porous structures of highly controlled morphology derived from co-continuous blends for tissue engineering applications. This approach allows the production of a variety of structures with controlled pore diameters with narrow pore size distribution and full interconnectivity. By using static annealing after melt blending as the principle approach, significant control over the phase dimensions in co-continuous morphologies can be exercised [16]. By using this method, many disadvantages of other fabrication techniques could be overcome, such as the use of toxic solvents, limitations imposed by the shape of the porogen phase, low levels of pore interconnectivity, high processing temperatures, large pore size distributions and high processing costs [18]. Rapid prototyping, as an example, has the advantage of structuring the pore geometry in terms of pore orientation and can control the pore size through the choice of strand diameter, but is limited in its ability to prepare small pore sizes [19, 20]. The melt blending approach together with the static annealing can be used to control pore sizes from less than 1 micron to hundreds of microns. Previous studies applied to polyethylene and polylactic acid based blends have shown that this can be done in a highly controlled and quantitative fashion [21, 22].

In this study, static annealing is applied to PCL/PEO blends leading to precisely controlled PCL phase/pore sizes. In addition, poly(ethylene oxide) (PEO) is used as a porogen in the blend, mainly due to its biocompatibility, high water solubility and its extensive use in many medical applications such as drug delivery systems using liposomes, nano- and micro-particle carriers [23-25]. A previous qualitative study has shown that PCL/PEO blends provided an uncontrolled porous morphology with anisotropic microstructure at the surface and in the core of the sample [26]. Moreover in this prior study, quantitative estimations of pore size, size distribution and pore interconnectivity were lacking.

The objective of this study is to prepare a range of highly controlled and quantitatively characterized isotropic, fully interconnected, porous PCL microstructures based on the melt blending of co-continuous immiscible polymers. The pore interconnectivity, the level of control over the pore size and pore size distribution will be evaluated in order to verify the applicability of such constructs as potential bone tissue engineering scaffolds. An *in vitro* approach using model bead infiltration to mimic bone-derived stromal cells will be developed to evaluate the capacity of the controlled interconnected pathways in the fabricated scaffolds to retain cells. Cell distribution within the scaffolds will also be examined and compared to that of the beads. The scaffolds will be further characterized for cytotoxicity and cell viability.

4.2 Materials and methods

4.2.1 Materials

The commercial-grade poly(ε-caprolactone) (PCL, CAPA 6800) was supplied by Solvay (Brussels, Belgium). Poly(ethylene) oxide (PEO) water-soluble polymers (POLYOX™ WSR-N10) was purchased from Dow (Midland, MI, USA). See Table 4.1 for further characteristics.

Table 4-1: Characteristics of the polymer materials used to create the porous scaffold

Materials	**Molecular Weight (M_w)**	**Density at 100°C (g/cm^3)**	**Zero Shear Viscosity (Pa.s)**	**Supplier**
PCL (Capa 6800)	80,000	0.961	7,261	Solvay
PEO (WSR-N10)	100,000	1.000	31,508	Dow Chemicals

4.2.2 Blend preparation

Blends of PCL and PEO were prepared at 45PCL/55PEO vol% in a Brabender internal mixer under a constant flow of dry nitrogen for the prevention of thermo-oxidative degradation of components. Mixing was done at 100°C for 7 min with the rotation speed of 50 rpm. The blends were quenched in liquid nitrogen right after mixing in order to freeze-in the morphology. The amount of material in every batch of mixing was maintained at 80% of the total capacity. All the concentrations are reported as volume percent and were estimated experimentally according to their melt densities at 100°C as tabulated in Table 4.1. Melt densities at 100°C were measured using a SWO pvT-100 apparatus.

4.2.3 Rheology

Discs of PCL Capa 6800 and PEO WSR-N10 were produced by a compression molding press at 100°C. The rheological characterization was performed using a Rheometric Scientific SR5000 stress-control rheometer under the flow of nitrogen and a parallel plate geometry with a 1 mm gap was selected. Time sweep tests were used to determine polymer stability while stress sweep tests were performed to determine the region of linear viscoelasticity. The zero shear viscosities of the polymers in Table 4.1 were estimated by the time weighted relaxation spectrum approach and were verified by the Carreau-Yasuda model [27].

4.2.4 Annealing and sample preparation

Static annealing of the PCL/PEO blends was performed in a compression molding press. Small pieces of the blend were cut, sandwiched in aluminum foil and subsequently transferred into the cavity of a frame. The blends and the frame were then put between the two metal plates of the press, so that the above press just touched the top of the samples while annealing took place. This arrangement imposed no external pressure on the samples and hence deformation and flow of the polymer blend were minimized. The annealing process was performed under constant flow of nitrogen in order to reduce the risk of thermo-oxidative degradation of the blend components. The annealing temperature was selected to be 160°C which is 30°C lower than the degradation temperature of PEO as measured by a thermogravimetric analysis apparatus (TGA Q-500 V6.7). After annealing, the samples were quenched in liquid nitrogen to freeze-in the morphology. The annealing times 0.5, 1, 1.5, 2, 2.5 and 3h were selected in order to ultimately generate a range of pore sizes suitable for tissue engineering applications. After annealing, samples were shaped into discs of 3 mm in diameter and 1.5-2 mm in thickness, by using a mechanical punch and a fresh razor blade.

4.2.5 Pore continuity/interconnectivity

Selective extraction of PEO in the blends was performed in deionized water at ambient temperature in 50 mL Fisherbrand tubes for 7 days. In order to calculate continuity, some scaffolds were subjected to two months of extraction to reach constant weight. Gravimetric measurements were used for the calculation of continuity of PEO as the porogen phase according to Equation 16. This approach allows for the quantitative estimation of pore interconnectivity.

$$\%Continuity = \frac{(Weight\ \mathrm{PEO_{init}} - \mathrm{Weight\ \ PEO_{final}})}{Weight\ \mathrm{PEO_{init}}} \qquad (16)$$

4.2.6 Scanning electron microscopy

For the purpose of visualization by scanning electron microscopy (SEM), annealed samples were cut into small pyramids and microtomed at -160˚C under liquid nitrogen using a glass knife, perpendicular to the machine direction. The instrument used for microtomy was a Leica-Jung RM 2165 equipped with a Leica LN 21 type cryochamber. After annealing for different durations, the microtomed samples were then subjected to extraction to remove the PEO porogen phase and yield porous structures. After drying for 24h the samples were coated with a gold-palladium alloy and observed by a Jeol JSM 840 scanning electron microscope operating at a voltage range of 5-10 kV.

4.2.7 Mercury intrusion porosimetry/sample designation

Volume average pore diameter and pore size distribution of the extracted samples were measured by an Autopore IV 9500 V1.06 mercury intrusion porosimeter. Mercury porosimetry is based on the capillary law governing the penetration of mercury as a non-wetting liquid into the small pores. Mercury porosimetry uses the Washburn equation (Equation 17) to describe the relation between the intrusion of mercury into the porous structure and the pressure applied to the mercury [28]:

$$P\,\mathrm{r} = -\,2\sigma\,\mathrm{Cos}\theta \qquad (17)$$

Where P is the applied pressure, r is the radius of the pores, σ is the surface tension and θ is the contact angle. For these experiments, a contact angle of 140° and surface tension of 0.48 N/m for mercury were considered.

Each blend was subsequently classified by its pore size and a number: 40 micron-Sample 1, 84 micron-Sample 2, 116 micron-Sample 3, 141 micron-Sample 4, 162 micron-Sample 5, and 212 micron-Sample 6. The non-annealed blend was designated as 0.87 micron-Sample 0.

4.2.8 Cell culture

Human bone marrow stromal cells (hBMSCs), obtained by bone marrow aspirates from healthy consented donors under institutional-approved protocols, were purchased from Texas A&M Institute for Regenerative Medicine (Temple, TX, USA). hBMSCs were cultured and expanded in complete culture media (CCM), which consisted of alpha minimum essential medium (αMEM, Sigma-Aldrich, Oakville, ON, Canada), 16% fetal bovine serum (FBS, Atlanta Biologicals, Atlanta, GA, USA), 2 mM L-glutamine (Sigma-Aldrich), and 100 units/ml Penicillin/100 μg/ml Streptomycin (Sigma-Aldrich). The cells were used between passage numbers of three and five in this study.

L929 cells (NCTC clone 929, American Type Culture Collection, Manassas, VA, USA) were cultured and expanded in αMEM supplemented with 10% FBS at 37 °C in an humidified atmosphere of 5% CO2.

4.2.9 Bead/cell infiltration

For bead/cell infiltration analysis, 2% agarose gels with 3 mm diameter holes were created into which each scaffold disc was press-fit, to study depth-wise infiltration of a controlled number of beads or cells, while minimizing escape or infiltration along the edges of the scaffold. Briefly, 1 mL of 2% warm agarose solution was pipetted into each well of a 24-well tissue culture plate (BD Biosciences, Mississauga, ON, Canada) and cooled down at 4°C. Once solidified, a 3 mm diameter hole was made in the center of the agarose gel by a 3 mm Miltex dermal biopsy punch. The cylindrical scaffolds were then fit to the bottom of the holes. Four pore sizes of scaffolds (84 micron-Sample 2, 116 micron-Sample 3, 141 micron-Sample 4 and 162 micron-Sample 5) were tested for bead/cell infiltration analysis in triplicate.

A novel approach of using polystyrene beads (size: 10 μm, dark red, Sigma-Aldrich) was first applied to mimic cell infiltration longitudinally into each scaffold cylinder. The particle size of the beads (n=462) was verified and determined to be 10 ± 0.1 microns through image analysis using a Nikon Optiphot-2 light microscope and StreamPix v.III and Sigmascan Pro v.5 software. As an economical model, beads closely mimic the size of trypsinized hBMSCs, which would be ultimately used for clinical bone regeneration applications. 126,500 beads in 2 μL water suspension were transferred to the top surface of the scaffold. After passive penetration by gravity for 30 min, the scaffolds were transferred to a new culture plate containing fresh 2% melted agarose solution and the beads fixed in place by solidification of agarose gel in 4°C. The scaffolds were then cut in half to generate two semi-cylinders and the transverse cross sections of the scaffold were photodocumented with a Zeiss AxioVert S100 microscope. The number of beads that passed through the scaffold and remained in the bottom of the well was quantified by the countess automated cell counter (Invitrogen). The number of retained beads in the scaffold is simply calculated by the subtraction of the number of escaped beads from the total number of seeded beads (126,500). Retention capacity was calculated by dividing the number of beads that remained in the scaffold by the original number of beads seeded.

For cell infiltration analysis, scaffolds were sterilized by 70% ethanol followed by sterile water washes and fit as described above into agarose wells. 126,500 freshly trypsinized hBMSCs suspended in 20 µL CCM were seeded on the scaffolds (N=4 per pore size). After 2h incubation at 37°C, the scaffolds were transferred to a new culture plate; cells escaped from the scaffolds were then trypsinized and seeded in a new 96-well culture plate containing a standard curve of increasing hBMSC number. Cells in the 96-well plate and scaffolds seeded with cells were maintained in CCM overnight, fixed with 4% Paraformaldehyde in PBS for 20 min and the cell nuclei stained with Hoechst 33342 (Invitrogen) for 5 min. The fixed cells were visualized with the Zeiss AxioVert S100 microscope and images were captured using the QImaging QICAM FAST 1394 digital camera and Northern Eclipse software. The total number of escaped cells was determined by automated counting using ImageJ software against the standard curve; cell retention capacity was calculated as the number of retained cells divided by total cells seeded; The scaffolds were cut in half into two semi-cylinders, and the cross sectional area of the semi-cylinder scaffolds was imaged with the Olympus FV1000-IX81 confocal microscope system.

4.2.10 Cell viability assays

L929 cells are commonly used for viability assays to assess the biocompatibility of scaffolds. $3x10^4$ cells were resuspended in CCM and seeded onto the scaffolds. After 20h culture at 37°C, AlamarBlue® cell viability reagent (Invitrogen) was added to each well at 1:10 v/v and cultured for 4h. The fluorescence of the conditioned media was read by a Tecan plate reader at 560 nm/590 nm excitation/emission. Cell viability was reported as relative fluorescence units and the test was repeated 4 times (N=4).

The viability of L929 cells attached on the scaffolds was also evaluated by a live/dead assay using 1 μM green-fluorescent Calcein AM (Invitrogen) and 1 μM red-fluorescent Ethidium homodimer-1 (Invitrogen) for 30 min at 37°C. The top of the scaffolds and the cells escaped from the scaffold were then imaged. For brightfield microscopic analysis, separate wells of seeded scaffolds were left undisturbed and were imaged by the Zeiss AxioVert S100 microscope.

4.2.11 Statistical analyses

Mean and standard deviation (SD) values were calculated for each group of data. Student's t-test was used to analyze experimental groups with two samples, with $p<0.05$ taken as statistically significant.

4.3 Results and discussion

4.3.1 Rheology

The rheology of the materials is important in determining how the co-continuous morphology is formed. Figure 4.1 demonstrates the trend of complex viscosity as a function of frequency for PCL and PEO pure materials. Time sweep tests were done to prove the stability of the polymers in the course of the rheological measurements. At 100°C PCL is mostly characterized by a Newtonian plateau in almost all the ranges of shear rate, as opposed to PEO which demonstrates a more shear thinning behavior in the probed frequency range. It is clear that for low frequencies (less than 3 rad/s), PEO is more viscous than PCL and for higher frequencies the opposite behaviour is observed. There was a similar frequency dependent behaviour in the storage modulus of the two polymers as a measure of their elastic properties.

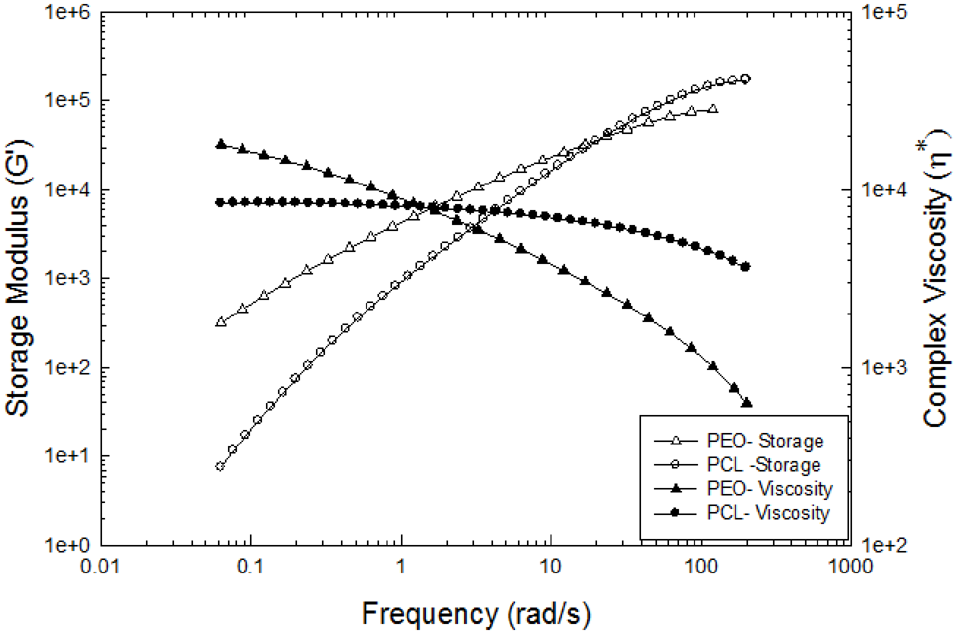

Figure 4.1: Complex viscosity and storage modulus as a function of frequency at 100°C

4.3.2 Morphology

SEM images in Figure 4.2 demonstrate the evolution of pore size in the co-continuous microstructure as a function of annealing time at a constant annealing temperature of 160°C.

Non-annealed constructs have a negligible pore size (0.87 microns) and their structure will be discussed in more detail below. The SEM photos qualitatively demonstrate a high level of continuity at all annealing times and this is further confirmed quantitatively below. Clearly, the increase in the annealing time leads to significantly increased phase/pore sizes over a very wide range of scale. This approach will be used to ultimately create a large window of pore sizes to be studied for cell retention capacity.

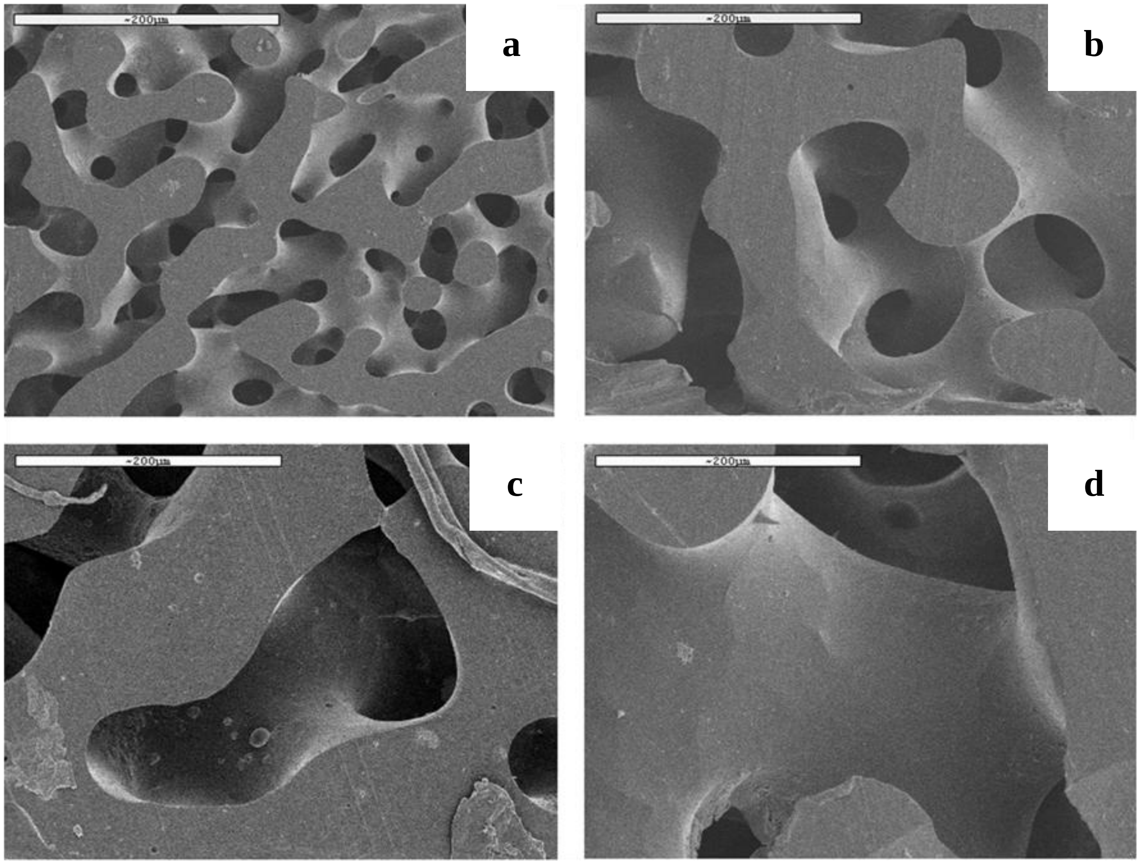

Figure 4.2: SEM micrographs of 45PCL/55PEO annealed at 160°C for a, b, c and d represent 30 min, 1h, 2h, and 3h, respectively. Scale bar = 200 microns

The increase in the volume average pore diameter as a function of annealing time at a given temperature (160°C) is also demonstrated in Figure 4.3 which demonstrates a linear correlation between the volume average pore diameter and the annealing time. This linear correlation in the phase coarsening follows an $R{\sim}kt$ relationship, where R is the average pore radius and t is the annealing time as suggested by Yuan et al. [17]. The coarsening rate dR/dt which is closely controlled by the interfacial tension and zero shear viscosity of the surrounding media is constant and was calculated as 33.4 µm/hr. This demonstrates that the average pore size can be highly controlled in a quantitative fashion by modifying the annealing time.

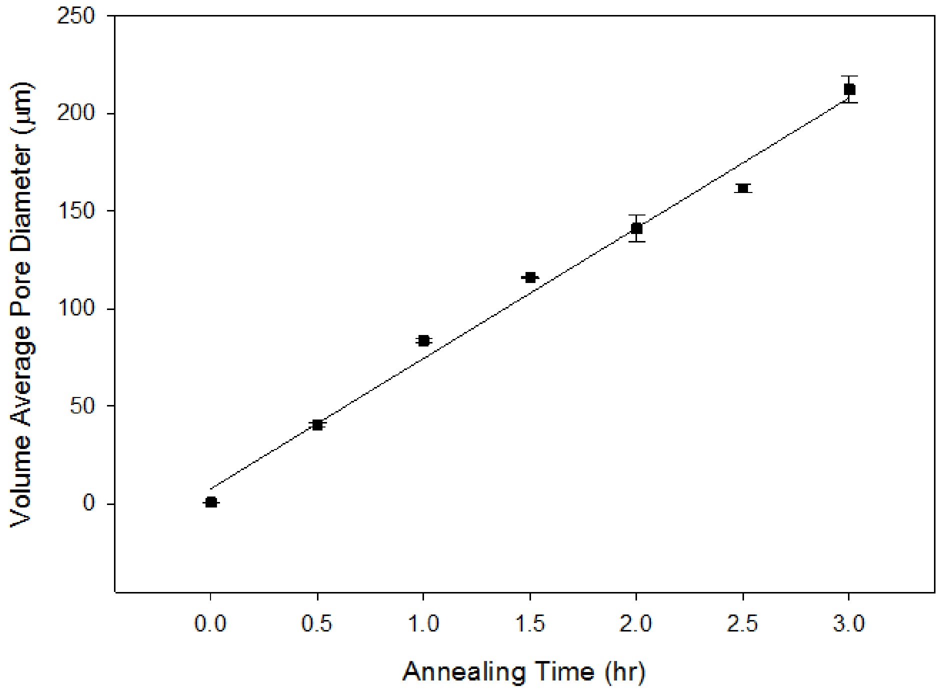

Figure 4.3: Volume average pore diameter as a function of annealing time. The pore diameter was directly proportional to the annealing time (r2 = 0.99), thus providing the ability to create pores between 40 and 212 µm by simply altering the duration of annealing

Such alterations in the annealing time could lead to a 230-fold increase in the pore size from approximately 0.87 microns in non-annealed samples to 212 microns in 3h annealed scaffolds. Table 4.2 summarizes the values of the volume average pore diameter as a function of the annealing time.

Table 4-2: Quantified volume average pore diameter as a function of annealing time for 45PCL/55PEO vol% after extraction of PEO

Sample Annealing Time	**Sample 0 0h**	**Sample 1 0.5h**	**Sample 2 1h**	**Sample 3 1.5h**	**Sample 4 2h**	**Sample 5 2.5h**	**Sample 6 3h**
Volume average pore diameter (μm)	0.87 ± 0.02	41 ± 1.2	84 ± 1.1	116 ± 0.3	141 ± 7	162 ± 1.9	212 ± 6.7
Continuity (%)	~ 100	98.7 ± 1.2	96.8 ± 2.2	97.1 ± 0.4	98.0 ± 0.8	99.2 ± 0.6	~ 100

Figures 4.4 and 4.5 depicts the pore size distribution of 4 different porous samples 0.87 micron-Sample 0 (non-annealed), 40 micron-Sample 1, 84 micron-Sample 2 and 141 micron-Sample 4. Peak analysis of the non-annealed samples in Fig. 4a showed the existence of two groupings of pore sizes at 890 nm and 12.5 μm, as well as shoulders occurring at 2 and 4 μm which indicate the polymodal/irregular nature of the pore size distribution for the non-annealed sample. As shown in Figure 4.4, these irregularities are absent for each annealed sample where only one sharp unimodal peak is observed (Figure 4.5). Evidently, the coarsening effect caused by static annealing of the samples eliminates the polymodal/irregular behaviour in the pore size distribution.

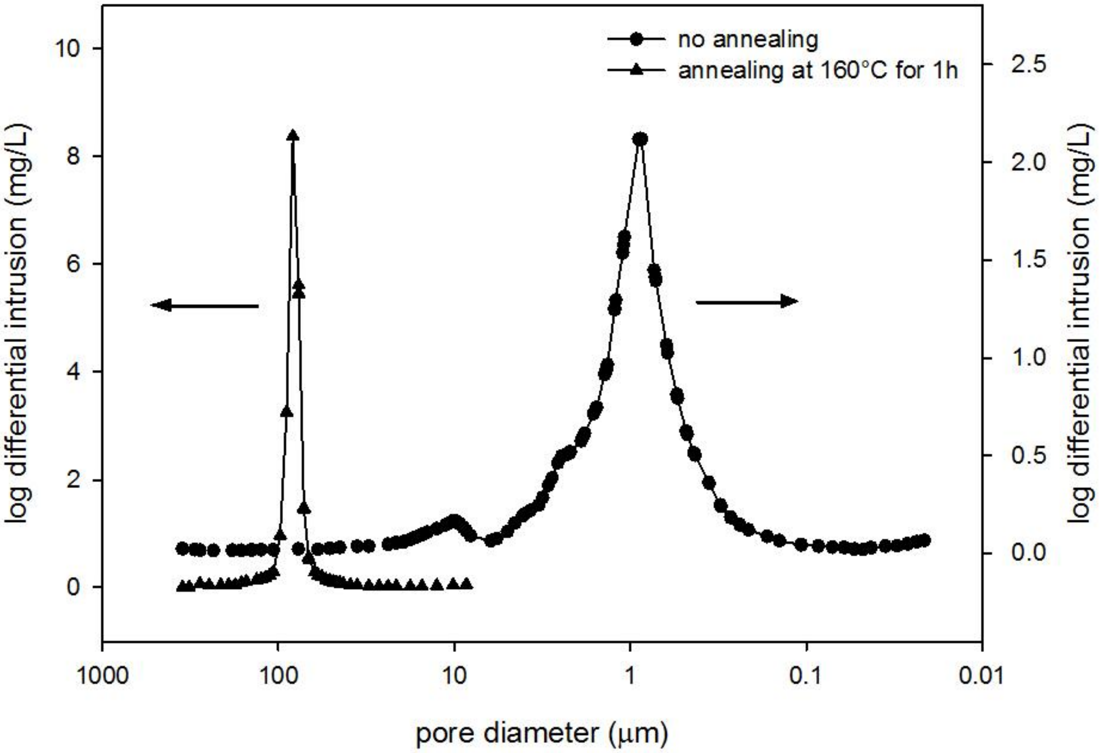

Figure 4.4: Pore size distribution as a function of annealing time for a non-annealed vs. 1h annealed scaffold. Non-annealed scaffolds display a polymodal pore distribution consisting of much smaller pores

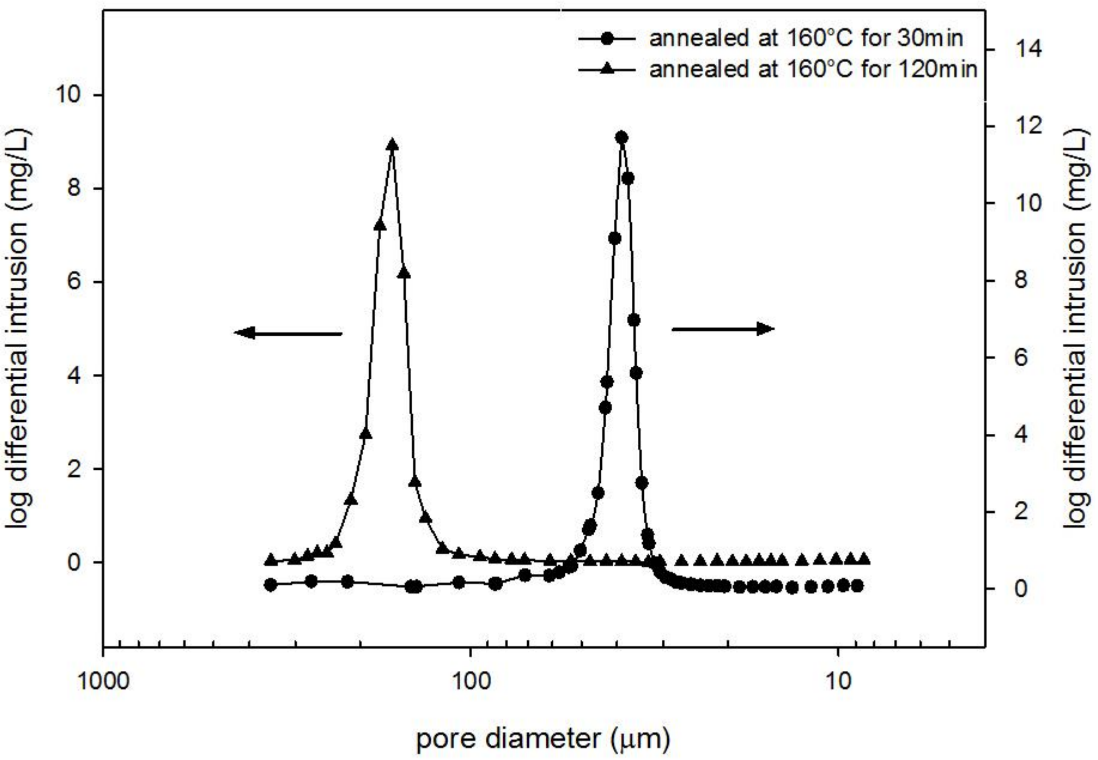

Figure 4.5: Pore size distribution as a function of annealing time for a 0.5h and 2h annealed scaffolds. Annealed scaffolds are made up of larger unimodal sized pores

4.3.3 Continuity measurements

The continuity percentage of the porogen phase in non-annealed scaffolds as a measure of pore interconnectivity was analyzed by gravimetric measurements in blends containing up to 55 vol% PEO and is illustrated in Figure 4.6. There was a broad region of PEO continuity starting from 35 v/v % up to 55% v/v PEO, which demonstrated that virtually all the pores in the samples were accessible to the solvent (water). This was a lucid indication of the high level of pore interconnectivity for this binary blend type scaffold. The blends containing 60 vol% PEO porogen phase and higher were not self-supporting and collapsed after extraction. In this article, all the co-continuous blends were prepared with the composition ratio of 45PCL/55PEO vol%. Calculation of the co-continuity as a measure of pore interconnectivity was also performed for the annealed blends and is shown in Table 4.2. For almost all annealing times, the quantitative level of continuity, and hence the pore interconnectivity, was nearly 100%. Hence the virtually perfect interconnectivity is maintained with annealing. Also, a constant weight in the gravimetric studies was obtained in a shorter period of time as the annealing time increased.

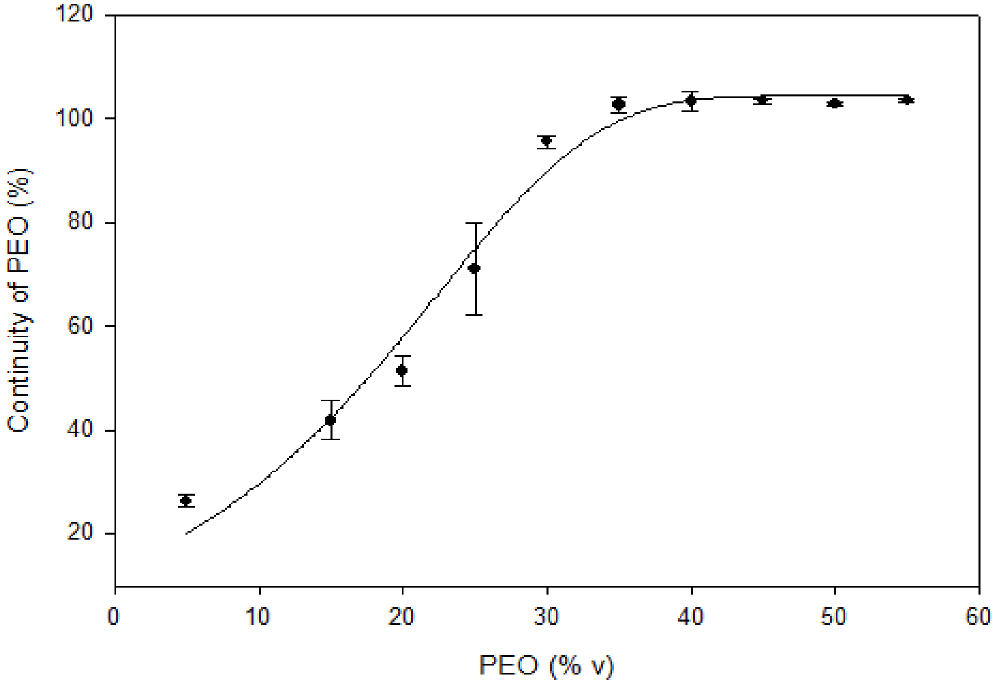

Figure 4.6: Continuity percentage of PEO porogen phase as a function of PEO composition. The broad region of continuity between 35% and 55% demonstrated that all the pores were accessible to the solvent, and thus pore interconnectedness was evident

The concentration of residual organic solvents in the course of the fabrication of scaffolds should be reduced to an acceptable window for them to be used in the human body [29]. By using water at ambient temperature as the solvent for the PEO phase, the added problems of toxicity due to residual solvent and deformations at high temperatures are fully overcome. Also, due to the hydrophobic nature of PCL, any low level residual PEO in the blend could in fact increase the hydrophilicity of the system since PEO has been previously used in the surface modification of PCL nanofiber webs to increase the hydrophilicity of the polymer surface [30]. As a result, even small amounts of PEO remaining in the blend could potentially enhance cell attachment.

4.3.4 Bead/cell infiltration

Due to the scarcity and high cost of primary hBMSCs, a rapid screening method using 10-micron polystyrene beads was developed to assess cell infiltration and retention in the scaffolds. The setup of the infiltration assay is illustrated in Figure 4.7.

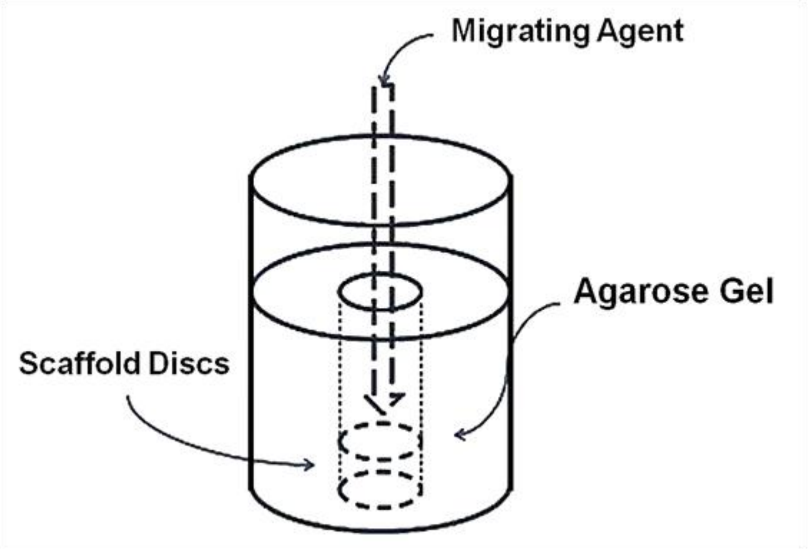

Figure 4.7: Infiltration assay setup where migrating agents seeded in the scaffolds can either be beads or hBMSCs

Figures 4.8 and 4.9 show the model bead retention behavior as a function of pore size and it can be seen that a linear relationship is obtained between bead escape/retention % and pore size. As an example, knowing that for 84 micron-Sample 2 with the smallest pore size, approximately 5,000 beads have escaped the scaffold (Figure 4.9) and total beads seeded inside were 126,500, the retention capacity (%) is calculated as [(126,500-5,000)/126,500] × 100 which gives 96% bead retention. This retention value is reported in Figure 4.8. The maximum bead retention capacity is 96%, observed for the 84 micron-Sample 2, and the minimum bead retention capacity is 83% for the 162 micron-Sample 5. Figure 4.10 shows that the beads infiltrate efficaciously into the center of the scaffold. Such a high level of infiltration into the scaffold reflects the high level of continuity of the porous structure and the tortuous pathways within the 3D constructs.

The cell escape/retention behavior is also depicted in Figures 4.8 and 4.9 and it can be seen that the pore size of the scaffold has little influence on cell escape/retention up to approximately 120 micron pore size. In that pore size range a very high retention and very low escape of cells is observed. This behavior differs markedly from the model beads.

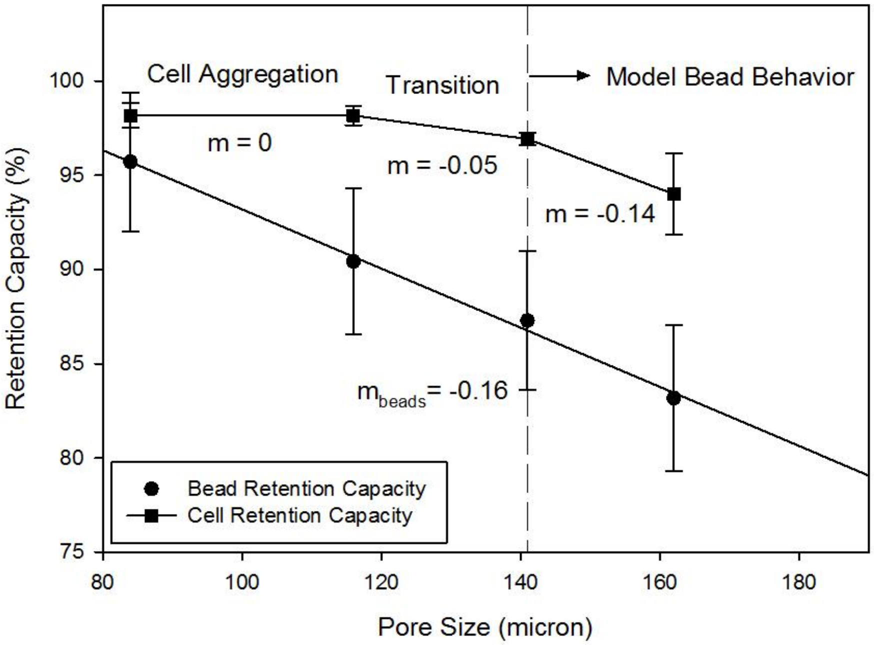

Figure 4.8: Cell/Bead retention capacity. 141 micron is the pore size threshold beyond which cells behave like model beads and infiltrate the scaffolds more homogeneously

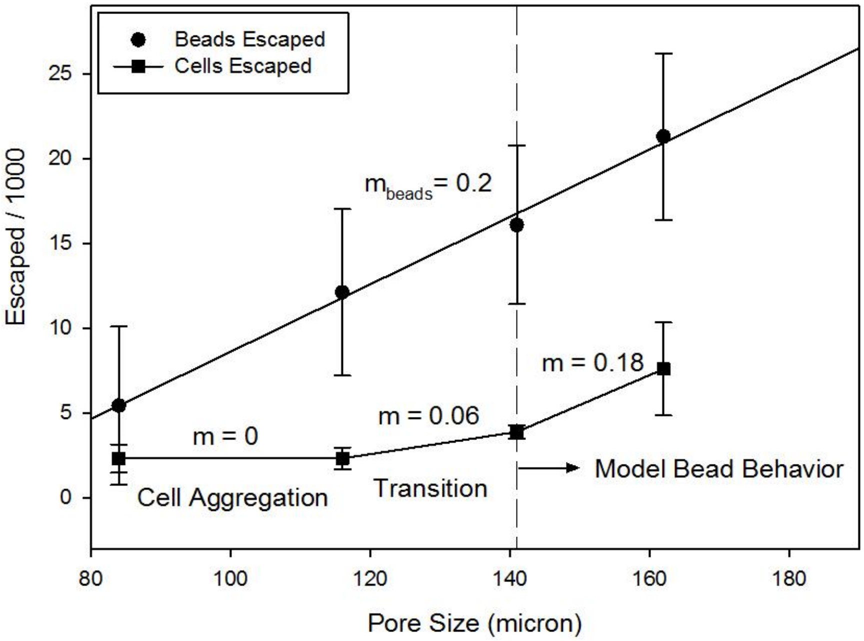

Figure 4.9: Cell/Bead escape. 141 micron is the pore size threshold beyond which cells behave like model beads and infiltrate the scaffolds more homogeneously

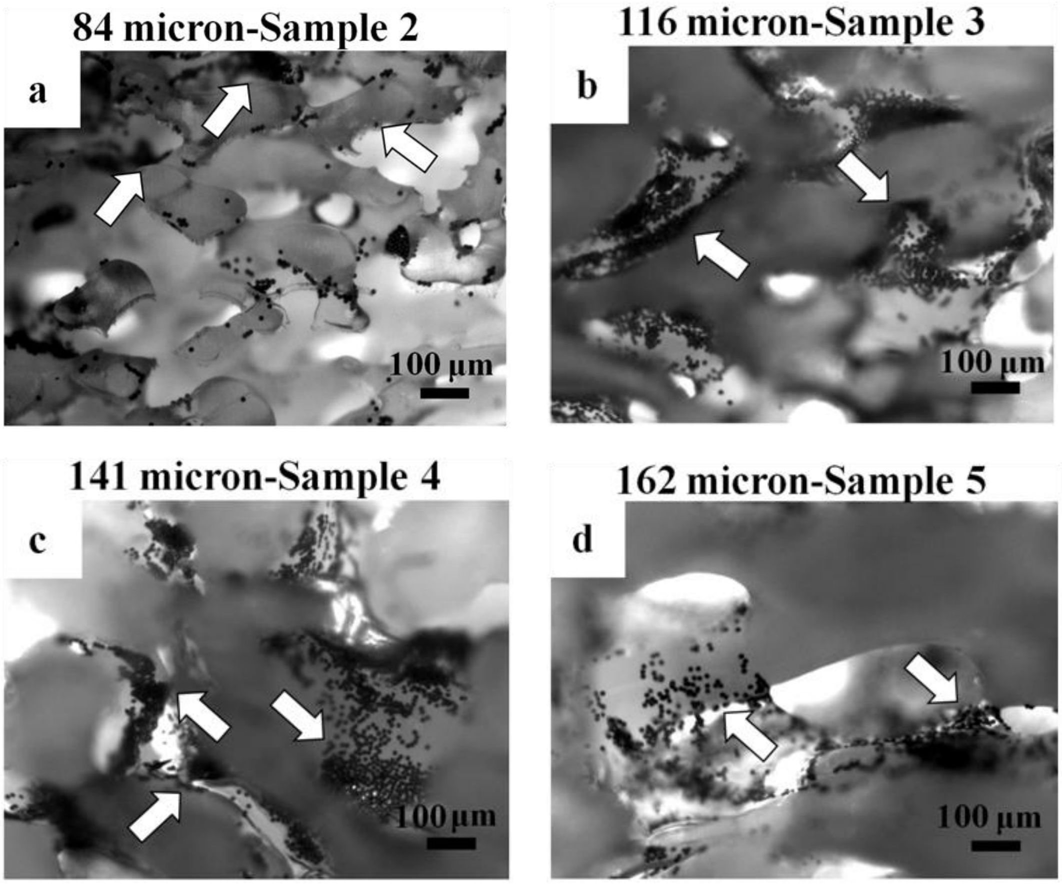

Figure 4.10: Phase contrast images of the rectangular cross section as a qualitative measure of bead penetration from the top toward the bottom of the scaffolds; dark spots (arrows) are beads. The panels correspond to 84 micron-Sample 2 (a), 116 micron-Sample 3 (b), 141 micron-Sample 4 (c) and 162 micron-Sample 5 (d) scaffolds. At low pore size, model beads penetrate toward the center. Scale bar = 100 microns

Figure 4.11(a, b) explains this discrepancy as high levels of surface aggregation of the cells at the top of the 3D scaffold are observed. Higher retention values of the cells as compared to those of the beads are explained by hBMSCs forming undesired cell-cell interactions in the seeding area, which limit their penetration into the lower pore size constructs. Clearly at 84 and 116 micron pore sizes (Figure 4.11(a, b)), the cells are aggregated at the top of the scaffold. At higher pore sizes (Figure 4.11(c, d)), the hBMSCs are able to penetrate the scaffold.

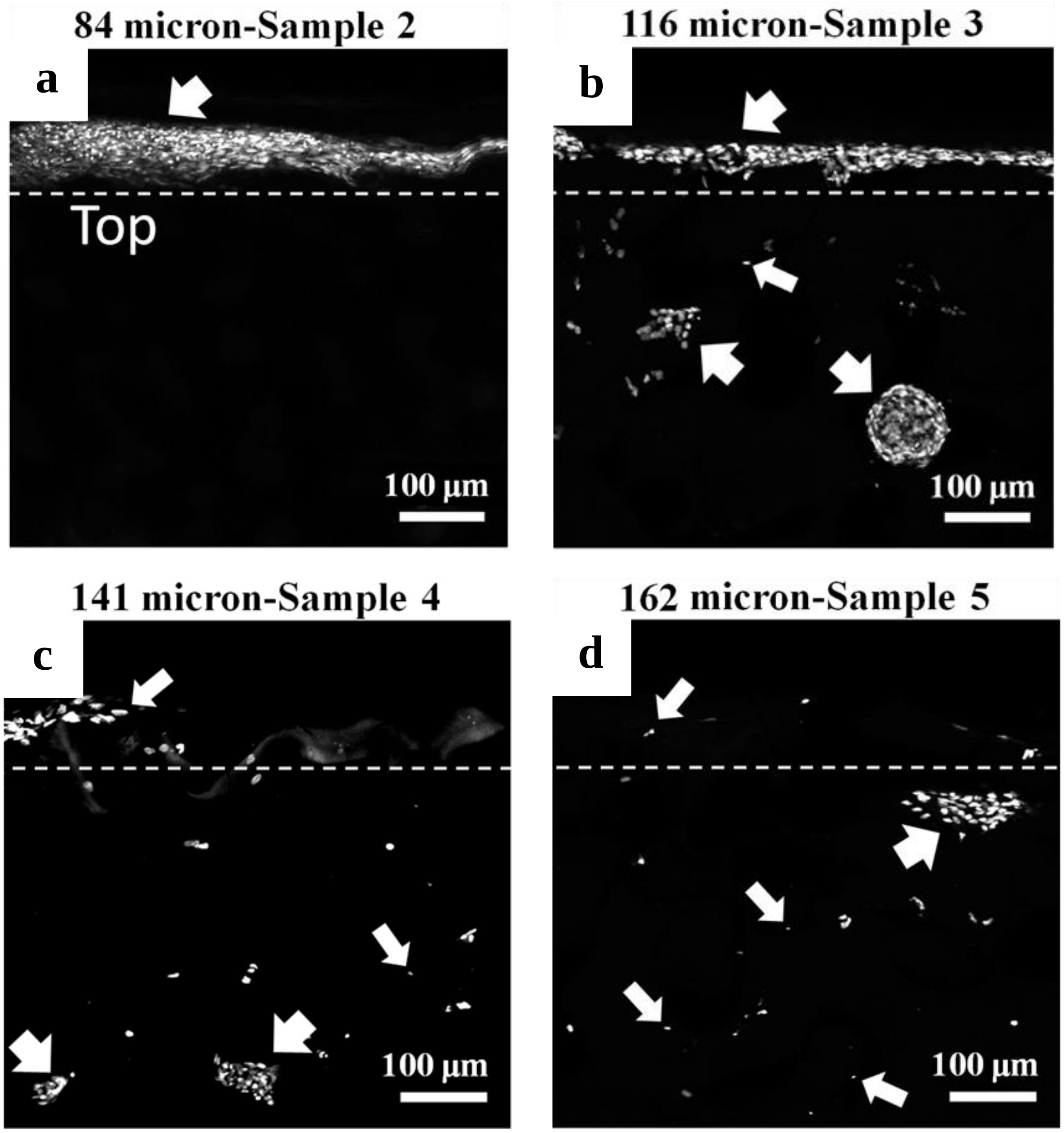

Figure 4.11: Confocal images of the scaffolds showing cell penetration from the top toward the bottom of the scaffolds; white spheres (arrows) are fluorescent cell nuclei, dashed line represents the seeding area or top of the scaffolds. The panels correspond to 84 micron-Sample 2 (a), 116 micron-Sample 3 (b), 141 micron-Sample 4 (c) and 162 micron-Sample 5 (d) scaffolds. At low pore size, cells tend to self-aggregate at the top of the scaffolds. Scale bar = 100 microns

Considering the slopes (m) on the graphs for cell escape/retention in Figure 4.8 and 4.9, three main regions with different characteristics are observed. At low pore sizes (84 and 116 microns), there is no dependence (zero slope) of cell escape/retention on pore size due to the cell aggregation at the top of the scaffold post-seeding. With an increase in the pore size (116-141 microns), a transition region is observed where more cells tend to pass the top surface barrier and enter the structure at deeper levels and a cell escape/retention dependence of positive/negative slope is observed. At pore sizes of 141 and 162 microns there is complete penetration of the cells into the 3D construct and the slope of cell escape/retention with pore size is identical to that of the model beads. It must be noted that the onset pore size above which the cells behave like model beads depends on various parameters such as cell type, cell-surface interactions and cell seeding density. It is expected that by reducing the cell seeding density, the model bead behavior could potentially be observed for cells at lower pore sizes.

These results indicate the value of carrying out model bead experiments as they can provide the baseline for perfectly non-aggregated systems. The above analysis also emphasizes the fact that cell aggregation behavior can have a significant role in determining optimum pore sizes for scaffolds in tissue engineering experiments, i.e. even if the trypsinized cells used in this study are nominally in the order of 10 microns in size, their effective aggregated size can be many times greater than that value.

In this study the 141 micron-Sample 4 (Figure 4.11c) and 162 micron-Sample 5 (Figure 4.11d) demonstrate a homogeneous distribution with a low amount of cell aggregation on the top in comparison with other pore sizes, indicating that the open network of pores allowed cells to settle from the top surface throughout the scaffold. However, the 162 micron-Sample 5 demonstrated the highest bead escape level of 17% and a 6% loss of cells as shown in Figure 4.9. Therefore, it can be stated that the 141 micron-Sample 4 demonstrates the best combination of cell retention capacity and distribution inside the scaffold and is hence considered to be the scaffold with optimum morphology. Moreover, according to results by Hulbert et al.[31], such a large pore size should be able to support bone ingrowth and qualify for optimal osteogenesis prerequisites.

4.3.5 Cytotoxicity and cell viability

AlamarBlue® assay was carried out to verify the cytotoxicity of the scaffolds. The exposure of L929 cells to PCL scaffolds induced a slight decrease of average cell metabolism, but the effect was not significant (p=0.11, Figure 4.12), implying that the PCL scaffolds were not cytotoxic.

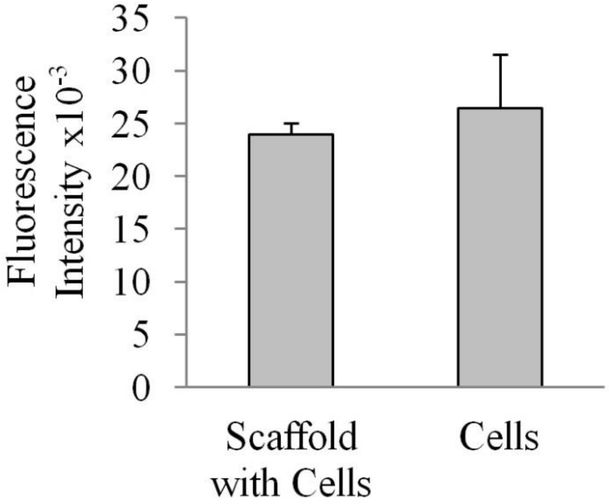

Figure 4.12: AlamarBlue® assay was used to measure cell viability of L929 cells cultured on PCL scaffolds as compared to a control monolayer culture, n=4

Live/dead cell assay in 141 micron-Sample 4 confirmed the cytocompatibility of the scaffold (Figure 4.13(a,b)). The monolayer cells were visualized to grow directly underneath the scaffold without necrosis or detachment and presented similar morphology (Figure 4.13d) to the control monolayer culture (Figure 4.13c). Nevertheless, there was a slight difference in cell morphology on tissue culture wells with a more elongated, spindle shaped and fibroblast-like phenotype, compared to that on the PCL scaffold where the majority of cells remained spherical. This was in agreement with results obtained by Mattanavee et al. who observed rounded L929 cells cultured on electrospun PCL scaffolds [32], which is best explained by an intrinsic hydrophobic PCL surface that is relatively non-adherent for cells [33]. Future work will focus on the surface modification of the melt-blended PCL scaffold to enhance cell attachment, spreading and differentiation into osteoblasts.

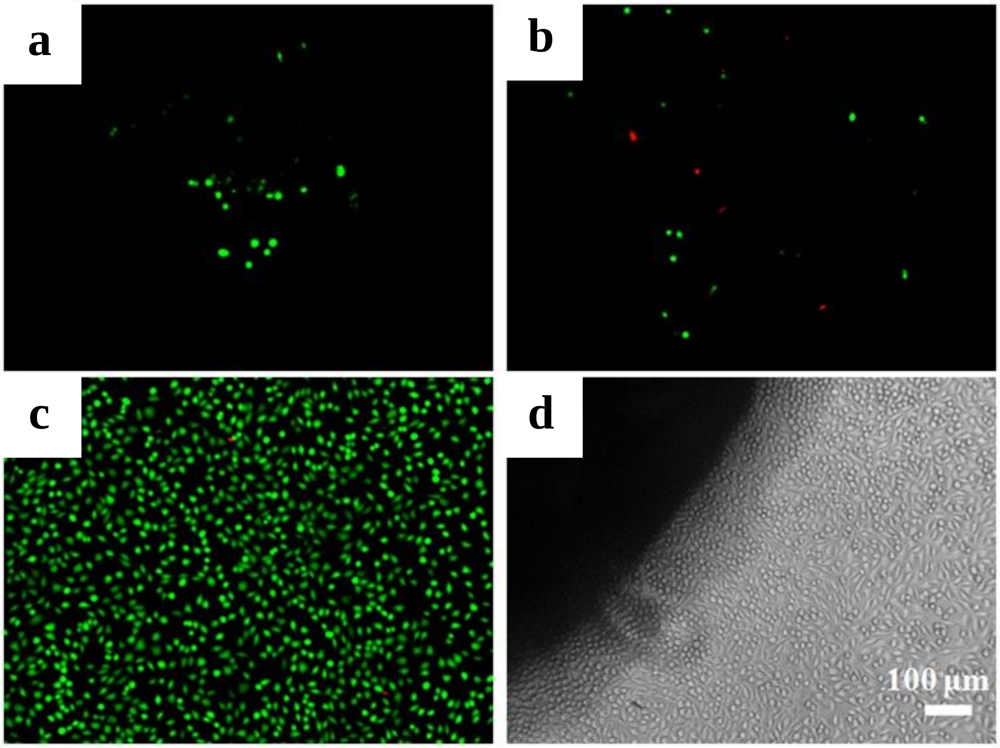

Figure 4.13: (a-b) Fluorescent images of L929 cells inside the scaffold, (c) Fluorescent image of subconfluent L929 cells on the tissue culture plate (positive control), Live and dead cells are represented by green and red color, respectively. (d) Phase contrast image of L929 cells and PCL scaffold. PCL scaffolds were not cytotoxic as the monolayer cells grow directly underneath the scaffold without necrosis. Scale bar = 100 microns

4.4 Conclusion

To date, a thorough investigation of tissue engineering scaffolds of significantly different and highly controlled pore sizes at the microscopic level including scaffold infiltration as a crucial parameter has not been done. The melt blending of PCL and PEO as a co-continuous immiscible polymer blend followed by static annealing is a robust approach for the creation of highly controlled 3-dimensional scaffolds destined for tissue engineering applications. Close to 100% pore interconnectivities, sharp unimodal pore size distribution, along with precise and unique control over the pore size varying over two orders of magnitude are the main advantages of the technique. Porosimetry measurements show that the static annealing of the blends can yield a sharp unimodal pore size distribution, as opposed to non-annealed structures that demonstrate a polymodal and irregular size dispersity. Infiltration studies using model 10-micron beads as a new approach show that the fabricated scaffolds bear high retention capacities and demonstrate effective infiltration of the beads into the scaffold. Such a high level of infiltration into the scaffold reflects the high level of continuity of the porous structure and the tortuous pathways within the 3D constructs.

However, it is shown that, unlike beads, cells do not act as single entities and tend to form aggregates on the seeding area of the small pore size scaffolds which impedes penetration into the porous device. This phenomenon necessitates the use of large pore size scaffolds to avoid such non-uniform cell distribution. The model bead experiments are important as they can provide the baseline for perfectly non-aggregated systems and the beads closely mimic trypsinized cells at pore sizes equal to or larger than 141 microns. The novel bead system reported in this paper can be used as a reference model for devising proper seeding protocols to overcome retention and distribution issues. According to our studies, PCL scaffolds of 141-micron average pore have the best bead/cell retention and distribution within the scaffold. Cytotoxicity assays demonstrate that there is no significant difference in cell viability after incubation of L929 cells in contact with the scaffold as compared to that of the control monolayer cells, and few necrotic cells were detected by a fluorescent live-dead cell assay.

Acknowledgements

The authors would like to thank Sylvie St-Amour and Sylvie Sauriol at FPInnovations for their valuable assistance in the porosimetric measurements and Guillaume Lessard at École Polytechnique de Montréal for his help in the preparation of the scaffolds. Also, financial support of the Natural Sciences and Engineering Research Council of Canada (NSERC) through its Network for Innovative Plastic Materials and Manufacturing Processes (NIPMMP), NSERC Discovery (to CDH), and salary support for XL and CDH from the Fonds de Recherche en Santé du Québec (FRQ-S, Bourse de Carrière Nationale to CDH) and the Mentor program for MBA is gratefully acknowledged.

References

1. Langer R, Vacanti JP. Tissue Engineering. Science (New York, NY). 1993;260(5110):920-6.

2. Hutmacher DW. Scaffolds in tissue engineering bone and cartilage. Biomaterials. 2000;21(24):2529-43.

3. Diana MY, John F. Polymeric Scaffolds for Tissue Engineering Applications. Tissue Engineering and Artificial Organs. Electrical Engineering Handbook: CRC Press; 2006. p. 37-1--18.

4. Santis RD, Catauro M, Silvio LD, Manto L, Raucci MG, Ambrosio L et al. Effects of polymer amount and processing conditions on the in vitro behaviour of hybrid titanium dioxide/polycaprolactone composites. Biomaterials. 2007;28(18):2801-9.

5. Gloria A, Russo T, D'Amora U, Zeppetelli S, D'Alessandro T, Sandri M et al. Magnetic poly(epsilon-caprolactone)/iron-doped hydroxyapatite nanocomposite substrates for advanced bone tissue engineering. J R Soc Interface. 2013;10(80):20120833.

6. Chang HI, Perrie Y, Coombes AGA. Delivery of the antibiotic gentamicin sulphate from precipitation cast matrices of polycaprolactone. Journal of Controlled Release. 2006;110(2):414-21.

7. Li W-J, Tuli R, Okafor C, Derfoul A, Danielson KG, Hall DJ et al. A three-dimensional nanofibrous scaffold for cartilage tissue engineering using human mesenchymal stem cells. Biomaterials. 2005;26(6):599-609.

8. Franco RA, Nguyen TH, Lee BT. Preparation and characterization of electrospun PCL/PLGA membranes and chitosan/gelatin hydrogels for skin bioengineering applications. J Mater Sci-Mater Med. 2011;22(10):2207-18.

9. Ng KW, Hutmacher DW, Schantz JT, Ng CS, Too HP, Lim TC et al. Evaluation of ultra-thin poly(epsilon-caprolactone) films for tissue-engineered skin. Tissue engineering. 2001;7(4):441-55.

10. Borriello A, Guarino V, Schiavo L, Alvarez-Perez MA, Ambrosio L. Optimizing PANi doped electroactive substrates as patches for the regeneration of cardiac muscle. J Mater Sci-Mater Med. 2011;22(4):1053-62.

11. Causa F, Netti PA, Ambrosio L, Ciapetti G, Baldini N, Pagani S et al. Poly-ϵ-caprolactone/hydroxyapatite composites for bone regeneration: In vitro characterization and human osteoblast response. Journal of Biomedical Materials Research Part A. 2006;76A(1):151-62.

12. Ghasemi-Mobarakeh L, Semnani D, Morshed M. A novel method for porosity measurement of various surface layers of nanofibers mat using image analysis for tissue engineering applications. Journal of Applied Polymer Science. 2007;106(4):2536-42.

13. Dalton PD, Woodfield, T., Hutmacher, W.D.,. SnapShot: Polymer Scaff olds for Tissue Engineering. Biomaterials. 2009;30(4):701-2.

14. Karageorgiou V, Kaplan D. Porosity of 3D biomaterial scaffolds and osteogenesis. Biomaterials. 2005;26(27):5474-91.

15. Willemse RC, Posthuma de Boer A, van Dam J, Gotsis AD. Co-continuous morphologies in polymer blends: the influence of the interfacial tension. Polymer. 1999;40(4):827-34.

16. Sarazin P, Favis BD. Morphology Control in Co-continuous Poly(l-lactide)/Polystyrene Blends: A Route towards Highly Structured and Interconnected Porosity in Poly(l-lactide) Materials. Biomacromolecules. 2003;4(6):1669-79.

17. Yuan Z, Favis BD. Coarsening of immiscible co-continuous blends during quiescent annealing. AIChE Journal. 2005;51(1):271-80.

18. Sarazin P, Roy X, Favis BD. Controlled preparation and properties of porous poly(l-lactide) obtained from a co-continuous blend of two biodegradable polymers. Biomaterials. 2004;25(28):5965-78.

19. Gloria A, Causa F, Russo T, Battista E, Della Moglie R, Zeppetelli S et al. Three-dimensional poly(epsilon-caprolactone) bioactive scaffolds with controlled structural and surface properties. Biomacromolecules. 2012;13(11):3510-21.

20. Dalton PD, Woodfield T, Hutmacher DW. Erratum to: SnapShot: Polymer Scaffolds for Tissue Engineering [Biomaterials 30/4 (2009) 701–702]. Biomaterials. 2009;30(12):2420.

21. Yuan Z, Favis BD. Influence of the efficacy of interfacial modification on the coarsening of cocontinuous PS/HDPE blends during quiescent annealing. Journal of Polymer Science Part B: Polymer Physics. 2006;44(4):711-21.

22. Yuan Z, Favis BD. Macroporous poly(l-lactide) of controlled pore size derived from the annealing of co-continuous polystyrene/poly(l-lactide) blends. Biomaterials. 2004;25(11):2161-70.

23. Anderson KE, Stevenson BR, Rogers JA. Folic acid–PEO-labeled liposomes to improve gastrointestinal absorption of encapsulated agents. Journal of Controlled Release. 1999;60(2–3):189-98.

24. Suh H, Jeong B, Rathi R, Kim SW. Regulation of smooth muscle cell proliferation using paclitaxel-loaded poly(ethylene oxide)–poly(lactide/glycolide) nanospheres. Journal of biomedical materials research. 1998;42(2):331-8.

25. Park S-J, Kim K-S, Kim S-H. Effect of poly(ethylene oxide) on the release behaviors of poly(ε-caprolactone) microcapsules containing erythromycin. Colloids and Surfaces B: Biointerfaces. 2005;43(3–4):238-44.

26. Washburn NR, Simon CG, Tona A, Elgendy HM, Karim A, Amis EJ. Co-extrusion of biocompatible polymers for scaffolds with co-continuous morphology. Journal of Biomedical Materials Research. 2002;60(1):20-9.

27. Carreau PJ, De Kee DCR, Chhabra RP. Rheology of Polymeric Systems: Principles and Applications. Hanser; 1997.

28. Washburn EW. The Dynamics of Capillary Flow. Physical Review. 1921;17(3):273-83.

29. Joerg T, Theresa H, Antonios M. Salt Leaching for Polymer Scaffolds. Scaffolding In Tissue Engineering. CRC Press; 2005. p. 111-24.

30. Kim G, Park J, Park S. Surface-treated and multilayered poly(ε-caprolactone) nanofiber webs exhibiting enhanced hydrophilicity. Journal of Polymer Science Part B: Polymer Physics. 2007;45(15):2038-45.

31. Hulbert SF, Young FA, Mathews RS, Klawitter JJ, Talbert CD, Stelling FH. Potential of ceramic materials as permanently implantable skeletal prostheses. Journal of biomedical materials research. 1970;4(3):433-56.

32. Mattanavee W, Suwantong O, Puthong S, Bunaprasert T, Hoven VP, Supaphol P. Immobilization of Biomolecules on the Surface of Electrospun Polycaprolactone Fibrous Scaffolds for Tissue Engineering. ACS Applied Materials & Interfaces. 2009;1(5):1076-85.

33. Sudarmadji N, Tan JY, Leong KF, Chua CK, Loh YT. Investigation of the mechanical properties and porosity relationships in selective laser-sintered polyhedral for functionally graded scaffolds. Acta Biomaterialia. 2011;7(2):530-7.

CHAPTER 5 ARTICLE 2: CHITOSAN SURFACE MODIFICATION OF FULLY INTERCONNECTED 3D POROUS POLY(E-CAPROLACTONE) BY THE LBL APPROACH

Although the PCL scaffolds generated in Chapter 4 were not cytotoxic, we attributed the observed rounded morphologies of some hBMSCs on the surface of the constructs to the hydrophobic surface chemistry of PCL. Hence, the surface modification of PCL scaffolds to increase their cytocompatibility is inevitable. Chapter 5 focuses on the surface modification of PCL with chitosan as a hydrophilic cytocompatible compound, which has been shown to improve osteogenesis *in vitro*. Layer-by-Layer (LbL) self assembly of polyelectrolytes has been vastly studied in our laboratory in the recent years. In this part of the study, we use the LbL technique to incorporate chitosan on the surface of 2D and 3D PCL and hence improve its surface wettability. The existence and homogeneity of a chitosan layer on the surface of the scaffolds are of ultimate significance, and their qualitative and quantitative evaluation becomes crucial in the case of 3D constructs with considerable and comparable dimensions. As a result, various characterization techniques such as gravimetric measurements, X-ray photoelectron spectroscopy (XPS) and time of flight secondary ion mass spectrometry (ToF-SIMS) are going to be used to assess the uniformity of the coatings.

This article has been submitted to the journal of “*ACS Applied Materials & Interfaces*”.

Chitosan Surface Modification of Fully Interconnected 3D Porous Poly(ε-caprolactone) by the LbL Approach

Nima Ghavidel Mehr[a,b], Caroline D. Hoemann[a,c,d], and Basil D. Favis[a,b,2]

[a] Department of Chemical Engineering, École Polytechnique, Montreal, QC, H3C 3A7 Canada

[b] Centre de Recherche sur les Systèmes Polymères et Composites à Haute Performance (CREPEC), École Polytechnique, Montréal, QC, H3C 3A7 Canada

[c] Institute of Biomedical Engineering, and Groupe de Recherches Sciences et Technologies (GRSTB), École Polytechnique, Montréal, QC, H3C 3A7 Canada

[d] Institute of Biomedical Engineering, École Polytechnique, Montreal, QC, H3C 3A7 Canada

Contribution of co-authors:

Caroline D. Hoemann: Co-director of this research study

Basil D. Favis: Director of this research study

---

[2] Corresponding author. Tel.: + 1 514 340 4711x4527; fax: + 1 514 340 4159.

E-mail address: basil.favis@polymtl.ca (B.D. Favis).

Abstract

In this study, the deposition of a homogeneous chitosan layer on the surface of a 3D interconnected porous network of poly(ε-caprolactone) (PCL), prepared from a co-continuous polymer blend of PCL/PEO (poly(ethylene oxide)), was achieved. A Layer-by-Layer (LbL) self-assembly of polyelectrolytes (PDADMAC as polycation and PSS as polyanion) followed by chitosan deposition was compared with a traditional dip-coating strategy of chitosan on pure PCL surfaces. LbL with polyelectrolytes and PSS as the final layer prior to chitosan addition potentially allows for the preparation of a negatively charged surface that can then subsequently interact with the positively charged chitosan. Gravimetric measurements were done to estimate the deposition efficiency of up to 8 layers of polyelectrolytes on the 3D porous substrate. Few layer depositions lead to an interpenetration of polyelectrolyte molecule chains, however upon increasing the number of layers, more well defined layers are formed. X-ray Photoelectron Spectroscopy (XPS) on 2D solid discs was used to compare the 4 layer deposited samples with the 8 layer deposited ones. The oxygen/carbon, nitrogen/carbon and sulfur/carbon ratios clearly showed that the PSS molecule dominated the surface as the last deposited layer at higher number of depositions (n=8). The further addition of chitosan as the top layer by LbL was demonstrated to be superior as compared to the dip-coating technique since uniform local deposition of chitosan on the LbL coating was observed in both 2D solid discs and 3D porous cubes at various depths within the scaffolds. SEM imaging shows the multilayer assembly ranges in thickness from 550 to 700 nanometers. These data demonstrate that the LbL technique of polyelectrolyte deposition followed by chitosan addition provides a route towards stable and homogeneous surface modification and has the potential to transform a classic fully interconnected porous synthetic polymer material to one with essentially complete chitosan-like surface characteristics.

Keywords: Poly(ε-caprolactone), scaffold, 3D, co-continuous, coating, Layer-by-Layer, X-ray Photoelectron Spectroscopy

5.1 Introduction

PCL is a biodegradable polyester that has been proposed for use in drug release, cutaneous wound repair and also cartilage and bone in-growth and regeneration [1-4]. Degradation of PCL occurs due to the bulk and surface hydrolysis of ester linkages which result in a slow biodegradation which can also be altered according to specifications needed for each application [5]. In addition, PCL is biocompatible, easily processable and does not elicit immune responses which add to its potential to be used in bone regeneration applications. The application of PCL and its composites in bone tissue engineering has been studied and a variety of porous PCL products have been investigated including PCL-only scaffolds (generated by Fused Deposition Modeling (FDM) [6], electrospun PCL [1], or solvent-extracted PCL [7]), loaded PCL scaffolds (scaffolds containing transforming growth factor beta-1 (TGF-β-1) [8] or BMPs [9, 10]) as well as PCL composites (PCL combined with PLLA [11], tricalcium phosphate (TCP) [12, 13], or collagen [14]). *In vitro* studies with cell-seeded PCL have shown alkaline phosphatase activity and mineral deposition. However, none of these scaffolds has yet achieved clinical use for non-union bone fractures, potentially due to lack of mechanical integrity and/or lack of structural requirements due to the limitations in the fabrication techniques as shown in a previous work [15].

Recently, the melt blending of polymers and copolymers based on component compositions and material properties such as interfacial tension and viscosity has been examined as a robust approach for the production of tissue engineering scaffolds of 100% pore interconnectivity [16-18]. In a recent study, this laboratory prepared PCL scaffolds of highly controlled porous structure with a fully interconnected internal network via melt blending of PCL and poly(ethylene oxide) (PEO) and it was shown that they have structural features compatible with bone tissue engineering [19]. However, the same study reported that L929 mouse fibroblasts tend to form spherical morphologies on the PCL scaffolds post-seeding which was also in accordance with previous results for the attachment of these cells on electrospun PCL scaffolds [20]. This phenomenon could be best explained by the intrinsic hydrophobicity of PCL, which makes its surface relatively non-adherent to cells and therefore is unfavorable for mesenchymal cell growth that normally requires substrate anchorage [21]. It is clear that the surface of PCL should be modified in order to enhance the cytocompatibility of PCL through hydrophilic interactions.

Numerous techniques such as plasma treatment, UV-induced or ozone grafting polymerization, and aminolysis have been put to use in order to incorporate hydrophilic components onto the PCL surface [22-26]. These hydrophilic third party groups that are used for surface modification of PCL are mostly extracellular matrix components such as collagen and chitosan or small peptide sequence molecules containing Arg-Gly-Asp (RGD). Most of the surface treatment techniques used to alter the surface of PCL involve grafting components containing hydroxyl, carboxyl or amine functional groups, upon which proper active bio-macromolecules could be incorporated. Since the surface of PCL is considered as a reaction site for these methods, common limitations exist such as steric hindrance leading to non-uniform grafting and inevitable non-specific interactions [27].

Layer-by-Layer (LbL) self-assembly of polyelectrolytes is a simple, straightforward yet powerful technique to physically modify the charge on the surface of a substrate without the need to a grafting reaction on the surface of the PCL scaffold. LbL surface deposition is based on the electrostatic attraction of oppositely charged polyelectrolytes while they adsorb on the surface[28]. Although poly(dialyldemethylammunium chloride) (PDADMAC) and polyanion poly(sodium 4-styrenesulfonate) (PSS) are not known as biodegradable polyelectrolytes, they have been used as LbL components for tissue engineering *in vitro* studies [29-31]. A qualitative study has investigated the LbL surface deposition of these polyelectrolytes on PCL nanofiber films [32]. Also, due to the fact that the PCL film is only weakly charged at the surface, this previous study lacks solid proof of the efficiency of the depositions. Chitosan, an important member of the polysaccharide family, is derived from the cuticle of crustaceans and has been widely used in various biomedical applications such as tissue engineering, drug delivery systems and wound dressing [33-35]. Also, glycol-chitosan/hyaluronic acid polyelectrolyte multilayer films have been recently used as a substrate mediated gene-delivery system [36]. Recent findings demonstrated that chitosan promotes bone formation through differentiation of human bone mesenchymal stem cells (h-BMSCs) via the upregulation of genes associated with calcium binding and mineralization [37]. While Guzman et al. showed that chitosan microparticles inhibit mineralization of hBMSCs [38], Amir et al. demonstrated that chitosan particles permit biomineralization of macaque dental pulp stromal cells [39]. With a high positive charge density in acidic solutions, chitosan can therefore be used as an apt polyelectrolyte osteogenic surface, provided it can be firmly adsorbed to a surface of adequate negative charge. Moreover, due to its degradation at low temperatures, chitosan is not melt processable and it is therefore deprived of the versatile structures provided by melt blending techniques.

In this study the objective is to use the LbL approach to manipulate the electric charge of the internal surface of a fully interconnected, porous 3D PCL construct, in order to be able to deposit chitosan as the bioactive macromolecule that provides hydrophilicity to the PCL surface. The rigorous examination of the LbL self–assembly process and the homogeneity of the chitosan deposition will be examined and compared to a classic dip-coating technique.

5.2 Materials and Methods

5.2.1 Materials

The commercial-grade poly(ε-caprolactone) (PCL, CAPA 6800, M_w=80kDa) was supplied by Solvay (Brussels, Belgium). Poly(ethylene) oxide (PEO) water-soluble polymers (POLYOX™ WSR-N10, M_w=100kDa) was purchased from Dow (Midland, MI, USA). Polycation poly(dialyldemethylammunium chloride) (PDADMAC), M_w 100000–200000, and polyanion poly(sodium 4-styrenesulfonate) (PSS), M_w 70000 were purchased from Sigma-Aldrich. Autoclave-sterile solutions of 20 mg/mL chitosan (DDA=98% and pre-autoclave weight-average molecular weight M_w=237,000) and 0.9% mol/mol RITC/chitosan, (DDA=98% and M_w=237,000) were supplied by the Biomaterials and Cartilage Laboratory (BCL) at École Polytechnique de Montréal. Chitosan was amine-derivatized with rhodamine isothiocyanate (RITC) as described by Ma et al [6].

5.2.2 Blend preparation

Blends of PCL and PEO were prepared at 45PCL/55PEO vol% in a Brabender internal mixer under a constant flow of dry nitrogen in order to prevent the thermo-oxidative degradation of components. The mixing was carried out at 100°C for 7 minutes with a rotation speed of 50rpm. The blends were quenched in liquid nitrogen right after mixing in order to freeze-in the morphology. The amount of material in every batch of mixing was maintained at 80% of the total capacity of the internal mixer. All the concentrations are reported as volume percent.

5.2.3 Annealing

For the purpose of increasing the phase sizes, static annealing of the blends was performed in a compression molding press. Small pieces of the blends were cut, sandwiched in aluminum foil and subsequently transferred into the cavity of a frame. The blends and the frame were then put between the two metal plates of the press, so that the above press just touched the top of the samples while annealing took place. This arrangement imposed no external pressure on the samples and hence deformation and flow of the polymer blend were minimized. The annealing process was performed under static conditions at 160°C for 2 hours under a constant flow of nitrogen in order to reduce the risk of thermo-oxidative degradation of the blend components.

5.2.4 Scaffold preparation and designation

After annealing, samples were cut into three distinct shapes: 1) 3D porous cubes of $5\times5\times5$ mm^3 dimension (razor cut); 2) 2D solid discs of 3mm in diameter and 2mm in thickness were mechanically punched from larger PCL discs and trimmed on the side with a fresh razor blade; and 3) large 3D porous substrates of 2cm (l) x 2cm (w) x 1cm (h). The 3D porous cubes and 2D solid discs were used for surface characterization. The 2D solid discs allowed for a more simplified and intermediate modeling step for the ToF SIMS and XPS of dip coated and LbL depositions. The use of the large 3D porous substrates was for the LbL gravimetric study in order to build up sufficient quantities for measurement.

5.2.5 Solvent extraction

The PEO porogen phase was selectively extracted from the 3D samples for 7 days in 50mL of deionized water at ambient temperature under constant shaking. Water was refreshed twice in this period. After the extraction, the samples were dried for 24h at 40°C in a vacuum oven.

5.2.6 Surface modification via dip coating and LbL deposition of polyelectrolytes

Dip-coating of pure PCL scaffold in chitosan was first tested as a coating strategy. PCL scaffolds were dip-coated by submerging in 300 µL of 50 µg/mL unlabeled (pH=4) or RITC-labeled chitosan solution (pH=5.6) and incubated at 37°C for 1 hour, followed by rinsing in cell culture media for 1 hour and air drying overnight. RITC-chitosan was only used for fluorescent microscopy.

PDADMAC polycation and PSS polyanion were used in aqueous solution containing 10 mg/mL of polyelectrolyte, 1 M NaCl, adjusted to pH=8 with NaOH, or pH=2 with HCl. A pH of 8 was selected for the precursor PDADMAC solution according to the work done by Manso et al [40]. In that study it was shown that at high pH values the zeta potential of PCL film lies at its highest negative values which is an indication of considerable negative surface charge. Also, pilot studies showed that a pH of 8 leads to the highest mass increase after the PDADMAC precursor layer deposition (Data not shown). These polyelectrolytes were used to alter the surface charge of the different PCL polymeric substrates. PCL samples (discs and cubes) were exposed to PDADMAC and PSS polyelectrolyte solutions with pH=2 for 1 hour. After each polyelectrolyte deposition, a water rinsing step was performed for 1 hour. In order to always keep the substrates in contact with the solution and increase the contact surface, metal wires were used to prevent the samples from floating. LbL deposition was performed on substrates up to layer n=4 and n=8 with PSS as the final deposited layer. Samples were then dipped in 2 mg/mL chitosan solution pH=4 for 4 hours at 37°C as the concluding layer followed by water rinsing for 1 hour.

5.2.7 Gravimetric measurements

In order to have a quantitative evaluation of the layers deposited on the surfaces of the large 3D porous PCL substrates, gravimetric measurement was done on a dedicated set of scaffolds following the deposition of each layer, deionized water (dd-H2O) rinsing and vacuum drying for 3 hours. The values are reported as the percentage of mass increase as compared to the initial sample weight. The experiment was repeated three times.

5.2.8 Fluorescent microscopy

3D porous cubes of pure PCL scaffold were dip-coated in RITC-chitosan solution, after which they were then cut in half and the transverse cross-section was imaged with an inverted Zeiss Axiovert fluorescence microscope (EC Plan-Neofluar 1.25x/0.3 NA objective, Carl-Zeiss Canada, Toronto, Ontario, Canada), CCD Hitachi camera (Tokyo, Japan), and Northern Eclipse software (Empix, Mississauga, Ontario, Canada). For the sake of comparison, the exposure settings on the Northern Eclipse software were kept constant for both cases of before and after RITC-chitosan dip-coating.

5.2.9 Time of flight secondary ion mass spectrometry (ToF-SIMS)

ToF-SIMS studies were performed on 2D solid discs dip-coated in chitosan by a ToF-SIMS IV (IONTOF, GmbH, Münster, Germany). Oxygen was leaked in the analyzing chamber to a pressure of 2×10^{-7} Torr during the measurements in order to limit surface charging of the sample. Samples were bombarded with Bi1 primary ions at an energy level of 15 keV in bunch mode with a pulse of 19.9 ns. The gun operated with a 2.3 pA pulsed ion current over a frame area of 500 μm × 500 μm for a dosage below the threshold level of 5×10^{11} ions/cm^2 for static SIMS. Measurements were taken with an acquisition time of 100 s. The maximum mass resolution, $R = m/\Delta m$, was ≥ 9000 on $29Si^+$, where m is the target ion mass and Δm is the resolved mass difference at the peak half-width. Effective charge compensation was obtained using the electron flood gun. Positive and negative ion spectra were calibrated using H^+, H_2^+, H_3^+, $C_xH_y^+$ and C^-, CH^-, C_2^-, C_2H^-, C_3^- and C_3H^- peaks, respectively. Integration of the signals was performed using the Poisson correction.

5.2.10 X-ray photoelectron spectroscopy (XPS)

The chemical composition of the coatings on 2D solid discs dip-coated with chitosan, and 3D porous cubes with LbL-only or LbL-chitosan coatings, were examined by X-ray photoelectron spectroscopy (XPS). An ESCALAB MKII apparatus (VA Scientific Limited, U.K.) was used to analyze the relative concentration of C, O, N and S according to their respective peaks. An Mg Kα X-ray source (hυ = 1253.6) with an analyzer pass energy of 100 eV was operated at 12 mA and 18 kV. For all the measurements, an ultrahigh-vacuum (UHV) chamber with a base pressure of less than 10^{-8} Torr was utilized. For the whole experiment, the binding energy of the C 1s core levels (285 eV) was used as an internal standard to determine the charge shift. Various elemental analyses were performed on cube and disc shaped PCL substrates with and without polyelectrolyte/chitosan coatings. Relative atomic concentration (%) is calculated with respect to the total number of present atoms (except H and He). For 2D solid discs and 3D porous cubes, measurements were done on right, center and left positions of each sample. As for the 3D porous cubes, regional relative atomic concentration were also measured in 1/4 thickness from the top and in the middle (1/2 from the top) level of the cubes as well as the top surface, in order to evaluate the existence of a homogeneous chitosan layer in the depth of a porous structure.

5.2.11 Scanning electron microscopy

2D solid discs and 3D porous cubes coated by LbL were treated with a gold-palladium alloy by plasma deposition and observed by a FEG-SEM scanning electron microscope, type JEOL(JSM-7600TFE), operated at a voltage of 2 keV–5 keV. SigmaScan Pro software was used for image analysis to determine the thickness of the layers deposited on the substrate.

5.3 Results and discussion

5.3.1 Dip coating pure PCL in slightly acidic chitosan solutions leads to an inhomogeneous surface coating

5.3.1.1 Fluorescent microscopy

Figure 5.1 demonstrates the fluorescent imaging of 3D porous cubes before and after dip-coating in RITC-chitosan. It is evident that there is an attractive driving force between the PCL surface and the RITC-chain molecules.

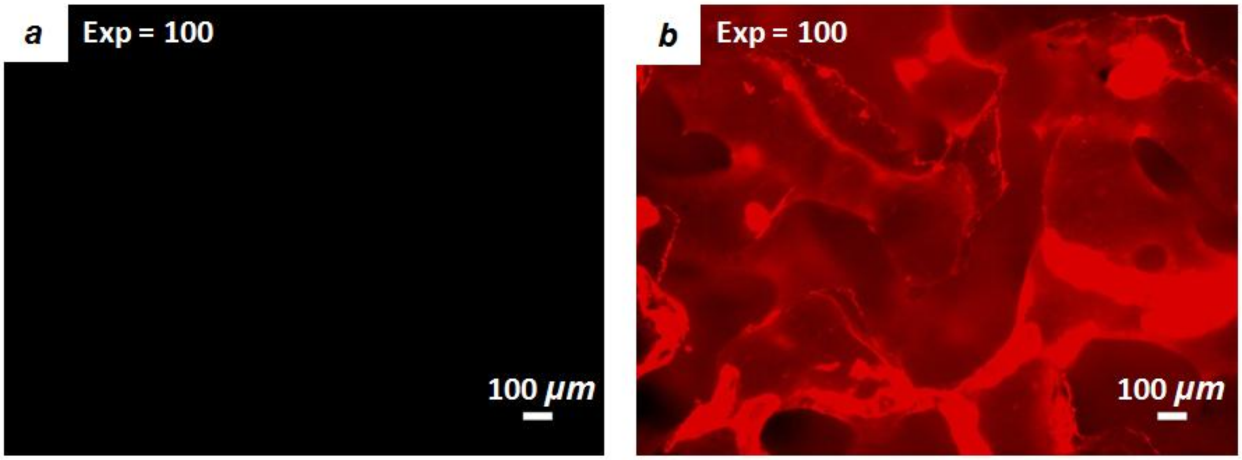

Figure 5.1 : Fluorescent imaging of 3D porous cubes (a) before and (b) after submersion in 50 µg/mL RITC-chitosan for 5 min, rinsing and drying. The exposure was maintained constant to permit a direct comparison

The red signal in this figure is RITC-chitosan, which clearly shows that even by using a very dilute solution of RITC-chitosan, and after rinsing and drying in the dip-coating procedure, there is an RITC-chitosan layer retained on the PCL scaffold surface. Since it is well known that chitosan contains positively charged amine groups at low pH [41] and PCL as a polyester contains partially negatively charged oxygen atoms in its carboxylic groups, the potential exists for electrostatic attraction. Manso et al. reported negative values of zeta potential in a wide range of pH for PCL films, which are in close relationship with their surface charge [40]. While this figure provides clear evidence that chitosan can bind to the PCL surface with a simple dip coating technique, it does not give any information on the quantity or surface homogeneity of the coating formed.

5.3.1.2 XPS and ToF-SIMS analysis

For PCL substrate surfaces coated with chitosan, the only source for nitrogen atoms is from the chitosan itself because PCL is devoid of nitrogen. Therefore, such nitrogen specificity can be used as a probe for the detection of chitosan at the surface by surface characterization techniques such as XPS or ToF-SIMS. Relative nitrogen concentrations (%) on two distinct 2D solid discs (PCL1 and PCL2) are shown in Figure 5.2b according to the positions 1, 2 and 3 depicted in Figure 5.2a.

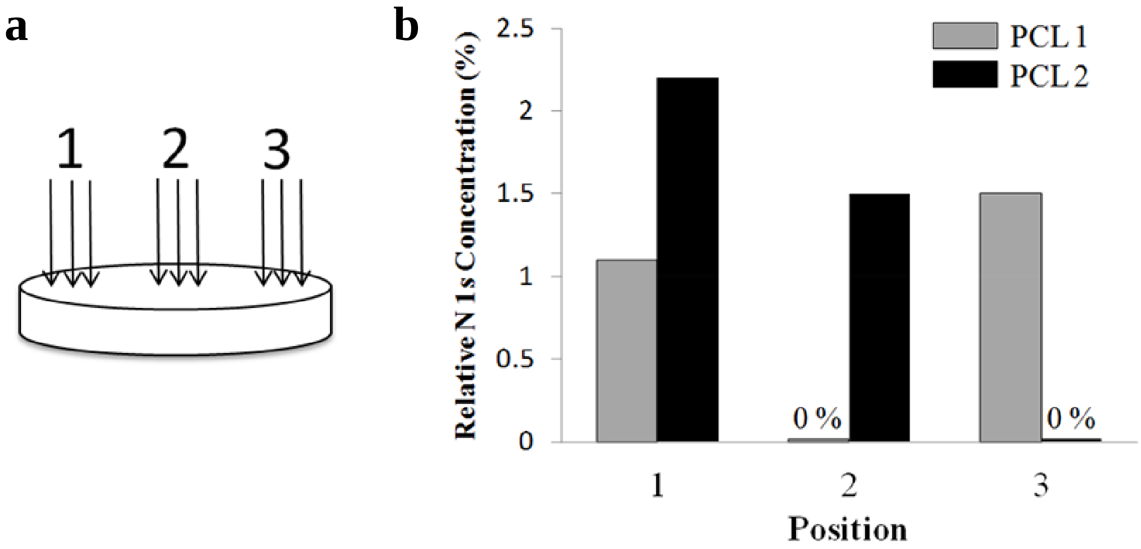

Figure 5.2: Evaluation of coating homogeneity using the dip-coating strategy on 2D solid discs of pure PCL: (a) Schematic of the 2D solid discs with X-ray emission at positions 1,2 and 3, (b) XPS measurements of the relative nitrogen concentration (%) on two identical random discs (PCL1 and PCL2) at positions 1, 2 and 3

PCL1 and PCL2 were subjected to exactly the same preparation process and dip-coating conditions nevertheless they clearly show non-uniform and more importantly zero chitosan depositions at different positions on the samples, i.e. for PCL1 there is no deposition detected at the center of the disc, whereas for PCL2, an absence of chitosan is recorded near the edge. These results demonstrate that the coating is deposited in a random non-homogeneous fashion with some areas rich, some poor and some even devoid of chitosan coating.

Figure 5.3 illustrates high resolution ToF-SIMS images of the surface distribution of $C_6H_{11}O_3^-$ and CNO^- ions that are specific to PCL and chitosan molecules, respectively.

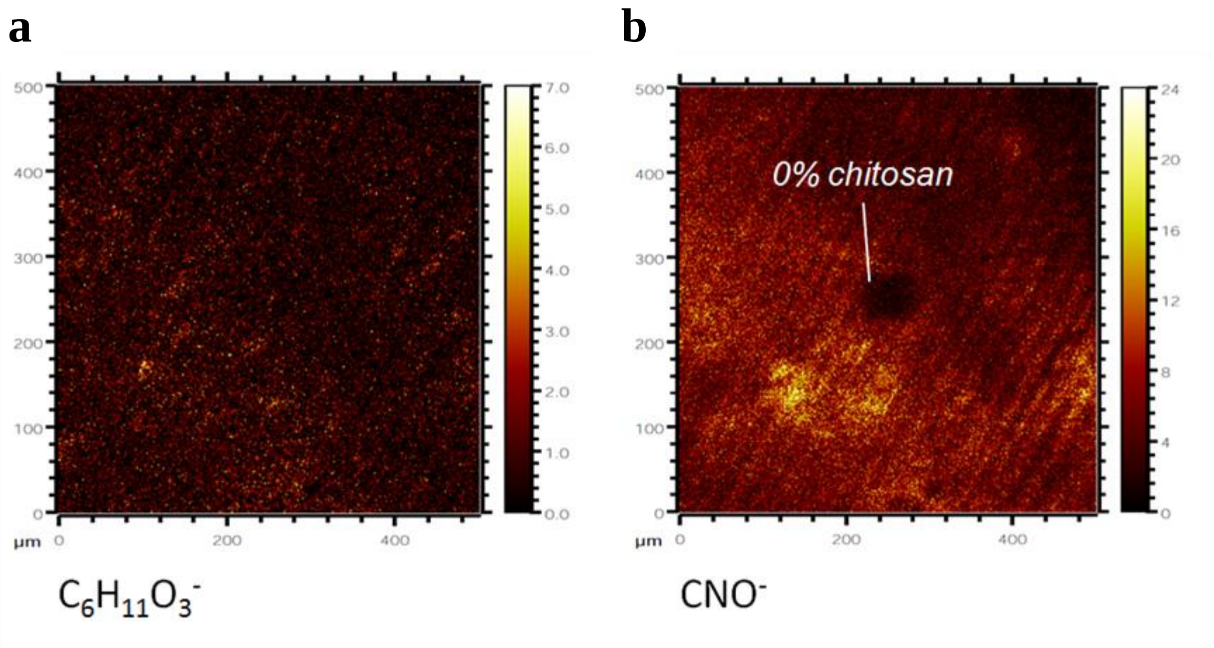

Figure 5.3: ToF-SIMS Analysis of (a) $C_6H_{11}O_3^-$ as the characteristic ion for PCL and (b) CNO^- as the characteristic ion for chitosan on the coated samples

While characteristic ions of PCL are distributed evenly across a 500 µm x 500 µm surface area, there is a large regional variation of concentration intensity of chitosan specific ions, i.e. the chitosan concentration appears to be higher on the bottom left corner of the coated surface (yellow areas, potentially chitosan aggregates), as opposed to the top right corner where a low amount of chitosan is detected. Also, in the center, zero CNO^- ions are detected, whereas in the same area, the presence of $C_6H_{11}O_3^-$ ions is evident, which shows that chitosan deposition failed in this specific position. Previously, negative zeta potentials for PCL nanofiber scaffolds have been measured which clearly demonstrates that the negative carbonyl oxygen is present at the surface [42, 43]. Clearly, the dip coating strategy carried out in this work fails to deposit a controlled homogeneous chitosan coating on both 2D solid discs of pure PCL. The principal explanation for the failure in achieving homogeneous layer deposition via the simple dip-coating technique is that the PCL surface is only slightly negatively charged [44] and the interaction with the positive charge on the chitosan chain is not strong enough. Evidently, the PCL surface will need to be modified in order to generate strong interactions with the positively charged chitosan. Ideally, such powerful bonds should exist throughout the scaffold area at various depths of the structure, i.e. the cells for future seeding experiments should all be in contact with such uniform chitosan coating layer all through the scaffold thickness. In the next section we examine the potential of LbL surface deposition of polyelectrolytes in order to prepare a more uniform chitosan surface coating.

5.3.2 LbL surface deposition of polyelectrolytes

5.3.2.1 Gravimetric measurements

Figure 5.4 illustrates the mass increase percentage after the deposition of each layer on the PCL surface followed by rinsing and freeze drying. In this figure, odd and even layer numbers are associated with the addition of the PDADMAC polycation and PSS polyanion, respectively. This graph determines the efficacy of LbL depositions and also how effective the polyelectrolytes are in building up layers on the surface of the PCL porous polymer. According to Figure 5.4, three characteristic regions can be distinguished: Region I, comprised of layers 1-3 includes a window of deposited layers with a % mass increase slope value of as low as 0.2% per added layer. It appears that indistinct interpenetrating layers are formed in this region likely resulting from a balanced, as opposed to a distinct and alternating charge deposition. Therefore, this window of initial disordered layers is named “Surface Preparation” region. The existence of a region of precursor layers with equal slopes for % mass increase was also witnessed in previous work by Roy et al which could be due to the interdiffusion of PDADMAC and PSS layers [45]. After the addition of the fourth PSS layer, there is an approximately 2-fold rise in the % mass increase of the samples, which leads to the formation of a transition Region II, comprised of layers 3-5. This region could potentially be attributed to the onset of the layer buildup phenomenon, where layer deposition starts to achieve a certain uniformity. It is clear that in Region III, comprised of layers 5-8, a significant and much more uniform buildup of layers is observed. In this latter window of layer depositions, therefore, it is believed that the polyelectrolytes transit from an interdiffusion of adjacent layers at low deposition number to apparently more well-defined layers at higher layer deposition numbers. Further analysis was carried out to confirm this hypothesis. The slopes of % mass increase highly depend on the internal surface, material density and surface charge, and therefore are different from polymer to polymer even when using the same polyelectrolytes. For instance, the three regions observed in Figure 5.4 for PCL were not observed in a previous work in this laboratory when depositing the same LbL coating on PLLA and HDPE substrates [46]. However, the slopes for the addition of PDADMAC and PSS layers on the PLLA substrate in that study are in accordance with the slopes obtained in Figure 5.4 where the addition of PSS leads to a higher mass increase than that of PDADMAC.

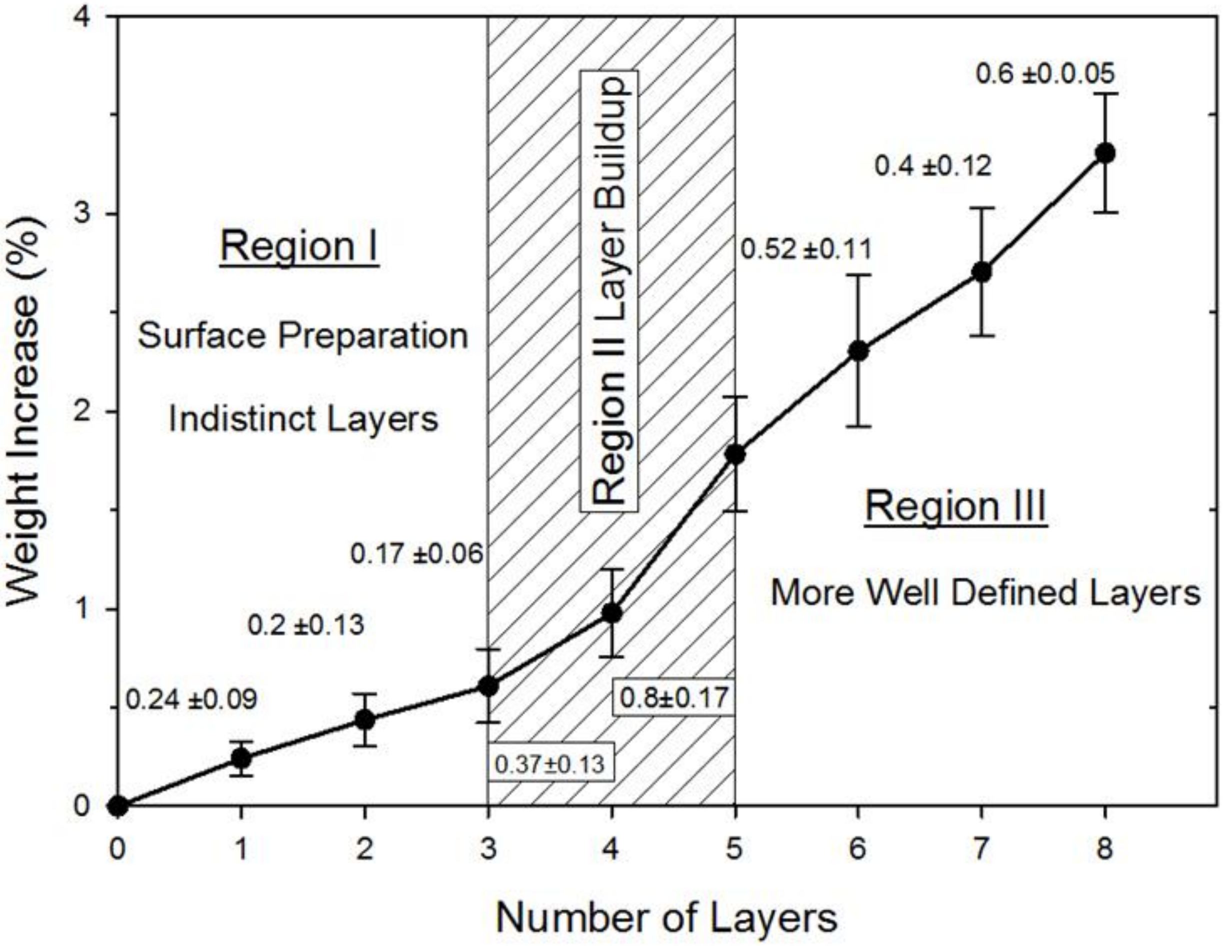

Figure 5.4: Weight increase (%) of large 3D substrates as a function of the number of deposited polyelectrolyte layers in the LbL approach. Odd and even layer numbers represent PDADMAC and PSS depositions respectively. Three main regions are detected according to point to point

slopes: Region I or the surface preparation region where interpenetration of layers is dominant. Region II as an onset for layer buildup phenomenon, and Region III where more well-defined layers are established

5.3.2.2 XPS analysis of the layers

In order to verify the results obtained by gravimetry, a more detailed surface characterization study by XPS was performed on the layers deposited by the LbL technique. Samples with four and eight deposited polyelectrolyte layers were considered in this experiment. Elemental relative compositions of carbon, oxygen, nitrogen and sulfur atoms were quantified according to C 1s, O 1s, N 1s and S 1s spectra given by XPS. It should be noted that after four or eight layers, PSS is the final layer deposited on the structure. In this study, the fourth and eighth layers fall into Region II and Region III of Figure 5.4, respectively. Figure 5.5 illustrates the chemical structure and molecular formula of PDADMAC and PSS.

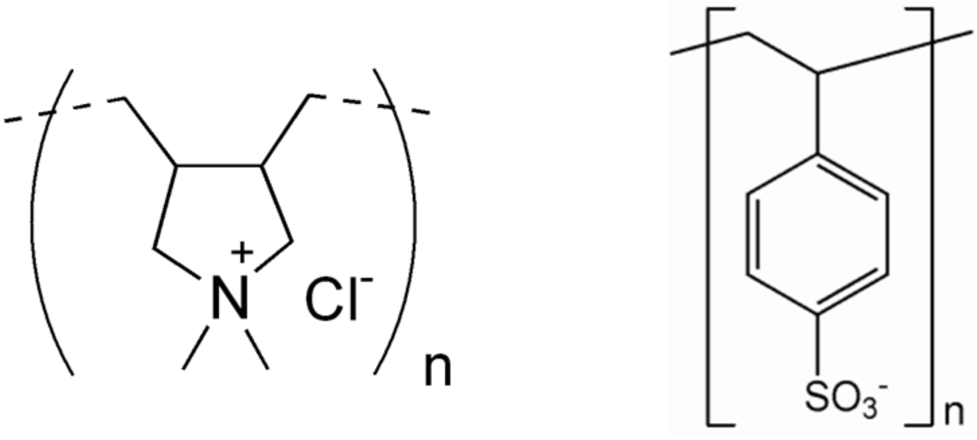

PDADMAC (+) PSS (-)

Figure 5.5: Chemical structures of PDADMAC and PSS polyelectrolytes

Figure 5.6 summarizes the O 1s:C 1s, N 1s:C 1s and S 1s:C 1s ratios after n=4 and n=8 layers are deposited. The XPS apparatus typically provides information about the elemental composition up to a maximum of 10 nm from the top surface. Bragaru et al. report on the average thickness of individual PSS or PDADMAC layers, on silica as being between 4.5-6.5 nm [47]. Roy et al.

report a thickness of 100 nm for 1 layer of PSS, 5 layers of PDADMAC and 4 layers of bovine serum albumin. When PSS and PDADMAC films are deposited in the presence of salt, as is the case in this study and all the studies reported above, the thickness of the layers has been reported to be as high as 15 nm per layer [48]. The thickness of individual PSS or PDADMAC layers established on silicon wafers according to the conditions used in this study (polyelectrolyte and salt concentrations) was approximately 5.6 nm [48]. Hence, although some XPS signal could potentially also be detected from the layer underneath the final layer [25], the principal peaks should be from the outer layer.

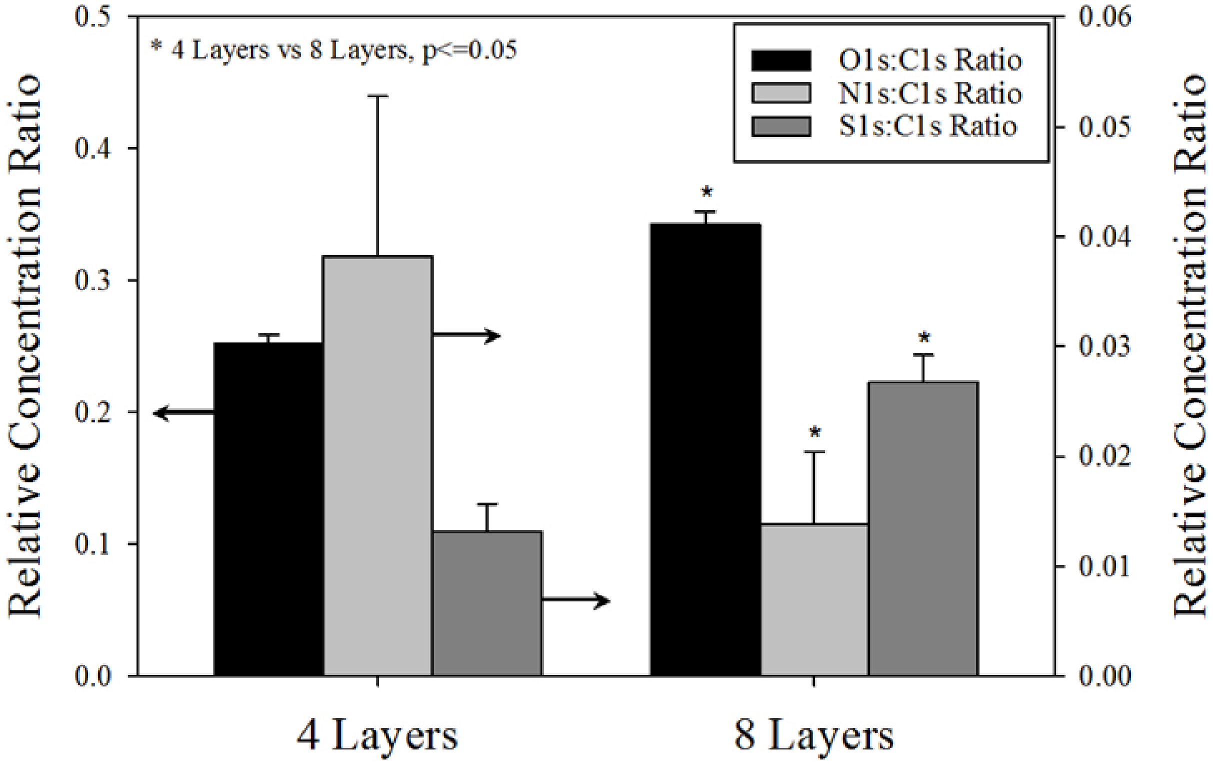

Figure 5.6: Effect of the number of deposited layers on the atomic composition of the outermost layers on the 2D solid disc substrate. n=4 and n=8 both represent PSS as the outermost layer. Data shown as mean ± standard deviation, N=3

This XPS study on 2D solid discs comparing layers 4 and 8 is used to confirm the observation that layers 5-8 are more distinct as presented in Figure 5.4. Figure 5.6 clearly shows that this is the case with a decrease in the N 1s:C 1s ratio (specific to PDADMAC); and an increase in the O

1s:C 1s and S 1s:C 1s ratios (specific to PSS). The O 1s:C 1s ratio increases from 0.25 after the deposition of 4 layers to 0.34 after that of 8 layers. This recorded ratio is very close to the actual value for the PSS repeating unit molecule which is 0.37. Moreover, knowing that the only source for the nitrogen atom in the polyelectrolyte assemblies is the PDADMAC polymer chain, low values for the N 1s:C 1s ratio necessarily concludes that the PDADMAC layer is well masked below the final PSS layer. A 60% reduction in the N 1s:C 1s ratio after 8 layers as compared to 4 layers indicates that the level of interdiffusion of PDADMAC polymer chains within those of the PSS has been dramatically reduced. Furthermore, the sulfur atom is only specific to the PSS repeating unit and, as a result, the higher the value of S 1s:C 1s and the closer it gets to 0.125 which is the value of the mentioned ratio in PSS molecule, the more distinct the final PSS layer becomes and the more homogeneous the negative surface charge is distributed. Figure 5.6 shows that the S 1s:C 1s ratio doubles when going from layer 4 to layer 8 again confirming the formation of more distinct PSS chains on the PCL surface. Data in Figure 5.6 therefore support the concept presented in Figure 5.4 of poorly defined polyelectrolyte layers 1 to 4 that become more well-defined as the number of layers is increased. However, Figure 5.6 demonstrates that even at 8 layers a significant level of interpenetration of layers is still occurring. In a recent work, Gilbert et al. also used the XPS approach for the analysis of interlayer diffusion in polyelectrolyte multilayers (PEMs) [25]. It has been reported that for the case of classic layer-by-layer deposition where strong polyelectrolytes such as PDADMAC and PSS are used, discrete polyelectrolyte layers are formed [49]. Our surface analysis studies demonstrate that the formation of more distinct layers in LbL occurs at higher numbers of layer depositions, whereas interdiffusion of layers always exists.

Having determined the optimal conditions for the LbL self-assembly of polyelectrolytes on the co-continuous PCL structure, the quality of the chitosan coating on the final negative layer has to be evaluated. To do so, three different cases were considered: 2D solid discs (2D-nonporous) as the positive control; top section of 3D porous cubes (Top-3D); and the middle section of the same samples (Inside-3D). The amount of chitosan coating on the top section of the scaffold is of importance, as it is the first part of the scaffold with which the cells establish initial contact post-seeding. Obtaining a homogeneous chitosan coating in the middle section of the scaffolds is of equal significance as the cells migrate toward deeper levels and therefore has to be taken into consideration in this study.

Figure 5.7 demonstrates XPS spectra for a 2D solid discs coated with chitosan by the LbL technique (LbL-chitosan), where the N 1s peak is evident at 401 eV as compared to 2D solid discs of PCL with LbL coating but without the addition of chitosan (LbL-only) where the nitrogen peak is present due to the existence of nitrogen containing PDADMAC underneath the final PSS layer but it appears to be very weak. The addition of chitosan on the LbL modified PCL amplifies the nitrogen on the surface which clearly points to a successful surface deposition.

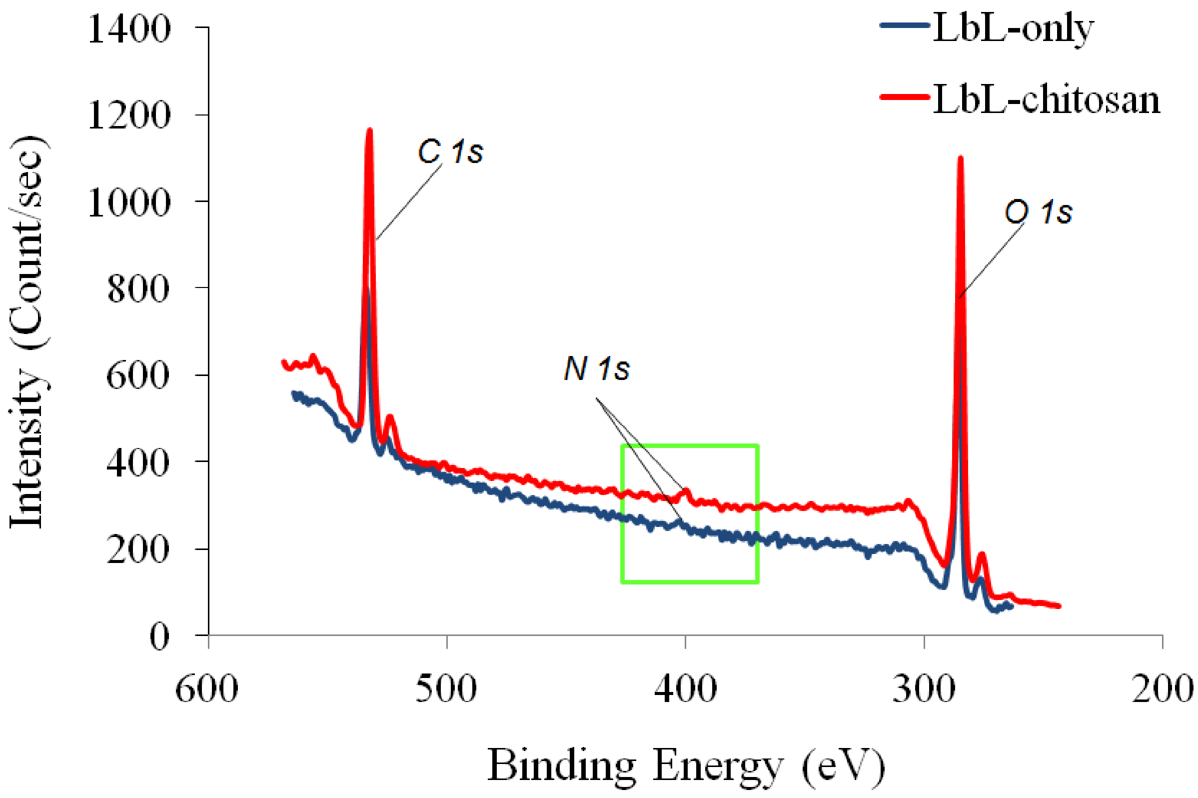

Figure 5.7: Efficiency evaluation of the chitosan layer deposition via the LbL approach on 2D solid discs: XPS spectra of neat and 8 layer LbL coated PCL. Nitrogen peak is observed at 401 eV for the coated sample

Local chitosan deposition by the LbL strategy on two identical 2D solid discs (designated as PCL1 and PCL2) is demonstrated in Figure 5.8 according to the same positions (1, 2 and 3) depicted in Figure 5.2a. The XPS results for the N 1s concentration after chitosan surface modification by LbL at the different positions in the disks show that none of the areas sampled have zero depositions with the LbL technique and indicate a homogeneous local distribution, as opposed to the dip-coating strategy (Figure 5.2b).

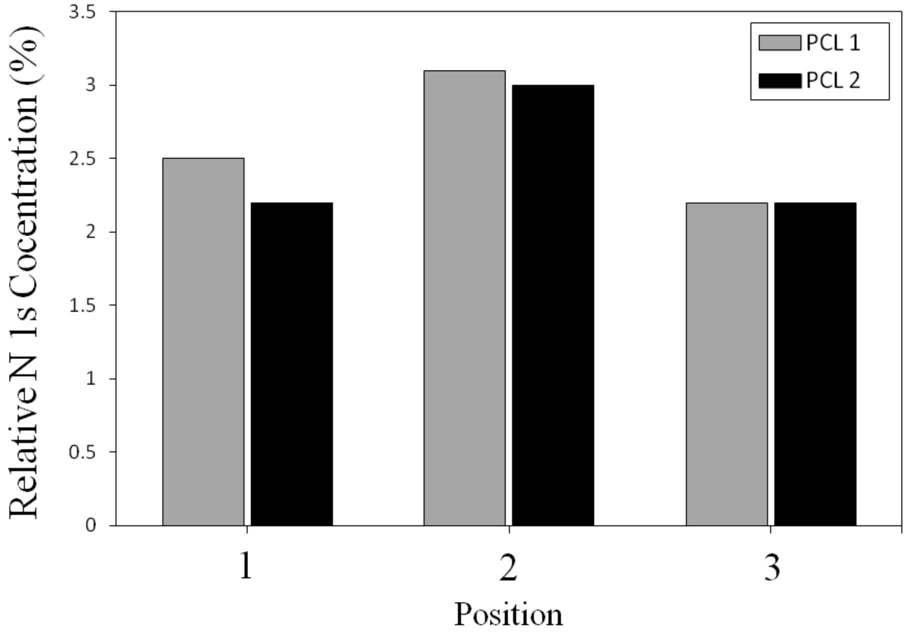

Figure 5.8: XPS measurements of the relative nitrogen concentration (%) on two random discs (PCL1 and PCL2) at positions 1, 2 and 3 mentioned in Figure 5.2a

Figure 5.9 summarizes the XPS readings of the relative nitrogen concentration % on the examined surfaces of 2D-solid, Top-3D porous cube and Inside 3D porous cube samples after chitosan surface modification by LbL. According to Figure 5.9, a high level of chitosan is detected on the surface of the 2D-solid, Top-3D cube and Inside 3D cube samples. This indicates a successful penetration of the LbL chitosan right into the middle of the 3D construct. It can also be seen that the nitrogen concentration decreases by 60% in going from 2D-solid to Top-3D cube to inside 3D cube. This decrease is expected due to the porous nature of the 3D construct. The 2D solid disc has no pores and possesses an even horizontal surface available for chitosan deposition and subsequent analysis. In the Top 3D cube sample the surface is porous, i.e. some of the top surface is horizontal/flat and the rest of the signal comes from pore depressions along the horizontal surface. Lastly the Inside 3D cube sample only provides the porous surface for chitosan deposition and the signal comes from the surface of pores that are oblique to the horizontal surface.

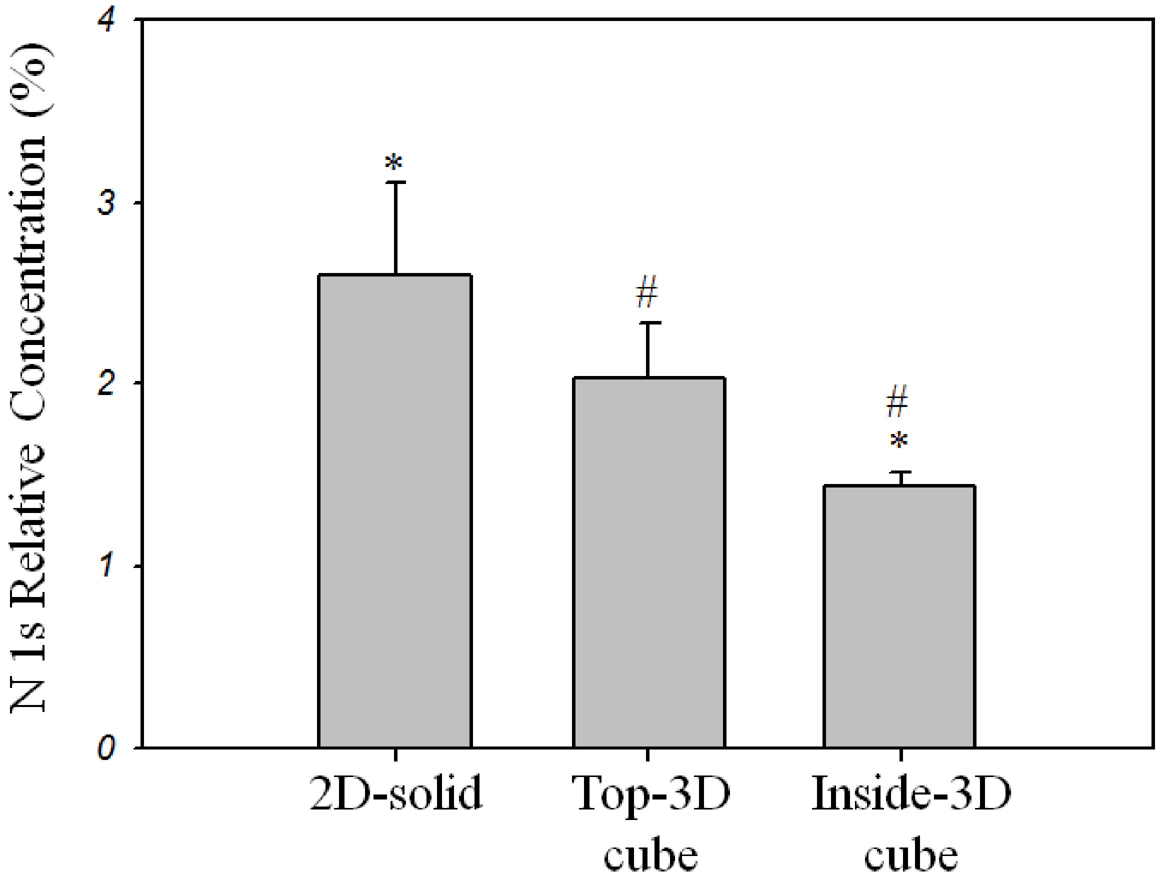

Figure 5.9: Effectiveness of chitosan coating by using the LbL approach in 3D porous cubes: Relative nitrogen concentration (%) on 2D solid discs (2D-solid) as the positive control; top section of 3D porous cubes (Top-3D cube); and the middle section of the same samples (Inside-3D cube). Data shown as mean ± standard deviation, N=3. Bars with the same symbols (*, #) show significant differences with $p < 0.05$

The X-ray emission at different positions and different depths for 3D porous cubes are illustrated in Figure 5.10a. Relative nitrogen concentrations are demonstrated in Figure 5.10b according to the positions 1, 2 and 3 and depths A, B and C. Levels D and E were not considered because due to symmetry they are redundant with A and B. Our results show a relatively uniform local distribution of chitosan with at least 1% relative nitrogen concentration (chitosan) detection at all the scanned points within the cubic construct. Also, the drop in the level of chitosan deposition is evident at levels B and C, in comparison to level A (Top-3D). There is no significant difference between the amounts of chitosan detected by the XPS at levels B and C. Our results show that chitosan can be uniformly deposited on a co-continuous porous structure even at deep levels of 3D porous cubes with the LbL self-assembly of polyelectrolytes.

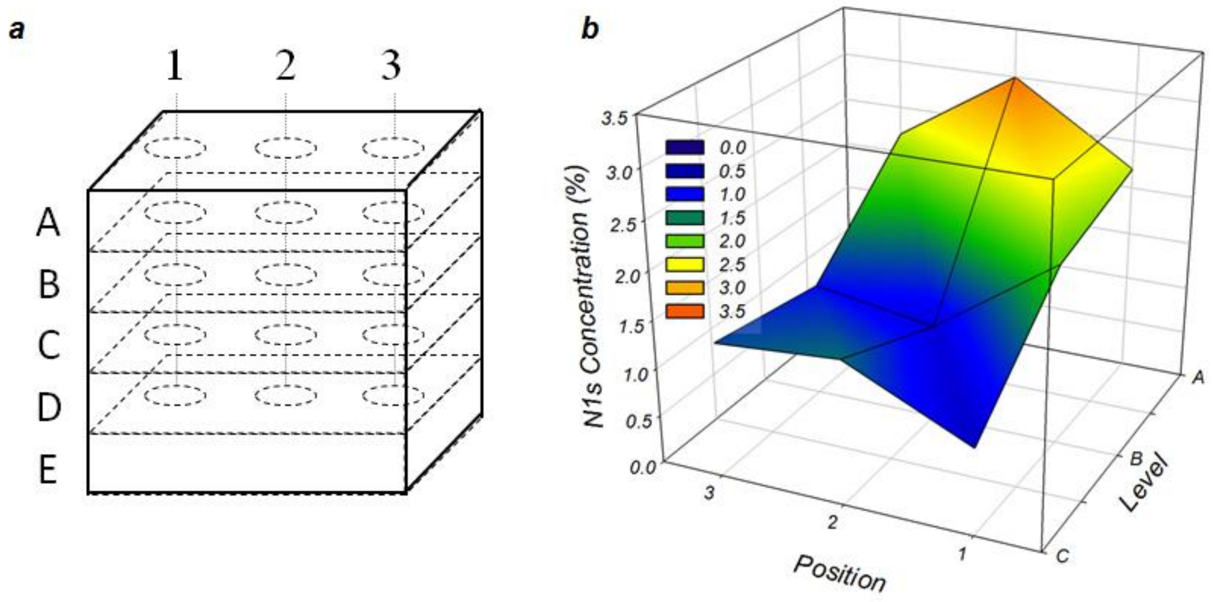

Figure 5.10: (a) Schematic of the 3D porous cubes with X-ray emission at different positions and different depths. (b) Local distribution of the LbL coated chitosan by XPS measurements performed at positions 1,2 and 3 and at levels A, B and C. At least 1% of chitosan was detected at all the scanned points

5.3.2.3 Scanning electron microscopy

SEM image on Figure 5.11a provides the morphology of the assembly of 8 polyelectrolyte layers with the final addition of chitosan on 2D solid discs. According to this figure, the assembly of layers form a microscopically rough surface morphology. The partial detachment of the layers for microscopic observation can be attributed to sample cutting by razor. Image analysis on high resolution FEG-SEM images demonstrated that the thickness of the multilayer assembly ranges from 550 up to 700 nm. Considering that the average layer thickness for PSS or PDADMAC is between 4.5-6.5 nm per layer [47, 48], the measured thickness in this study could mostly be attributed to chitosan. Furthermore, SEM imaging of PCL with the LbL coating (Figure 5.11b) clearly demonstrates that the addition of chitosan creates the observed surface roughness. According to Deligianni et al., cell adhesion and proliferation of human bone marrow cells increased with the level of roughness on hydroxyapatite surfaces [50]. Thus, the surface roughness observed in this surface preparation approach may have advantageous effects for the adhesion and proliferation of cells.

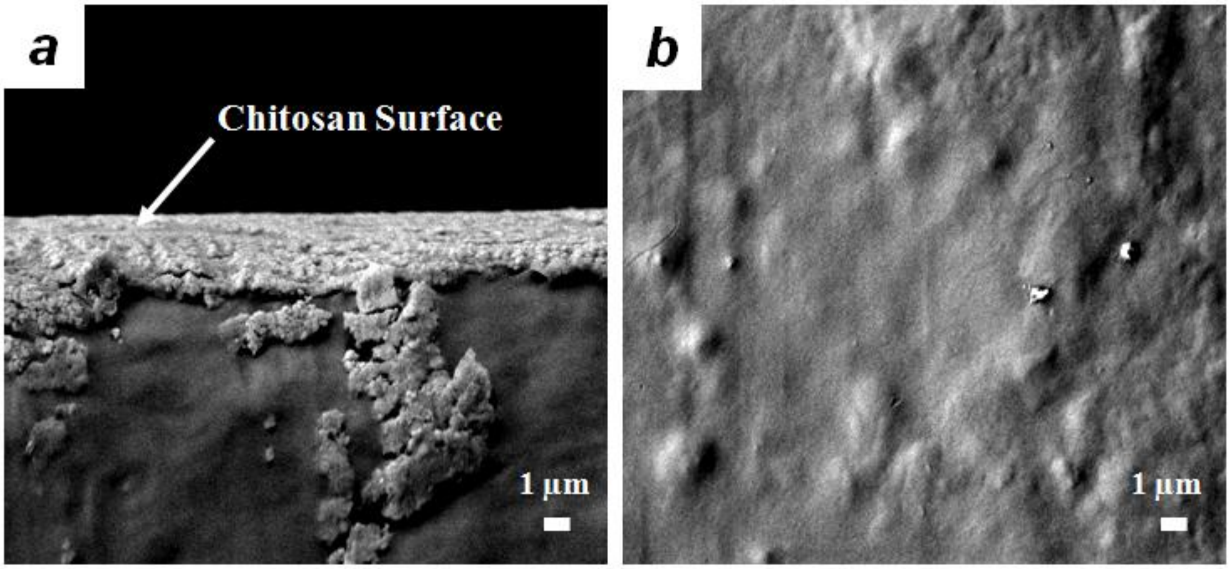

Figure 5.11: FEG-SEM images of the LbL chitosan coated sample: (a) Microscopic roughness of the final layer assembly. An average thickness value of 610 nm was estimated using image analysis; and (b) Pore surface of a 3D porous cube after LbL but without chitosan coating. The scale bar represents 1 micron

5.4 Conclusion

To our knowledge, a thorough investigation of chitosan coating on porous PCL constructs using LbL self-assembly of polyelectrolytes has never been done. PCL structures of highly controlled morphologies using co-continuous polymer blends have been tested via dip-coating and LbL in both 2D and 3D for the evaluation of the efficacy of chitosan coating. Gravimetric measurements, fluorescence microscopy, ToF-SIMS analysis, x-ray photoelectron spectroscopy and scanning electron microscopy were used to examine these deposition strategies. The classic dip coating technique succeeded in the deposition of chitosan on PCL scaffolds due to the intrinsic attraction between the positively charged chitosan and slightly negatively charged PCL, but failed to produce homogeneous deposits, and hence areas devoid of chitosan were detected. In the layer-by-layer deposition approach, gravimetric measurements revealed the existence of three main regions according to the number of assembled layers: a surface preparation region comprised of indistinct layers; an onset region for layer buildup; and a more well-defined layer region. The existence of these regions was strongly suggested by higher Sulfur/Carbon and lower Nitrogen/Carbon ratios for 8 layers of polyelectrolytes as compared to 4 layers reflecting a more uniform PSS final layer. The LbL strategy was found to be superior to the dip-coating technique since uniform local deposition of chitosan was observed in both 2D solid discs and 3D porous cubes at various depths within the scaffolds. SEM imaging revealed that there is a microscopically rough coating ranging in total thickness from 550 to 700 nanometers. This layer thickness appears to be principally related to the chitosan part of the coating. This study proposes an adaptation of the LbL technique as a solution to the existing issues related to chitosan coating, such as heterogeneous local distribution in virtually 3D constructs, and provides characterization and analysis techniques to support the methodologies used. This work shows that the LbL technique of polyelectrolyte deposition followed by chitosan addition provides a route towards stable and homogeneous surface modification and has the potential to transform a classic fully interconnected porous synthetic PCL polymer material to one with essentially complete chitosan-like surface characteristics. In a future work, the produced scaffolds with hydrophilic chitosan coating will be put into practice in order to evaluate their potential to support human mesenchymal stem cell osteoblastic differentiation and biomineralization.

Acknowledgements

The financial support of the Natural Sciences and Engineering Research Council of Canada (NSERC) through its Network for Innovative Plastic Materials and Manufacturing Processes (NIPMMP) is gratefully acknowledged. The authors would also like to thank Suzie Poulin and Josianne Lefebvre in the department of Engineering Physics at the École Polytechnique de

Montréal for their valuable assistance in the XPS and ToF-SIMS analyses. Appreciation is also extended to Guillaume Lessard for his help in the preparation of the scaffolds and Elias Mansour for his contribution in the LbL experiments.

References

1. Yoshimoto H, Shin YM, Terai H, Vacanti JP. A biodegradable nanofiber scaffold by electrospinning and its potential for bone tissue engineering. Biomaterials. 2003;24(12):2077-82.

2. Chang HI, Perrie Y, Coombes AGA. Delivery of the antibiotic gentamicin sulphate from precipitation cast matrices of polycaprolactone. Journal of Controlled Release. 2006;110(2):414-21.

3. Ng KW, Hutmacher DW, Schantz JT, Ng CS, Too HP, Lim TC et al. Evaluation of ultra-thin poly(epsilon-caprolactone) films for tissue-engineered skin. Tissue Engineering. 2001;7(4):441-55.

4. Alves da Silva ML, Martins A, Costa-Pinto AR, Costa P, Faria S, Gomes M et al. Cartilage Tissue Engineering Using Electrospun PCL Nanofiber Meshes and MSCs. Biomacromolecules. 2010;11(12):3228-36.

5. Diana MY, John F. Polymeric Scaffolds for Tissue Engineering Applications. Tissue Engineering and Artificial Organs. Electrical Engineering Handbook: CRC Press; 2006. p. 37-1--18.

6. Choong C, Triffitt JT, Cui ZF. Polycaprolactone scaffolds for bone tissue engineering - Effects of a calcium phosphate coating layer on osteogenic cells. Food and Bioproducts Processing. 2004;82(C2):117-25.

7. Ciapetti G, Ambrosio L, Savarino L, Granchi D, Cenni E, Baldini N et al. Osteoblast growth and function in porous poly ε-caprolactone matrices for bone repair: a preliminary study. Biomaterials. 2003;24(21):3815-24.

8. Huang Q, Hutmacher DW, Lee EH. In Vivo Mesenchymal Cell Recruitment by a Scaffold Loaded with Transforming Growth Factor [beta]1 and the Potential for in Situ Chondrogenesis. Tissue Engineering. 2002;8(3):469-82.

9. Williams JM, Adewunmi A, Schek RM, Flanagan CL, Krebsbach PH, Feinberg SE et al. Bone tissue engineering using polycaprolactone scaffolds fabricated via selective laser sintering. Biomaterials. 2005;26(23):4817-27.

10. Savarino L, Baldini N, Greco M, Capitani O, Pinna S, Valentini S et al. The performance of poly-epsilon-caprolactone scaffolds in a rabbit femur model with and without autologous stromal cells and BMP4. Biomaterials. 2007;28(20):3101-9.

11. Landis WJ, Jacquet R, Hillyer J, Lowder E, Yanke A, Siperko L et al. Design and assessment of a tissue-engineered model of human phalanges and a small joint. Orthodontics & Craniofacial Research. 2005;8(4):303-12.

12. Shao X, Hutmacher DW, Lee EH. Repair of Large Articular Osteochondral Defects Using Hybrid Scaffolds and Bone Marrow-Derived Mesenchymal Stem Cells in a Rabbit Model. Tissue Engineering. 2006;12(6):1539-51.

13. Yeo A, Wong WJ, Teoh S-H. Surface modification of PCL-TCP scaffolds in rabbit calvaria defects: Evaluation of scaffold degradation profile, biomechanical properties and bone healing patterns. Journal of Biomedical Materials Research: Part A. 2010;93A(4):1358-67.

14. Srouji S, Kizhner T, Suss-Tobi E, Livne E, Zussman E. 3-D Nanofibrous electrospun multilayered construct is an alternative ECM mimicking scaffold. Journal of Materials Science: Materials in Medicine. 2008;19(3):1249-55.

15. Sarazin P, Roy X, Favis BD. Controlled preparation and properties of porous poly(l-lactide) obtained from a co-continuous blend of two biodegradable polymers. Biomaterials. 2004;25(28):5965-78.

16. Willemse RC, Posthuma de Boer A, van Dam J, Gotsis AD. Co-continuous morphologies in polymer blends: the influence of the interfacial tension. Polymer. 1999;40(4):827-34.

17. Sarazin P, Favis BD. Morphology Control in Co-continuous Poly(l-lactide)/Polystyrene Blends: A Route towards Highly Structured and Interconnected Porosity in Poly(l-lactide) Materials. Biomacromolecules. 2003;4(6):1669-79.

18. Yuan Z, Favis BD. Coarsening of immiscible co-continuous blends during quiescent annealing. AIChE Journal. 2005;51(1):271-80.

19. Ghavidel Mehr N, Li X, Ariganello MB, Hoemann CD, Favis BD. Poly(epsilon-caprolactone) scaffolds of highly controlled porosity and interconnectivity derived from co-continuous polymer blends: model bead and cell infiltration behavior. Journal of Materials Science: Materials in Medicine. 2014.

20. Mattanavee W, Suwantong O, Puthong S, Bunaprasert T, Hoven VP, Supaphol P. Immobilization of Biomolecules on the Surface of Electrospun Polycaprolactone Fibrous Scaffolds for Tissue Engineering. ACS Applied Materials & Interfaces. 2009;1(5):1076-85.

21. Sudarmadji N, Tan JY, Leong KF, Chua CK, Loh YT. Investigation of the mechanical properties and porosity relationships in selective laser-sintered polyhedral for functionally graded scaffolds. Acta Biomaterialia. 2011;7(2):530-7.

22. Zander NE, Orlicki JA, Rawlett AM, Beebe TP. Quantification of Protein Incorporated into Electrospun Polycaprolactone Tissue Engineering Scaffolds. ACS Applied Materials & Interfaces. 2012;4(4):2074-81.

23. Fisher ER. Challenges in the Characterization of Plasma-Processed Three-Dimensional Polymeric Scaffolds for Biomedical Applications. ACS Applied Materials & Interfaces. 2013;5(19):9312-21.

24. Darain F, Chan WY, Chian KS. Performance of Surface-Modified Polycaprolactone on Growth Factor Binding, Release, and Proliferation of Smooth Muscle Cells. Soft Materials. 2010;9(1):64-78.

25. Zhu Y, Gao C, Shen J. Surface modification of polycaprolactone with poly(methacrylic acid) and gelatin covalent immobilization for promoting its cytocompatibility. Biomaterials. 2002;23(24):4889-95.

26. Zhu YB, Gao CY, Liu XY, Shen JC. Surface modification of polycaprolactone membrane via aminolysis and biomacromolecule immobilization for promoting cytocompatibility of human endothelial cells. Biomacromolecules. 2002;3(6):1312-9.

27. Edmondson S, Osborne VL, Huck WTS. Polymer brushes via surface-initiated polymerizations. Chemical Society Reviews. 2004;33(1):14-22.

28. Decher G, Hong JD, Schmitt J. Buildup of ultrathin multilayer films by a self-assembly process .3. Consecutively alternating adsorption of anionic and cationic polyelectrolytes on charged surfaces. Thin Solid Films. 1992;210(1-2):831-5.

29. Kidambi S, Lee I, Chan C. Controlling primary hepatocyte adhesion and spreading on protein-free polyelectrolyte multilayer films. Journal of the American Chemical Society. 2004;126(50):16286-7.

30. Ricotti L, Taccola S, Bernardeschi I, Pensabene V, Dario P, Menciassi A. Quantification of growth and differentiation of C2C12 skeletal muscle cells on PSS-PAH-based polyelectrolyte layer-by-layer nanofilms. Biomedical Materials. 2011;6(3).

31. Pastorino L, Soumetz FC, Ruggiero C. Nanofunctionalisation for the treatment of peripheral nervous system injuries. IEE Proceedings - Nanobiotechnology. 2006;153(2):16-20.

32. Dubas ST, Kittitheeranun P, Rangkupan R, Sanchavanakit N, Potiyaraj P. Coating of polyelectrolyte multilayer thin films on nanofibrous scaffolds to improve cell adhesion. Journal of Applied Polymer Science. 2009;114(3):1574-9.

33. Ma L, Gao CY, Mao ZW, Zhou J, Shen JC, Hu XQ et al. Collagen/chitosan porous scaffolds with improved biostability for skin tissue engineering. Biomaterials. 2003;24(26):4833-41.

34. Sinha VR, Singla AK, Wadhawan S, Kaushik R, Kumria R, Bansal K et al. Chitosan microspheres as a potential carrier for drugs. International Journal of Pharmaceutics. 2004;274(1-2):1-33.

35. Ong SY, Wu J, Moochhala SM, Tan MH, Lu J. Development of a chitosan-based wound dressing with improved hemostatic and antimicrobial properties. Biomaterials. 2008;29(32):4323-32.

36. Holmes CA, Tabrizian M. Substrate-Mediated Gene Delivery from Glycol-Chitosan/Hyaluronic Acid Polyelectrolyte Multilayer Films. ACS Applied Materials & Interfaces. 2013;5(3):524-31.

37. Mathews S, Gupta PK, Bhonde R, Totey S. Chitosan enhances mineralization during osteoblast differentiation of human bone marrow-derived mesenchymal stem cells, by upregulating the associated genes. Cell Proliferation. 2011;44(6):537-49.

38. Guzmán-Morales J, El-Gabalawy H, Pham MH, Tran-Khanh N, McKee MD, Wu W et al. Effect of chitosan particles and dexamethasone on human bone marrow stromal cell osteogenesis and angiogenic factor secretion. Bone. 2009;45(4):617-26.

39. Amir LR, Suniarti DF, Utami S, Abbas B. Chitosan as a potential osteogenic factor compared with dexamethasone in cultured macaque dental pulp stromal cells. Cell and Tissue Research. 2014.

40. Manso M, Valsesia A, Lejeune M, Gilliland D, Ceccone G, Rossi F. Tailoring surface properties of biomedical polymers by implantation of Ar and He ions. Acta Biomaterialia. 2005;1(4):431-40.

41. Pillai CKS, Paul W, Sharma CP. Chitin and chitosan polymers: Chemistry, solubility and fiber formation. Progress in Polymer Science. 2009;34(7):641-78.

42. Chen H, Fan X, Xia J, Chen P, Zhou X, Huang J et al. Electrospun chitosan-graft-poly (varepsilon-caprolactone)/poly (varepsilon-caprolactone) nanofibrous scaffolds for retinal tissue engineering. International Journal of Nanomedicine. 2011;6:453-61.

43. Vaquette C, Babak VG, Baros F, Boulanouar O, Dumas D, Fievet P et al. Zeta-potential and morphology of electrospun nano- and microfibers from biopolymers and their blends used as scaffolds in tissue engineering. Mendeleev Communications. 2008;18(1):38-41.

44. Ramgopal Y, Mondal D, Venkatraman SS, Godbey WT, Yuen GY. Controlled release of complexed DNA from polycaprolactone film: Comparison of lipoplex and polyplex release. Journal of Biomedical Materials Research Part B: Applied Biomaterials. 2009;89B(2):439-47.

45. Roy X, Sarazin P, Favis BD. Ultraporous Nanosheath Materials by Layer-by-Layer Deposition onto Co-continuous Polymer-Blend Templates. Advanced Materials. 2006;18(8):1015-9.

46. Salehi P, Sarazin P, Favis BD. Porous devices derived from co-continuous polymer blends as a route for controlled drug release. Biomacromolecules. 2008;9(4):1131-8.

47. Bragaru A, Kusko M, Radoi A, Danila M, Simion M, Craciunoiu F et al. Microstructures and growth characteristics of polyelectrolytes on silicon using layer-by-layer assembly. Central European Journal of Chemistry. 2013;11(2):205-14.

48. Dubas ST, Schlenoff JB. Factors Controlling the Growth of Polyelectrolyte Multilayers. Macromolecules. 1999;32(24):8153-60.

49. Ravati S, Favis BD. Low percolation threshold conductive device derived from a five-component polymer blend. Polymer. 2010;51(16):3669-84.

50. Deligianni DD, Katsala N, Ladas S, Sotiropoulou D, Amedee J, Missirlis YF. Effect of surface roughness of the titanium alloy Ti–6Al–4V on human bone marrow cell response and on protein adsorption. Biomaterials. 2001;22(11):1241-51.

CHAPTER 6 ARTICLE 3: OSTEOGENIC MESENCHYMAL STEM CELLS POPULATE 3-D POLY(E-CAPROLACTONE) SCAFFOLDS WITH INTERCONNECTED PORES AND PREFERENTIALLY MINERALIZE LBL CHITOSAN-COATED SURFACES

Having successfully modified the surface of the intrinsically hydrophobic PCL by chitosan, and hence giving chitosan a fully interconnected porous microstructure, we will finish this thesis by evaluating the osteogenic potential of such hybrid scaffold in bone tissue engineering. The effect of pore size as well as that of the chitosan coating is of central attention in this chapter. However, since the pore size highly influences the scaffold infiltration behavior as demonstrated in Chapter 4, optimization of the cell seeding protocol is essential in order to have comparable cell densities and distributions within scaffolds of different pore sizes. Therefore, several seeding protocols will be presented and assessed in order to obtain the optimal infiltration conditions. Then, hBMSCs will be seeded according to the optimal seeding protocol onto the scaffolds of two pore sizes (one above and one under 100 μm) in the presence or absence of the chitosan coating. Therefore the effects of pore size and LbL surface modification by chitosan on the matrix mineralization of hBMSCs during three weeks of osteogenesis are studied via scanning electron microscopy, micro-CT, and qualitative/quantitative histological analysis.

This article has been submitted to the journal of "*Tissue Engineering, Part A*".

Osteogenic mesenchymal stem cells populate 3-D poly(ε-caprolactone) scaffolds with interconnected pores and preferentially mineralize LbL chitosan-coated surfaces

Nima Ghavidel Mehr[a,b], Xian Li[a,c], Gaoping Chen[a], Basil D. Favis[a,b] and Caroline D. Hoemann[a,c,d,3]

[a] Department of Chemical Engineering, École Polytechnique, Montreal, QC, H3C 3A7 Canada

[b] Centre de Recherche sur les Systèmes Polymères et Composites à Haute Performance (CREPEC), École Polytechnique, Montreal, QC, H3C 3A7 Canada

[c] Biomedical Science and Technology Research Group/Groupe de Recherches Sciences et Technologies (GRSTB), École Polytechnique, Montreal, QC, H3C 3A7 Canada

[d] Institute of Biomedical Engineering, École Polytechnique, Montreal, QC, H3C 3A7 Canada

Contribution of co-authors:

Xian Li: Assistance in the cell experiments

Gaoping Chen: Assistance in histology and histomorphometry

Basil D. Favis: Co-director of this research study

Caroline D. Hoemann: Director of this research study

Abstract

---

[3] Corresponding author. Tel.: + 1 514 340 4711x4848; fax: + 1 514 340 2980.

E-mail address: caroline.hoemann@polymtl.ca (C.D. Hoemann).

Poly(ε-caprolactone) (PCL) is a promising but hydrophobic material for bone tissue engineering applications. We tested the hypothesis that human bone mesenchymal stem cells (hBMSC) seeded in 3D PCL scaffolds with fully interconnected pores of 84 micron or 141 micron average diameter show more biomineralization when pore surfaces are coated with chitosan, via Layer-by-Layer (LbL)-deposited polyelectrolytes. Optimization studies revealed that freshly trypsinized hBMSCs best populated all depths of the 1mm-thick scaffolds when seeded at 4°C in a medium containing 2% FBS. hBMSCs cold-seeded in scaffolds coated or not with LbL-chitosan were cultured for 10 days in proliferation medium then 21 days in osteogenic medium. At day 2, hBMSCs formed sparse monolayers with rounded cell morphologies in PCL-only pores, and a more spread morphology in chitosan-coated pores. At day 10, cells migrated onto secreted collagen networks that filled interpore spaces, proliferated on LbL-chitosan-coated pore surfaces, and formed external monolayers. At day 31, a similar level of tissue formed in scaffolds with and without LbL-chitosan coating, with higher tissue deposition in edge vs inner pores, and significantly more biomineralized matrix in the inner 84 micron pores with LbL-chitosan coating ($p<0.05$). Haphazard mineral deposits formed in outer layers and highly colonized inner 141 micron pores of all scaffolds. On 2D control surfaces, hBMSCs showed higher alkaline phosphatase staining but failed to mineralize on chitosan coatings. This study showed that hBMSCs survive, proliferate, and attach to fibrotic matrix rather than the PCL-only scaffold pore surfaces. LbL-chitosan-coating guided osteogenesis to the pore surfaces and promoted mineralization deeper in smaller-pore size scaffolds.

Keywords: PCL, 3D, pore size, chitosan, hBMSC, osteogenesis, mineralization, cell infiltration

6.1 Introduction

An important aim and challenge of bone tissue engineering is to develop three-dimensional porous constructs that can serve as temporary bone void fillers to repair non-union bone fractures. Structurally stable bone voids can self-repair through woven bone growth at the edges of bone wounds [1]. In scaffold-assisted repair, a 3D structure needs to serve as a supportive bridge or skeleton which due to its specific microstructure facilitates the migration, attachment and distribution of the cells involved in vascular bone in-growth and healing of the target defect [2]. Biocompatibility, biodegradability, mechanical properties, surface chemistry and highly interconnected porous networks with adequate pore size and pore size distributions can influence the performance of a substitute bone graft [3-7]. Transitioning from an inert scaffold to a living tissue requires osteoconduction, or new bone deposition on the scaffold surface. Cues that guide stem cells to deposit bone on the scaffold inner surfaces are still under investigation.

Poly(ε-caprolactone) (PCL) shows much promise as a bone scaffold polymer for its biocompatibility, high toughness, ability to support early loads, and slow biodegradability [8, 9]. PCL scaffolds fabricated using a unique melt-blend approach were previously shown to create fully-interconnected pore structures with discrete pore diameters from 40 to 200 µm [10], and present novel scaffolds for bone reconstruction; however the ideal pore size for obtaining *in vitro* mineralization is unclear. One purpose of the current study was to test the hypothesis that osteogenesis can take place in the 3D environments created by co-continuous PCL scaffolds of different pore sizes (84 or 141 µm pores). Nevertheless, the hydrophobic nature of PCL makes it an unfavorable surface for cell adhesion and growth, and therefore needs to be altered by the proper surface modification technique [11, 12].

To improve cell attachment to PCL, the polymer surface can be rendered hydrophilic (plasma treatment, UV/ozone grafting, aminolysis) [13-16], or by immobilization of bioactive agents (Arg-Gly-Asp (RGD), adenoviral Runx2, bone morphogenetic protein-2, BMP-2) [17-19]. Layer-by-Layer (LbL) self-assembly of polyelectrolytes has also been used to deposit hydrophilic compounds on the surface of PCL fibers and films [20, 21]. Chitosan is a cationic linear polysaccharide used in wound dressings and drug delivery [22-25], and was also shown to support the attachment, proliferation, and end-stage differentiation of human mesenchymal stem cells to osteoblasts [26, 27]. Since chitosan is not melt-processable because of its low degradation temperature which occurs before melting, production of chitosan scaffolds has been limited to solution-based fabrication techniques such as phase separation and lyophilization [26]. Furthermore, chitosan can be deposited uniformly on PCL pore surfaces using an LbL approach (Ghavidel Mehr et al, submitted). When chitosan is incorporated on a PCL scaffold produced by melt-processing, chitosan is given the versatile skeletal design as well as the more robust mechanical properties of the PCL polymer.

Although many cell infiltration protocols have been developed for 3D scaffolds [28, 29], static seeding remains the most common method, despite low seeding efficiencies as well as poor cell distribution [30]. Although strenuous efforts have been made to overcome these limitations, in dynamic, vacuum, magnetic, electrostatic, and centrifugal seeding, static seeding is still the preferred approach for scaffold infiltration due to its simplicity. In this study, we developed an innovative modification of static cell seeding to obtain a more uniform initial cell infiltration, to test the hypothesis that an LbL-chitosan coating promotes human primary bone mesenchymal stem cell (hBMSC) cell attachment, extracellular matrix deposition and mineralization in the three-dimensional environment.

6.2 Materials and methods

6.2.1 Materials

Commercial-grade poly(ε-caprolactone) (PCL, CAPA 6800) was supplied by Solvay (Brussels, Belgium). Poly(ethylene) oxide (PEO) water-soluble polymers (POLYOX™ WSR-N10) was purchased from Dow (Midland, MI, USA). Poly(dialyldemethylammunium chloride) (PDADMAC), M_w 100000–200000, and Poly(sodium 4-styrenesulfonate) (PSS), M_w 70000 were purchased from Sigma-Aldrich. Chitosan (DDA=98% and M_w=237,000, <500 EU, <0.2% protein and <5ppm heavy metals) free-base powder was generated from raw materials and characterized by the Biomaterials and Cartilage Laboratory (BCL) at École Polytechnique de Montréal.

6.2.2 Scaffold fabrication

As previously described [31, 32], PCL and PEO blend components were melt-blended at the co-continuous composition of 45PCL/55PEO vol% in a Brabender internal mixer at 100°C for 7 min with the rotation speed of 50 rpm and under a constant flow of dry nitrogen, then the blends were immediately quenched in liquid nitrogen to freeze-in the morphology. The blends were then annealed at 160°C in a compression molding press under a constant flow of nitrogen for one and two hours. Annealed samples were then quenched in liquid nitrogen and shaped into discs of 3 mm in diameter and 1.5-2 mm in thickness, by using a mechanical punch and a fresh razor blade. PEO was finally selectively extracted in 50 mL deionized water for 7 days under agitation at ambient temperature, leaving a microporous structure. One and two hour annealing of the samples led to the production of scaffolds with 84 and 141 micron average pore diameter, respectively as determined by mercury intrusion porosimetry [10]. PCL scaffolds were designated as PCL1 (84 micron) and PCL2 (141 micron).

6.2.3 Surface modification of PCL via LbL self-assembly

Aqueous 10 mg/mL solutions of PDADMAC (polycation) and PSS (polyanion) were used as polyelectrolytes. PCL discs were first incubated in PDADMAC solution of pH=8 for an hour, rinsed in deionized water, then exposed to alternating polyelectrolyte solutions of opposite charges in 1 M NaCl, pH=2 for 1 hour until the eighth layer is deposited corresponding to the negatively charged PSS outermost layer. After each polyelectrolyte deposition, an hour of water rinsing was performed to remove the unbound polyelectrolyte material. Metal wires were used to keep the discs submerged in the solutions and water at all times. Samples with negatively charged surface were then sterilized in 70% v/v ethanol, rinsed in water 3 times, dipped in 0.22 µm filter sterilized 0.2% w/v chitosan HCl solution with a positive charge at pH=4 for 4 hours under slow shaking as the concluding layer followed by rinsing in sterile deionized water for 1 hour.

6.2.4 Scaffold characterization by micro-computed tomography (µ-CT)

Scaffolds were freeze-dried, stacked vertically with thin separators in tubes made from yellow pipette tips and scanned (Skyscan-1172, version 1.5, Belgium) at 33 kV, 198 µA, 5 µm pixel size; no filter applied; 0.42° rotation step and 3s frame averaging. Each scan lasted ~30 min. 3D sample reconstruction was carried out using NRecon software (version 1.6.2.0; Skyscan), and data analyses performed by CTAnalyser software (version 1.10.1.1; Skyscan).

6.2.5 Cell expansion and static cell seeding

Under institutional-approved protocols, hBMSCs from bone marrow aspirate from a single healthy consented donor at passage 2 were purchased from Texas A&M Institute for Regenerative Medicine (Temple, TX, USA). Primary cells were cultured and expanded in tissue culture flasks at 37 °C in a humidified atmosphere of 5% CO2 in complete culture media (CCM): alpha minimum essential medium (αMEM, Invitrogen, Life Sciences, Burlington, Ontario), 16% fetal bovine serum (FBS, Atlanta Biologicals, Atlanta, GA, USA), 2 mM L-glutamine (Sigma-Aldrich), and 100 units/ml Penicillin/100 µg/ml Streptomycin (Sigma-Aldrich). The cells were passaged twice before seeding in the scaffolds. Scaffolds were sterilized in 70% ethanol for 1 hour and rinsed 3 times in sterile water, air-dried overnight and fully sealed into sterile Petri dishes until further use.

A cell infiltration protocol was optimized with 140 µm scaffold discs, 3 mm diameter and 1 mm thick, press-fit into 3 mm diameter holes generated with a biopsy punch in sterile 2% agarose solidified in 24-well culture plates, as previously described [10]. Three different seeding protocols using 250,000 freshly trypsinized hBMSCs were investigated: 1) classic seeding of cells in 25 µL warm CCM with 16% FBS then incubated for 2 hours at 37°C, 2) cold seeding with cells in 25 µL in 2% FBS medium at 4°C, incubated at 4°C for 1 hour, then at 37°C for 2 hours; 3) a 2-step seeding protocol, where 12.5 µL with 125,000 cells is applied twice with a one hour interval at room temperature, followed by 2 hours at 37°C. N=3 scaffolds were tested for each seeding protocol. Scaffolds were covered with medium at all times. After seeding, scaffolds were transferred to 24-well culture plates, and % escaped cells in the seeding plate determined indirectly by AlamarBlueR assay (Invitrogen). Seeded scaffolds were cultured overnight, fixed in

4% paraformaldehyde in PBS for 20 minutes, stained with Hoechst 33342 (Invitrogen), and cut transversely in half, for fluorescence microscopy of cell nuclei retained at the scaffold surface, using a Zeiss AxioVert S100 microscope, QImaging QICAM FAST 1394 digital camera and Northern Eclipse software (Empix, Mississauga, Ontario, Canada), and for imaging the transverse cut plane with an Olympus FV1000-IX81 confocal microscope system. The cross-section of the scaffold image was divided into top, center and bottom levels, and the cell nuclei in each level counted by automated counting using ImageJ software. The percentage of cells observed at each level was calculated with respect to the total number of counted cells at all the levels, considering that 33% of all cells should ideally populate each of the three different penetration depths. The deviation from the homogeneity (i.e., 33%) at each level is calculated similarly to the calculation of the standard deviation according to the following general equation:

$$\alpha_{Level}(\%) = \left[\frac{\left(\bar{P}_{Level} - \frac{100}{L}\right)^2}{N}\right]^{1/2} \qquad (18)$$

where α_{Level} (%) is the deviation from homogeneity, $\bar{P}_{Level}$ is the average percentage of cells observed at the specific level. L is number of level sections in the scaffold thickness (L=3) and N is the total number of samples studied (N=3).

6.2.6 Osteogenic culture in 2D and 3D

For 2D monolayer control cultures, 33 µL filter-sterile chitosan (0.5 µg/mL) was allowed to air-dry in 96 well plate a sterile laminar flow hood. 150 µL of CCM containing 600 live trypsinized hBMSCs were seeded on chitosan-coated and uncoated wells. For 3D cultures, 250,000 hBMSCs in 25 µL of media were cold-seeded in PCL1 and PCL2 scaffolds press-fit in sterile agarose wells, as described in section 6.2.5. The scaffolds were transferred to 96-well plates and 200 µL of CCM added. The medium for both 2D and 3D cultures was changed twice weekly for 10 days, then the medium was replaced with an osteogenic medium containing CCM supplemented with 5 mM disodium β-glycerophosphate, 100 µM L-Ascorbic acid 2-phosphate and 10 nM dexamethasone (all from Sigma-Aldrich), and changed twice a week until day 31. Some samples were observed to become flipped during medium replacement. 2D cultures were stained at days 10 and 31 for in situ alkaline phosphatase and alizarin red. 3D discs were harvested at days 2, 10 and 31 for ESEM, micro-CT, and histological evaluations. At harvesting, scaffolds with any monolayer attached were carefully scraped from the well bottom with a small weigh spatula then fixed in 4% paraformaldehyde in PBS (pH=7.4) for 20 min and rinsed 3X in PBS.

6.2.7 Microscopic evaluations using environmental scanning electron microscopy (ESEM)

2% glutaraldehyde-fixed PCL1 and PCL2 samples from culture days 2, 10 and 31, and unseeded scaffolds cultured in parallel, were cut in half using a fresh razor, rinsed in water, air-dried and gold coated using plasma deposition and imaged (ESEM, Quanta 200 FEG, FEI Company, Czech Republic) under high vacuum pressure mode and at a voltage of 20kV.

6.2.8 Histology and quantitative histomorphometry

Scaffolds were cryoprotected in graded sucrose solutions, embedded in Tissue-Tek OCT (4583S, Cederlane, Hornby, Ontario, Canada), and cryosections 10 μm thick collected using the CryoJane tape transfer system. Sections were stained with hematoxylin and eosin (H&E), and alizarin red. Sections were either dried overnight and mounted directly in Permount® to retain PCL or carried through toluene which cleared the PCL. Images were obtained with a Zeiss Axiolab microscope equipped with a digital Hitachi HV-F22F camera.

Histomorphometric analyses were performed by 2 blinded observers (N.G.M. and G.C.) on H&E and AR stained sections from N=4 distinct day 31 scaffold samples per condition, with day 2, with day 10 and cell-free scaffolds as negative controls. 10x magnification images were taken systematically from the corner of each PCL cross-section with the highest cell density, then regions of interest were cropped: “edge” containing the 300 μm thick scaffold top and side-wall excluding any monolayer growing on the surface, and “inner” rectangular area 300 μm to 600 μm deep in the scaffold. An ImageJ plug-in was used to adjust the HSV thresholds to quantify positively stained pixels distinct from background stain. It was assumed that the regions stained pink or purple with H&E constitute tissue and those stained dark red with AR were calcium deposits. The percentage of *in vitro* tissue (H&E stain, matrix %) and mineralized matrix (AR stain, mineral %) was determined by dividing the stained pixels by the total pixels in the image by an in-house MATLAB (Mathworks) routine (R2011a) [33].

6.2.9 Statistical analyses

The mean and standard deviation were calculated for each dataset. Student’s t-test was used to analyze differences between two experimental groups. $p<0.05$ was taken as statistically significant.

6.3 Results

6.3.1 Scaffold structural characterization with and without LbL-chitosan

μ-CT scans of PCL scaffolds with 84 and 141 micron pore size (PCL1 and PCL2, respectively) showed a relatively uniform 3D structure of interconnecting pores (Figure 6.1(a, b)). The unmodified PCL scaffolds showed smooth pore surfaces after 2 days incubation in CCM (Figure 6.1(c-f)), that after LbL-chitosan surface modification changed to a rough microstructure (white arrows, Figure 6.1 (g,h)). The irregular structure of the LbL-chitosan coating may be partly due to aldehyde fixation, which leads to chitosan aggregates via inter- and intra-chain cross-links of free amine groups [34]. These results demonstrated that the LbL-chitosan coating was effectively deposited throughout the PCL scaffold at both pore sizes.

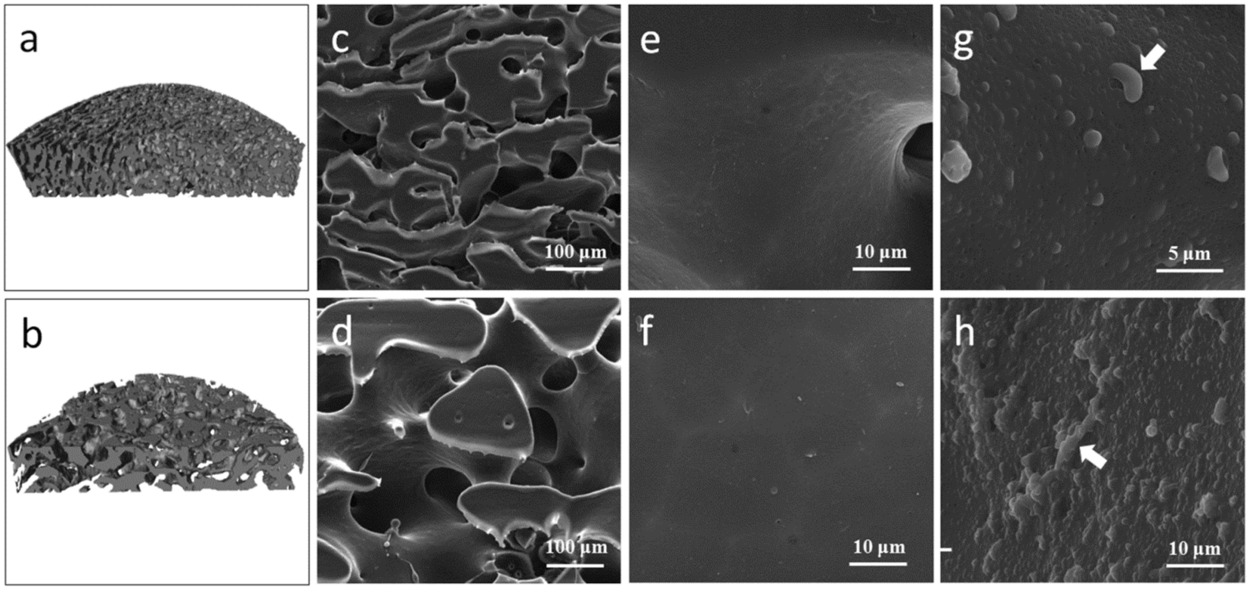

Figure 6.1: (a, b) Micro-computed tomography and (c, d) SEM images exhibiting the macrostructure of the scaffolds. SEM micrographs showing the surface topography of the samples of (e, f) pure and (g, h) chitosan modified PCL surface. The panels correspond to PCL1 (a, c, e, g) and PCL2 (b, d, f, h). The pore surface topography of PCL demonstrates a change from smooth toward rough microstructures for both PCL1 and PCL2. White arrows represent chitosan layer aggregates. Scale bars (c to h) are 5 to 100 microns, as indicated.

6.3.2 Cold seeding improves cell seeding distribution in PCL scaffolds

Scaffolds with Hoechst-stained cell nuclei were analyzed at day 1 post seeding by top and transverse views, following classic, cold, and 2-step methods (Figure 6.2). The white contours in panels A-C represent “clean” areas on the scaffold surface in which the cells have freely penetrated through and left the top surface, and settled in the pores. Cold-seeded cells with 2% serum penetrated to the deeper pores (open arrowheads, Figure 6.2e), and escaped through the scaffold to the bottom of the culture well (Figure 6.3a) leading to 13.6 % deviation from the ideal 33% cell distribution in each of the 3 layers (Figure 6.3b). Cells seeded at 37°C (1-step or 2-step seeding) collected mostly at the surface (white arrowheads, Figure 6.2(d, f)). The 2-step seeding procedure led to the lowest number of escaped cells (Figure 6.3a), and the highest % deviation from 33% cell distribution at different penetration depths (Figure 6.3b). These data showed that cold-seeding generates the most uniform cell distribution in the scaffold.

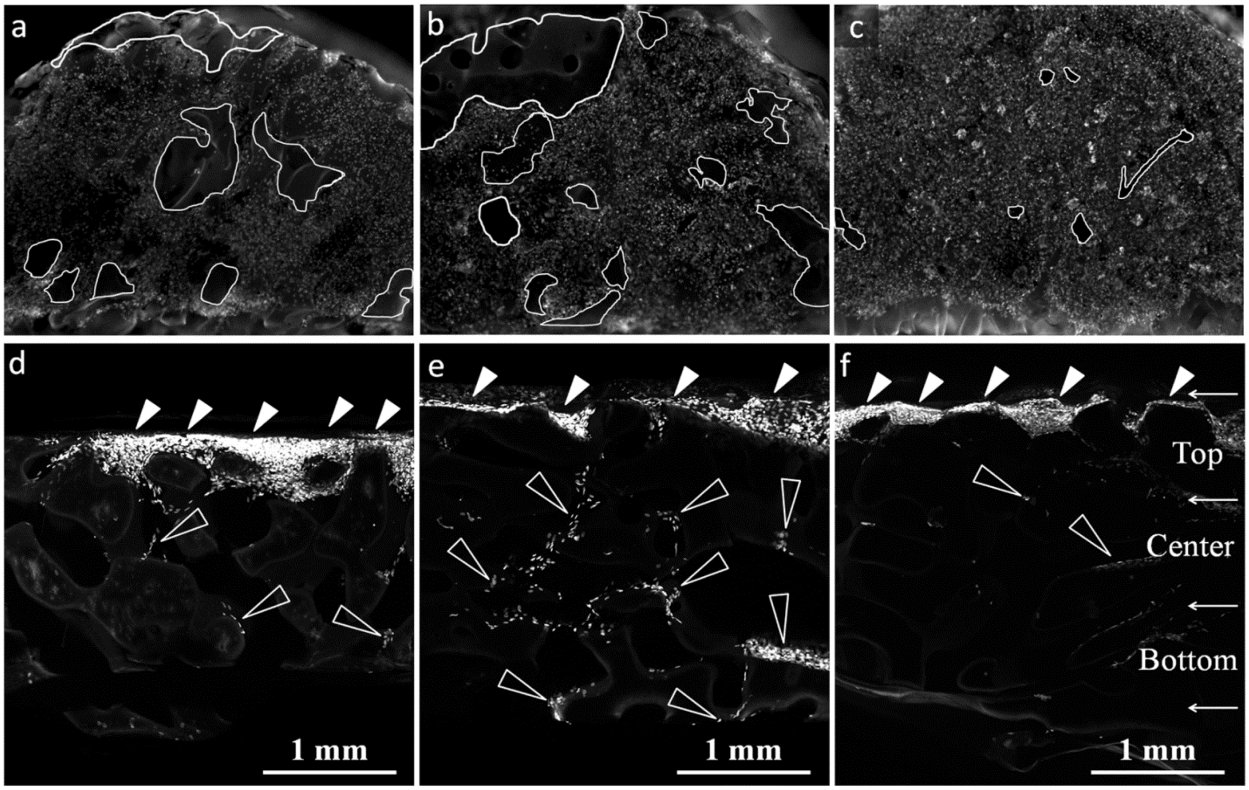

Figure 6.2: Fluorescent images of the Hoechst stained hBMSCs on the seeding area, where white contours represent the top view porous areas where the cells have freely penetrated through and completely left the top surface (a-c) or infiltrated the depth of the scaffold cross-section (d-f), as shown by confocal images of the Hoechst stained cells in the rectangular cross section of PCL2 scaffolds. The panels represent classical seeding at 37°C (a, d), cold seeding at 4°C with 2% FBS (b, e) and 2-step seeding at 37°C (c, f). Cold seeding exhibits the most uniform cell distribution across the PCL scaffold. Scale bar = 1 mm

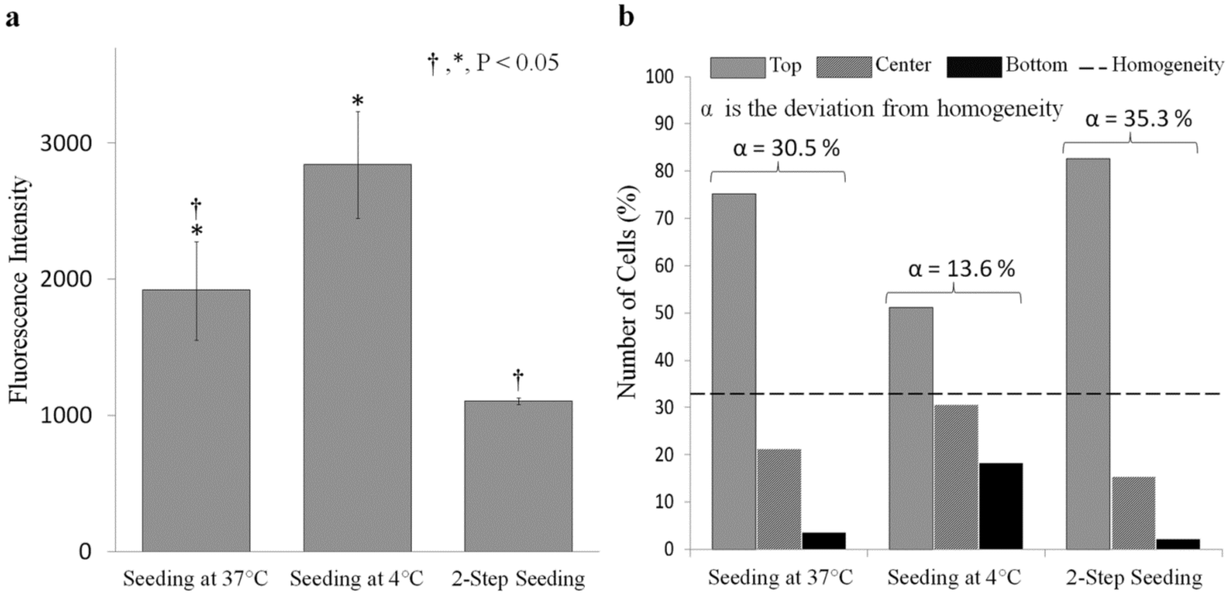

Figure 6.3: (a) AlamarBlue® metabolic assay as an indirect method to compare the number of cells that completely passed through the PCL2 scaffolds seeded with different seeding protocols: classical seeding at 37°C, cold seeding at 4°C with 2% FBS and 2-step seeding at 37°C. The cold seeding protocol with 2% FBS demonstrates the highest number of escaped beads which corresponds to the best cell penetration. The classical seeding protocol gave lower escape than cold-seeding and higher than the 2-step condition ($P < 0.05$); and (b) Average percentage of cell numbers counted at each penetration depth for each seeding protocol. α is the deviation from homogeneity of cell distribution at each penetration depth calculated. The homogeneity percentage for three penetration depth is 33%. The cold seeding protocol with 2% FBS displays the lowest deviation from homogeneity.

6.3.3 Cell attachment, proliferation and matrix deposition

hBMSCs cold-seeded and cultured 2 days in 3D scaffolds in proliferation medium had a rounded morphology with thin filopodia anchored to the PCL-only pore surfaces (Figure 6.4a), and a spread morphology on chitosan-coated pore surfaces (Figure 6.4b), for both 84 and 141 µm pore sizes.

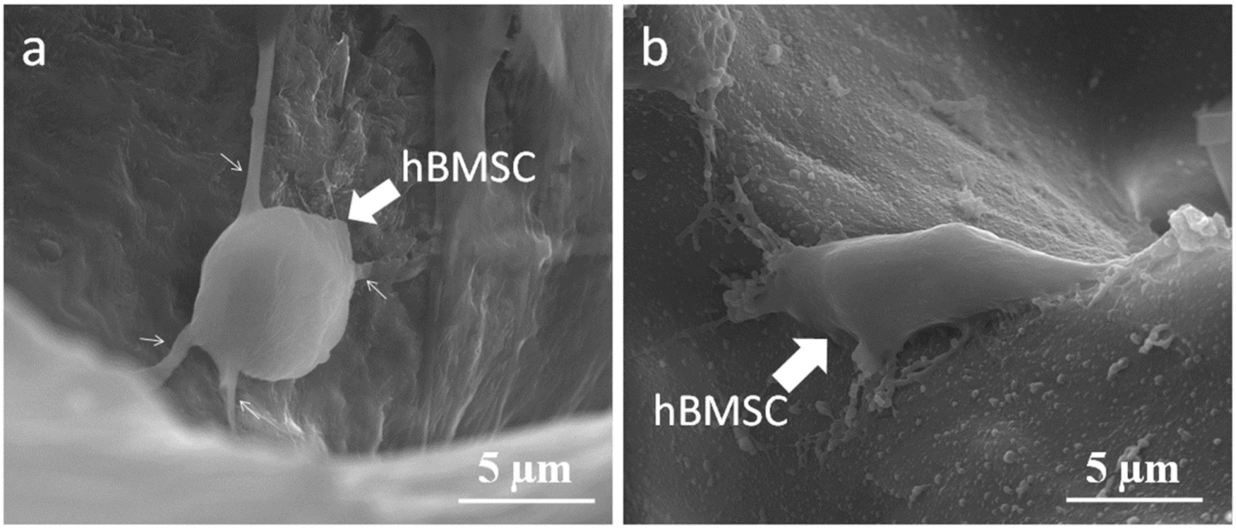

Figure 6.4: ESEM micrographs of hBMSCs on (a) uncoated and (b) chitosan coated pores of PCL at day 2. Isolated hBMSCs (thick arrow) form rounded morphologies with filopodia (thin arrows) on the uncoated pores, whereas they fully spread on the chitosan coated pores of the scaffold.

After 2 days in culture, hBMSC cell clusters were observed in larger PCL2 pores (Figure 6.5(i, m), with heavy deposition of ECM fibers and sheets along chitosan-coated pore surfaces (Figure 6.5(a, e)). In the 84 micron PCL1 scaffolds, hBMSCs were more restricted to top edge pores (white rectangle, Figure 6.5e). Sparse cells with round morphologies were detected on unmodified PCL1 pore surfaces, with and without chitosan coating (Figure 6.5(a, b)). These data suggest that cells thrive and take root as colonies rather than isolated single cells, given the more elongated and spread features with ECM accumulation in highly colonized areas in the PCL2 scaffolds (Figure 6.5(i, j)). Cells were found to rapidly secrete a fibrous matrix in unmodified PCL pores (Figure 6.5(b, c, j, k)), and to adopt a more fully elongated and packed morphology in flattened sheets on the LbL-chitosan coated PCL surfaces (Figure 6.5(f, g, n, o)). Some hBMSCs appear to be partly detached from the surface of LbL-chitosan modified which could be due to likely detachment of chitosan from the surface by pulling forces of the contractile apparatus of the hBMSC (open arrowhead, Figure 6.5g). At day 31, rubbled surfaces were observed that may represent mineralized matrix (Figure 6.5(h, p)).

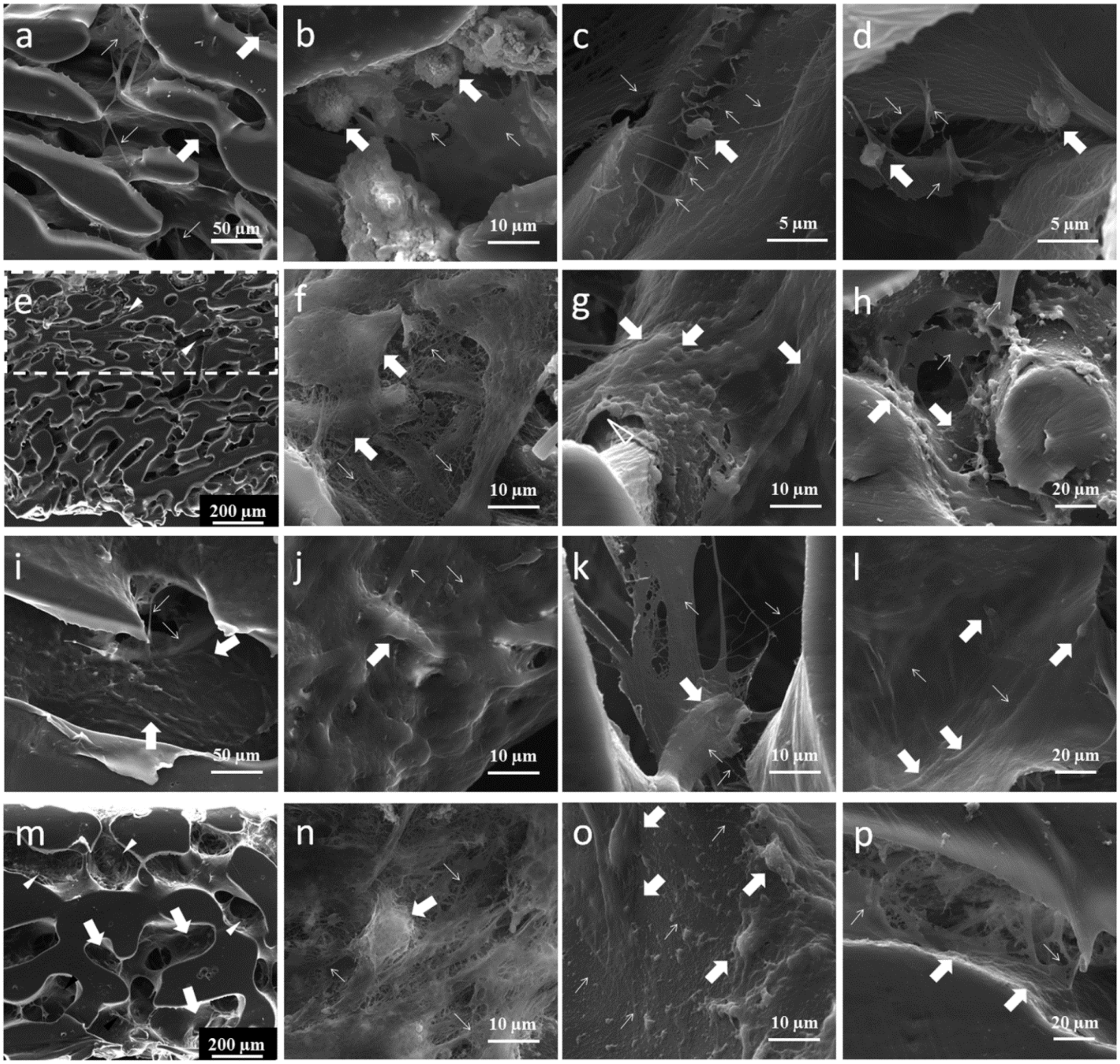

Figure 6.5: ESEM images of the pore interspacial area for (a-d) PCL1, (e-h) chitosan surface modified PCL1, (i-l) PCL2, (m-p) chitosan surface modified PCL2. The panels represent PCL scaffolds cultured at day 2 (a, b, e, f, i, j, m, n), day 10 (c, g, k, o) and day 31 (d, h, l, p). White rectangle in panel E upper zone represents the fully colonized area. Thin arrows represent collagen fibers and ECM sheets, whereas thick white arrows illustrate hBMSCs. White arrow-heads represent pores with dense ECM fibers. The open white arrowhead in panel G illustrates the likely detachment of the chitosan layer. Scale bar in panels (c, d), (b, f, g, j, k, n, o), (h, l, p), (a, i), and (e, m) = 5, 10, 20, 50 and 200 microns, respectively

According to H&E stained sections at culture day 10, hBMSCs colonized ECM filling the unmodified PCL pores (white arrowheads, Figure 6.6(a, e)), while in chitosan-coated pores, hBMSCs were detected both in pore ECM and on pore surfaces (black arrowheads, Figure 6.6(b, f)). At day 31, cells formed thick outer layers that showed ingrowth into the edge pores with less infiltration in the inner pores (dashed rectangle, Figure 6.6(c, g)). The surface modification by chitosan led to a homogeneous matrix deposition all across the scaffold thickness (Figure 6.6(d, h) versus (Figure 6.6(c, g)).

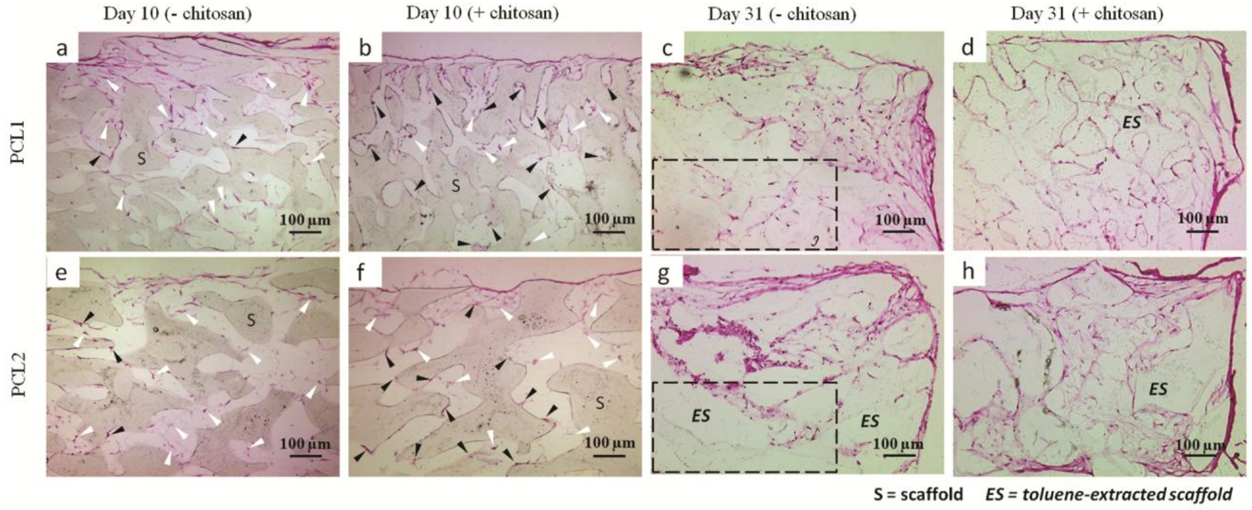

Figure 6.6: Histological images of H&E stained extracellular matrix illustrating the rectangular cross section of (a-d) PCL1, (e-h) PCL2, at (a, b, e, f) day 10 and (c, d, g, h) day 31 in the (a, c, e, g) absence and (b, d, f, h) presence of chitosan coating. hBMSCs on the ECM in the pore interspace area and on the pore surface is represented by white and black arrow-heads. The black rectangle represents the depth of the constructs. At day 10, hBMSCs in unmodified scaffolds prefer to remain on the deposited matrix in the space between the pores, whereas they spread on the pore surface of chitosan coated scaffolds. At day 31, chitosan coated scaffolds exhibit a more uniform matrix deposition across the scaffold. Panels a, b, e, f: dry-mount sections to retain PCL scaffold (S). Panels c, d, g, h: toluene-extracted PCL scaffold (ES). White arrowheads: interpore cells. Black arrowheads: cells adhering to pore surfaces. Scale bar = 100 microns

6.3.4 Histological analysis of matrix mineralization

At day 10, constructs showed no sign of calcium deposits (Figure 6.7(a, b, e, f)). Therefore, chitosan was insufficient to accelerate osteogenesis in the absence of dexamethasone. At day 31, punctate matrix calcification was detected in PCL-only scaffolds, mainly in the outer monolayers of the PCL1-only scaffolds (Figure 6.7c) and larger PCL2 edge pores containing MSC aggregates (white rectangles and arrows, Figure 6.7g). These data show that mineralization in unmodified PCL scaffolds only occurs in areas where the scaffold is highly colonized. A similar outer layer of calcified matrix was detected in chitosan-coated scaffolds, along with a more uniform punctate calcification of inner pores (white rectangles and arrows, Figure 6.7(d, h)). Data in Fig 6.7(d, h) suggest that mineralization in LbL-chitosan scaffolds occurs by the hBMSCs depositing a collagenous matrix on the surface of the pores that is competent to calcify. Thus, chitosan guides the osteogenic process. Micro-CT images of LbL-chitosan modified PCL1 and PCL2 scaffolds (Figure 6.7(i, k)) show evidence of mineral deposition at the edges (thick white arrows). However, minerals could not be detected deep inside the scaffolds most probably due to the similar radio-opacity of PCL and minerals (see outer mineralized layer, thin white arrows, Figure 6.7(i, k)).

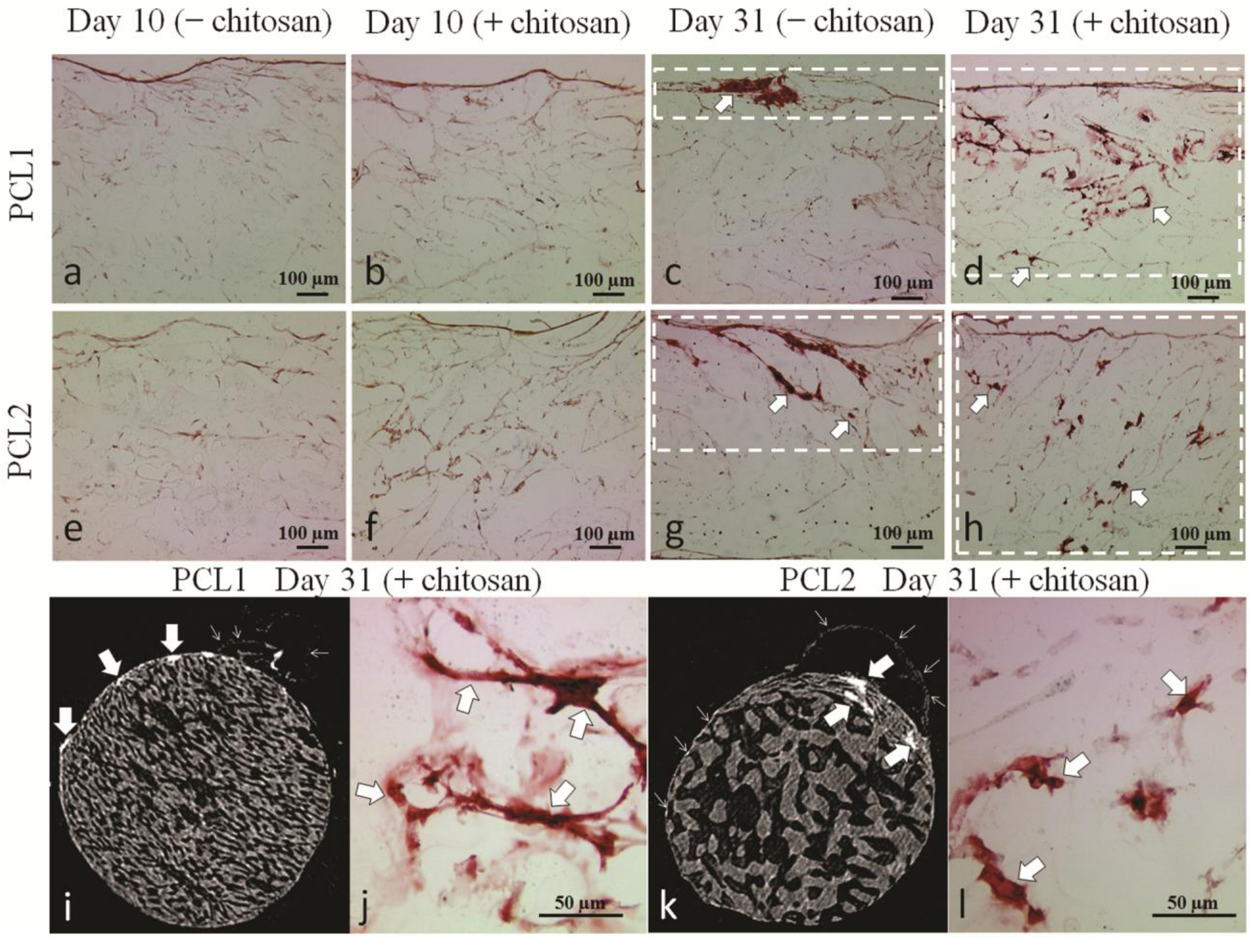

Figure 6.7: Alizarin red stained (a-d, J) PCL1 and (e-h, L) PCL2 sections at (a, b, e, f) day 10 and (c, d, g, h, j, l) day 31 in the (a, c, e, g) absence and (b, d, f, h, j, l) presence of chitosan coating. White dashed rectangles represent the areas inside the PCL scaffolds where minerals are observed. Thick white arrows show the deposited calcium nodules; micro-CT images of chitosan surface modified (i) PCL1 and (k) PCL2 scaffolds. Thin and thick arrows respectively represent an outer skin of partly mineralized ECM, and likely minerals at the periphery of the scaffolds. Minerals are deposited in the highly colonized top and inner sections of uncoated PCL1 and PCL2 scaffolds, whereas they were deposited along the surfaces of the edge and inner pores in chitosan coated samples. Scale bar for panels (a-h, j, l) = 100 microns

3-fold more tissue was detected in outer pores of uncoated samples at day 31, with the highest ECM in the outer pores of PCL2 samples (12% vs. 7% other conditions, $p<0.05$, Figure 6.8a). Around 2% to 4% ECM formed in deeper levels of the scaffolds (white bars, Figure 6.8a). More mineralized tissue was observed in the edge (0.3% to 1.5%) compared to inner pores in uncoated-PCL1 and PCL2 (0.02% to 0.7%, Figure 6.8b).

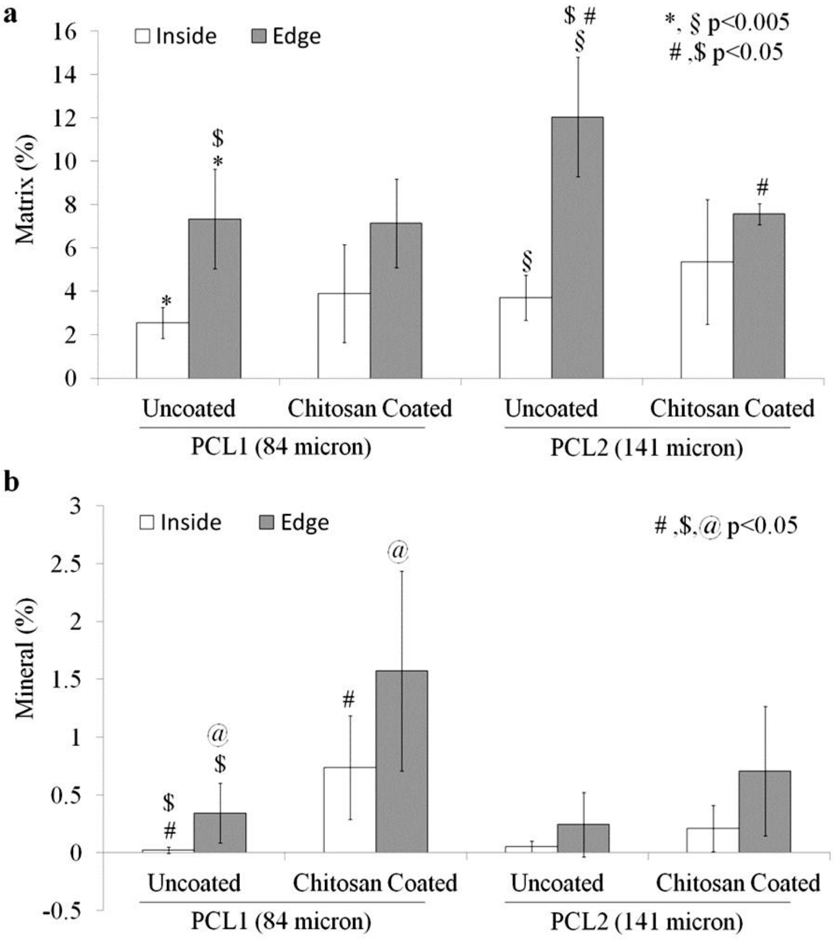

Figure 6.8: (a) Extracellular matrix % on the edge and in the depth of the sections for PCL1 and PCL2 scaffolds in the presence or absence of chitosan coating according to quantitative histomorphometry. Although chitosan coating does not significantly affect the amount of ECM deposited, the formation of ECM becomes more uniform across the surface-modified scaffolds; (b) Mineral % on the edge and in the depth of the sections for PCL1 and PCL2 scaffolds in the presence or absence of chitosan coating. There is a significant increase in the mineral % on the edge and in the depth of PCL1 scaffolds by modifying the surface with chitosan. This effect was not significant for PCL2 discs. Statistical significance was observed for (*, §) and (#, \$, @) conditions at $p < 0.005$ and $p<0.05$, respectively

Compared to the unmodified PCL1, LbL-chitosan coated PCL1 scaffolds showed 5-fold higher Ca2+ deposition in the edge pores, and 12-fold more in the inner pores ($p<0.05$, Figure 6.8b). Although a similar trend for higher % mineral deposition was observed for the chitosan-coated vs uncoated PCL2 samples, no statistical significance was found between the data, mainly due to sporadic calcification in some highly colonized uncoated PCL2 pores.

In 2D monolayer control osteogenic cultures, chitosan enhanced alkaline phosphatase activity compared to tissue culture plastic (Figure 6.9(a, c)). However, chitosan was unable to guide the hBMSCs towards the terminal osteoblast differentiation, since the mineralization was suppressed by chitosan as shown in Figure 6.9(b, d).

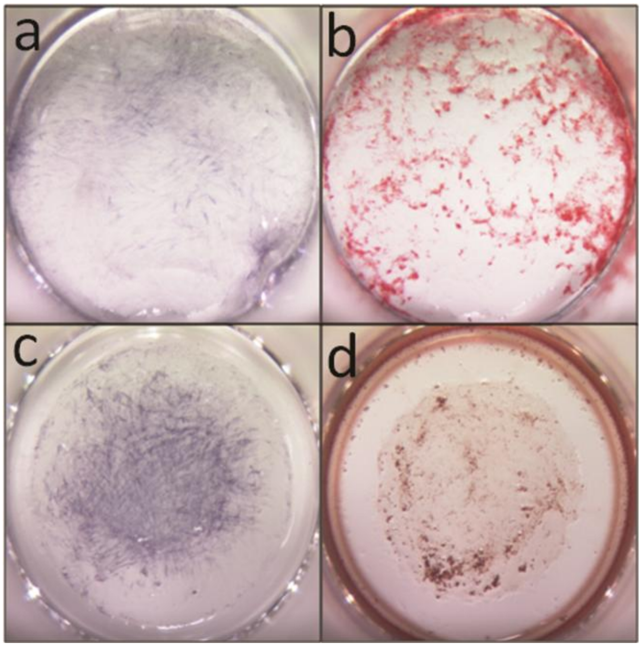

Figure 6.9: (a, c) Alkaline phosphatase and (b, d) alizarin red staining of the 2D cultured monolayer hBMSCs at day 31 in the (a, b) absence and (b, c) presence of chitosan coating on the wells. Although there is an increase in the ALP activity of the cells, chitosan suppresses the matrix mineralization

6.4 Discussion

This study reports the novel effects of LbL-chitosan coating in promoting a more uniform mineralization in 84 micron PCL scaffold pores. The result was achieved in part by using an optimized cold cell-seeding protocol. In previous work, we observed that cell aggregation during static seeding prevents cells from infiltrating the interconnecting pores whereas 10 micron latex beads show good penetration for scaffolds with at least 80 micron pore diameter [10]. Cold seeding reduces metabolic activity and a lower 2% FBS potentially reduces PCL surface biofouling, allowing cells to behave more like individual inert beads.

The rounded hBMSC morphology of isolated cells in unmodified PCL scaffolds in this study is in accordance with a previous observation of rounded morphologies of L929 mouse fibroblasts on electrospun PCL scaffolds [35]. It is well established that cell-biomaterial interactions can influence ECM and mineral deposition, hence biomaterial properties can influence hBMSCs to differentiate to osteoblasts [36]. In this study, we show that hBMSCs tend to migrate onto the freshly secreted collagen fibers in the space-filling area of the pores rather than remain on the hydrophobic PCL surface after 10 days of culture in CCM. Cell proliferation in these hydrophobic niches led to mineralization in some pores, without requiring cell attachment. By contrast, chitosan coated PCL surfaces drive the cells to form active attachments on the surface of the pores through fully elongated morphologies even in the smaller pore size scaffold. Cell adhesion to the chitosan coating can significantly promote mineralizing behavior and physical interfacing of the cells and scaffold.

Pure or surface-modified 3D PCL scaffolds with or without the incorporation of bioactive agents such as Bone Morphogenetic Protein-2 (BMP2) and RGD have already been tested for *in vitro* osteogenesis [37-40]. These previous investigations most often examined either the cell response, or the scaffold morphology, and few studies carefully characterized or quantified the ability of hBMSCs to biomineralize in a 3D environment. Previous studies analyzed PCL scaffolds impregnated with osteoconductive materials such as hydroxyapatite to improve mechanical properties required for cortical bone repair [41], but there is still a lack of knowledge regarding the cell/PCL interaction and biomineralization in pure 3D PCL scaffolds seeded with hBMSCs. Low levels of mineralization have been generally associated with pure PCL scaffolds pre-seeded with various cell types including hBMSCs [41-43]. Our results clearly show that even the hydrophobic PCL can stimulate a disorderly *in vitro* biomineralization process, in ~5% of the matrix area (i.e., 0.3% mineral for 7% tissue formed, Figure 6.8). Although the distribution of minerals at the outer and inner pores of the scaffolds is a determining factor for osseointegration of the scaffolds *in vivo* [44], to our knowledge, the investigation of pore size *in vitro*, in 3D PCL constructs has seen little activity. In this study, we showed that a change in the pore size could not independently induce biomineralization. This is in agreement with the results obtained by Akay et al. who showed that the pore size has minimal effect on *in vitro* bone ingrowth [45].

Chitosan improved the formation of mineral deposits in the lower pore size, however the effect is less pronounced in PCL2 scaffolds (Figure 6.8b). BMSCs have previously been shown to exhibit higher levels of osteogenic differentiation of in 3D as opposed to 2D systems [46]. The weaker biomineralization of larger pore sizes could be related to suppressed mineralization of chitosan-coated 2D surfaces (Figure 6.9). It was previously shown that hBMSCs are capable of ingesting chitosan particles in a 2D system, which interferes with biomineralization [47]. Therefore, it is possible that in our system, the less curved surfaces of PCL2 mimic a 2D suppressed osteogenic behavior, while the more highly curved pore surfaces of PCL1 scaffolds could potentially interfere with the ingestion of chitosan particles.

The deposition of minerals across the chitosan-coated scaffolds is non-uniform and accounts for approximately 20% of the matrix area (i.e., 1.6% mineral for 7% tissue formed), and the low mineral signal in micro-CT images of Figure 6.7(i, k) is consistent with sparse mineral deposits. In a study by Abrahamsson et al, 3D PCL scaffolds with pore dimensions similar to and larger than those in our PCL2 scaffolds were used to demonstrate qualitatively that hBMSCs can deposit mineral [37], in agreement with our findings for PCL-only scaffolds. Chastain et al. investigated the osteogenic differentiation of hBMSCs on 2D and 3D PCL substrates and speculated that vitronectin, a serum protein, may be adsorbed to PCL surfaces and inhibit biomineralization [48], although quantitative mineralization assays were not done. The lack of mineral deposition in the deeper levels of unmodified PCL scaffolds in our study, brings us to speculate that the migration of hBMSCs onto the ECM fibers and sheets (Figure 6.6(a, e)) and the lack of a solid osteogenic ground for the cells to adhere to inhibits the mineralization process.

This study is the first to report the effect of chitosan surface modification of porous 3D PCL scaffolds on the *in vitro* osteogenic behavior of osteoprogenitor cells. Yang et al. demonstrated that chitosan incorporated inside PCL electrospun nanofibers improved the adhesion, proliferation and calcification of calvarial MC3T3-E1 preosteoblasts [49]. However, the influence of the pore size and chitosan on the mineralization of the stem cells was not independently investigated. Our study proved that a 3D PCL scaffold alone and chitosan-coated 2D culture cannot actively promote the process of matrix mineralization; our results clearly demonstrate that the combinatory effect of chitosan and porous PCL structure specifically at the lower pore size can highly improve mineral deposition.

The limitations regarding the sporadic deposition of minerals inside chitosan coated constructs emphasize that the *in vitro* static cultures in 3D PCL scaffolds are insufficient for achieving a biomechanically stable bone formation. Therefore, given the cost and limitations of perfusion bioreactors, it would be necessary to further develop an *in vivo* system in which vasculature can form and invade the 3D PCL scaffold, which may require at least 100 μm and potentially up to 600 μm [50]. Therefore, although a better *in vitro* performance was observed for 84 μm scaffolds in the presence of chitosan, PCL scaffolds of 141 μm may show better performance *in vivo*. This hypothesis will be verified in a future work.

Acknowledgements

The authors would like to thank Monica Iliescu Nelea, Guillaume Lessard, Geneviève Picard and Geoffrey Li for their precious assistance in the ESEM, scaffolds preparation, histology and micro-CT. Also, the authors would like to acknowledge the financial support of the Natural Sciences and Engineering Research Council of Canada (NSERC) through its Network for Innovative Plastic Materials and Manufacturing Processes (NIPMMP), Canadian Institutes of Health Research (CIHR, to CDH), NSERC Discovery (to CDH), and salary support for XL and CDH from the Fonds de Recherche en Santé du Québec (FRQ-S, Bourse de Carrière Nationale to CDH).

References

1. Hoemann CD, El-Gabalawy H, McKee MD. In vitro osteogenesis assays: Influence of the primary cell source on alkaline phosphatase activity and mineralization. Pathologie Biologie. 2009;57(4):318-23.

2. Bauer TW, Muschler GF. Bone graft materials. An overview of the basic science. Clinical Orthopaedics and Related Research. 2000(371):10-27.

3. Ratner BD, Hoffman, A.S., Schoen, F.J., Lemons, J.E. Biomaterials Science: an Introduction to Materials in Medicine. 2nd Edn ed. San Diego, USA: Academic Press; 2005.

4. Roy TD, Simon JL, Ricci JL, Rekow ED, Thompson VP, Parsons JR. Performance of degradable composite bone repair products made via three-dimensional fabrication techniques. Journal of Biomedical Materials Research: Part A. 2003;66(2):283-91.

5. Woodard JR, Hilldore AJ, Lan SK, Park CJ, Morgan AW, Eurell JAC et al. The mechanical properties and osteoconductivity of hydroxyapatite bone scaffolds with multi-scale porosity. Biomaterials. 2007;28(1):45-54.

6. Graziano A, d'Aquino R, Cusella-De Angelis MG, De Francesco F, Giordano A, Laino G et al. Scaffold's surface geometry significantly affects human stem cell bone tissue engineering. Journal of Cellular Physiology. 2008;214(1):166-72.

7. Bai F, Wang Z, Lu J, Liu J, Chen G, Lv R et al. The correlation between the internal structure and vascularization of controllable porous bioceramic materials in vivo: a quantitative study. Tissue Engineering: Part A. 2010;16(12):3791-803.

8. Hutmacher DW. Scaffolds in tissue engineering bone and cartilage. Biomaterials. 2000;21(24):2529-43.

9. Oh SH, Park IK, Kim JM, Lee JH. In vitro and in vivo characteristics of PCL scaffolds with pore size gradient fabricated by a centrifugation method. Biomaterials. 2007;28(9):1664-71.

10. Ghavidel Mehr N, Li X, Ariganello MB, Hoemann CD, Favis BD. Poly(epsilon-caprolactone) scaffolds of highly controlled porosity and interconnectivity derived from co-continuous polymer blends: model bead and cell infiltration behavior. Journal of Materials Science: Materials in Medicine. 2014.

11. Ma Z, Mao Z, Gao C. Surface modification and property analysis of biomedical polymers used for tissue engineering. Colloids and Surfaces B: Biointerfaces. 2007;60(2):137-57.

12. Sudarmadji N, Tan JY, Leong KF, Chua CK, Loh YT. Investigation of the mechanical properties and porosity relationships in selective laser-sintered polyhedral for functionally graded scaffolds. Acta Biomaterialia. 2011;7(2):530-7.

13. Darain F, Chan WY, Chian KS. Performance of Surface-Modified Polycaprolactone on Growth Factor Binding, Release, and Proliferation of Smooth Muscle Cells. Soft Materials. 2010;9(1):64-78.

14. Domingos M, Intranuovo F, Gloria A, Gristina R, Ambrosio L, Bártolo PJ et al. Improved osteoblast cell affinity on plasma-modified 3-D extruded PCL scaffolds. Acta Biomaterialia. 2013;9(4):5997-6005.

15. Siri S, Wadbua P, Amornkitbamrung V, Kampa N, Maensiri S. Surface modification of electrospun PCL scaffolds by plasma treatment and addition of adhesive protein to promote fibroblast cell adhesion. Materials Science and Technology. 2010;26(11):1292-7.

16. Zhu Y, Gao C, Shen J. Surface modification of polycaprolactone with poly(methacrylic acid) and gelatin covalent immobilization for promoting its cytocompatibility. Biomaterials. 2002;23(24):4889-95.

17. Zhang Y, Deng X, Scheller EL, Kwon T-G, Lahann J, Franceschi RT et al. The effects of Runx2 immobilization on poly (ε-caprolactone) on osteoblast differentiation of bone marrow stromal cells in vitro. Biomaterials. 2010;31(12):3231-6.

18. Drevelle O, Daviau A, Lauzon M-A, Faucheux N. Effect of BMP-2 and/or BMP-9 on preosteoblasts attached to polycaprolactone functionalized by adhesive peptides derived from bone sialoprotein. Biomaterials. 2013;34(4):1051-62.

19. Zhang H, Lin C-Y, Hollister SJ. The interaction between bone marrow stromal cells and RGD-modified three-dimensional porous polycaprolactone scaffolds. Biomaterials. 2009;30(25):4063-9.

20. Dubas ST, Kittitheeranun P, Rangkupan R, Sanchavanakit N, Potiyaraj P. Coating of polyelectrolyte multilayer thin films on nanofibrous scaffolds to improve cell adhesion. Journal of Applied Polymer Science. 2009;114(3):1574-9.

21. Lv NJ, Meng S, Guo Z, Wu LX, Liu ZJ, Jin HG et al. Improving the biocompatibility of poly(epsilon-caprolactone) by surface Immobilization of chitosan and heparin. e-Polymers. 2008.

22. Ma L, Gao C, Mao Z, Zhou J, Shen J, Hu X et al. Collagen/chitosan porous scaffolds with improved biostability for skin tissue engineering. Biomaterials. 2003;24(26):4833-41.

23. Sinha VR, Singla AK, Wadhawan S, Kaushik R, Kumria R, Bansal K et al. Chitosan microspheres as a potential carrier for drugs. International journal of pharmaceutics. 2004;274(1–2):1-33.

24. Ong S-Y, Wu J, Moochhala SM, Tan M-H, Lu J. Development of a chitosan-based wound dressing with improved hemostatic and antimicrobial properties. Biomaterials. 2008;29(32):4323-32.

25. Cai K, Yao K, Cui Y, Lin S, Yang Z, Li X et al. Surface modification of poly (D,L-lactic acid) with chitosan and its effects on the culture of osteoblasts in vitro. Journal of Biomedical Materials Research. 2002;60(3):398-404.

26. Seol Y-J, Lee J-Y, Park Y-J, Lee Y-M, Ku Y, Rhyu I-C et al. Chitosan sponges as tissue engineering scaffolds for bone formation. Biotechnology Letters. 2004;26(13):1037-41.

27. Mathews S, Gupta PK, Bhonde R, Totey S. Chitosan enhances mineralization during osteoblast differentiation of human bone marrow-derived mesenchymal stem cells, by upregulating the associated genes. Cell Proliferation. 2011;44(6):537-49.

28. Yow KH, Ingram J, Korossis SA, Ingham E, Homer-Vanniasinkam S. Tissue engineering of vascular conduits. British Journal of Surgery. 2006;93(6):652-61.

29. Parikh SA, Edelman ER. Endothelial cell delivery for cardiovascular therapy. Advanced Drug Delivery Reviews. 2000;42(1–2):139-61.

30. Villalona GA, Udelsman B, Duncan DR, McGillicuddy E, Sawh-Martinez RF, Hibino N et al. Cell-seeding techniques in vascular tissue engineering. Tissue Engineering: Part B, Reviews. 2010;16(3):341-50.

31. Yuan Z, Favis BD. Macroporous poly(l-lactide) of controlled pore size derived from the annealing of co-continuous polystyrene/poly(l-lactide) blends. Biomaterials. 2004;25(11):2161-70.

32. Yuan Z, Favis BD. Coarsening of immiscible co-continuous blends during quiescent annealing. AIChE Journal. 2005;51(1):271-80.

33. Marchand C, Chen G, Tran-Khanh N, Sun J, Chen H, Buschmann MD et al. Microdrilled Cartilage Defects Treated with Thrombin-Solidified Chitosan/Blood Implant Regenerate a More Hyaline, Stable, and Structurally Integrated Osteochondral Unit Compared to Drilled Controls. Tissue Engineering: Part A. 2012;18(5-6):508-19.

34. Iliescu M, Hoemann CD, Shive MS, Chenite A, Buschmann MD. Ultrastructure of hybrid chitosan-glycerol phosphate blood clots by environmental scanning electron microscopy. Microscopy Research and Technique. 2008;71(3):236-47.

35. Mattanavee W, Suwantong O, Puthong S, Bunaprasert T, Hoven VP, Supaphol P. Immobilization of biomolecules on the surface of electrospun polycaprolactone fibrous scaffolds for tissue engineering. ACS Applied Materials & Interfaces. 2009;1(5):1076-85.

36. Marquis ME, Lord E, Bergeron E, Drevelle O, Park H, Cabana F et al. Bone cells-biomaterials interactions. Frontiers in Bioscience (Landmark Ed). 2009;14:1023-67.

37. Abrahamsson CK, Yang F, Park H, Brunger JM, Valonen PK, Langer R et al. Chondrogenesis and mineralization during in vitro culture of human mesenchymal stem cells on three-dimensional woven scaffolds. Tissue Engineering: Part A. 2010;16(12):3709-18.

38. Yildirim ED, Pappas D, Güçeri S, Sun W. Enhanced Cellular Functions on Polycaprolactone Tissue Scaffolds by O2 Plasma Surface Modification. Plasma Processes and Polymers. 2011;8(3):256-67.

39. Zhang H, Migneco F, Lin CY, Hollister SJ. Chemically-conjugated bone morphogenetic protein-2 on three-dimensional polycaprolactone scaffolds stimulates osteogenic activity in bone marrow stromal cells. Tissue Engineering: Part A. 2010;16(11):3441-8.

40. Gloria A, Causa F, Russo T, Battista E, Della Moglie R, Zeppetelli S et al. Three-dimensional poly(epsilon-caprolactone) bioactive scaffolds with controlled structural and surface properties. Biomacromolecules. 2012;13(11):3510-21.

41. Xia Y, Zhou PY, Cheng XS, Xie Y, Liang C, Li C et al. Selective laser sintering fabrication of nano-hydroxyapatite/poly-epsilon-caprolactone scaffolds for bone tissue engineering applications. International Journal of Nanomedicine. 2013;8:4197-213.

42. Kim M, Jung WK, Kim G. Bio-composites composed of a solid free-form fabricated polycaprolactone and alginate-releasing bone morphogenic protein and bone formation peptide for bone tissue regeneration. Bioprocess and Biosystems Engineering. 2013;36(11):1725-34.

43. Venugopal J, Low S, Choon AT, Kumar AB, Ramakrishna S. Electrospun-modified nanofibrous scaffolds for the mineralization of osteoblast cells. Journal of Biomedical Materials Research: Part A. 2008;85(2):408-17.

44. Keogh MB, O'Brien FJ, Daly JS. Substrate stiffness and contractile behaviour modulate the functional maturation of osteoblasts on a collagen–GAG scaffold. Acta Biomaterialia. 2010;6(11):4305-13.

45. Akay G, Birch MA, Bokhari MA. Microcellular polyHIPE polymer supports osteoblast growth and bone formation in vitro. Biomaterials. 2004;25(18):3991-4000.

46. Hosseinkhani H, Hosseinkhani M, Tian F, Kobayashi H, Tabata Y. Osteogenic differentiation of mesenchymal stem cells in self-assembled peptide-amphiphile nanofibers. Biomaterials. 2006;27(22):4079-86.

47. Guzmán-Morales J, El-Gabalawy H, Pham MH, Tran-Khanh N, McKee MD, Wu W et al. Effect of chitosan particles and dexamethasone on human bone marrow stromal cell osteogenesis and angiogenic factor secretion. Bone. 2009;45(4):617-26.

48. Chastain SR, Kundu AK, Dhar S, Calvert JW, Putnam AJ. Adhesion of mesenchymal stem cells to polymer scaffolds occurs via distinct ECM ligands and controls their osteogenic differentiation. Journal of Biomedical Materials Research: Part A. 2006;78(1):73-85.

49. Yang X, Chen X, Wang H. Acceleration of Osteogenic Differentiation of Preosteoblastic Cells by Chitosan Containing Nanofibrous Scaffolds. Biomacromolecules. 2009;10(10):2772-8.

50. Kuboki Y, Jin Q, Takita H. Geometry of carriers controlling phenotypic expression in BMP-induced osteogenesis and chondrogenesis. The Journal of Bone and Joint Surgery: American volume. 2001;83-A Suppl 1(Pt 2):S105-15.

CHAPTER 7 GENERAL DISCUSSION

This research study involved many unknown parameters starting from finding suitable materials for the fabrication of the scaffolds to the surface modification protocols, to the *in vitro* osteogenic assays. Therefore, developing the project from scratch and optimizing the experimental methods in order to achieve unbiased data were always accompanied by scientific and technical issues which had to be overcome in every single step. This chapter concentrates on the problems encountered during this thesis. According to the works done, three major categories are going to be discussed in this section: PCL scaffold fabrication and infiltration studies, surface modification of PCL scaffolds and finally osteogenic potential of the surface modified PCL scaffolds.

7.1 PCL scaffold fabrication and infiltration studies

The choice of PEO as the porogen phase was because of its water solubility as a factor that eliminates the issue of solvent toxicity. Due to the immiscibility of PCL and PEO, the use of PCL greatly facilitated the production of porous PCL scaffolds. However, we had first considered the production of PLA scaffolds. In that case, PEO could not be used as the porogen phase due to its partial miscibility with PLA. The morphology of non-annealed PLA-PEO samples as compared to PCL-PEO both at 50/50 vol% composition is demonstrated in Figure 7.1. Although sparse pores are observed on the surface of the partially miscible PLA/PEO blend after solvent extraction, the co-continuous morphology (pore interconnectivity) cannot be reached.

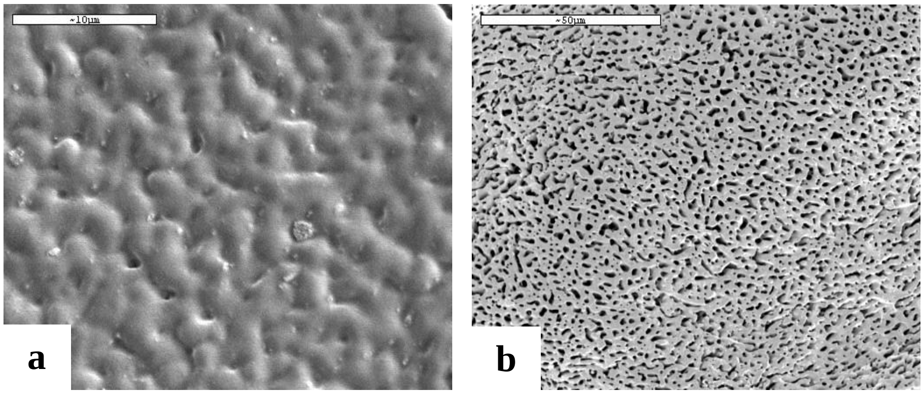

Figure 7.1: SEM microstructure of a) 50PLA/50PEO vol% and b) 50PCL/50PEO vol%. Scale bar = 10 microns

This is also in accordance with the results obtained by (Nijenhuis et al., 1996). Selection of another porogen phase could potentially need another solvent which could not have been as biocompatible as water. Therefore, we decided to change the polymer of interest according to the works in the literature without compromising the biocompatibility of the system.

However, the problems also existed even in the case of the PCL/PEO blend. The coarsening phenomenon achieved by the static annealing after the melt blending was carried out at 160°C which is 100°C higher than the melting temperatures of both PCL and PEO. The reason for the use of such high temperature is the fact the PCL/PEO blend appears to resist the coarsening phenomenon at lower temperatures and short annealing times (lower than 30min). SEM micrographs in Figure 7.2 demonstrates how the blend resists phase growth at 100°C and for annealing periods up to 30 min, which itself is considered to be a long time as compared to the reaction of other polymer blend systems to annealing. As a result, in order to achieve the required morphology for the production of scaffolds, the annealing times and temperature were respectively increased to 160°C and minimum 30 min, which led to the formation of pore sizes adequate for the bone tissue engineering application, as demonstrated in Figure 4.2.

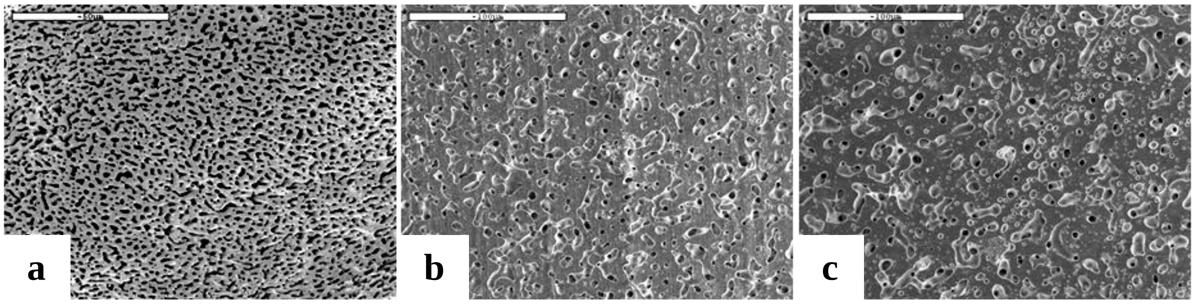

Figure 7.2: Resistance of co-continuous PCL/PEO blend to annealing at 100°C. (a) non-annealed; (b) t= 20 min; and c) t= 30 min

Knowing that virtually all the PEO in the annealed samples is extracted according to the results in Table 4.2, the scaffolds produced by 45PCL/55PEO vol% blends possess 55% porosity. Although the porosity of the scaffolds could have increased by partial extraction of PCL, or the incorporation of a third component to the system, we decided to keep the porosity unchanged.

This was because adding the porosity as another variable to the system would just overcomplicate this study. Although some studies report the neutral effect of porosity on *in vitro* osteogenesis, Takahashi et al. explained that lower porosities could in fact stimulate the osteogenesis due to cell aggregation (Itoh et al., 2004; Takahashi & Tabata, 2004). Our study only considered the effect of pore size at constant porosity. However, considering the effect of porosity and investigating more complicated morphologies could be a route to future works, which is discussed in the next section.

In order to investigate the effect of pore size on the infiltration of scaffolds by beads, several attempts have been done which failed due to the fact that the bead suspension escaped from the edges of the discs onto the culture plate. This led to a false reading of the number of beads that were supposed to fully pass through the scaffolds, and also caused a lot of variations in the data. In order to settle this issue, the agarose gel setup was devised as mentioned in Chapter 4 in order to confine the edges of the discs and only allow for the longitudinal penetration of beads/cells by gravity.

In order to verify how closely the beads could mimic hBMSCs for scaffold infiltration, the experiments had to be repeated with cells. However, unlike beads, the cells could not have been simply counted using a cell counter, since some cells adhered to the culture plate underneath the scaffolds during the infiltration time; the fact that increased the amount of experimental error and led to biased data. This issue was overcome by the hypothesis that the cells that fully penetrated the scaffolds and accumulated at the bottom of the pores would proliferate negligibly if trypsinized and resuspended into another culture plate after the infiltration assay. Consequently, fixing and staining the cell nuclei with the Hoechst dye could then be effectively performed, in order for us to be able to count the cells by image analysis.

7.2 Surface modification of PCL scaffolds

The deposition of a homogeneous chitosan layer on the PCL took a long time and energy, because of preliminary misleading results. The dip coating strategy was first employed to modify the surface of PCL. According to the pilot tests performed by (Guzmán-Morales et al., 2009) the concentration of 50 μg/mL was chosen for the chitosan solution. Fluorescent microscopy images of the PCL scaffolds treated with chitosan having rhodamine isothiocyanate (RITC) as the fluorophore (DDA=98% and M_w=237,000) showed promising results when PCL glowed only after the chitosan dip-coating, which determined that there certainly was a change in the surface chemistry of PCL. However, fluorescent microscopy was the only technique which confirmed the existence of chitosan material on the surface and kept us still trying to detect the layer by other techniques such as atomic force microscopy and SEM. Figure 7.3 shows some of these inconsistent results.

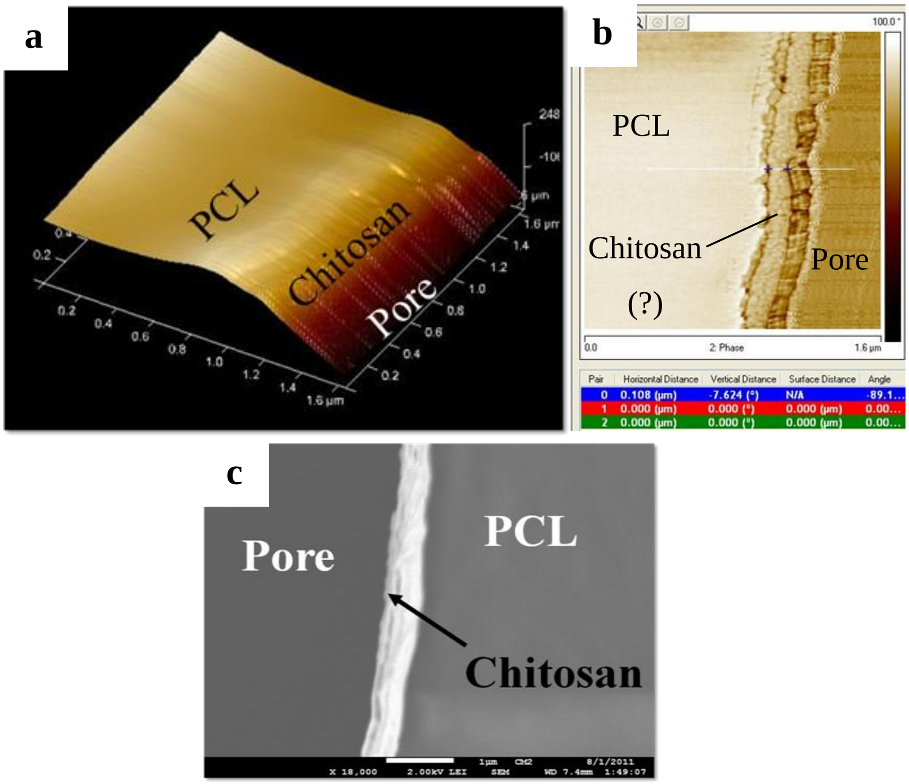

Pair	Horizontal Distance	Vertical Distance	Surface Distance	Angle
0	0.108 (μm)	-7.624 (°)	N/A	-89.1...
1	0.000 (μm)	0.000 (°)	0.000 (μm)	0.00...
2	0.000 (μm)	0.000 (°)	0.000 (μm)	0.00...

Figure 7.3: (a,b) Atomic force microscopy images (phase mode) of the interface between the PCL and a pore; and (c) SEM image of the same area showing an external layer with a considerable submicron thickness

Failed surface experiments one after another added to the confusion whether there was a coating on the surface or rather aggregates of chitosan which led to the fluorescence of the construct. By increasing the concentration of chitosan, the XPS measurements finally detected signals related to chitosan. However, the peaks detected by the survey mode of the XPS were not consistent at various positions on the scaffolds, which brought us to asking the question which according to literature is normally neglected by the researchers: is the chitosan coating uniformly deposited in every studied position inside the scaffold or not? Since our scaffold is 3D, i.e. the third dimension is in the same order of magnitude as the other two), it becomes extremely important to verify if the chitosan exists at various positions at various depths inside the constructs. The local non-homogeneity of the chitosan coating could lead to controversial cellular behavior and therefore lead to unreliable results. The idea of LbL deposition of polyelectrolytes on the PCL scaffolds was then put forward in order to solve the issue of data inconsistency related to the dip coating strategy, as explained in Chapter 5.

7.3 Osteogenic potential of surface modified PCL scaffolds

The topics discussed in this section are divided into two subsections: technical and scientific challenges.

7.3.1 Technical challenges

One of the technical problems that existed in our osteogenic assays was the fact that the cells failed to infiltrate the scaffolds of 41 μm pore average diameter. This scaffold was first selected to act as our small pore size sample (PCL1). However, such limitation in the scaffold infiltration led to an influential idea to improve the cell seeding strategy by modifying our cell seeding protocol. The results regarding the inefficient cell infiltration in the scaffolds of 40 μm pore size are separately included in Appendix 4 of this thesis and will not be discussed here.

Also, when analyzing the H&E and VK stained sections using toluene as the commonly used clearing agent in histological staining, PCL scaffolds were accidentally eluted from the slides, whose effect was both positive and negative. Visualizing the scaffolds in microscopic evaluations is of great importance, as the boundaries between the scaffold material and pores are evident. However, although this could be appealing for illustrating the ECM, cells and minerals in the space-filling areas between the pores, a lot of information is masked in the shadow of the scaffolds at the surfaces of the pores. We have discussed in Chapter 6 that by modifying the surface with chitosan, the cells are driven toward the PCL surface rather than migrating onto the collagenous fibers and sheets in the space-filling areas of the pores. However, this information is lost when the PCL scaffold is present on the slide. Therefore, to solve this issue, we decided to finally use toluene and extract PCL in order to include all data possible especially for histomorphometric measurements. The difference in the H&E, VK and alizarin red stained sections are elaborated in Appendix 4 of this thesis.

7.3.2 Scientific challenges

Since this last part of the thesis led to unexpected findings, the results produced in Chapter 6 are going to be discussed more in this section. Many researchers have previously studied the ability of various cell sources to biomineralize 3D scaffolds composed of different materials, including rodent, canine, and human primary MSCs, as well as iPS and osteoblast cell lines (Abrahamsson et al., 2010; Holy et al., 2000; Poh et al., 2013; Rai et al., 2004; Sun et al., 2012; Zou et al., 2013). However, as mentioned in section 2.2.3.3, attempts for determining pore size requirements for both *in vitro* and *in vivo* assays are still ongoing, and contradictory results do exist in this matter. Our histomorphometric results in Chapter 6, confirmed the neutral effect of pore size on the amount of minerals deposited, as previously reported by (Akay et al., 2004).

For unmodified PCL scaffolds, biomineralization occurred in highly colonized areas of PCL1 (top edge) and PCL2 (top edge and nearly top areas) scaffolds. Quantitative evaluation of by histomorphometry, however, showed low amounts of deposited minerals inside the constructs, which is greatly enhanced specifically for PCL1 scaffolds by the addition of chitosan to the pore surface. No effect was observed for the PCL2 samples. Therefore, two points have to be addressed:

1) Matrix mineralization across the scaffold thickness is not uniform for chitosan modified scaffolds, i.e. minerals are deposited sporadically, whereas areas with no minerals are observed. In Chapter 5, the homogeneity of the chitosan layer inside the scaffolds was ascertained. Therefore, hBMSCs were all supposedly in contact with roughly same surface components at all levels inside the structure. The reason for the occurrence of punctate minerals is therefore unclear.

2) Chitosan seems to improve biomineralization in the lower pore size, but not in the bigger pore size sample. The 2D osteogenic assay supported the theory that chitosan could be potentially ingested by hBMSCs and therefore the osteogenesis is suppressed, which is also in agreement

with the results obtained by (Guzmán-Morales et al., 2009). By increasing the pore size (from 84 μm to 141 μm), we are actually moving toward a more 2D system with more flat surfaces. As a result, hBMSCs seem to be able to dislodge and ingest chitosan particles from the surface of the pores, which can hold back the biomineralization process. However, in PCL1 scaffolds, chitosan actually promotes the deposition of minerals. We speculate that in the lower pore size, hBMSCs are somehow unable to internalize and consume chitosan particles present on the surface of the pores because of the higher curvature of the structure. Consequently, chitosan seems to enhance the process of biomineralization through mediation by cell-chitosan interactions rather than suppression by chitosan ingestion. It is reported that chitosan promotes bone formation through differentiation of h-BMSCs (Mathews et al., 2011). In the latter study, we believe that the cells were also unable to internalize chitosan and therefore a positive effect on the osteogenesis was observed. However, the arguments above are all speculations and therefore need to be backed up by future experiments, some of which are proposed in the next section.

CONCLUSION AND RECOMMENDATIONS

To date, a comprehensive examination of bone tissue engineering scaffolds of significantly different pore sizes including scaffold infiltration as an essential factor for the quality of tissue ingrowth, has not been carried out. Highly controlled 3D scaffolds destined for tissue engineering applications were fabricated from the melt blending of PCL and PEO at the co-continuous composition followed by static annealing and selective extraction of PEO. The generated scaffolds demonstrate complete pore interconnectivity, sharp unimodal pore size distribution, together with precise control over the pore size varying over two orders of magnitude. While non-annealed structures exhibit a polymodal and irregular size dispersity, our results show that the static annealing of the blends can lead to a sharp unimodal pore size distribution. For the purpose of investigating the effect of pore size on the infiltration of scaffolds by hBMSCs, a novel *in vitro* approach using model 10-micron beads was employed. These results demonstrated that a threshold in the scaffold pore size exists beyond which the hBMSCs can follow the linear behavior of the beads for the infiltration of the 3D constructs. This was attributed to the cell aggregation of hBMSCs near the seeding area for smaller pore sizes, whereas beads provided a baseline for non-aggregated systems at all ranges of pore size. Therefore, the novel bead system can be used as a reference model for devising proper seeding protocols to overcome retention and cell distribution issues within the scaffolds. PCL scaffolds of 141 μm average pore size in this study show the best bead/cell retention and distribution inside the scaffolds. According to cytotoxicity assays, no significant difference in L929 cell viability exists while in contact with the scaffolds, as compared to the control monolayer cells and few necrotic cells were detected. Nevertheless, there was a slight difference in cell morphology on tissue culture wells with a more elongated and fibroblast-like phenotype, compared to that on the PCL scaffold where the cells appeared to remain spherical. The sphericity of cells on the PCL scaffolds originates from its hydrophobic nature which has to be overcome by surface modification techniques.

In order to modify the surface of the PCL scaffolds, chitosan was selected as the bioactive agent that can bring hydrophilicity and cytocompatibility to the surface. For this purpose, Layer-by-Layer self assembly of polyelectrolytes was used and compared with the classic dip-coating technique. Chitosan surface modification of virtually 3D porous PCL constructs by the LbL technique has been done for the first time in this study. Since there is an intrinsic force of attraction between the positively charged chitosan and the slightly negatively charged PCL, the classic deep coating succeeds to deposit chitosan on the surface, yet fails to produce a homogeneous coating, which is confirmed by ToF-SIMS and XPS analysis. Gravimetric measurements demonstrate that three main regions exist according to the number of deposited layers: a surface preparation region, an onset for layer buildup region and a more well-defined layer region. These regions are confirmed by the XPS analysis examining the evolution of O/C, N/C and S/C ratios from 4 layers to 8 layers of assembled polyelectrolytes. These analyses were also performed at various depths of 3D constructs and demonstrate that a uniform local deposition of chitosan was observed. SEM imaging revealed that there is a microscopically rough assembly of layers ranging in total thickness from 550 to 700 nanometers. The hydrophilic surface of PCL after chitosan surface modification has the potential to be used in cell culture studies to evaluate the potential of the scaffolds for inducing hBMSC differentiation and osteoblasts mineralization.

For the first time, a novel static cell seeding at 4°C in a medium containing 2% serum is presented to maximize the efficiency of scaffold infiltration and improve the homogeneity of cell distribution at different depths within the scaffolds. Conventional cell seeding at 37°C as well as a 2-step seeding protocol at 37°C were proved inefficient by AlamarBlue® assay and image analysis. hBMSCs were cold-seeded in PCL scaffolds with and without chitosan coating, cultured for 10 days in CCM and another 21 days in an osteogenic medium. At day 2, sparse rounded hBMSCs were observed with filopodia anchoring to the unmodified PCL, while they formed elongated morphologies on chitosan coated pore surfaces. ESEM and histological evaluations at day 10 demonstrated that the cells prefer to migrate onto the secreted ECM in the space-filling area of the unmodified pores, whereas they actively spread on the pore surface of LbL-chitosan scaffolds. The % matrix formed in the structures is always higher at the outer pores (near the edge), which is not particularly influenced by the pore size and chitosan surface modification. Mineral deposits were observed at highly colonized areas of the unmodified scaffolds (near the top edge), but accumulated sporadically at deeper levels inside the LbL-chitosan modified scaffolds. Histomorphometric measurements demonstrate that chitosan promotes biomineralization in the smaller pore size scaffolds, while not influencing that in the larger pore size structures. Increasing the pore size drives the microstructure toward more flat surfaces and close to a 2D system, where the ingestion of chitosan particles by the hBMSCs appears to suppress the osteogenesis. On the other hand, the cells seem to be unable to dislodge chitosan particles at the smaller pore size potentially due to the higher curvature of the system. Hence, the biomineralization is enhanced through effective cell-chitosan interactions.

We hope that our efforts in the production of highly structured and surface modified porous PCL scaffolds have been fruitful, and that we have come one step closer to a sustainable treatment for bone fracture nonunions. There is still a long way ahead, but we are hopeful that someday will come that no Canadian is forced to suffer from painful complications following a bone injury.

The following recommendations for future work are worth considering:

1. For the sake of simplicity and to earn the basic knowledge about the properties of our scaffolds, this research study was carried out with PCL constructs with 55% porosity as imposed by the volume percentage of the PEO porogen phase. However, it would be interesting to investigate also the effect of porosity on cellular functions. This could be easily done by the partial extraction of PCL after PEO removal. Or, by adding another biodegradable blend component to the PCL/PEO system. Thermoplastic starch could be a fit candidate for the purpose, as it is also water-soluble like PEO. Actually, the blend of PCL/TPS has already been reported to resist annealing according to (Li & Favis, 2010), while we showed that the blend of PCL/PEO reacted to annealing at 160°C. Therefore, there might be a possibility of forming a bimodal pore size distribution depending on the thermodynamics of the ternary blend of PCL/PEO/TPS. Here is the morphology of the non-annealed ternary blend 40PCL/40PEO/20TPS36 vol% (as a pilot study in this thesis) with a higher porosity after the extraction of PEO and TPS. Scale bar = 1 micron.

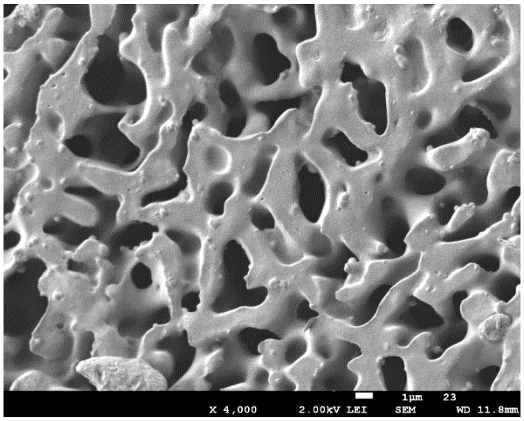

2. It would be also interesting to generate a microporous continuous network (<5 μm pore size) inside the matrix of the PCL scaffolds. These micropores could serve as pathways for the transfer of oxygen, nutrients and wastes, whereas the macropores can act as attachment sites for cells. This could be possible by developing an A/B/C–B–C ternary blend system in which one of the components has affinity to migrate into the PCL phase and form co-continuous structure while also reaching the interface, i.e. a co-continuous in co-continuous structure is formed. An example of this kind of morphology has been reported by (Wang et al., 2014)
3. In this study, PDADMAC and PSS polyelectrolytes were used for the LbL surface modification of PCL. Although these two materials are not exactly biocompatible, they did not show negative impact on our osteogenic and other cell experiments. Despite this limitation, these polyelectrolytes have been already used in tissue engineering *in vitro* experiments (Kidambi et al., 2004; Pastorino et al., 2006; Ricotti et al., 2011). Nevertheless, in our study, the LbL modified PCL surface was completely covered with chitosan. However, in order to reduce the risks of exposure to bio-incompatible compounds, we therefore suggest using bio and cell-compatible polyelectrolyte pairs that can replace PDADMAC and PSS while not compromising the strong positive and negative charges needed.
4. The elastic modulus of PCL has been reported in the literature to be in the range of 0.21-0.44 GPa which is in accordance with that of the proximal trabecular bone (Linde & Hvid, 1989). Although PCL can mechanically support the ingrowth of trabecular bone, it will fail to assist the formation of cortical bone with a high elastic modulus of 11.5-17 GPa (Cullinane & Einhorn, 2002). Therefore, it is essential to mechanically reinforce PCL by incorporating nano and microparticles in the PCL matrix or mixing PCL and PEO in a ternary blend with HA which is the inorganic part of the bone matrix.
5. It would also be interesting to investigate the effect of chitosan concentration and molecular weight on the efficiency of LbL deposition as well as osteogenesis in the 3D PCL structure. We should note that high chitosan concentrations might lead to cell apoptosis during osteogenesis (Guzmán-Morales et al., 2009). Also, we might be able to find a critical molecular weight for chitosan which can reverse the role of chitosan in

osteogenesis, i.e. chitosan ingestion by hBMSCs and suppression of mineralization, as opposed to effective cell-chitosan interactions that can promote osteogenesis. Other positively charged bioactive agents such as positively charged liposomes which release growth factors can also be potentially deposited on the surface whose effects on osteogenesis can be studied.

6. The evaluation of bone regeneration *in vivo* at higher pore sizes of PCL scaffolds (to permit vascularization) in the presence or absence of the chitosan coating could lead to valuable information about the efficiency of these scaffolds in potential clinical applications. It would be interesting to see whether the increase in the pore size in the presence of chitosan, would follow our *in vitro* results and lead to lower levels of bone formation *in vivo*, the formation of vasculature inside the bigger pores as suggested by (Kuboki et al., 2001) can yield high levels of new bone formation.

7. In Chapter 6, we speculated that superior biomineralization in the smaller pore size of the LbL-chitosan modified PCL could be attributed to the higher curvature in these scaffolds. In order to prove this hypothesis, we can simplify the system to hollow cylindrical substrates (PCL or not) with different diameters: small representing high curvature; and large representing low curvature systems. The surface of these cylindrical substrates should be chitosan coated via the LbL technique (same procedure as in Chapter 5). hBMSCs can now be seeded on the external and/or internal surface of these tubes and cultured in proliferation and osteogenic medium for 10 and another 21 days, respectively. The hypothesis is that there will be more mineralization on the smaller diameter tube than the larger one.

8. The cylindrical systems mentioned above can also be combined in concentric cylinders with different diameters (as depicted in the figure below, $\phi_1<\phi_2$) to mimic the ring structure of the osteon. In the presence of chitosan, concentric cell monolayers can be formed with a likely mineral concentration gradient from low on the outer layers to high on the inner layers close to the center.

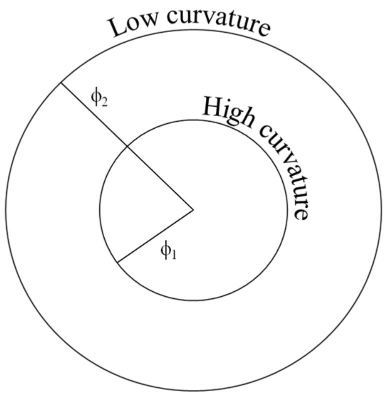

9. A substitute for the cylindrical systems above which would perhaps be more feasible is the use of flat substrates yet with a jagged structure with shallow cavities between the surface stripes. The distance between the “bumpy” stripes determines the curvature of the system; the smaller the distance, the higher the curvature.

At the end, I would like to wish the best of luck to the researcher(s) that follow me in this project in order to bring our product closer to clinical applications and hopefully benefit mankind.

REFERENCES

Canadian Community Health Survey, 2009-2010. Canadian Community Health Survey- Annual Component. 2009-2010 combined.: Statistics Canada.

Aarvold, A., Smith, J. O., Tayton, E. R., Lanham, S. A., Chaudhuri, J. B., Turner, I. G., & Oreffo, R. O. C. 2013. The effect of porosity of a biphasic ceramic scaffold on human skeletal stem cell growth and differentiation in vivo. *Journal of Biomedical Materials Research Part A*, 101(12): 3431-3437.

AATB. September 2010. 2007 Annual Survey Results for AATB-Accredited Tissue Banks in the United States

Abbasi, F., Mirzadeh, H., & Katbab, A.-A. 2002. Bulk and surface modification of silicone rubber for biomedical applications. *Polymer International*, 51(10): 882-888.

Abrahamsson, C. K., Yang, F., Park, H., Brunger, J. M., Valonen, P. K., Langer, R., Welter, J. F., Caplan, A. I., Guilak, F., & Freed, L. E. 2010. Chondrogenesis and mineralization during in vitro culture of human mesenchymal stem cells on three-dimensional woven scaffolds. *Tissue Engineering Part A*, 16(12): 3709-3718.

Abramson, S. D., Seyda, A., Sit, P. S., & Kohn, J. 2002. *Characterization of degradable polymers for orthopedic application - Examining tyrosine-derived polycarbonates for tissue engineering of bone*. Dordrecht: Springer.

Adusumilli, M., & Bruening, M. L. 2009. Variation of Ion-Exchange Capacity, ζ Potential, and Ion-Transport Selectivities with the Number of Layers in a Multilayer Polyelectrolyte Film. *Langmuir*, 25(13): 7478-7485.

Agarwal, R. 2013. Unfavourable results with distraction in craniofacial skeleton. *Indian Journal of Plastic Surgery*, 46(2): 194-203.

Akay, G., Birch, M. A., & Bokhari, M. A. 2004. Microcellular polyHIPE polymer supports osteoblast growth and bone formation in vitro. *Biomaterials*, 25(18): 3991-4000.

Amemiya, T., Nakaoka, K., Hamada, Y., & Hayakawa, T. 2012. Effect of Porosity of Titanium Web on Cortical Bone Response. *Journal of Hard Tissue Biology*, 21(2): 103-108.

Amir, L. R., Suniarti, D. F., Utami, S., & Abbas, B. 2014. Chitosan as a potential osteogenic factor compared with dexamethasone in cultured macaque dental pulp stromal cells. *Cell and Tissue Research*.

Angelatos, A. S., Wang, Y., & Caruso, F. 2008. Probing the Conformation of Polyelectrolytes in Mesoporous Silica Spheres. *Langmuir*, 24(8): 4224-4230.

Anseth Kristi, S., Svaldi Dina, C., Laurencin Cato, T., & Langer, R. 1997. Photopolymerization of Novel Degradable Networks for Orthopedic Applications, *Photopolymerization*, Vol. 673: 189-202: American Chemical Society.

Anseth, K. S., Metters, A. T., Bryant, S. J., Martens, P. J., Elisseeff, J. H., & Bowman, C. N. 2002. In situ forming degradable networks and their application in tissue engineering and drug delivery. *Journal of Controlled Release*, 78(1–3): 199-209.

Antunes, C. F., van Duin, M., & Machado, A. V. 2011. Morphology and phase inversion of EPDM/PP blends – Effect of viscosity and elasticity. *Polymer Testing*, 30(8): 907-915.

Arends, C. B. 1992. Percolation in injection molded polymer blends. *Polymer Engineering & Science*, 32(13): 841-844.

Arns, C. H., Knackstedt, M. A., Roberts, A. P., & Pinczewski, V. W. 1999. Morphology, Cocontinuity, and Conductive Properties of Anisotropic Polymer Blends. *Macromolecules*, 32(18): 5964-5966.

Aslan, M., Simsek, G., & Dayi, E. 2006. The effect of hyaluronic acid-supplemented bone graft in bone healing: experimental study in rabbits. *Journal of Biomaterials Applications*, 20(3): 209-220.

Athanasiou, K. A., Agrawal, C. M., Barber, F. A., & Burkhart, S. S. 1998. Orthopaedic applications for PLA-PGA biodegradable polymers. *Arthroscopy*, 14(7): 726-737.

Athanasiou, K. A., Niederauer, G. G., & Agrawal, C. M. 1996. Sterilization, toxicity, biocompatibility and clinical applications of polylactic acid/polyglycolic acid copolymers. *Biomaterials*, 17(2): 93-102.

Attawia, M., Kadiyala, S., Fitzgerald, K., . 2003. Cell Based Approaches for Bone Graft Substitutes. In C. T. Laurencin (Ed.), *Bone Graft Substitutes*, 1st Edn ed.: 126. West Conshohocken, Philadelphia: ASTM International.

Aubin, J. 2001. Regulation of Osteoblast Formation and Function. *Reviews in Endocrine and Metabolic Disorders*, 2(1): 81-94.

Aulin, C., Varga, I., Claesson, P. M., Wågberg, L., & Lindström, T. 2008. Buildup of Polyelectrolyte Multilayers of Polyethyleneimine and Microfibrillated Cellulose Studied by in Situ Dual-Polarization Interferometry and Quartz Crystal Microbalance with Dissipation. *Langmuir*, 24(6): 2509-2518.

Avgeropoulos, G. N., Weissert, F. C., Biddison, P. H., & Böhm, G. G. A. 1976. Heterogeneous Blends of Polymers. Rheology and Morphology. *Rubber Chemistry and Technology*, 49(1): 93-104.

Ayers, R. A., Simske, S. J., Bateman, T. A., Petkus, A., Sachdeva, R. L., & Gyunter, V. E. 1999. Effect of nitinol implant porosity on cranial bone ingrowth and apposition after 6 weeks. *Journal of Biomedical Materials Research*, 45(1): 42-47.

Baad-Hansen, T., Kold, S., Nielsen, P. T., Laursen, M. B., Christensen, P. H., & Soballe, K. 2011. Comparison of trabecular metal cups and titanium fiber-mesh cups in primary hip arthroplasty: a randomized RSA and bone mineral densitometry study of 50 hips. *Acta Orthopaedica*, 82(2): 155-160.

Bai, F., Wang, Z., Lu, J., Liu, J., Chen, G., Lv, R., Wang, J., Lin, K., Zhang, J., & Huang, X. 2010. The correlation between the internal structure and vascularization of controllable porous bioceramic materials in vivo: a quantitative study. *Tissue Engineering Part A*, 16(12): 3791-3803.

Bai, F., Zhang, J. K., Wang, Z., Lu, J. X., Chang, J. A., Liu, J. A., Meng, G. L., & Dong, X. 2011. The effect of pore size on tissue ingrowth and neovascularization in porous bioceramics of controlled architecture in vivo. *Biomedical Materials*, 6(1).

Banes, A. J., Lee, G., Graff, R., Otey, C., Archambault, J., Tsuzaki, M., Elfervig, M., & Qi, J. 2001. Mechanical forces and signaling in connective tissue cells: cellular mechanisms of detection, transduction, and responses to mechanical deformation. *Current Opinion in Orthopaedics*, 12(5): 389-396.

Barralet, J. E., Wang, L., Lawson, M., Triffitt, J. T., Cooper, P. R., & Shelton, R. M. 2005. Comparison of bone marrow cell growth on 2D and 3D alginate hydrogels. *Journal of Materials Science: Materials in Medicine*, 16(6): 515-519.

Bartels, K. E. 1987. Nonunion. *Veterinary Clinics of North America: Small Animal Practice*, 17(4): 799-809.

Bartis, D., Pongracz, J. . 2011. Three dimensional tissue cultures and tissue engineering – Basic principles, *Three dimensional tissue cultures and tissue engineering – Basic principles*: 1-3. Pécs, Hungary: University of Pécs.

Batorsky, A., Liao, J., Lund, A. W., Plopper, G. E., & Stegemann, J. P. 2005. Encapsulation of adult human mesenchymal stem cells within collagen-agarose microenvironments. *Biotechnology and Bioengineering*, 92(4): 492-500.

Bauer, T. W., & Muschler, G. F. 2000. Bone graft materials. An overview of the basic science. *Clinical Orthopaedics and Related Research,* (371): 10-27.

Bernhardt, A., Lode, A., Mietrach, C., Hempel, U., Hanke, T., & Gelinsky, M. 2009. In vitro osteogenic potential of human bone marrow stromal cells cultivated in porous scaffolds from mineralized collagen. *Journal of Biomedical Materials Research Part A*, 90A(3): 852-862.

Betz, R. R. 2002. Limitations of autograft and allograft: new synthetic solutions. *Orthopedics*, 25(5 Suppl): s561-570.

Bhamidipati, M., Sridharan, B., Scurto, A. M., & Detamore, M. S. 2013. Subcritical CO2 sintering of microspheres of different polymeric materials to fabricate scaffolds for tissue engineering. *Materials Science and Engineering: C*, 33(8): 4892-4899.

Bhardwaj, N., & Kundu, S. C. 2010. Electrospinning: A fascinating fiber fabrication technique. *Biotechnology Advances*, 28(3): 325-347.

Boland, E. D., Wnek, G. E., Simpson, D. G., Pawlowski, K. J., & Bowlin, G. L. 2001. Tailoring Tissue Engineering Scaffolds Using Electrostatic Processing Techniques: A Study Of Poly(Glycolic Acid) Electrospinning. *Journal of Macromolecular Science, Part A*, 38(12): 1231-1243.

Bonewald, L. F., Harris, S. E., Rosser, J., Dallas, M. R., Dallas, S. L., Camacho, N. P., Boyan, B., & Boskey, A. 2003. Von Kossa Staining Alone Is Not Sufficient to Confirm that Mineralization In Vitro Represents Bone Formation. *Calcified Tissue International*, 72(5): 537-547.

Bosnakovski, D., Mizuno, M., Kim, G., Takagi, S., Okumura, M., & Fujinaga, T. 2005. Isolation and multilineage differentiation of bovine bone marrow mesenchymal stem cells. *Cell and Tissue Research*, 319(2): 243-253.

Boukhechba, F., Balaguer, T., Michiels, J.-F., Ackermann, K., Quincey, D., Bouler, J.-M., Pyerin, W., Carle, G. F., & Rochet, N. 2009. Human Primary Osteocyte Differentiation in a 3D Culture System. *Journal of Bone and Mineral Research*, 24(11): 1927-1935.

Boulmedais, F., Ball, V., Schwinte, P., Frisch, B., Schaaf, P., & Voegel, J.-C. 2002. Buildup of Exponentially Growing Multilayer Polypeptide Films with Internal Secondary Structure. *Langmuir*, 19(2): 440-445.

Bourry, D., & Favis, B. D. 1998. Cocontinuity and phase inversion in HDPE/PS blends: Influence of interfacial modification and elasticity. *Journal of Polymer Science Part B: Polymer Physics*, 36(11): 1889-1899.

Bryant, S. J., & Anseth, K. S. 2001. The effects of scaffold thickness on tissue engineered cartilage in photocrosslinked poly(ethylene oxide) hydrogels. *Biomaterials*, 22(6): 619-626.

Buttafoco, L., Engbers-Buijtenhuijs, P., Poot, A. A., Dijkstra, P. J., Daamen, W. F., van Kuppevelt, T. H., Vermes, I., & Feijen, J. 2006. First steps towards tissue engineering of small-diameter blood vessels: Preparation of flat scaffolds of collagen and elastin by means of freeze drying. *Journal of Biomedical Materials Research Part B: Applied Biomaterials*, 77B(2): 357-368.

Caplan, A. I. 2005. Review: mesenchymal stem cells: cell-based reconstructive therapy in orthopedics. *Tissue Engineering*, 11(7-8): 1198-1211.

Carmagnola, D., Adriaens, P., & Berglundh, T. 2003. Healing of human extraction sockets filled with Bio-Oss®. *Clinical Oral Implants Research*, 14(2): 137-143.

Caruso, F., Niikura, K., Furlong, D. N., & Okahata, Y. 1997. 1. Ultrathin Multilayer Polyelectrolyte Films on Gold: Construction and Thickness Determination. *Langmuir*, 13(13): 3422-3426.

Chanlalit, C., Shukla, D. R., Fitzsimmons, J. S., An, K. N., & O'Driscoll, S. W. 2012. Stress shielding around radial head prostheses. *Journal of Hand Surgery (American Volume)*, 37(10): 2118-2125.

Chao, E. Y., & Inoue, N. 2003. Biophysical stimulation of bone fracture repair, regeneration and remodelling. *European Cells & Materials*, 6: 72-84; discussion 84-75.

Chen, F., Mao, T., Tao, K., Chen, S., Ding, G., & Gu, X. 2002. Bone graft in the shape of human mandibular condyle reconstruction via seeding marrow-derived osteoblasts into porous coral in a nude mice model. *Journal of Oral and Maxillofacial Surgery*, 60(10): 1155-1159.

Chiu, R., Ma, T., Smith, R. L., & Goodman, S. B. 2006. Polymethylmethacrylate particles inhibit osteoblastic differentiation of bone marrow osteoprogenitor cells. *Journal of Biomedical Materials Research Part A*, 77A(4): 850-856.

Cho, J., Char, K., Hong, J. D., & Lee, K. B. 2001. Fabrication of Highly Ordered Multilayer Films Using a Spin Self-Assembly Method. *Advanced Materials*, 13(14): 1076-1078.

Choong, C., Triffitt, J. T., & Cui, Z. F. 2004. Polycaprolactone Scaffolds for Bone Tissue Engineering: Effects of a Calcium Phosphate Coating Layer on Osteogenic Cells. *Food and Bioproducts Processing*, 82(2): 117-125.

Chu, C. C. 1981. Hydrolytic degradation of polyglycolic acid: Tensile strength and crystallinity study. *Journal of Applied Polymer Science*, 26(5): 1727-1734.

Ciapetti, G., Ambrosio, L., Savarino, L., Granchi, D., Cenni, E., Baldini, N., Pagani, S., Guizzardi, S., Causa, F., & Giunti, A. 2003. Osteoblast growth and function in porous poly ε-caprolactone matrices for bone repair: a preliminary study. *Biomaterials*, 24(21): 3815-3824.

Coelho, M. J., Trigo Cabral, A., & Fernandes, M. H. 2000. Human bone cell cultures in biocompatibility testing. Part I: osteoblastic differentiation of serially passaged human bone marrow cells cultured in α-MEM and in DMEM. *Biomaterials*, 21(11): 1087-1094.

Costa-Pinto, A. R., Correlo, V. M., Sol, P. C., Bhattacharya, M., Charbord, P., Delorme, B., Reis, R. L., & Neves, N. M. 2009. Osteogenic Differentiation of Human Bone Marrow Mesenchymal Stem Cells Seeded on Melt Based Chitosan Scaffolds for Bone Tissue Engineering Applications. *Biomacromolecules*, 10(8): 2067-2073.

Croll, T. I., O'Connor, A. J., Stevens, G. W., & Cooper-White, J. J. 2006. A Blank Slate? Layer-by-Layer Deposition of Hyaluronic Acid and Chitosan onto Various Surfaces. *Biomacromolecules*, 7(5): 1610-1622.

Cui, Y., Liu, Y., Cui, Y., Jing, X., Zhang, P., & Chen, X. 2009. The nanocomposite scaffold of poly(lactide-co-glycolide) and hydroxyapatite surface-grafted with l-lactic acid oligomer for bone repair. *Acta Biomaterialia*, 5(7): 2680-2692.

Cui, Y. L., Qi, A. D., Liu, W. G., Wang, X. H., Wang, H., Ma, D. M., & Yao, K. D. 2003. Biomimetic surface modification of poly(L-lactic acid) with chitosan and its effects on articular chondrocytes in vitro. *Biomaterials*, 24(21): 3859-3868.

Cullinane, D. M., & Einhorn, T. A. 2002. Chapter 2 - Biomechanics of Bone. In J. P. Bilezikian, L. G. Raisz, & G. A. Rodan (Eds.), *Principles of Bone Biology (Second Edition)*: 17-32. San Diego: Academic Press.

Dalton, P. D., Woodfield, T., & Hutmacher, D. W. 2009. Erratum to: SnapShot: Polymer Scaffolds for Tissue Engineering [Biomaterials 30/4 (2009) 701–702]. *Biomaterials*, 30(12): 2420.

Damien, E., Hing, K., Saeed, S., & Revell, P. A. 2003. A preliminary study on the enhancement of the osteointegration of a novel synthetic hydroxyapatite scaffold in vivo. Journal of Biomedical Materials Research Part A, 66(2): 241-246.

Daniels, A. U., Chang, M. K., & Andriano, K. P. 1990. Mechanical properties of biodegradable polymers and composites proposed for internal fixation of bone. *Journal of Applied Biomaterials*, 1(1): 57-78.

Darain, F., Chan, W. Y., & Chian, K. S. 2010. Performance of Surface-Modified Polycaprolactone on Growth Factor Binding, Release, and Proliferation of Smooth Muscle Cells. *Soft Materials*, 9(1): 64-78.

Dawson, J. I., & Oreffo, R. O. C. 2008. Bridging the regeneration gap: Stem cells, biomaterials and clinical translation in bone tissue engineering. *Archives of Biochemistry and Biophysics*, 473(2): 124-131.

De Vasconcellos, Y. R. C., Renata Falchete do Prado, Luis Gustavo Oliveira de Vasconcellos, Mário Lima de Alencastro Graça,Carlos Alberto Alves Cairo 2012. Porous Titanium by Powder Metallurgy for Biomedical Application: Characterization, Cell Citotoxity and in vivo Tests of Osseointegration. In R. Hudak (Ed.), *Biomedical Engineering - Technical Applications in Medicine*. : InTech.

DeAngelis, M. P. 1975. Causes of delayed union and nonunion of fractures. *Veterinary Clinics of North America*, 5(2): 251-258.

Decher, G. 1997. Fuzzy Nanoassemblies: Toward Layered Polymeric Multicomposites. *Science*, 277(5330): 1232-1237.

Decher, G., Hong, J. D., & Schmitt, J. 1992. Buildup of ultrathin multilayer films by a self-assembly process: III. Consecutively alternating adsorption of anionic and cationic polyelectrolytes on charged surfaces. *Thin Solid Films*, 210–211, Part 2(0): 831-835.

Dedecker, K., Groeninckx, G., & Inoue, T. 1998. Reactive compatibilization of A/(B/C) polymer blends. Part 3. Quantitative analysis of the interfacial thickness and the interfacial reaction. *Polymer*, 39(21): 5001-5010.

Dementjev, A. P., de Graaf, A., van de Sanden, M. C. M., Maslakov, K. I., Naumkin, A. V., & Serov, A. A. 2000. X-Ray photoelectron spectroscopy reference data for identification of the C3N4 phase in carbon–nitrogen films. *Diamond and Related Materials*, 9(11): 1904-1907.

Domb, A. J., Mathiowitz, E., Ron, E., Giannos, S., & Langer, R. 1991. Polyanhydrides. IV. Unsaturated and crosslinked polyanhydrides. *Journal of Polymer Science Part A: Polymer Chemistry*, 29(4): 571-579.

Domingos, M., Intranuovo, F., Gloria, A., Gristina, R., Ambrosio, L., Bártolo, P. J., & Favia, P. 2013. Improved osteoblast cell affinity on plasma-modified 3-D extruded PCL scaffolds. *Acta Biomaterialia*, 9(4): 5997-6005.

Dong, J., Kojima, H., Uemura, T., Kikuchi, M., Tateishi, T., & Tanaka, J. 2001. In vivo evaluation of a novel porous hydroxyapatite to sustain osteogenesis of transplanted bone marrow-derived osteoblastic cells. *Journal of Biomedical Materials Research*, 57(2): 208-216.

Dubas, S. T., Kittitheeranun, P., Rangkupan, R., Sanchavanakit, N., & Potiyaraj, P. 2009. Coating of polyelectrolyte multilayer thin films on nanofibrous scaffolds to improve cell adhesion. *Journal of Applied Polymer Science*, 114(3): 1574-1579.

Dubas, S. T., & Schlenoff, J. B. 1999. Factors Controlling the Growth of Polyelectrolyte Multilayers. *Macromolecules*, 32(24): 8153-8160.

Edmondson, S., Osborne, V. L., & Huck, W. T. S. 2004. Polymer brushes via surface-initiated polymerizations. *Chemical Society Reviews*, 33(1): 14-22.

Ehashi, T., Takemura, T., Hanagata, N., Minowa, T., Kobayashi, H., Ishihara, K., & Yamaoka, T. 2014. Comprehensive Genetic Analysis of Early Host Body Reactions to the Bioactive and Bio-Inert Porous Scaffolds. *PLoS ONE*, 9(1): e85132.

Einhorn, T. A. 1995. Enhancement of fracture-healing. *Journal of bone and joint surgery. American volume*, 77(6): 940-956.

El-Ghannam, A. R. 2004. Advanced bioceramic composite for bone tissue engineering: design principles and structure-bioactivity relationship. *Journal of Biomedical Materials Research Part A*, 69(3): 490-501.

El Haitami, A. E., Martel, D., Ball, V., Nguyen, H. C., Gonthier, E., Labbé, P., Voegel, J.-C., Schaaf, P., Senger, B., & Boulmedais, F. 2009. Effect of the Supporting Electrolyte Anion on the Thickness of PSS/PAH Multilayer Films and on Their Permeability to an Electroactive Probe. *Langmuir*, 25(4): 2282-2289.

Elemans, P. H. M., Janssen, J. M. H., & Meijer, H. E. H. 1990. The measurement of interfacial tension in polymer/polymer systems: The breaking thread method. *Journal of Rheology (1978-present)*, 34(8): 1311-1325.

Eslaminejad, M. B., Bagheri, F., Zandi, M., Nejati, E., & Zomorodian, E. 2011. Study of Mesenchymal Stem Cell Proliferation and Bone Differentiation on Composite Scaffolds of PLLA and Nano Hydroxyapatite with Different Morphologies. *Yakhteh*, 12(4): 469-476.

Farhat, T. R., & Schlenoff, J. B. 2002. Corrosion control using polyelectrolyte multilayers. *Electrochemical and Solid-State Letters*, 5(4): B13-B15.

Favis, B. D., & Chalifoux, J. P. 1988. Influence of composition on the morphology of polypropylene/polycarbonate blends. *Polymer*, 29(10): 1761-1767.

Ferreira, M., & Rubner, M. F. 1995. Molecular-Level Processing of Conjugated Polymers. 1. Layer-by-Layer Manipulation of Conjugated Polyions. *Macromolecules*, 28(21): 7107-7114.

Filippone, G., Dintcheva, N. T., La Mantia, F. P., & Acierno, D. 2010. Selective localization of organoclay and effects on the morphology and mechanical properties of LDPE/PA11 blends with distributed and co-continuous morphology. *Journal of Polymer Science Part B: Polymer Physics*, 48(5): 600-609.

Fischer, E. M., Layrolle, P., Van Blitterswijk, C. A., & De Bruijn, J. D. 2003. Bone formation by mesenchymal progenitor cells cultured on dense and microporous hydroxyapatite particles. *Tissue Engineering*, 9(6): 1179-1188.

Fisher, J. P., Holland, T. A., Dean, D., Engel, P. S., & Mikos, A. G. 2001. Synthesis and properties of photocross-linked poly(propylene fumarate) scaffolds. *Journal of biomaterials science. Polymer Edition*, 12(6): 673-687.

Fisher, J. P., Jo, S., Mikos, A. G., & Reddi, A. H. 2004. Thermoreversible hydrogel scaffolds for articular cartilage engineering. *Journal of Biomedical Materials Research Part A*, 71(2): 268-274.

Fisher, J. P., Vehof, J. W. M., Dean, D., van der Waerden, J. P. C. M., Holland, T. A., Mikos, A. G., & Jansen, J. A. 2002. Soft and hard tissue response to photocrosslinked poly(propylene fumarate) scaffolds in a rabbit model. *Journal of Biomedical Materials Research*, 59(3): 547-556.

Fleer, G. 1993. *Polymers at Interfaces*: Springer.

Fleming, J. E., Jr., Cornell, C. N., & Muschler, G. F. 2000. Bone cells and matrices in orthopedic tissue engineering. *Orthopedic Clinics of North America*, 31(3): 357-374.

Fox, S. M. 1984. Cancellous bone grafting in the dog: an overview. *Journal American Animal Hospital Association*, 20: 840-848.

Frazza, E. J., & Schmitt, E. E. 1971. A new absorbable suture. *J Biomed Mater Res*, 5(2): 43-58.

Fukuda, T., Goto, A., & Ohno, K. 2000. Mechanisms and kinetics of living radical polymerizations. *Macromolecular Rapid Communications*, 21(4): 151-165.

Gabbay, J. S., Heller, J. B., Mitchell, S. A., Zuk, P. A., Spoon, D. B., Wasson, K. L., Jarrahy, R., Benhaim, P., & Bradley, J. P. 2006. Osteogenic potentiation of human adipose-derived stem cells in a 3-dimensional matrix. *Annals of Plastic Surgery*, 57(1): 89-93.

Galloway, J. A., & Macosko, C. W. 2004. Comparison of methods for the detection of cocontinuity in poly(ethylene oxide)/polystyrene blends. *Polymer Engineering & Science*, 44(4): 714-727.

Garg, A., Heflin, J. R., Gibson, H. W., & Davis, R. M. 2008. Study of Film Structure and Adsorption Kinetics of Polyelectrolyte Multilayer Films: Effect of pH and Polymer Concentration. *Langmuir*, 24(19): 10887-10894.

Gergen W.P., L. R. G., Davison S. 1996. Hydrogenated block copolymers in thermoplastic elastomer interpenetrating polymer networks. In L. N. R. Holden G., Quirk R.P., Schroeder H.E., (Ed.), *Thermoplastic Elastomers*, 2nd Ed. ed. New York: Hanser Publishers.

Ghavidel Mehr, N., Hoemann, C. D., & Favis, B. D. 2014a. Chitosan Surface Modification of Fully Interconnected 3D Porous Poly(ε-caprolactone) by the LbL Approach. *ACS Applied Materials & Interfaces*.

Ghavidel Mehr, N., Li, X., Ariganello, M., Hoemann, C., & Favis, B. 2014b. Poly(ε-caprolactone) scaffolds of highly controlled porosity and interconnectivity derived from co-continuous polymer blends: model bead and cell infiltration behavior. *Journal of Materials Science: Materials in Medicine*, 25(9): 2083-2093.

Ghavidel Mehr, N., Li, X., Favis, B. D., & Hoemann, C. D. 2014c. Osteogenic mesenchymal stem cells populate 3D poly(ε-caprolactone) scaffolds with interconnected pores and preferentially mineralize LbL chitosan-coated surfaces. *Tissue Engineering Part A*.

Glowacki, J., & Mizuno, S. 2008. Collagen scaffolds for tissue engineering. *Biopolymers*, 89(5): 338-344.

Gogolewski, S. 2000. Bioresorbable polymers in trauma and bone surgery. *Injury*, 31 Suppl 4: 28-32.

Gong, W., Abdelouas, A., & Lutze, W. 2001. Porous bioactive glass and glass-ceramics made by reaction sintering under pressure. *Journal of Biomedical Materials Research*, 54(3): 320-327.

Graul, T. W., & Schlenoff, J. B. 1999. Capillaries Modified by Polyelectrolyte Multilayers for Electrophoretic Separations. *Analytical Chemistry*, 71(18): 4007-4013.

Graziano, A., d'Aquino, R., Cusella-De Angelis, M. G., De Francesco, F., Giordano, A., Laino, G., Piattelli, A., Traini, T., De Rosa, A., & Papaccio, G. 2008. Scaffold's surface geometry significantly affects human stem cell bone tissue engineering. *Journal of Cellular Physiology*, 214(1): 166-172.

Gronthos, S., Graves, S. E., Ohta, S., & Simmons, P. J. 1994. The STRO-1+ fraction of adult human bone marrow contains the osteogenic precursors. *Blood*, 84(12): 4164-4173.

Groth, T., Klosz, K., Campbell, E. J., New, R. R., Hall, B., & Goering, H. 1994. Protein adsorption, lymphocyte adhesion and platelet adhesion/activation on polyurethane ureas is related to hard segment content and composition. *Journal of Biomaterials Science, Polymer Edition*, 6(6): 497-510.

Groth, T., Liu, Z.-M., Niepel, M., Peschel, D., Kirchhof, K., Altankov, G., & Faucheux, N. 2010. Chemical and Physical Modifications of Biomaterial Surfaces to Control Adhesion of Cells. In V. P. Shastri, G. Altankov, & A. Lendlein (Eds.), *Advances in Regenerative Medicine: Role of Nanotechnology, and Engineering Principles*: 253-284: Springer Netherlands.

Gunatillake, P. A., & Adhikari, R. 2003. Biodegradable synthetic polymers for tissue engineering. *European Cells & Materials*, 5: 1-16; discussion 16.

Guo, L., Kawazoe, N., Fan, Y., Ito, Y., Tanaka, J., Tateishi, T., Zhang, X., & Chen, G. 2008. Chondrogenic differentiation of human mesenchymal stem cells on photoreactive polymer-modified surfaces. *Biomaterials*, 29(1): 23-32.

Guo, X., Wang, C., Duan, C., Descamps, M., Zhao, Q., Dong, L., Lu, S., Anselme, K., Lu, J., & Song, Y. Q. 2004. Repair of osteochondral defects with autologous chondrocytes seeded onto bioceramic scaffold in sheep. *Tissue Engineering*, 10(11-12): 1830-1840.

Guzmán-Morales, J., El-Gabalawy, H., Pham, M. H., Tran-Khanh, N., McKee, M. D., Wu, W., Centola, M., & Hoemann, C. D. 2009. Effect of chitosan particles and dexamethasone on human bone marrow stromal cell osteogenesis and angiogenic factor secretion. *Bone*, 45(4): 617-626.

Guzman, E., Ritacco, H., Rubio, J. E. F., Rubio, R. G., & Ortega, F. 2009. Salt-induced changes in the growth of polyelectrolyte layers of poly(diallyl-dimethylammonium chloride) and poly(4-styrene sulfonate of sodium). *Soft Matter*, 5(10): 2130-2142.

Hadjipanayi, E., Brown, R. A., & Mudera, V. 2009. Interface integration of layered collagen scaffolds with defined matrix stiffness: implications for sheet-based tissue engineering. *Journal of Tissue Engineering and Regenerative Medicine*, 3(3): 230-241.

Harris, J. J., & Bruening, M. L. 1999. Electrochemical and in Situ Ellipsometric Investigation of the Permeability and Stability of Layered Polyelectrolyte Films. *Langmuir*, 16(4): 2006-2013.

Harris, L. D., Kim, B. S., & Mooney, D. J. 1998. Open pore biodegradable matrices formed with gas foaming. *Journal of Biomedical Materials Research*, 42(3): 396-402.

Harvey, E. J., Bobyn, J. D., Tanzer, M., Stackpool, G. J., Krygier, J. J., & Hacking, S. A. 1999. Effect of flexibility of the femoral stem on bone-remodeling and fixation of the stem in a canine total hip arthroplasty model without cement. *Journal of Bone and Joint Surgery American Edition*, 81(1): 93-107.

Hattori, K., Yoshikawa, T., Takakura, Y., Aoki, H., Sonobe, M., & Tomita, N. 2005. Bio-artificial periosteum for severe open fracture--an experimental study of osteogenic cell/collagen sponge composite as a bio-artificial periosteum. *Bio-Medical Materials and Engineering*, 15(3): 127-136.

Heinegard, D., King, K., Morgelin, M., Rosenberg, K., Wiberg, C.,. 2001. Matrix Molecules with Roles in Cartilage Assembly. In R. Rosier, Evans, C., (Ed.), *Molecular Biology in Orthopaedics*: 315–323. Scottsdale: American Academy of Orthopaedic Surgeons.

Hillsley, M. V., & Frangos, J. A. 1994. Review: Bone tissue engineering: The role of interstitial fluid flow. *Biotechnology and Bioengineering*, 43(7): 573-581.

Hing, K. A. 2004. Bone repair in the twenty-first century: biology, chemistry or engineering? *Philosophical transactions. Series A, Mathematical, Physical, and Engineering Sciences*, 362(1825): 2821-2850.

Hoefle, W. D. 1993. Delayed union and nonunion of fractures. In M. J. Bojrab, Smeak, D.D., Bloomberg, M.S. (Ed.), *Disease Mechanisms in Small Animal Surgery*, 2nd ed. ed.: 689-691. Philadelphia: Lea & Febiger.

Hoemann, C., Guzmán-Morales, J., Tran-Khanh, N., Lavallée, G., Jolicoeur, M., & Lavertu, M. 2013. Chitosan Rate of Uptake in HEK293 Cells is Influenced by Soluble versus Microparticle State and Enhanced by Serum-Induced Cell Metabolism and Lactate-Based Media Acidification. *Molecules*, 18(1): 1015-1035.

Hoemann, C. D., El-Gabalawy, H., & McKee, M. D. 2009. In vitro osteogenesis assays: Influence of the primary cell source on alkaline phosphatase activity and mineralization. *Pathologie Biologie*, 57(4): 318-323.

Hollinger, J. O. 1983. Preliminary report on the osteogenic potential of a biodegradable copolymer of polyactide (PLA) and polyglycolide (PGA). *Journal of Biomedical Materials Research*, 17(1): 71-82.

Hollinger, J. O., & Battistone, G. C. 1986. Biodegradable bone repair materials. Synthetic polymers and ceramics. *Clinical Orthopaedics and Related Research*, (207): 290-305.

Holy, C. E., Shoichet, M. S., & Davies, J. E. 2000. Engineering three-dimensional bone tissue in vitro using biodegradable scaffolds: investigating initial cell-seeding density and culture period. *Journal of Biomedical Materials Research*, 51(3): 376-382.

Hong, S.-J., Jeong, I., Noh, K.-T., Yu, H.-S., Lee, G.-S., & Kim, H.-W. 2009. Robotic dispensing of composite scaffolds and in vitro responses of bone marrow stromal cells. *Journal of Materials Science: Materials in Medicine*, 20(9): 1955-1962.

Hosseinkhani, H., Hosseinkhani, M., Tian, F., Kobayashi, H., & Tabata, Y. 2006. Osteogenic differentiation of mesenchymal stem cells in self-assembled peptide-amphiphile nanofibers. *Biomaterials*, 27(22): 4079-4086.

Hsu, W. Y., & Wu, S. 1993. Percolation behavior in morphology and modulus of polymer blends. *Polymer Engineering & Science*, 33(5): 293-302.

Hu, Y., Grainger, D. W., Winn, S. R., & Hollinger, J. O. 2002. Fabrication of poly(α-hydroxy acid) foam scaffolds using multiple solvent systems. *Journal of Biomedical Materials Research*, 59(3): 563-572.

Huang, Q., Goh, J. C., Hutmacher, D. W., & Lee, E. H. 2002. In vivo mesenchymal cell recruitment by a scaffold loaded with transforming growth factor beta1 and the potential for in situ chondrogenesis. *Tissue Engineering*, 8(3): 469-482.

Huang, W., Carlsen, B., Wulur, I., Rudkin, G., Ishida, K., Wu, B., Yamaguchi, D. T., & Miller, T. A. 2004. BMP-2 exerts differential effects on differentiation of rabbit bone marrow stromal cells grown in two-dimensional and three-dimensional systems and is required for in vitro bone formation in a PLGA scaffold. *Experimental Cell Research*, 299(2): 325-334.

Huang, Z., Nelson, E. R., Smith, R. L., & Goodman, S. B. 2007. The sequential expression profiles of growth factors from osteoprogenitors [correction of osteroprogenitors] to osteoblasts in vitro. *Tissue Engineering*, 13(9): 2311-2320.

Hübsch, E., Ball, V., Senger, B., Decher, G., Voegel, J.-C., & Schaaf, P. 2004. Controlling the Growth Regime of Polyelectrolyte Multilayer Films: Changing from Exponential to Linear Growth by Adjusting the Composition of Polyelectrolyte Mixtures. *Langmuir*, 20(5): 1980-1985.

Hulbert, S. F., Young, F. A., Mathews, R. S., Klawitter, J. J., Talbert, C. D., & Stelling, F. H. 1970. Potential of ceramic materials as permanently implantable skeletal prostheses. *Journal of Biomedical Materials Research*, 4(3): 433-456.

Huri, Pinar Y., Ozilgen, B. A., Hutton, D. L., & Grayson, W. L. 2014. Scaffold pore size modulates in vitro osteogenesis of human adipose-derived stem/stromal cells. *Biomedical Materials*, 9(4): 045003.

Itoh, M., Shimazu, A., Hirata, I., Yoshida, Y., Shintani, H., & Okazaki, M. 2004. Characterization of CO3Ap-collagen sponges using X-ray high-resolution microtomography. *Biomaterials*, 25(13): 2577-2583.

Jana, S., Florczyk, S. J., Leung, M., & Zhang, M. 2012. High-strength pristine porous chitosan scaffolds for tissue engineering. *Journal of Materials Chemistry*, 22(13): 6291-6299.

Jayakumar, P., & Di Silvio, L. 2010. Osteoblasts in bone tissue engineering. *Proceedings of the Institution of Mechanical Engineers, Part H*, 224(12): 1415-1440.

Jin, H.-H., Kim, D.-H., Kim, T.-W., Shin, K.-K., Jung, J. S., Park, H.-C., & Yoon, S.-Y. 2012. In vivo evaluation of porous hydroxyapatite/chitosan–alginate composite scaffolds for bone tissue engineering. *International Journal of Biological Macromolecules*, 51(5): 1079-1085.

Karageorgiou, V., & Kaplan, D. 2005. Porosity of 3D biomaterial scaffolds and osteogenesis. *Biomaterials*, 26(27): 5474-5491.

Keating, J. F., & McQueen, M. M. 2001. Substitutes for autologous bone graft in orthopaedic trauma. *Journal of Bone and Joint Surgery - British Volume*, 83(1): 3-8.

Khan, Y., Yaszemski, M. J., Mikos, A. G., & Laurencin, C. T. 2008. Tissue engineering of bone: material and matrix considerations. *Journal of Bone and Joint Surgery - American Volume*, 90 Suppl 1: 36-42.

Kidambi, S., Lee, I., & Chan, C. 2004. Controlling primary hepatocyte adhesion and spreading on protein-free polyelectrolyte multilayer films. *Journal of the American Chemical Society*, 126(50): 16286-16287.

Kim, H.-W., Knowles, J. C., & Kim, H.-E. 2004. Hydroxyapatite/poly(ε-caprolactone) composite coatings on hydroxyapatite porous bone scaffold for drug delivery. *Biomaterials*, 25(7–8): 1279-1287.

Kim, H. D., & Valentini, R. F. 2002. Retention and activity of BMP-2 in hyaluronic acid-based scaffolds in vitro. *Journal of Biomedical Materials Research*, 59(3): 573-584.

Kim, H. J., Park, I. K., Kim, J. H., Cho, C. S., & Kim, M. S. 2012. Gas Foaming Fabrication of Porous Biphasic Calcium Phosphate for Bone Regeneration. *Tissue Engineering and Regenerative Medicine*, 9(2): 63-68.

Kim, J., Magno, M. H. R., Alvarez, P., Darr, A., Kohn, J., & Hollinger, J. O. 2011. Osteogenic Differentiation of Pre-Osteoblasts on Biomimetic Tyrosine-Derived Polycarbonate Scaffolds. *Biomacromolecules*, 12(10): 3520-3527.

Kim, S. H., Lee, J. H., Hyun, H., Ashitate, Y., Park, G., Robichaud, K., Lunsford, E., Lee, S. J., Khang, G., & Choi, H. S. 2013. Near-infrared fluorescence imaging for noninvasive trafficking of scaffold degradation. *Scientific Reports*, 3: 1198.

Klee, D., Ademovic, Z., Bosserhoff, A., Hoecker, H., Maziolis, G., & Erli, H.-J. 2003. Surface modification of poly(vinylidenefluoride) to improve the osteoblast adhesion. *Biomaterials*, 24(21): 3663-3670.

Klokkevold , P. R. J. S. A. 2003. Advanced implant surgery and bone grafting techniques. In T. Carranza, Newman (Ed.), *Clinical Periodontology*, 9th ed. ed.: p. 90521: Saunders: Elsevier Science.

Krieger, I. M., & Dougherty, T. J. 1959. A Mechanism for Non-Newtonian Flow in Suspensions of Rigid Spheres. *Transactions of The Society of Rheology (1957-1977)*, 3(1): 137-152.

Kruyt, M. C., de Bruijn, J. D., Wilson, C. E., Oner, F. C., van Blitterswijk, C. A., Verbout, A. J., & Dhert, W. J. 2003. Viable osteogenic cells are obligatory for tissue-engineered ectopic bone formation in goats. *Tissue Engineering*, 9(2): 327-336.

Kuboki, Y., Jin, Q., & Takita, H. 2001. Geometry of carriers controlling phenotypic expression in BMP-induced osteogenesis and chondrogenesis. *Journal of Bone and Joint Surgery - American Volume*, 83-A Suppl 1(Pt 2): S105-115.

Kucharczyk, P., Otgonzu, O., Kitano, T., Gregorova, A., Kreuh, D., Cvelbar, U., Sedlarik, V., & Saha, P. 2012. Correlation of Morphology and Viscoelastic Properties of Partially Biodegradable Polymer Blends Based on Polyamide 6 and Polylactide Copolyester. *Polymer-Plastics Technology and Engineering*, 51(14): 1432-1442.

Kujawa, P., Moraille, P., Sanchez, J., Badia, A., & Winnik, F. M. 2005. Effect of Molecular Weight on the Exponential Growth and Morphology of Hyaluronan/Chitosan Multilayers: A Surface Plasmon Resonance Spectroscopy and Atomic Force Microscopy Investigation. *Journal of the American Chemical Society*, 127(25): 9224-9234.

Labet, M., & Thielemans, W. 2009. Synthesis of polycaprolactone: a review. *Chemical Society Reviews*, 38(12): 3484-3504.

Ladd, A., & Pliam, N. 1999. Use of bone-graft substitutes in distal radius fractures. *Journal of the American Academy of Orthopaedic Surgeons*, 7(5): 279-290.

Lam, C. X. F., Hutmacher, D. W., Schantz, J.-T., Woodruff, M. A., & Teoh, S. H. 2009. Evaluation of polycaprolactone scaffold degradation for 6 months in vitro and in vivo. *Journal of Biomedical Materials Research Part A*, 90A(3): 906-919.

Landis, W. J., Jacquet, R., Hillyer, J., Lowder, E., Yanke, A., Siperko, L., Asamura, S., Kusuhara, H., Enjo, M., Chubinskaya, S., Potter, K., & Isogai, N. 2005. Design and assessment of a tissue-engineered model of human phalanges and a small joint. *Orthodontics & Craniofacial Research*, 8(4): 303-312.

Lavalle, P., Picart, C., Mutterer, J., Gergely, C., Reiss, H., Voegel, J.-C., Senger, B., & Schaaf, P. 2003. Modeling the Buildup of Polyelectrolyte Multilayer Films Having Exponential Growth ✗. *The Journal of Physical Chemistry B*, 108(2): 635-648.

Lee, C. H., Singla, A., & Lee, Y. 2001a. Biomedical applications of collagen. *International Journal of Pharmaceutics*, 221(1-2): 1-22.

Lee, C. R., Grodzinsky, A. J., & Spector, M. 2001b. The effects of cross-linking of collagen-glycosaminoglycan scaffolds on compressive stiffness, chondrocyte-mediated contraction, proliferation and biosynthesis. *Biomaterials*, 22(23): 3145-3154.

Lee, H.-Y., Jin, G.-Z., Shin, U., Kim, J.-H., & Kim, H.-W. 2012. Novel porous scaffolds of poly(lactic acid) produced by phase-separation using room temperature ionic liquid and the assessments of biocompatibility. *Journal of Materials Science: Materials in Medicine*, 23(5): 1271-1279.

Lee, K. Y., & Mooney, D. J. 2001. Hydrogels for tissue engineering. *Chemical Reviews*, 101(7): 1869-1879.

Lewandrowski, K. U., Gresser, J. D., Bondre, S., Silva, A. E., Wise, D. L., & Trantolo, D. J. 2000. Developing porosity of poly(propylene glycol-co-fumaric acid) bone graft substitutes and the effect on osteointegration: a preliminary histology study in rats. *Journal of Biomaterials Science. Polymer Edition*, 11(8): 879-889.

Lewandrowski, K. U., Hile, D. D., Thompson, B. M., Wise, D. L., Tomford, W. W., & Trantolo, D. J. 2003. Quantitative measures of osteoinductivity of a porous poly(propylene fumarate) bone graft extender. *Tissue Engineering*, 9(1): 85-93.

Li, G., & Favis, B. D. 2010. Morphology Development and Interfacial Interactions in Polycaprolactone/Thermoplastic-Starch Blends. *Macromolecular Chemistry and Physics*, 211(3): 321-333.

Li, J., & Favis, B. D. 2001. Characterizing co-continuous high density polyethylene/polystyrene blends. *Polymer*, 42(11): 5047-5053.

Li, J., & Favis, B. D. 2002. Strategies to measure and optimize the migration of the interfacial modifier to the interface in immiscible polymer blends. *Polymer*, 43(18): 4935-4945.

Li, J., Ma, P. L., & Favis, B. D. 2002a. The Role of the Blend Interface Type on Morphology in Cocontinuous Polymer Blends. *Macromolecules*, 35(6): 2005-2016.

Li, W.-J., Tuli, R., Okafor, C., Derfoul, A., Danielson, K. G., Hall, D. J., & Tuan, R. S. 2005. A three-dimensional nanofibrous scaffold for cartilage tissue engineering using human mesenchymal stem cells. *Biomaterials*, 26(6): 599-609.

Li, W. J., Laurencin, C. T., Caterson, E. J., Tuan, R. S., & Ko, F. K. 2002b. Electrospun nanofibrous structure: a novel scaffold for tissue engineering. *Journal of Biomedical Materials Research*, 60(4): 613-621.

Liao, C. J., Chen, C. F., Chen, J. H., Chiang, S. F., Lin, Y. J., & Chang, K. Y. 2002. Fabrication of porous biodegradable polymer scaffolds using a solvent merging/particulate leaching method. *Journal of Biomedical Materials Research*, 59(4): 676-681.

Lickorish, D., Ramshaw, J. A. M., Werkmeister, J. A., Glattauer, V., & Howlett, C. R. 2004. Collagen–hydroxyapatite composite prepared by biomimetic process. *Journal of Biomedical Materials Research Part A*, 68A(1): 19-27.

Linde, F., & Hvid, I. 1989. The effect of constraint on the mechanical behaviour of trabecular bone specimens. *Journal of Biomechanics*, 22(5): 485-490.

Liu, J., Liu, C., Sun, B., Shi, C., Qiao, C., Ke, X., Liu, S., Liu, X., & Sun, H. 2014. Differentiation of Rabbit Bone Mesenchymal Stem Cells into Endothelial Cells In Vitro and Promotion of Defective Bone Regeneration In Vivo. *Cell Biochemistry and Biophysics*, 68(3): 479-487.

Liu, X., & Ma, P. X. 2004. Polymeric scaffolds for bone tissue engineering. *Annals of Biomedical Engineering*, 32(3): 477-486.

Livingston, T., Ducheyne, P., & Garino, J. 2002. In vivo evaluation of a bioactive scaffold for bone tissue engineering. *Journal of Biomedical Materials Research*, 62(1): 1-13.

Lösche, M., Schmitt, J., Decher, G., Bouwman, W. G., & Kjaer, K. 1998. Detailed Structure of Molecularly Thin Polyelectrolyte Multilayer Films on Solid Substrates as Revealed by Neutron Reflectometry. *Macromolecules*, 31(25): 8893-8906.

Lü, L.-X., Zhang, X.-F., Wang, Y.-Y., Ortiz, L., Mao, X., Jiang, Z.-L., Xiao, Z.-D., & Huang, N.-P. 2012. Effects of Hydroxyapatite-Containing Composite Nanofibers on Osteogenesis of Mesenchymal Stem Cells In vitro and Bone Regeneration In vivo. *ACS Applied Materials & Interfaces*, 5(2): 319-330.

Lu, L., & Mikos, A. G. 1996. The importance of new processing techniques in tissue engineering. *MRS Bull*, 21(11): 28-32.

Lulevich, V. V., & Vinogradova, O. I. 2004. Effect of pH and Salt on the Stiffness of Polyelectrolyte Multilayer Microcapsules. *Langmuir*, 20(7): 2874-2878.

Luthen, F., Lange, R., Becker, P., Rychly, J., Beck, U., & Nebe, J. G. 2005. The influence of surface roughness of titanium on beta1- and beta3-integrin adhesion and the organization of fibronectin in human osteoblastic cells. *Biomaterials*, 26(15): 2423-2440.

Lv, N. J., Meng, S., Guo, Z., Wu, L. X., Liu, Z. J., Jin, H. G., Zhong, W., & Tomasik, P. 2008. Improving the biocompatibility of poly(epsilon-caprolactone) by surface Immobilization of chitosan and heparin. *E-Polymers*.

Lvov, Y., Decher, G., & Moehwald, H. 1993. Assembly, structural characterization, and thermal behavior of layer-by-layer deposited ultrathin films of poly(vinyl sulfate) and poly(allylamine). *Langmuir*, 9(2): 481-486.

Lyngaae-Jørgensen, J., & Utracki, L. A. 1991. Dual phase continuity in polymer blends. *Makromolekulare Chemie. Macromolecular Symposia*, 48-49(1): 189-209.

M. Lvov, Y., F. Rusling, J., Laurence Thomsen, D., Papadimitrakopoulos, F., Kawakami, T., & Kunitake, T. 1998. High-speed multilayer film assembly by alternate adsorption of silica nanoparticles and linear polycation. *Chemical Communications*(11): 1229-1230.

Ma, P. X., Zhang, R., Xiao, G., & Franceschi, R. 2001. Engineering new bone tissue in vitro on highly porous poly(α-hydroxyl acids)/hydroxyapatite composite scaffolds. *Journal of Biomedical Materials Research*, 54(2): 284-293.

Ma, Z., Mao, Z., & Gao, C. 2007. Surface modification and property analysis of biomedical polymers used for tissue engineering. *Colloids and Surfaces B: Biointerfaces*, 60(2): 137-157.

Madihally, S. V., & Matthew, H. W. T. 1999. Porous chitosan scaffolds for tissue engineering. *Biomaterials*, 20(12): 1133-1142.

Mano, J. F., Reis, R. L., & Cunha, A. M. 2002. Dynamic Mechanical Analysis in Polymers for Medical Applications. In R. Reis, & D. Cohn (Eds.), *Polymer Based Systems on Tissue Engineering, Replacement and Regeneration*, Vol. 86: 139-164: Springer Netherlands.

Marin, N., & Favis, B. D. 2002. Co-continuous morphology development in partially miscible PMMA/PC blends. *Polymer*, 43(17): 4723-4731.

Mark, J. E. 2009. *The Polymer Data Handbook* (2nd Edn ed.). USA: Oxford University Press.

Maspero, F. A., Ruffieux, K., Muller, B., & Wintermantel, E. 2002. Resorbable defect analog PLGA scaffolds using CO2 as solvent: structural characterization. *Journal of Biomedical Materials Research*, 62(1): 89-98.

Mathews, S., Gupta, P. K., Bhonde, R., & Totey, S. 2011. Chitosan enhances mineralization during osteoblast differentiation of human bone marrow-derived mesenchymal stem cells, by upregulating the associated genes. *Cell Proliferation*, 44(6): 537-549.

Matos, M., Favis, B. D., & Lomellini, P. 1995. Interfacial modification of polymer blends—the emulsification curve: 1. Influence of molecular weight and chemical composition of the interfacial modifier. *Polymer*, 36(20): 3899-3907.

Matsuzaka, K., Walboomers, F., de Ruijter, A., & Jansen, J. A. 2000. Effect of microgrooved poly-l-lactic (PLA) surfaces on proliferation, cytoskeletal organization, and mineralized matrix formation of rat bone marrow cells. *Clinical Oral Implants Research*, 11(4): 325-333.

Mattanavee, W., Suwantong, O., Puthong, S., Bunaprasert, T., Hoven, V. P., & Supaphol, P. 2009. Immobilization of biomolecules on the surface of electrospun polycaprolactone fibrous scaffolds for tissue engineering. *ACS Appl Mater Interfaces*, 1(5): 1076-1085.

McAloney, R. A., Sinyor, M., Dudnik, V., & Goh, M. C. 2001. Atomic Force Microscopy Studies of Salt Effects on Polyelectrolyte Multilayer Film Morphology. *Langmuir*, 17(21): 6655-6663.

Meinel, L., Hofmann, S., Betz, O., Fajardo, R., Merkle, H. P., Langer, R., Evans, C. H., Vunjak-Novakovic, G., & Kaplan, D. L. 2006. Osteogenesis by human mesenchymal stem cells cultured on silk biomaterials: Comparison of adenovirus mediated gene transfer and protein delivery of BMP-2. *Biomaterials*, 27(28): 4993-5002.

Mekhilef, N., Favis, B. D., & Carreau, P. J. 1997. Morphological stability, interfacial tension, and dual-phase continuity in polystyrene-polyethylene blends. *Journal of Polymer Science Part B: Polymer Physics*, 35(2): 293-308.

Metelkin, V., & Blekht, V. 1984. Formation of a continuous phase in heterogeneous polymer mixtures. *Colloid Journal of the USSR*, 46(3): 425-429.

Miao, D., Tong, X. K., Chan, G. K., Panda, D., McPherson, P. S., & Goltzman, D. 2001. Parathyroid hormone-related peptide stimulates osteogenic cell proliferation through protein kinase C activation of the Ras/mitogen-activated protein kinase signaling pathway. *The Journal of Biological Chemistry*, 276(34): 32204-32213.

Middleton, J. C., & Tipton, A. J. 2000. Synthetic biodegradable polymers as orthopedic devices. *Biomaterials*, 21(23): 2335-2346.

Mikos, A. G., Bao, Y., Cima, L. G., Ingber, D. E., Vacanti, J. P., & Langer, R. 1993. Preparation of poly(glycolic acid) bonded fiber structures for cell attachment and transplantation. *Journal of Biomedical Materials Research*, 27(2): 183-189.

Mikos, A. G., Thorsen, A. J., Czerwonka, L. A., Bao, Y., Langer, R., Winslow, D. N., & Vacanti, J. P. 1994. Preparation and characterization of poly(l-lactic acid) foams. *Polymer*, 35(5): 1068-1077.

Miles, I. S., & Zurek, A. 1988. Preparation, structure, and properties of two-phase co-continuous polymer blends. *Polymer Engineering & Science*, 28(12): 796-805.

Mooney, D. J., Baldwin, D. F., Suh, N. P., Vacanti, J. P., & Langer, R. 1996. Novel approach to fabricate porous sponges of poly(D,L-lactic-co-glycolic acid) without the use of organic solvents. *Biomaterials*, 17(14): 1417-1422.

Moreira, P. L., An, Y. H., Santos, A. R., Jr., & Genari, S. C. 2004. In vitro analysis of anionic collagen scaffolds for bone repair. *Journal of Biomedical Materials Research Part B: Applied Biomaterials*, 71(2): 229-237.

Morishita, T., Honoki, K., Ohgushi, H., Kotobuki, N., Matsushima, A., & Takakura, Y. 2006. Tissue Engineering Approach to the Treatment of Bone Tumors: Three Cases of Cultured Bone Grafts Derived From Patients' Mesenchymal Stem Cells. *Artificial Organs*, 30(2): 115-118.

Muschler, G. F., & Midura, R. J. 2002. Connective tissue progenitors: practical concepts for clinical applications. *Clinical Orthopaedics and Related Research,* (395): 66-80.

Muzzarelli, R. A. A., Mattioli-Belmonte, M., Tietz, C., Biagini, R., Ferioli, G., Brunelli, M. A., Fini, M., Giardino, R., Ilari, P., & Biagini, G. 1994. Stimulatory effect on bone formation exerted by a modified chitosan. *Biomaterials*, 15(13): 1075-1081.

Nam, Y. S., & Park, T. G. 1999. Porous biodegradable polymeric scaffolds prepared by thermally induced phase separation. *Journal of Biomedical Materials Research*, 47(1): 8-17.

Nazarov, R., Jin, H.-J., & Kaplan, D. L. 2004. Porous 3-D Scaffolds from Regenerated Silk Fibroin. *Biomacromolecules*, 5(3): 718-726.

Nienhuijs, M. E., Walboomers, X. F., Merkx, M. A., Stoelinga, P. J., & Jansen, J. A. 2006. Bone-like tissue formation using an equine COLLOSS E-filled titanium scaffolding material. *Biomaterials*, 27(16): 3109-3114.

Niinomi, M., & Nakai, M. 2011. Titanium-based biomaterials for preventing stress shielding between implant devices and bone. *International journal of biomaterials*, 2011.

Nijenhuis, A. J., Colstee, E., Grijpma, D. W., & Pennings, A. J. 1996. High molecular weight poly(l-lactide) and poly(ethylene oxide) blends: thermal characterization and physical properties. *Polymer*, 37(26): 5849-5857.

Niu, X. F., Fan, Y. B., Liu, X. H., Li, X. M., Li, P., Wang, J. X., Sha, Z. Y., & Feng, Q. L. 2011. Repair of Bone Defect in Femoral Condyle Using Microencapsulated Chitosan, Nanohydroxyapatite/Collagen and Poly(L-Lactide)-Based Microsphere-Scaffold Delivery System. *Artificial Organs*, 35(7): E119-E128.

Nunley, J. A. 2001. Fractures of the base of the fifth metatarsal: the Jones fracture. *Orthopedic Clinics of North America*, 32(1): 171-180.

Oh, S. H., Kang, S. G., Kim, E. S., Cho, S. H., & Lee, J. H. 2003. Fabrication and characterization of hydrophilic poly(lactic-co-glycolic acid)/poly(vinyl alcohol) blend cell scaffolds by melt-molding particulate-leaching method. *Biomaterials*, 24(22): 4011-4021.

Oh, S. H., Kang, S. G., & Lee, J. H. 2006. Degradation behavior of hydrophilized PLGA scaffolds prepared by melt-molding particulate-leaching method: comparison with control hydrophobic one. *Journal of Materials Science: Materials in Medicine*, 17(2): 131-137.

Oliveira, J. M., Sousa, R. A., Kotobuki, N., Tadokoro, M., Hirose, M., Mano, J. F., Reis, R. L., & Ohgushi, H. 2009. The osteogenic differentiation of rat bone marrow stromal cells cultured with dexamethasone-loaded carboxymethylchitosan/poly(amidoamine) dendrimer nanoparticles. *Biomaterials*, 30(5): 804-813.

Orthopedics Network News. 2011. Bone Grafts and Bone Substitutes *Orthopedics Network News*, Vol. 22.

Pachence, J. M., Kohn, J.,. 1997. Biodegradable Polymers for Tissue Engineering. In R. Lanza, Langer, R., (Ed.), *Principles of Tissue Engineering*: 273–293. San Diego: Academic Press.

Park, S., Lee, S., & Kim, W. 2011. Fabrication of porous polycaprolactone/hydroxyapatite (PCL/HA) blend scaffolds using a 3D plotting system for bone tissue engineering. *Bioprocess and Biosystems Engineering*, 34(4): 505-513.

Park, S. N., Park, J. C., Kim, H. O., Song, M. J., & Suh, H. 2002. Characterization of porous collagen/hyaluronic acid scaffold modified by 1-ethyl-3-(3-dimethylaminopropyl)carbodiimide cross-linking. *Biomaterials*, 23(4): 1205-1212.

Pastorino, L., Soumetz, F. C., & Ruggiero, C. 2006. Nanofunctionalisation for the treatment of peripheral nervous system injuries. *Iee Proceedings-Nanobiotechnology*, 153(2): 16-20.

Paul, D. R., & Barlow, J. W. 1980. Polymer Blends. *Journal of Macromolecular Science, Part C*, 18(1): 109-168.

Penk, A., Förster, Y., Scheidt, H. A., Nimptsch, A., Hacker, M. C., Schulz-Siegmund, M., Ahnert, P., Schiller, J., Rammelt, S., & Huster, D. 2013. The pore size of PLGA bone implants determines the de novo formation of bone tissue in tibial head defects in rats. *Magnetic Resonance in Medicine*, 70(4): 925-935.

Pietrzak, W. S., & Woodell-May, J. 2005. The composition of human cortical allograft bone derived from FDA/AATB-screened donors. *Journal of Craniofacial Surgery*, 16(4): 579-585.

Pilliar, R. M. 1998. Overview of surface variability of metallic endosseous dental implants: textured and porous surface-structured designs. Implant Dentistry, 7(4): 305-314.

Pitt, C. G., Chasalow, F. I., Hibionada, Y. M., Klimas, D. M., & Schindler, A. 1981. Aliphatic polyesters. I. The degradation of poly(ϵ-caprolactone) in vivo. *Journal of Applied Polymer Science*, 26(11): 3779-3787.

Poh, P. S., Hutmacher, D. W., Stevens, M. M., & Woodruff, M. A. 2013. Fabrication and in vitro characterization of bioactive glass composite scaffolds for bone regeneration. *Biofabrication*, 5(4): 045005.

Poncin-Epaillard, F., Chevet, B., & Brosse, J.-C. 1994. Modification of isotactic polypropylene by a cold plasma or an electron beam and grafting of the acrylic acid onto these activated polymers. *Journal of Applied Polymer Science*, 53(10): 1291-1306.

Porcel, C., Lavalle, P., Decher, G., Senger, B., Voegel, J. C., & Schaaf, P. 2007. Influence of the Polyelectrolyte Molecular Weight on Exponentially Growing Multilayer Films in the Linear Regime. *Langmuir*, 23(4): 1898-1904.

Porcel, C. H., Izquierdo, A., Ball, V., Decher, G., Voegel, J. C., & Schaaf, P. 2004. Ultrathin Coatings and (Poly(glutamic acid)/Polyallylamine) Films Deposited by Continuous and Simultaneous Spraying. *Langmuir*, 21(2): 800-802.

Quarles, L. D., Yohay, D. A., Lever, L. W., Caton, R., & Wenstrup, R. J. 1992. Distinct proliferative and differentiated stages of murine MC3T3-E1 cells in culture: An in vitro model of osteoblast development. *Journal of Bone and Mineral Research*, 7(6): 683-692.

Rai, B., Teoh, S. H., Ho, K. H., Hutmacher, D. W., Cao, T., Chen, F., & Yacob, K. 2004. The effect of rhBMP-2 on canine osteoblasts seeded onto 3D bioactive polycaprolactone scaffolds. *Biomaterials*, 25(24): 5499-5506.

Ramsden, J. J., Lvov, Y. M., & Decher, G. 1995. Determination of optical constants of molecular films assembled via alternate polyion adsorption. *Thin Solid Films*, 254(1–2): 246-251.

Ratner, B. D., Hoffman, A.S., Schoen, F.J., Lemons, J.E. 2005. *Biomaterials Science: an Introduction to Materials in Medicine* (2nd Edn ed.). San Diego, USA: Academic Press.

Raudino, A., Sarpietro, M., & Pannuzzo, M. 2011. The thermodynamics of simple biomembrane mimetic systems. *Journal of Pharmacy And Bioallied Sciences*, 3(1): 15-38.

Ravati, S., & Favis, B. D. 2011. 3D porous polymeric conductive material prepared using LbL deposition. *Polymer*, 52(3): 718-731.

Reignier, J., & Favis, B. D. 2000. Control of the Subinclusion Microstructure in HDPE/PS/PMMA Ternary Blends. *Macromolecules*, 33(19): 6998-7008.

Reignier, J., & Favis, B. D. 2003. On the presence of a critical shell volume fraction leading to pseudo-pure droplet behavior in composite droplet polymer blends. *Polymer*, 44(18): 5061-5066.

Remedios, A. 1999. Bone and bone healing. *Veterinary Clinics of North America: Small Animal Practice*, 29(5): 1029-1044, v.

Rengachary, S. S., Benzel, E. C., & Committee, A. P. 1998. *Calvarial and Dural Reconstruction*: American Association of Neurological Surgeons.

Richert, L., Lavalle, P., Payan, E., Shu, X. Z., Prestwich, G. D., Stoltz, J.-F., Schaaf, P., Voegel, J.-C., & Picart, C. 2003. Layer by Layer Buildup of Polysaccharide Films: Physical Chemistry and Cellular Adhesion Aspects. *Langmuir*, 20(2): 448-458.

Ricotti, L., Taccola, S., Bernardeschi, I., Pensabene, V., Dario, P., & Menciassi, A. 2011. Quantification of growth and differentiation of C2C12 skeletal muscle cells on PSS-PAH-based polyelectrolyte layer-by-layer nanofilms. *Biomedical Materials*, 6(3).

Rocha, L. B., Goissis, G., & Rossi, M. A. 2002. Biocompatibility of anionic collagen matrix as scaffold for bone healing. *Biomaterials,* 23(2): 449-456.

Rosenberg, G. A., & Sferra, J. J. 2000. Treatment Strategies for Acute Fractures and Nonunions of the Proximal Fifth Metatarsal. *Journal of the American Academy of Orthopaedic Surgeons*, 8(5): 332-338.

Roy, T. D., Simon, J. L., Ricci, J. L., Rekow, E. D., Thompson, V. P., & Parsons, J. R. 2003. Performance of degradable composite bone repair products made via three-dimensional fabrication techniques. *Journal of Biomedical Materials Research Part A*, 66(2): 283-291.

Rubin, J. P., & Yaremchuk, M. J. 1997. Complications and toxicities of implantable biomaterials used in facial reconstructive and aesthetic surgery: a comprehensive review of the literature. *Plastic and Reconstructive Surgery*, 100(5): 1336-1353.

Rudra, J. S., Dave, K., & Haynie, D. T. 2006. Antimicrobial polypeptide multilayer nanocoatings. *Journal of Biomaterials Science. Polymer Edition*, 17(11): 1301-1315.

Ruths, J., Essler, F., Decher, G., & Riegler, H. 2000. Polyelectrolytes I: Polyanion/Polycation Multilayers at the Air/Monolayer/Water Interface as Elements for Quantitative Polymer Adsorption Studies and Preparation of Hetero-superlattices on Solid Surfaces†. *Langmuir*, 16(23): 8871-8878.

Salgado, A. J., Coutinho, O. P., & Reis, R. L. 2004. Bone tissue engineering: state of the art and future trends. *Macromolecular Bioscience*, 4(8): 743-765.

Salomäki, M., Laiho, T., & Kankare, J. 2004. Counteranion-Controlled Properties of Polyelectrolyte Multilayers. *Macromolecules*, 37(25): 9585-9590.

Sarazin, P., & Favis, B. D. 2003. Morphology Control in Co-continuous Poly(l-lactide)/Polystyrene Blends: A Route towards Highly Structured and Interconnected Porosity in Poly(l-lactide) Materials. *Biomacromolecules*, 4(6): 1669-1679.

Sarazin, P., Roy, X., & Favis, B. D. 2004. Controlled preparation and properties of porous poly(l-lactide) obtained from a co-continuous blend of two biodegradable polymers. *Biomaterials*, 25(28): 5965-5978.

Savarino, L., Baldini, N., Greco, M., Capitani, O., Pinna, S., Valentini, S., Lombardo, B., Esposito, M. T., Pastore, L., Ambrosio, L., Battista, S., Causa, F., Zeppetelli, S., Guarino, V., & Netti, P. A. 2007. The performance of poly-ε-caprolactone scaffolds in a rabbit femur model with and without autologous stromal cells and BMP4. *Biomaterials*, 28(20): 3101-3109.

Scaglione, S., Giannoni, P., Bianchini, P., Sandri, M., Marotta, R., Firpo, G., Valbusa, U., Tampieri, A., Diaspro, A., & Bianco, P. 2012. Order versus Disorder: in vivo bone formation within osteoconductive scaffolds. *Scientific Reports*, 2.

Schaefer, D., Martin, I., Shastri, P., Padera, R. F., Langer, R., Freed, L. E., & Vunjak-Novakovic, G. 2000. In vitro generation of osteochondral composites. *Biomaterials*, 21(24): 2599-2606.

Schantz, J. T., Lim, T. C., Ning, C., Teoh, S. H., Tan, K. C., Wang, S. C., & Hutmacher, D. W. 2006. Cranioplasty after trephination using a novel biodegradable burr hole cover: technical case report. *Neurosurgery*, 58(1 Suppl): ONS-E176; discussion ONS-E176.

Schantz, J. T., Teoh, S. H., Lim, T. C., Endres, M., Lam, C. X., & Hutmacher, D. W. 2003. Repair of calvarial defects with customized tissue-engineered bone grafts I. Evaluation of osteogenesis in a three-dimensional culture system. *Tissue Engineering*, 9 Suppl 1: S113-126.

Schlenoff, J. B., & Dubas, S. T. 2001. Mechanism of Polyelectrolyte Multilayer Growth: Charge Overcompensation and Distribution. *Macromolecules*, 34(3): 592-598.

Schlenoff, J. B., Ly, H., & Li, M. 1998. Charge and Mass Balance in Polyelectrolyte Multilayers. *Journal of the American Chemical Society*, 120(30): 7626-7634.

Schwarz, B., & Schönhoff, M. 2002. A 1H NMR relaxation study of hydration water in polyelectrolyte mono and multilayers adsorbed to colloidal particles. *Colloids and Surfaces A: Physicochemical and Engineering Aspects*, 198–200(0): 293-304.

Seol, Y.-J., Lee, J.-Y., Park, Y.-J., Lee, Y.-M., Ku, Y., Rhyu, I.-C., Lee, S.-J., Han, S.-B., & Chung, C.-P. 2004. Chitosan sponges as tissue engineering scaffolds for bone formation. *Biotechnology Letters*, 26(13): 1037-1041.

Seong, J. M., Kim, B. C., Park, J. H., Kwon, I. K., Mantalaris, A., & Hwang, Y. S. 2010. Stem cells in bone tissue engineering. *Biomedical Materials*, 5(6): 062001.

Shao, X., Goh, J. C., Hutmacher, D. W., Lee, E. H., & Zigang, G. 2006. Repair of large articular osteochondral defects using hybrid scaffolds and bone marrow-derived mesenchymal stem cells in a rabbit model. *Tissue Engineering*, 12(6): 1539-1551.

Shen, J. A., Li, Y. B., Zuo, Y., Zou, Q., Cheng, L., Zhang, L., Gong, M., & Gao, S. B. 2010. Characterization and cytocompatibility of biphasic calcium phosphate/polyamide 6 scaffolds for bone regeneration. *Journal of Biomedical Materials Research Part B-Applied Biomaterials*, 95B(2): 330-338.

Shim, J. K., Na, H. S., Lee, Y. M., Huh, H., & Nho, Y. C. 2001. Surface modification of polypropylene membranes by γ-ray induced graft copolymerization and their solute permeation characteristics. *Journal of Membrane Science*, 190(2): 215-226.

Shiratori, S. S., & Rubner, M. F. 2000. pH-Dependent Thickness Behavior of Sequentially Adsorbed Layers of Weak Polyelectrolytes. *Macromolecules*, 33(11): 4213-4219.

Shirley, D. A. 1972. High-Resolution X-Ray Photoemission Spectrum of the Valence Bands of Gold. *Physical Review B*, 5(12): 4709-4714.

Siegbahn, K. K. V.-s. i. U. 1967. *ESCA; atomic, molecular and solid state structure studied by means of electron spectroscopy*. Uppsala: Almqvist & Wiksells.

Siri, S., Wadbua, P., Amornkitbamrung, V., Kampa, N., & Maensiri, S. 2010. Surface modification of electrospun PCL scaffolds by plasma treatment and addition of adhesive protein to promote fibroblast cell adhesion. *Materials Science and Technology*, 26(11): 1292-1297.

Skalak, R., & Fox, C. F. 1988. *Tissue Engineering: Proceedings of a workshop, held at Granlibakken, Lake Tahoe, California, February 26-29, 1988*: Liss.

Sperling, L. H. 2005. *Introduction to Physical Polymer Science*: Wiley.

Srouji, S., Kizhner, T., Suss-Tobi, E., Livne, E., & Zussman, E. 2008. 3-D Nanofibrous electrospun multilayered construct is an alternative ECM mimicking scaffold. *Journal of Materials Science: Materials in Medicine*, 19(3): 1249-1255.

Steffens, G. C. M., Nothdurft, L., Buse, G., Thissen, H., Höcker, H., & Klee, D. 2002. High density binding of proteins and peptides to poly(d,l-lactide) grafted with polyacrylic acid. *Biomaterials*, 23(16): 3523-3531.

Steinmann, S., Gronski, W., & Friedrich, C. 2001. Cocontinuous polymer blends: influence of viscosity and elasticity ratios of the constituent polymers on phase inversion. *Polymer*, 42(15): 6619-6629.

Steinmann, S., Gronski, W., & Friedrich, C. 2002. Influence of selective filling on rheological properties and phase inversion of two-phase polymer blends. *Polymer*, 43(16): 4467-4477.

Story, B. J., Wagner, W. R., Gaisser, D. M., Cook, S. D., & Rust-Dawicki, A. M. 1998. In vivo performance of a modified CSTi dental implant coating. *The International Journal of Oral & Maxillofacial Implants*, 13(6): 749-757.

Sudarmadji, N., Tan, J. Y., Leong, K. F., Chua, C. K., & Loh, Y. T. 2011. Investigation of the mechanical properties and porosity relationships in selective laser-sintered polyhedral for functionally graded scaffolds. *Acta Biomaterialia*, 7(2): 530-537.

Sugiura, F., Kitoh, H., & Ishiguro, N. 2004. Osteogenic potential of rat mesenchymal stem cells after several passages. *Biochemical and Biophysical Research Communications*, 316(1): 233-239.

Sun, L., Parker, S. T., Syoji, D., Wang, X., Lewis, J. A., & Kaplan, D. L. 2012. Direct-Write Assembly of 3D Silk/Hydroxyapatite Scaffolds for Bone Co-Cultures. *Advanced Healthcare Materials*, 1(6): 729-735.

Swieszkowski, W., Tuan, B. H. S., Kurzydlowski, K. J., & Hutmacher, D. W. 2007. Repair and regeneration of osteochondral defects in the articular joints. *Biomolecular Engineering*, 24(5): 489-495.

Takahashi, Y., & Tabata, Y. 2004. Effect of the fiber diameter and porosity of non-woven PET fabrics on the osteogenic differentiation of mesenchymal stem cells. *Journal of Biomaterials Science, Polymer Edition*, 15(1): 41-57.

Tarvainen, T., Tunturi, T., Rautavuori, J., Tormala, P., Patiala, H., & Rokkanen, P. 1986. Shear strength of loaded porous-glassy-carbon/bone interface--an experimental study on rabbits. *Annals of Biomedical Engineering*, 14(5): 417-424.

Taylor, J. 1992. Delayed Union and Non-union Fractures. In A. H. Crenshaw (Ed.), *Campbell's Operative Orthopaedics*, 8th ed. ed.: 1287–1345. St. Louis: Mosby.

Thomson, R. C., Yaszemski, M. J., Powers, J. M., & Mikos, A. G. 1995. Fabrication of biodegradable polymer scaffolds to engineer trabecular bone. *Journal of Biomaterials Science, Polymer Edition*, 7(1): 23-38.

Timmer, M. D., Carter, C., Ambrose, C. G., & Mikos, A. G. 2003. Fabrication of poly(propylene fumarate)-based orthopaedic implants by photo-crosslinking through transparent silicone molds. *Biomaterials*, 24(25): 4707-4714.

Trantolo, D. J., Sonis, S. T., Thompson, B. M., Wise, D. L., Lewandrowski, K. U., & Hile, D. D. 2003. Evaluation of a porous, biodegradable biopolymer scaffold for mandibular reconstruction. *The International Journal of Oral & Maxillofacial Implants*, 18(2): 182-188.

Tsuruga, E., Takita, H., Itoh, H., Wakisaka, Y., & Kuboki, Y. 1997. Pore size of porous hydroxyapatite as the cell-substratum controls BMP-induced osteogenesis. *The Journal of Biochemistry*, 121(2): 317-324.

Tziampazis, E., Kohn, J., & Moghe, P. V. 2000. PEG-variant biomaterials as selectively adhesive protein templates: model surfaces for controlled cell adhesion and migration. *Biomaterials*, 21(5): 511-520.

Utracki, L. A. 2002. *Polymer Blends Handbook*: Kluwer Academic Pub.

van den Dolder, J., Farber, E., Spauwen, P. H., & Jansen, J. A. 2003. Bone tissue reconstruction using titanium fiber mesh combined with rat bone marrow stromal cells. *Biomaterials*, 24(10): 1745-1750.

van Luyn, M. J., van Wachem, P. B., Damink, L. O., Dijkstra, P. J., Feijen, J., & Nieuwenhuis, P. 1992. Relations between in vitro cytotoxicity and crosslinked dermal sheep collagens. *Journal of Biomedical Materials Research*, 26(8): 1091-1110.

Vanoene, H. 1972. Modes of dispersion of viscoelastic fluids in flow. *Journal of Colloid and Interface Science*, 40(3): 448-467.

Vater, C., Kasten, P., & Stiehler, M. 2011. Culture media for the differentiation of mesenchymal stromal cells. *Acta Biomaterialia*, 7(2): 463-477.

Veenstra, H., Van Dam, J., & Posthuma de Boer, A. 2000. On the coarsening of co-continuous morphologies in polymer blends: effect of interfacial tension, viscosity and physical cross-links. *Polymer*, 41(8): 3037-3045.

Vert, M., Li, S. M., Spenlehauer, G., & Guerin, P. 1992. Bioresorbability and biocompatibility of aliphatic polyesters. *Journal of Materials Science: Materials in Medicine*, 3(6): 432-446.

Virgilio, N., Favis, B. D., Pépin, M.-F., Desjardins, P., & L'Espérance, G. 2005. High Contrast Imaging of Interphases in Ternary Polymer Blends Using Focused Ion Beam Preparation and Atomic Force Microscopy. *Macromolecules*, 38(6): 2368-2375.

Vonarbourg, A., Passirani, C., Saulnier, P., & Benoit, J.-P. 2006. Parameters influencing the stealthiness of colloidal drug delivery systems. *Biomaterials*, 27(24): 4356-4373.

Wagner, C. D., & Muilenberg, G. E. 1979. *Handbook of x-ray photoelectron spectroscopy: a reference book of standard data for use in x-ray photoelectron spectroscopy*: Physical Electronics Division, Perkin-Elmer Corp.

Wang, J., Lessard, B. H., Maric, M., & Favis, B. D. 2014. Hierarchically porous polymeric materials from ternary polymer blends. *Polymer*.

Wang, L., Fu, Y., Wang, Z., Fan, Y., & Zhang, X. 1999. Investigation into an Alternating Multilayer Film of Poly(4-Vinylpyridine) and Poly(acrylic acid) Based on Hydrogen Bonding. *Langmuir*, 15(4): 1360-1363.

Wang, X., Nyman, J., Dong, X., & Leng, H. 2010. *Fundamental Biomechanics in Bone Tissue Engineering*: Morgan & Claypool Publishers.

Washburn, E. W. 1921. The Dynamics of Capillary Flow. *Physical Review*, 17(3): 273-283.

Wei, G., & Ma, P. X. 2004. Structure and properties of nano-hydroxyapatite/polymer composite scaffolds for bone tissue engineering. *Biomaterials*, 25(19): 4749-4757.

Weigel, J. P. 1993. Bone Grafting. In M. J. Bojrab, Smeak, D.D., Bloomberg, M.S. (Ed.), *Disease Mechanisms in Small Animal Surgery*, 2nd ed. ed.: 679-683. Philadelphia: Lea & Febiger.

Weis, C., Leukel, J., Borkenstein, K., Maier, D., Gronski, W., Friedrich, C., & Honerkamp, J. 1998. Morphological and rheological detection of the phase inversion of PMMA/PS polymer blends. *Polymer Bulletin*, 40(2-3): 235-241.

Whang, K., Healy, K. E., Elenz, D. R., Nam, E. K., Tsai, D. C., Thomas, C. H., Nuber, G. W., Glorieux, F. H., Travers, R., & Sprague, S. M. 1999. Engineering bone regeneration with bioabsorbable scaffolds with novel microarchitecture. *Tissue Engineering*, 5(1): 35-51.

Whang, K., Thomas, C. H., Healy, K. E., & Nuber, G. 1995. A NOVEL METHOD TO FABRICATE BIOABSORBABLE SCAFFOLDS. *Polymer*, 36(4): 837-842.

Willemse, R. C. 1999. Co-continuous morphologies in polymer blends: stability. *Polymer*, 40(8): 2175-2178.

Willemse, R. C., Posthuma de Boer, A., van Dam, J., & Gotsis, A. D. 1998. Co-continuous morphologies in polymer blends: a new model. *Polymer*, 39(24): 5879-5887.

Willemse, R. C., Ramaker, E. J. J., Van Dam, J., & De Boer, A. P. 1999. Coarsening in molten quiescent polymer blends: The role of the initial morphology. *Polymer Engineering & Science*, 39(9): 1717-1725.

Williams, C. G., Kim, T. K., Taboas, A., Malik, A., Manson, P., & Elisseeff, J. 2003. In vitro chondrogenesis of bone marrow-derived mesenchymal stem cells in a photopolymerizing hydrogel. *Tissue Engineering*, 9(4): 679-688.

Williams, J. M., Adewunmi, A., Schek, R. M., Flanagan, C. L., Krebsbach, P. H., Feinberg, S. E., Hollister, S. J., & Das, S. 2005. Bone tissue engineering using polycaprolactone scaffolds fabricated via selective laser sintering. *Biomaterials*, 26(23): 4817-4827.

Willis, J. M., Caldas, V., & Favis, B. D. 1991. Processing-morphology relationships of compatibilized polyolefin/polyamide blends. *Journal of Materials Science*, 26(17): 4742-4750.

Willis, J. M., & Favis, B. D. 1988. Processing-morphology relationships of compatibilized polyolefin/polyamide blends. Part I: The effect of an lonomer compatibilizer on blend morphology. *Polymer Engineering & Science*, 28(21): 1416-1426.

Wolfe, M. S., Dean, D., Chen, J. E., Fisher, J. P., Han, S., Rimnac, C. M., & Mikos, A. G. 2002. In vitro degradation and fracture toughness of multilayered porous poly(propylene fumarate)/β-tricalcium phosphate scaffolds. *Journal of Biomedical Materials Research*, 61(1): 159-164.

Wu, C., Fan, W., Zhou, Y., Luo, Y., Gelinsky, M., Chang, J., & Xiao, Y. 2012. 3D-printing of highly uniform CaSiO3 ceramic scaffolds: preparation, characterization and in vivo osteogenesis. *Journal of Materials Chemistry*, 22(24): 12288-12295.

Wu, C., Luo, Y., Cuniberti, G., Xiao, Y., & Gelinsky, M. 2011. Three-dimensional printing of hierarchical and tough mesoporous bioactive glass scaffolds with a controllable pore architecture, excellent mechanical strength and mineralization ability. *Acta Biomaterialia*, 7(6): 2644-2650.

Wu, T., Zivanovic, S., Draughon, F. A., Conway, W. S., & Sams, C. E. 2005. Physicochemical properties and bioactivity of fungal chitin and chitosan. *Journal of Agricultural and Food Chemistry*, 53(10): 3888-3894.

Xiang, Z., Sarazin, P., & Favis, B. D. 2009. Controlling Burst and Final Drug Release Times from Porous Polylactide Devices Derived from Co-continuous Polymer Blends. *Biomacromolecules*, 10(8): 2053-2066.

Xiao, Y., Li, D., Chen, X., Lu, J., Fan, H., & Zhang, X. 2008. Preparation and cytocompatibility of chitosan-modified polylactide. *Journal of Applied Polymer Science*, 110(1): 408-412.

Xie, X.-M., Matsuoka, M., & Takemura, K. 1992. Formation of gradient phase structure during annealing of a polymer blend. *Polymer*, 33(9): 1996-1998.

Xu, H., Han, D., Dong, J.-S., Shen, G.-X., Chai, G., Yu, Z.-Y., Lang, W.-J., & Ai, S.-T. 2010a. Rapid prototyped PGA/PLA scaffolds in the reconstruction of mandibular condyle bone defects. *The International Journal of Medical Robotics and Computer Assisted Surgery*, 6(1): 66-72.

Xu, M., Li, Y., Suo, H., Yan, Y., Liu, L., Wang, Q., Ge, Y., & Xu, Y. 2010b. Fabricating a pearl/PLGA composite scaffold by the low-temperature deposition manufacturing technique for bone tissue engineering. *Biofabrication*, 2(2): 025002.

Xynos, I. D., Hukkanen, M. V., Batten, J. J., Buttery, L. D., Hench, L. L., & Polak, J. M. 2000. Bioglass 45S5 stimulates osteoblast turnover and enhances bone formation In vitro: implications and applications for bone tissue engineering. *Calcified Tissue International*, 67(4): 321-329.

Yamagiwa, H., Endo, N., Tokunaga, K., Hayami, T., Hatano, H., & Takahashi, H. E. 2001. In vivo bone-forming capacity of human bone marrow-derived stromal cells is stimulated by recombinant human bone morphogenetic protein-2. *Journal of Bone and Mineral Metabolism*, 19(1): 20-28.

Yang, K., & Han, C. D. 1996. Effects of shear flow and annealing on the morphology of rapidly precipitated immiscible blends of polystyrene and polyisoprene. *Polymer*, 37(26): 5795-5805.

Yang, S., Leong, K. F., Du, Z., & Chua, C. K. 2002. The design of scaffolds for use in tissue engineering. Part II. Rapid prototyping techniques. *Tissue Engineering*, 8(1): 1-11.

Yang, Y. F., Zhao, J., Zhao, Y. H., Wen, L., Yuan, X. Y., & Fan, Y. B. 2008. Formation of porous PLGA scaffolds by a combining method of thermally induced phase separation and porogen leaching. *Journal of Applied Polymer Science*, 109(2): 1232-1241.

Yeo, A., Wong, W. J., & Teoh, S. H. 2010. Surface modification of PCL-TCP scaffolds in rabbit calvaria defects: Evaluation of scaffold degradation profile, biomechanical properties and bone healing patterns. *Journal of Biomedical Materials Research Part A*, 93(4): 1358-1367.

Yoo, D., Shiratori, S. S., & Rubner, M. F. 1998. Controlling Bilayer Composition and Surface Wettability of Sequentially Adsorbed Multilayers of Weak Polyelectrolytes. *Macromolecules*, 31(13): 4309-4318.

Yoo, J. U., & Johnstone, B. 1998. The role of osteochondral progenitor cells in fracture repair. *Clinical Orthopaedics and Related Research*, (355 Suppl): S73-81.

Yoshimoto, H., Shin, Y. M., Terai, H., & Vacanti, J. P. 2003. A biodegradable nanofiber scaffold by electrospinning and its potential for bone tissue engineering. *Biomaterials*, 24(12): 2077-2082.

Yuan, H., de Bruijn, J. D., Zhang, X., van Blitterswijk, C. A., & de Groot, K. 2001. Bone induction by porous glass ceramic made from Bioglass (45S5). *Journal of Biomedical Materials Research*, 58(3): 270-276.

Yuan, Z., & Favis, B. D. 2004. Macroporous poly(l-lactide) of controlled pore size derived from the annealing of co-continuous polystyrene/poly(l-lactide) blends. *Biomaterials*, 25(11): 2161-2170.

Yuan, Z., & Favis, B. D. 2005. Coarsening of immiscible co-continuous blends during quiescent annealing. *AIChE Journal*, 51(1): 271-280.

Zaffe, D. 2005. Some considerations on biomaterials and bone. *Micron*, 36(7–8): 583-592.

Zajac, R., & Chakrabarti, A. 1995. Irreversible polymer adsorption from semidilute and moderately dense solutions. *Physical Review E,* 52(6): 6536-6549.

Zhang, J., Liu, G., Wu, Q., Zuo, J., Qin, Y., & Wang, J. 2012. Novel Mesoporous Hydroxyapatite/Chitosan Composite for Bone Repair. *Journal of Bionic Engineering*, 9(2): 243-251.

Zhang, Y., & Zhang, M. 2002. Three-dimensional macroporous calcium phosphate bioceramics with nested chitosan sponges for load-bearing bone implants. *Journal of Biomedical Materials Research*, 61(1): 1-8.

Zhao, F., Yin, Y., Lu, W. W., Leong, J. C., Zhang, W., Zhang, J., Zhang, M., & Yao, K. 2002. Preparation and histological evaluation of biomimetic three-dimensional hydroxyapatite/chitosan-gelatin network composite scaffolds. *Biomaterials*, 23(15): 3227-3234.

Zhu, Y., Gao, C., Liu, X., & Shen, J. 2002a. Surface modification of polycaprolactone membrane via aminolysis and biomacromolecule immobilization for promoting cytocompatibility of human endothelial cells. *Biomacromolecules*, 3(6): 1312-1319.

Zhu, Y., Gao, C., & Shen, J. 2002b. Surface modification of polycaprolactone with poly(methacrylic acid) and gelatin covalent immobilization for promoting its cytocompatibility. *Biomaterials*, 23(24): 4889-4895.

Zou, L. J., Luo, Y. L., Chen, M. W., Wang, G., Ding, M., Petersen, C. C., Kang, R., Dagnaes-Hansen, F., Zeng, Y. L., Lv, N. H., Ma, Q., Le, D. Q. S., Besenbacher, F., Bolund, L., Jensen, T. G., Kjems, J., Pu, W. T., & Bunger, C. 2013. A simple method for deriving functional MSCs and applied for osteogenesis in 3D scaffolds. *Scientific Reports*, 3.

APPENDIX 1 – BONE TISSUE ENGINEERING MATERIALS

Extensive studies have investigated the nature of the materials that have the potential to be used as bone tissue engineering scaffolds. These studies have placed these materials into the following categories: metals, ceramics, natural polymers, synthetic polymers, and combinations of these materials to form composites (Glowacki & Mizuno, 2008; Gong et al., 2001; Hadjipanayi et al., 2009; Hollinger & Battistone, 1986; Liu & Ma, 2004; Nienhuijs et al., 2006). Apart from all differences due to diversity of these materials, they should all have common specific characteristics for being used as bone grafts. They must be inherently biocompatible, biodegradable, and highly cell adhesive. Also, they all must have porous, mechanically stable and three dimensional structure. As long as biodegradability is concerned for bone tissue engineering applications, medium to long-term material stability is required for the newly formed tissue to withstand early functional loads and become self-supporting (Gogolewski, 2000; Roy et al., 2003). The ease of manufacturing and processability of these substances are also determining parameters in selecting bone graft materials.

Metals

As a result of their superior mechanical properties, metals are number one implant materials used in orthopedics. However, their main drawback is their lack of biodegradation, which results in the necessity of performing a second surgery for their removal or accepting the toxicity risk due to the accumulation of metal ions in case they remain inside the patient’s body (Rubin & Yaremchuk, 1997). In literature, metals such as stainless steel, titanium and titanium alloys have been shown to exhibit good osteoconductive yet weak osteoinductive properties (Khan et al., 2008; Zaffe, 2005). The concept of porosity for the metal implants is often different from other types of grafts or scaffolds, as the bulk of the implant is only the solid metal but the outer surface is covered with porous titanium coatings whose pore size ranges from a nanometer scale to hundreds of microns depending on the fabrication technique (Harvey et al., 1999; Story et al., 1998). The reason for such external porous coating is to overcome their inherent lack of tissue adherence (Hulbert et al., 1970). Plasma spraying of titanium was used to fabricate such coatings with 200-400 μm and 50-60% porosity in order to treat dog femoral defects (Pilliar, 1998). Apart from solid metals with porous coatings on their surface, fully porous metal scaffolds do exist. For instance, fiber meshes made of titanium with 86% porosity and a 250 μm average pore size have been used for the *in vitro* culture of rat bone mesenchymal cells (van den Dolder et al., 2003). These mesh materials have also been successfully used as fixation grafts in hip arthroplasty as demonstrated in Figure A1.1 (Baad-Hansen et al., 2011).

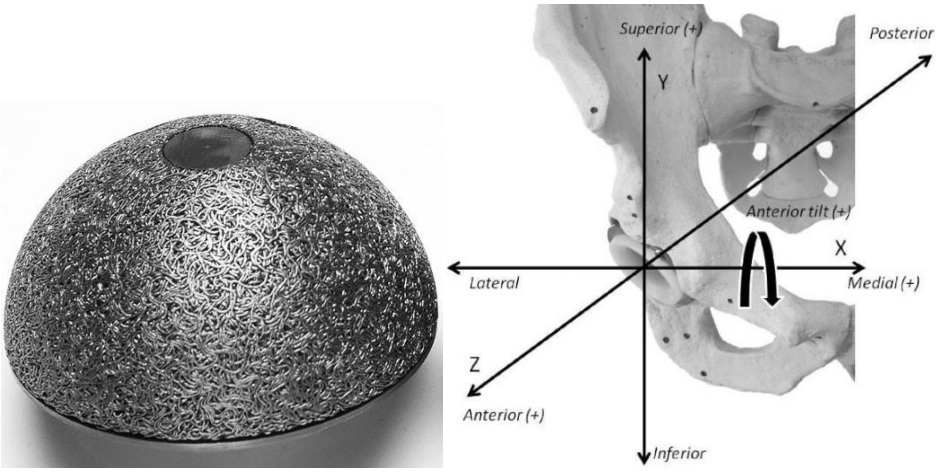

Figure A1.1: Cups made of titanium-aluminum-vanadium alloy core with a pure titanium fiber mesh on the surface (adapted from (Baad-Hansen et al., 2011))

Ceramics

Ceramics and ceramic composites used for osteogenesis are materials whose foundation lies upon the existence of hydroxyapatite, which is the inorganic calcium phosphate phase of the bone. As a result, ceramics are known for their impeccable osteoconductive properties in bone regeneration applications. Also, their stiffness fully complies with that of the real bone. However, the elastic moduli of the ceramic materials deviating from those of the bone and the fact that ceramics lack osteoinductivity could be considered as disadvantages for these bone grafts (Khan et al., 2008; Zaffe, 2005). There are mainly two types of ceramics:

Crystalline ceramics

As the name suggests, these ceramics have crystalline structure and are usually processed by sintering the ceramic powder at high temperatures to produce block and cylinder scaffolds which have approximately 80% porosity and 400-600 µm pore size. These scaffolds have been used to induce ectopic bone formation in mice and effectively treat rat femoral defects (Damien et al., 2003; Dong et al., 2001). As another example, natural coral, also a type of crystalline ceramic, molded into the form of a human mandibular condyle and pre-seeded with rabbit mesenchymal stem cells, induced ectopic bone formation in mice (Chen et al., 2002). Figure A1.2 demonstrates $CaSiO_3$ ceramics and their osteogenic potential in healing rat femoral defects. The level of bone formation after 8 weeks is higher than TCP scaffolds (Wu et al., 2012).

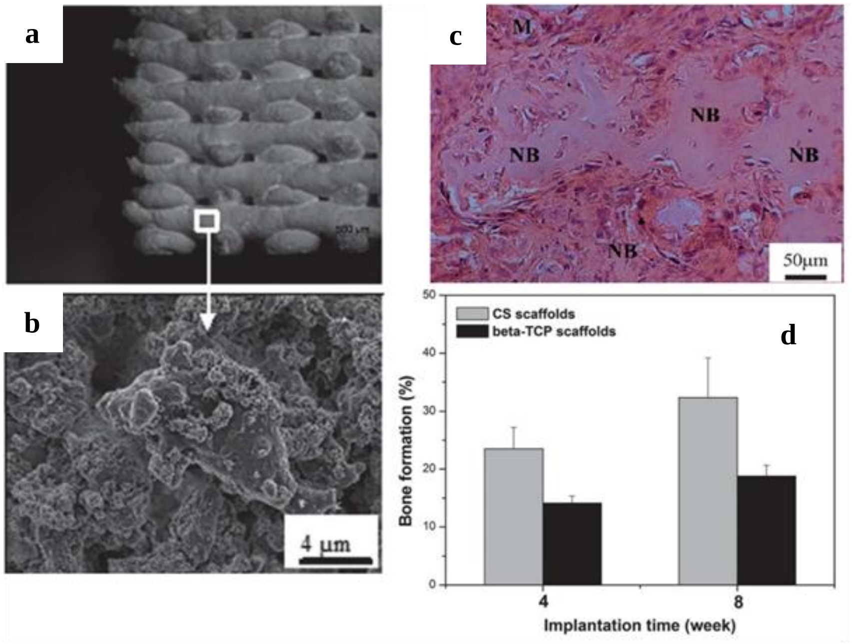

Figure A1.2: (a, b) SEM images of CaSiO3 scaffolds, (c) H&E images of explanted scaffolds 8-weeks post-surgery: NB stands for new bone, and d) % bone formation by micro-CT analysis (adapted from (Wu et al., 2012))

Glass and glass-ceramics

Amorphous glass and polycrystalline glass-ceramics are also members of the ceramics family. While crystallization is avoided in the fabrication of amorphous glass by rapid cooling, a so-called “controlled crystallization” is performed to form amorphous and crystalline phases together in the ceramics. Glass scaffolds with a low porosity level of 5% and a wide range of pore sizes from 10-200 µm induced bone ingrowth in rabbit tibia defects (Tarvainen et al., 1986).

Bioglass, a trademark material with chemical compositions different from those of regular glass, was also used to fabricate scaffolds with interconnected porous networks to support human primary osteoblasts, as well as induce ectopic bone formation in thigh muscles of dogs (Xynos et al., 2000; Yuan et al., 2001). Also, glass-ceramics with pore sizes ranging from 10-300 µm with around 50% porosity have been proven effective in the restoration of femoral defects in rabbits (El-Ghannam, 2004). Wu et al. demonstrated that 3D mesoporous bioactive glass (MBG) can enhance ALP activity of mesenchymal stem cells *in vitro* 7 days post-seeding as shown in Figure A1.3 (Wu et al., 2011).

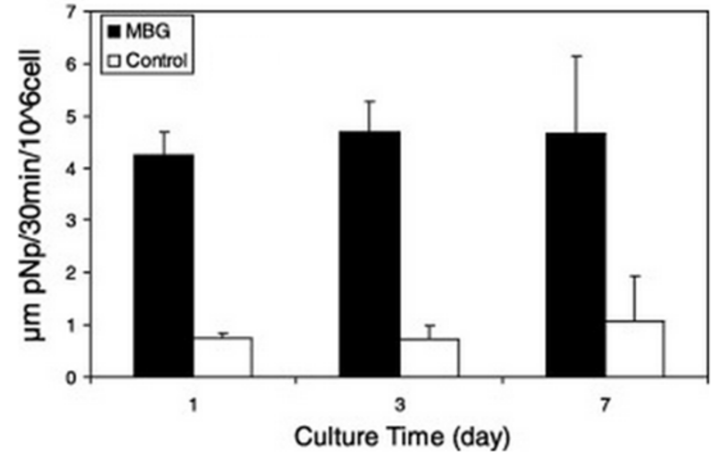

Figure A1.3: ALP activity of MSCs seeded in the mesoporous bioactive glass scaffolds at Days 1, 3 and 7. ALP activity is considerably higher than that of the control culture plate (Wu et al., 2011)

Natural polymers

Biomaterials obtained from natural resources such as collagen and glycosaminoglycans mostly comprise of structural tissue materials and therefore are biocompatible, biodegradable and hydrophilic. Consequently, these materials can encourage bone tissue development by directing cell adhesion and other cellular functions at the site of injury (Lee & Mooney, 2001). However, rapid biodegradation of these natural polymers along with their poor mechanical properties are considered as a downside to their application in bone tissue engineering. In order to reduce their degradation rate and reinforce their mechanical properties, natural polymers are commonly chemically modified by cross-linking or are blended with other materials, which on the other hand might compromise their biocompatibility and limit their use (van Luyn et al., 1992). In this section, common natural polymers are introduced.

Collagen

Collagen as the most abundant natural polymer accounts for approximately 30% of all body proteins and is the main component of mammalian connective tissue. It is found in every tissue that requires stability and flexibility at the same time. Among fourteen types of collagens that have been identified so far, the major constituent of orthopedic tissues are the fibrillar collagen (type I and type II) (Heinegard, 2001). Such fibrillar structure originating from its triple-helix structure leads to high tensile strengths (Lee et al., 2001a). Collagen is mostly used for soft orthopedic tissue regeneration. However, its mechanical properties can be easily enhanced for use in other applications by cross-linking chemically by aldehydes (glutaraldehyde and formaldehyde) and diimides (carbodiimide) or physically by UV irradiation or heat (Lee et al., 2001b; Park et al., 2002). Tibia defects in rats have been treated by using collagen scaffolds with pore sizes ranging from 11-105 µm and 14-134 µm (Rocha et al., 2002). Furthermore, *in vitro* studies with bovine osteoblasts within anionic collagen scaffolds prepared by hydrolysis demonstrated increased alkaline phosphatase over three weeks (Moreira et al., 2004).

Glycosaminoglycans

Glycosaminoglycans (GAGs), which consist of repeating disaccharide units in linear arrangement, usually include an uronic acid component (glucuronic or iduronic acid) and an amino sugar (such as n-acetyl-d-glucosamine). The largest GAG is Hyaluronic acid (HA) or hyaluronan which is an anionic polysaccharide composed of repeating disaccharide units of N-acetylglucosamine and glucuronic acid and can either be isolated from natural sources like rooster comb or be obtained from microbial fermentation routes. HA is also the major component of cartilage extracellular matrix from which it can be easily isolated (Pachence, 1997). Although HA is mostly used for chondrogenesis due to its ability to encourage chondrocyte proliferation and ECM production, HA based scaffolds with 80–90% porosity and pore sizes ranging from

100-600 μm were employed for the osteogenic differentiation of the murine pluripotent cell line C3H10T1/2 (Kim & Valentini, 2002). Also, Figure A1.4 demonstrates that bone grafts supplemented with HA have proved promising in healing tibia defects in rabbits (Aslan et al., 2006).

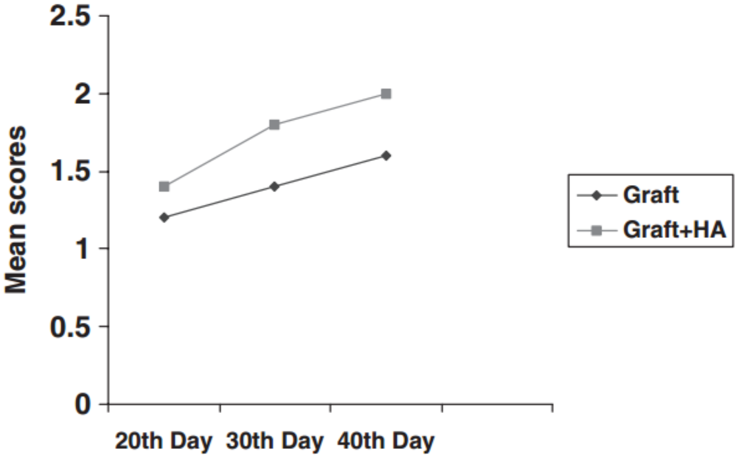

Figure A1.4: Bone healing scores in tibia defects (0 = empty cavity, 7 = bone only) (Aslan et al., 2006)

Synthetic polymers

Chemically synthesized polymers are advantageous over natural biomaterials due to their versatility and ability to transform into scaffolds with various shapes, porosities, pore sizes, molecular weights, molecular weight distributions and degradation rates through numerous fabrication techniques. In this matter, the effect of fabrication parameters has been investigated on the scaffold properties generated from poly(a-hydroxy acid), (poly(D,L-lactide), and poly(lactide-co-glycolide) (Hu et al., 2002). Several synthetic polymers have been used for orthopedic grafts, including poly(α-hydroxy esters), poly(ε-caprolactone), poly(orthoesters), poly(anhydrides), PEG-based materials (including PEO), poly(amino acids), and fumarate-based materials. Some of these materials are discussed in this section.

Poly(α-hydroxy esters)

Due to the FDA approval for poly(glycolic acid) (PGA) and poly(lactic acid) (PLA) to be used as drug delivery and suture materials, these polymers have been widely studied in tissue engineering applications. These two polymers and their copolymer are discussed in this subsection.

Poly(glycolic acid) (PGA)

Poly(glycolic acid) (PGA) is a linear aliphatic polyester which is by far the most studied synthetic polymer in tissue engineering. Depending on the synthesis procedure of PGA -being mainly by ring-opening polymerization- its crystallinity can reach 46-52%, which leads to a low level of solubility in organic solvents (except highly halogenated solvents) and a high melting point (224-226°C). PGA is highly hydrophilic which makes it collapse and lose its mechanical strength rapidly in the period of 2-4 weeks. This property of PGA makes it a suitable material for surgical sutures but not a mechanically stable one for load-bearing applications such as bone grafts (Frazza & Schmitt, 1971). Like other polyesters, PGA goes through a hydrolytic bulk degradation of ester linkages depending on its level of crystallinity (Athanasiou et al., 1998; Mikos et al., 1993). This polymer also has good processability features as it can be processed in extrusion and injection molding equipments. The VK staining images of PGA porous scaffolds seeded with umbilical cord mesenchymal stromal cells at 3 and 6 weeks post-seeding (Figure A1.5) clearly exhibits high levels of calcium mineral deposition within the scaffolds, and hence emphasizes on the osteogenic potential of this polymeric material.

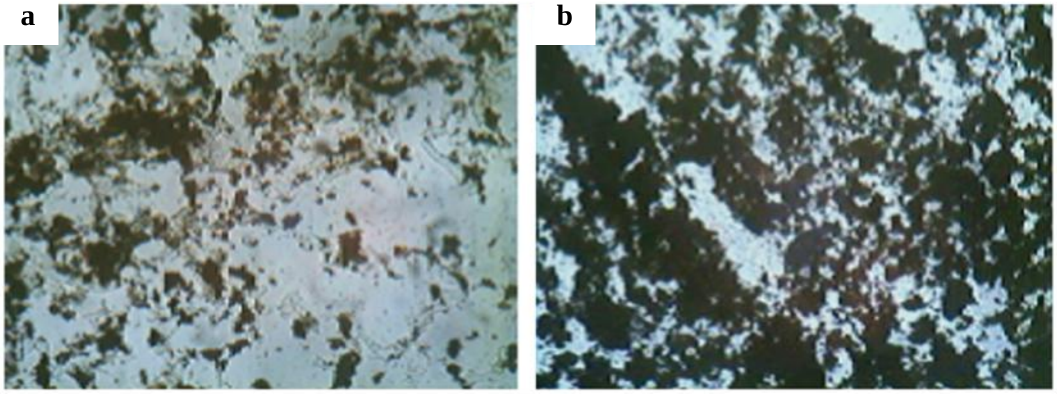

Figure A1.5: VK staining of PGA sections at (a) 3 and (b) 6 weeks post-seeding. Mineral deposition increased considerably with time (adapted from (Wang, Dormer, Bonewald, & Detamore, 2010))

Poly(lactic acid)

Poly(lactic acid) (PLA) is another aliphatic polyester in the poly(α-hydroxy ester) family which has similar characteristics to those of PGA. However, the hydrophilicity of PLA is less than that of PGA due to the existence of an extra methyl group in its backbone. This relative hydrophobic nature of PLA prolongs its degradation time and reinforces its mechanical properties as compared to PGA, and makes it a desirable material for orthopedic fixation devices (Athanasiou et al., 1998; Daniels et al., 1990; Mikos et al., 1994). PLA goes through the same degradation mechanism as the PGA, except that lactic acid is the by-product of the hydrolytic degradation reaction of PLA. Also, in comparison to PGA, PLA is more soluble in organic solvents such as methylene chloride and chloroform.

Since PLA is a chiral molecule, it is mainly consisted of two distinct stereoisomeric forms: PDLA and PLLA enantiomers. PDLLA is the racemic polymer obtained from the combination of these two enantiomers. Generally PLLA is more used compared to the other two stereoisomers. The main difference between these forms of PLA is their crystallinity. Both PDLA and PLLA are semi-crystalline polymers. However, the addition of more than 15% of PDLA to PLLA makes it amorphous (Vert et al., 1992). Normally PDLLA is used in drug delivery applications because of its amorphous nature that leads to a homogeneous dispersion of drug in the matrix. Moreover this amorphous nature of PDLLA leads to a drop in its melting point as well as mechanical properties such as tensile stress and modulus, yet an increase in the elongation at break. Also it degrades faster than the two PDLA and PLLA free forms (Mark, 2009). The melting point of PLA as a function of molecular weight ranges between 145-180°C (normally reported as 170°C) and its glass transition temperature ranges from 50-64°C (normally reported as 56°C) (Mark, 2009).

In the case of bone tissue engineering, the proliferation and mineralized matrix formation by rat BMSCs have been reported to improve significantly on PLA scaffolds (Matsuzaka et al., 2000). Nonetheless, very few works have investigated only PLA as a bone implant in the recent years.

Poly(lactide-co-glycolide)

The principal goal for the copolymerization of PLA and PGA in order to synthesize Poly(lactide-co-glycolic acid) (PLGA) is to either decrease the hydrophilicity of PGA or to increase the hydrophilicity of PLA in order for them to be used in wider ranges of applications. The properties of the PLGA copolymer are completely different from those of the pure PLA and PGA homopolymers. As opposed to PLA and PGA which are semi-crystalline polymers, PLGA is completely amorphous almost at all ranges of copolymer ratios, because of the disruption of the crystalline phases. As a result, hydrolytic degradation of PLGA occurs at a much faster rate than its constituting homopolymers (Athanasiou et al., 1998; Hollinger, 1983; Pachence, 1997).

PLGA copolymer has been a much more investigated material in the literature for osteogenic purposes than PLA and PGA, as it does not have the low hydrophilicity issue of PLA and degrades much slower than PGA as an implant. For instance, 2D and 3D PLGA scaffolds impregnated with human bone morphogenetic protein-2 (hBMP-2) and seeded with rabbit BMSCs induced osteogenic differentiation and extracellular matrix production over a period of two months *in vitro* (Huang et al., 2004). Also, alveolar bone atrophies right after tooth extraction have been prevented by using PLGA dental implants with interconnected porous structures (Maspero et al., 2002). Furthermore, Penk et al. have studied the potential of PLGA scaffolds for bone regeneration in rat tibial head defects. Figure A1.6 shows that the scaffold (S) is completely invaded with lamellar bone (L) (Penk et al., 2013).

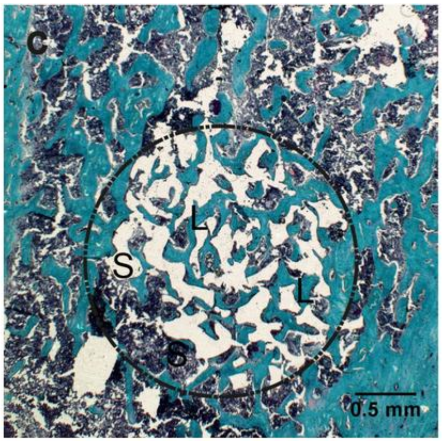

Figure A1.6: Goldner-Masson stained image of a rat tibial head defect: PLGA scaffold (S) has been completely invaded by newly formed lamellar bone (adapted from (Penk et al., 2013))

Other synthetic polymers

Apart from the discussed synthetic polymers and the biomaterials of interest elaborated in section 2.2.4, other materials have been investigated for bone tissue engineering applications. These materials include poly(anhydrides) (Anseth Kristi et al., 1997; Domb et al., 1991; Gunatillake & Adhikari, 2003), Poly(amino acids) (Abramson et al., 2002; Kim et al., 2011; Pachence, 1997) and Fumarate-based polymers (Fisher et al., 2001; Fisher et al., 2002; Lewandrowski et al., 2003; Timmer et al., 2003). The use of these synthetic polymers in bone tissue engineering has seen very little activity in the past recent year.

Composites

The main reason why composites were developed was to overcome likely drawbacks of the individual biomaterials, while benefiting from their advantages at the same time. For example, ceramics as explained above are excellent osteoconductive materials. However, their brittleness hinders their use as a single material to be used as bone implants. Therefore, by incorporating ceramics with other materials like synthetic polymers such as PCL, their osteoconductivity can still be used while PCL adds to their toughness. For instance, hydroxyapatite scaffolds were coated with a composite coating of hydroxyapatite/PCL which led to a higher compressive strength and elastic modulus (Kim et al., 2004). On the other hand, porous polymeric scaffolds often suffer from lower compressive strengths and moduli as compared to those of the human bone, which compromises the compatibility of the polymer implants with the surrounding tissue and increases the risk of scaffold debonding from the tissue under stress conditions. Park et al. also fabricated the PCL/HA scaffolds and demonstrated that incorporating hydroxyapatite powder to the molten PCL improves the ALP activity of human osteosarcoma MG63 cell lines at all culture periods, as illustrated in Figure A1.7 (Park et al., 2011). Stress shielding as explained in section 2.2.3.5 is another issue which could happen in the case of bone implants, and whose risks could be highly reduces by the use of blends and composites.

Hydroxyapatite ceramic materials have also been processed with two natural biomaterials chitosan and gelatin to make a composite material which supported the proliferation and mineralization of rat calvarial osteoblasts *in vitro* (Zhao et al., 2002). In another study collagen scaffolds have been coated with hydroxyapatite to enhance the osseointegration of the implant, which supported the attachment and proliferation of rabbit periosteal cells (Lickorish et al., 2004). Also, adding fillers or coatings like hydroxyapatite or TCP could also improve the mechanical properties of natural and synthetic polymers and render them closer to those of the natural bone. Some of these composites include Poly(L-lactide-co-D,L-lactide)/TCP, Poly(propylene fumarate)/TCP and Hydroxyapatite/TCP/chitosan (Roy et al., 2003; Wolfe et al., 2002; Zhang & Zhang, 2002).

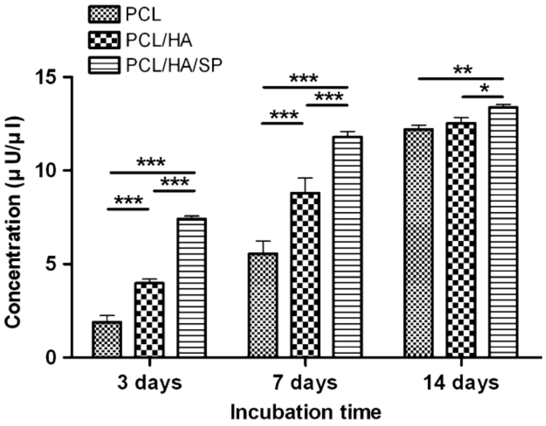

Figure A1.7 : ALP activity of MG63 cells on the scaffolds. Asterisks denote significant differences (*p<0.05, **p<0.01, ***p<0.001) (Park et al., 2011)

APPENDIX 2 – SCAFFOLD FABRICATION TECHNIQUES

Sintering

Sintering is the most common method to produce ceramic scaffolds. There are many variations in the process of sintering; however, the basics are the same for all of them. Sintering is defined as the condensation of ceramic powder at high temperatures (below their melting point) into a solid ceramic bulk. In this method, after the formation of slurry from the ceramic powder and putting it in the mold, compression is applied to form a "green body" which is the unsintered ceramic. Then the temperature is risen to 1100-1300 °C depending on the powder used. After sintering, pressure is applied isotactically. By applying certain modifications in the process, microporous or macroporous structures can be obtained. By using the standard sintering process, random pores with 5 μm diameter are obtained. However, for achieving a pore size of 100-500 μm, the most common approach is to use appropriately sized naphthalene particles with the ceramics powder before the formation of the green body. Therefore, during the sintering process, naphthalene particles are sublimated and macropores are generated. Another method is by using hydrogen peroxide to make the slurry which produces oxygen bubbles during sintering and makes the macropores (Rengachary et al., 1998).

Solvent casting and particulate leaching

Solvent casting and particulate leaching is the most commonly used approach for the production of porous polymeric tissue engineering scaffolds. In this approach, water soluble salts such as sodium chloride, sodium citrate and occasionally sugars and lipids are mixed with a polymer solution and cast into a mold of the desired scaffold shape. The evaporation or lyophilization of the solvent together with the extraction of the porogen phase by immersion in water (in the case of salts) leads to the solidification of the polymer and the formation of a porous network. This method was used to fabricate PLGA scaffolds in order to engineer trabecular bone as explained by (Thomson et al., 1995).

The porosity produced via this technique can reach up to 98% and the pore size can be 100-600 μm depending on the size of the porogen particles (Kim & Valentini, 2002; Nazarov et al., 2004).

Type, amount and size of the porogen particles are key parameters in controlling the porosity and pore size criteria which limit the control over the porous structure in this process. The main disadvantages of this approach include the residual solvent and porogen material in the system and the limitation in the thickness of the scaffolds produced. As a matter of fact, all the scaffolds produced by the solvent casting and porogen leaching technique are limited to a thickness range of 0.5-2 mm (Liao et al., 2002). In addition, achieving complete pore interconnectivity is very limited in this technique, which makes it unfavourable for uniform cell seeding and tissue ingrowth.

Gas foaming

The major problem of the solvent casting/particulate leaching method is the residual solvent that can be a threat for *in vivo* applications. Gas foaming is a technique that does not use solvents for the generation of porosity and therefore the effect of solvent is completely eliminated. This method was first introduced by Mooney et al. for tissue engineering applications (Mooney et al., 1996). In this approach, CO_2 gas is used to create polymer foams. Compression-molded polymer disks are exposed to high pressure CO_2 in order to saturate the gas in the discs. CO_2 is then released from the system by a pressure drop, which causes a thermodynamic instability. This instability is then compensated by the nucleation and growth of gas bubbles in the discs which make the pores in the polymer matrix. The porosity and pore size highly depend on the amount of gas and the pressure drop rate. The gas foaming method generates relatively high pore sizes ranging from 100-800 µm in diameter, and porosities as high as 97% (Kim et al., 2012; Nazarov et al., 2004; Trantolo et al., 2003). However, because of the gas bubbles in the polymer discs, gas foaming alone leads to the formation of a closed-pore and non-interconnected porous structure. As a matter of fact, only 10-30% of the pores generated by this technique are interconnected (Harris et al., 1998; Mooney et al., 1996). Therefore, this method is often combined with other techniques such as solvent casting and particulate leaching (Harris et al., 1998). Recently, the gas foaming fabrication technique has been used for the production of porous calcium phosphate scaffolds with pore sizes ranging from 300-800 µm and porosities up to 85% for *in vitro* (mouse BMSCs) and *in vivo* (rat jawbone and tibia) bone regeneration (Kim et al., 2012).

Thermally-induced phase separation (TIPS)

Phase separation in general is based on the demixing phenomenon of a polymer solution into polymer rich and solvent rich phases. Such demixing usually occurs either by exposure to another immiscible solvent or in the case of thermally-induced phase separation (TIPS), thermal manipulation (change in temperature). In section 2.2.4.3, this method was introduced as the most common approach for the production of three-dimensional chitosan scaffolds. In this technique, the polymer is dissolved in its specific solvent at high temperature. The temperature is then dropped rapidly usually by freezing and falling from a single homogeneous phase region into a biphasic region according to the phase diagram of a binary fluid (Figure A2.1), which leads to phase separation. Then, the solvent phase is subsequently removed by sublimation (Freeze-drying) which leaves a porous polymer scaffold (Nam & Park, 1999)

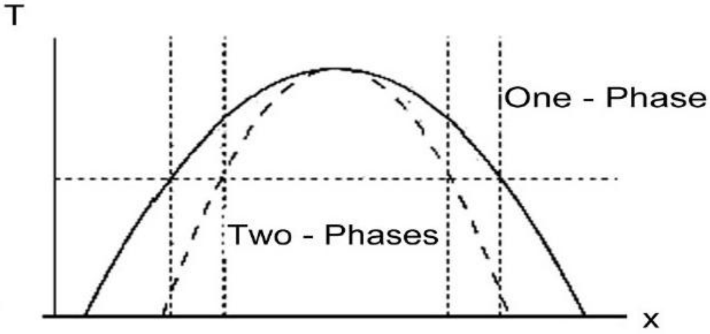

Figure A2.1: Phase diagram of a binary fluid (Raudino et al., 2011)

One advantage of this technique over solvent casting-particulate leaching is better mechanical properties of the produced scaffolds. It was proved that PLA scaffolds produced by this technique with the same porosity as those produced by solvent-casting particulate leaching demonstrated 20 times higher modulus (Ma et al., 2001). Nevertheless, there is an important drawback to this technique, which is the limitation for the generation of large pore sizes; this method is commonly used for the production of pore sizes of 10-100 μm which might not be ideal for seeding bone forming cells as discussed in section 2.2.3.3.2. As a result, a combination of this technique with other methods must be used to push the pore size into an acceptable window (Wei & Ma, 2004; Yang et al., 2008). The TIPS method does not always involve freezing as the agent for phase separation, as sometimes heating might as well lead to phase segregation (Shen et al., 2010). This technique has been proposed for use in bone tissue engineering, yet its *in vivo* application started in the recent past, when nanohydroxyapatite/collagen (nHAC), and PLLA-composite scaffolds produced by this method have been used for rabbit femoral condyle repair (Niu et al., 2011).

Freeze-drying

Freeze-drying is a rapid method for the fabrication of bone tissue engineering scaffolds with a relatively high degree of control over the porosity and pore size. The procedure consists of mixing an organic solution containing a dissolved polymer with water until a homogeneous emulsion is achieved. The emulsion is then poured into a metal mold of a pre-defined shape and is exposed to a rapid cooling by liquid nitrogen to freeze-in the liquid structure. Freeze-drying removes the water and solvent from the emulsion which leads to the formation of a scaffold with highly interconnected pores, porosity of more than 90% and the average pore size ranging from 20-500 µm (Whang et al., 1995; Zhao et al., 2002). One main disadvantage of this method is the formation of a closed-pore structure which again has to be overcome by its combination with other techniques. The applications of this approach for the formation of porous 3D structures for osteogenic purposes are numerous. Hydroxyapatite/chitosan-gelatin, Collagen/hydroxyapatite and hydroxyapatite/chitosan composite scaffolds with pore sizes of 30-500 µm have been fabricated to examine the *in vitro* attachment and proliferation behavior of rat osteoblasts, rabbit periosteal cells and mice osteoblastic cell line (MC-3T3-E1) (Lickorish et al., 2004; Zhang et al., 2012; Zhao et al., 2002).

Melt molding/particulate leaching

Melt molding technique is a simple method which can combine the porogen leaching principle and polymer processing for the fabrication of scaffolds in diverse geometries. In this approach, porogen and polymer particles are mixed and put in a mold and heated above the polymer glass transition temperature (for amorphous polymers) or polymer melting temperature (for semi-crystalline polymers). The mixture is then removed from the mold, quenched and soaked in a proper solvent to leach the porogen out of the mixture and yield a three-dimensional porous structure. The controlling parameters and basics of solvent casting and particulate leaching in this appendix also apply for melt molding. This method was used by Thomson et al. to fabricate scaffolds out of melt molding of PLGA with gelatin microparticles as porogen (Thomson et al., 1995). PLGA/poly(vinyl alcohol) (PVA) scaffolds with 90% porosity and 200-300 µm pore size have also been fabricated by this approach in order to evaluate their degradation behavior *in vivo* by using a rat model (Oh et al., 2006). Nanocomposite scaffolds made of PLGA and surface modified hydroxyapatite with 90% porosity and 100-300 µm pore size are another products of this method which exhibited rapid healings of rabbit radius defects (Cui et al., 2009).

Electrospinning

Electrostatic fiber spinning or electrospinning is a modern technique for the fabrication of nano and micro-scale porous structures. The principle of electrospinning is the electrostatic spraying of polymer fibers on a conductive target substrate by use of an electric field that controls the quality of the final product (Boland et al., 2001). A schematic of the vertical setup of the electrospinning apparatus is illustrated in Figure A2.2.

In this technique, a polymer solution or melt is injected with an electric potential which produces a charge imbalance between the injector and the target substrate. For polymer solutions, the most important factor is determining the critical entanglement concentration above which fibers can be formed. Should the charge imbalance overcome the surface tension of the polymer solution or melt (critical voltage), an electrically charged polymer jet is formed. During the fiber deposition or after, the solvent evaporates and porous structures are produced.

Biocompatible polymers like PCL, PGA and PLGA can be electrospun to form nanofiber scaffolds with porosities higher than 90%. Fiber thickness, average pore diameter and other scaffold properties can be controlled by parameters like polymer concentration in the solution, ejection rate, type of the solvent, applied voltage, capillary diameter, the collecting surface material and the distance between the capillary and the collecting surface. The fiber diameter can range from hundreds of nanometers up to several microns (Li et al., 2002b).

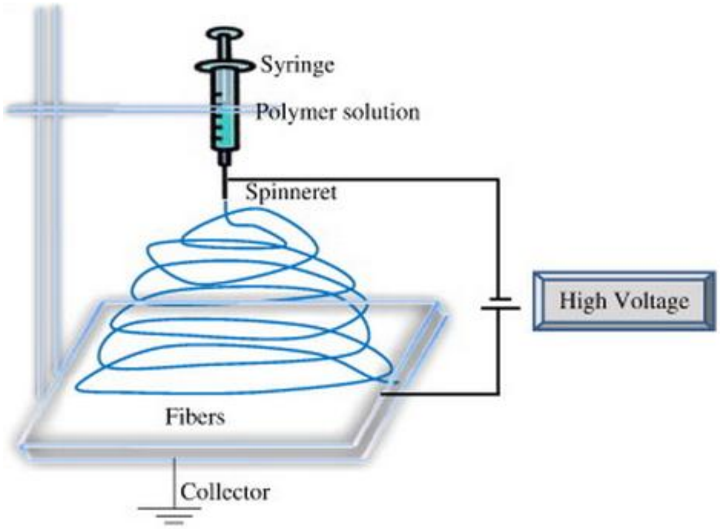

Figure A2.2: Schematic of an electrospinning set up (Bhardwaj & Kundu, 2010)

Famous work by Yoshimoto et al. discusses the electrospinning process for PCL by using chloroform as the solvent and 10-15 kV as the voltage (Yoshimoto et al., 2003). The scaffolds produced by the same study were seeded with rat BMSCs, and their *in vitro* osteogenic behavior was studied at week 4 post-seeding. It was shown that cell multilayers were formed, and minerals and collagen type I were detected on the scaffolds in this period. Two main interrelated drawbacks observed in this approach are the limited mechanical properties of the scaffolds produced and the decrease of porosity with the increase of the fiber thickness. Also, creating various shapes using the electrospun fibers has always been an issue and has limited the use of this technique in bone tissue engineering.

Rapid-prototyping techniques

Developed by the advanced industrial technology and computer science, rapid-prototyping techniques are now able to fabricate a complex product based on a computer-aided design model. These techniques include 3D printing (3DP), selective laser sintering (SLS) and fusion deposition modeling (FDM) (Yang et al., 2002). The aforementioned methods are known for their precision and control over the fabricated porous structure. However, the most important inconvenience of rapid-prototyping methods is their inability to design and fabricate scaffolds of fine microstructures due to their resolution limitations. Therefore, the porosities of the produced scaffolds are mainly low and their mechanical properties are evidently compromised. An example for the application of 3D printed structures in bone tissue engineering, is the use of PGA/PLA scaffolds pre-seeded with dog BMSCs for healing craniomaxillofacial bone injuries (Xu et al., 2010a). In addition, PCL and PCL-TCP composite scaffolds fabricated by fused-deposition modeling aimed to repair and regenerate osteochondral defects in articular joints by pre-seeded rabbit BMSCs (Swieszkowski et al., 2007).

APPENDIX 3 – XPS ANALYSIS OF MULTILAYER FILMS

Since XPS establishes the main surface characterization technique for the analysis of various layers in the LbL technique as explained in Chapter 5, this appendix is concentrated on the fundamentals of XPS and experimental conditions of the performed tests.

XPS fundamentals

X-ray photoelectron spectroscopy is a surface characterization technique which is based on Einstein's photoelectric effect discovery, and was developed by Siegbahn et al. at the University of Uppsala, Sweden (Siegbahn, 1967). XPS is a technique to obtain surface information about composition and chemical state. The technique is based on the irradiation of X-ray photons with a constant wavelength on a sample material and therefore causing electrons to be ejected from their original state. The kinetic energies of the ejected photoelectrons are measured which permits the detection of various elements. In the case of our study, the relative concentration of the elements is determined by ratios of these photoelectron intensities. According to Equation 16, the detected kinetic energies of the electrons are actually the energies remaining from the initial photon energy (hν) after consuming the binding energy of the specific excited electron (B.E) to reach the valence band and finally reach the detector ($\varphi_{\text{spectrometer}}$):

$$K.E = h\upsilon - B.E - \varphi_{\text{spectrometer}} \quad (19)$$

Where K.E is the kinetic energy of the photoelectron, $h\upsilon$ is the X-ray photon energy, B.E is the binding energy associated with the excited electron in a particular orbital and $\varphi_{\text{spectrometer}}$ is the spectrometer (concentric hemispherical analyzer) work function. Since the binding energy of the excited core electron in its orbital is specific to a unique element, the detected kinetic energy could be used as a fingerprint for the identification of elements and compounds. Also, since the excited photoelectrons have low kinetic energies, XPS experiments must be performed in an ultra-high vacuum (UHV) chamber of 10^{-9}–10^{-10} Torr. Figure A3.1 illustrates the penetration depth of the X-ray beams and the detection depth by the XPS apparatus. It is clear that although a large area is bombarded with X-ray beams and they can penetrate approximately 1 micron deep inside the substrate, a small area of 1 mm^2 is analyzed whose sampling depth is less than ~10nm. Nevertheless, electrons of deeper layers can still escape out of the sample but due to their collisions with other electrons and atoms, they would only be translated as background noise in the final spectra.

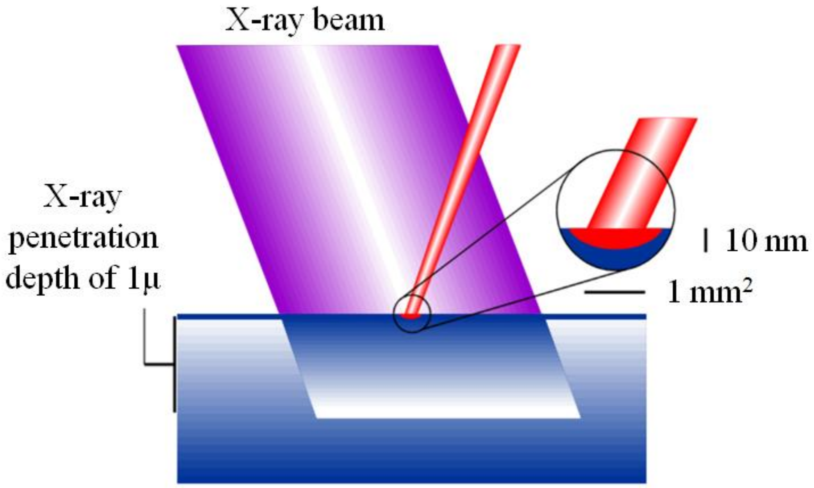

Figure A3.1: Penetration depth of X-ray and detection depth by XPS (adapted from (Shu))

A typical XPS spectrum plots the photoemission intensity as a function of the binding energy as shown in Figure A3.2. It is clear that any specific atom is exhibited at a specific binding energy which is a function of the state of their electronegativity and surrounding bonded atoms and hence corresponding to that unique atom (Dementjev et al., 2000).

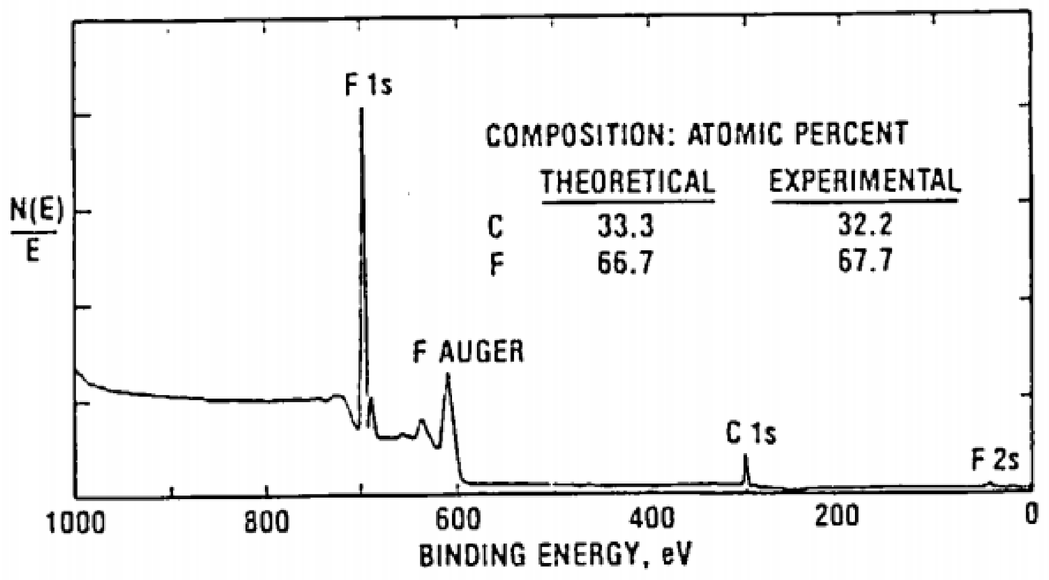

Figure A3.2: Typical XPS spectrum (Wagner & Muilenberg, 1979)

Experimental conditions and analysis

The details of the XPS characterization settings for the detection of N 1s (nitrogen) specific to the chitosan molecule, and/or other atoms in the case of LbL coatings are presented in Table A3.1.

Table A3.1: Experimental Conditions of the XPS analysis

Apparatus		ESCALAB 3 MKII de VG
Source		Mg Kα
Power		216W (12kV, 18mA)
Analyzed Surface		2mmx3mm
Analyzed Depth		50-100 Ǻ
Survey Scans	Energy Step Size	1.0 eV
	Pass Energy	100 eV
High Resolution Scans	Energy Step Size	0.05 eV
	Pass Energy	20 eV
Background Subtractions		Shirley Method (Shirley, 1972)
Sensitivity factor table		Wagner (Wagner & Muilenberg, 1979)
Charge correction with respect to C1s at		285.0eV

The relative atomic percentage is calculated according to Equation 17:

$$(Relative\ Atomic\ Percentage\ (\%))_1 = \frac{A_1/SF_1}{\sum_{n=1} A_n/SF_n} \quad (20)$$

Where A1 represents the peak area for element 1 and SF1 is the sensitivity factor for that element. SF values are taken from Table A3.2.

Table A3.2: Atomic sensitivity factors (ASFs) (Wagner & Muilenberg, 1979)

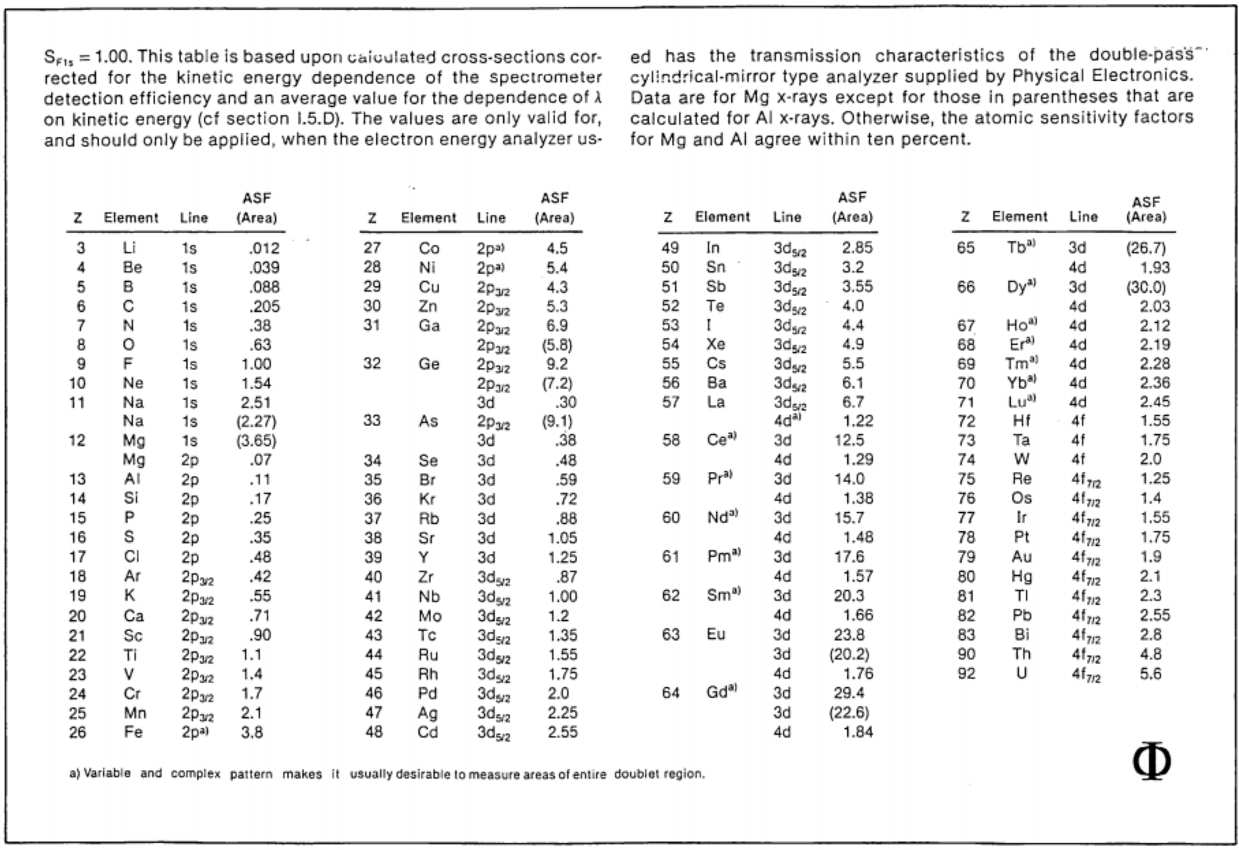

$S_{F1s} = 1.00$. This table is based upon calculated cross-sections corrected for the kinetic energy dependence of the spectrometer detection efficiency and an average value for the dependence of λ on kinetic energy (cf section I.5.D). The values are only valid for, and should only be applied, when the electron energy analyzer used has the transmission characteristics of the double-pass cylindrical-mirror type analyzer supplied by Physical Electronics. Data are for Mg x-rays except for those in parentheses that are calculated for Al x-rays. Otherwise, the atomic sensitivity factors for Mg and Al agree within ten percent.

Z	Element	Line	ASF (Area)
3	Li	1s	.012
4	Be	1s	.039
5	B	1s	.088
6	C	1s	.205
7	N	1s	.38
8	O	1s	.63
9	F	1s	1.00
10	Ne	1s	1.54
11	Na	1s	2.51
	Na	1s	(2.27)
12	Mg	1s	(3.65)
	Mg	2p	.07
13	Al	2p	.11
14	Si	2p	.17
15	P	2p	.25
16	S	2p	.35
17	Cl	2p	.48
18	Ar	$2p_{3/2}$	.42
19	K	$2p_{3/2}$	.55
20	Ca	$2p_{3/2}$	.71
21	Sc	$2p_{3/2}$	.90
22	Ti	$2p_{3/2}$	1.1
23	V	$2p_{3/2}$	1.4
24	Cr	$2p_{3/2}$	1.7
25	Mn	$2p_{3/2}$	2.1
26	Fe	2p[a]	3.8
27	Co	2p[a]	4.5
28	Ni	2p[a]	5.4
29	Cu	$2p_{3/2}$	4.3
30	Zn	$2p_{3/2}$	5.3
31	Ga	$2p_{3/2}$	6.9
		$2p_{3/2}$	(5.8)
32	Ge	$2p_{3/2}$	9.2
		$2p_{3/2}$	(7.2)
		3d	.30
33	As	$2p_{3/2}$	(9.1)
		3d	.38
34	Se	3d	.48
35	Br	3d	.59
36	Kr	3d	.72
37	Rb	3d	.88
38	Sr	3d	1.05
39	Y	3d	1.25
40	Zr	$3d_{5/2}$	.87
41	Nb	$3d_{5/2}$	1.00
42	Mo	$3d_{5/2}$	1.2
43	Tc	$3d_{5/2}$	1.35
44	Ru	$3d_{5/2}$	1.55
45	Rh	$3d_{5/2}$	1.75
46	Pd	$3d_{5/2}$	2.0
47	Ag	$3d_{5/2}$	2.25
48	Cd	$3d_{5/2}$	2.55
49	In	$3d_{5/2}$	2.85
50	Sn	$3d_{5/2}$	3.2
51	Sb	$3d_{5/2}$	3.55
52	Te	$3d_{5/2}$	4.0
53	I	$3d_{5/2}$	4.4
54	Xe	$3d_{5/2}$	4.9
55	Cs	$3d_{5/2}$	5.5
56	Ba	$3d_{5/2}$	6.1
57	La	$3d_{5/2}$	6.7
		4d[a]	1.22
58	Ce[a]	3d	12.5
		4d	1.29
59	Pr[a]	3d	14.0
		4d	1.38
60	Nd[a]	3d	15.7
		4d	1.48
61	Pm[a]	3d	17.6
		4d	1.57
62	Sm[a]	3d	20.3
		4d	1.66
63	Eu	3d	23.8
		3d	(20.2)
		4d	1.76
64	Gd[a]	3d	29.4
		3d	(22.6)
		4d	1.84
65	Tb[a]	3d	(26.7)
		4d	1.93
66	Dy[a]	3d	(30.0)
		4d	2.03
67	Ho[a]	4d	2.12
68	Er[a]	4d	2.19
69	Tm[a]	4d	2.28
70	Yb[a]	4d	2.36
71	Lu[a]	4d	2.45
72	Hf	4f	1.55
73	Ta	4f	1.75
74	W	4f	2.0
75	Re	$4f_{7/2}$	1.25
76	Os	$4f_{7/2}$	1.4
77	Ir	$4f_{7/2}$	1.55
78	Pt	$4f_{7/2}$	1.75
79	Au	$4f_{7/2}$	1.9
80	Hg	$4f_{7/2}$	2.1
81	Tl	$4f_{7/2}$	2.3
82	Pb	$4f_{7/2}$	2.55
83	Bi	$4f_{7/2}$	2.8
90	Th	$4f_{7/2}$	4.8
92	U	$4f_{7/2}$	5.6

a) Variable and complex pattern makes it usually desirable to measure areas of entire doublet region.

APPENDIX 4 – SUPPLEMENTARY HISTOLOGICAL DATA

Effect of toluene

The use of toluene as the clearing agent in our histological data had an obvious influence on the results obtained. PCL is soluble in toluene and therefore is eluted from the slides in its presence in the final steps of the staining protocols. Figure A4.1 shows how the extraction of PCL using toluene reveals the information that were previously missing or being masked in the shadow of the scaffolds. Additionally, there seems to be an interaction between the hematoxylin and eosin stain as well as Toluidine Blue (in the VK assay) with PCL, as the scaffold picks up some of the stain color and becomes purple at some areas.

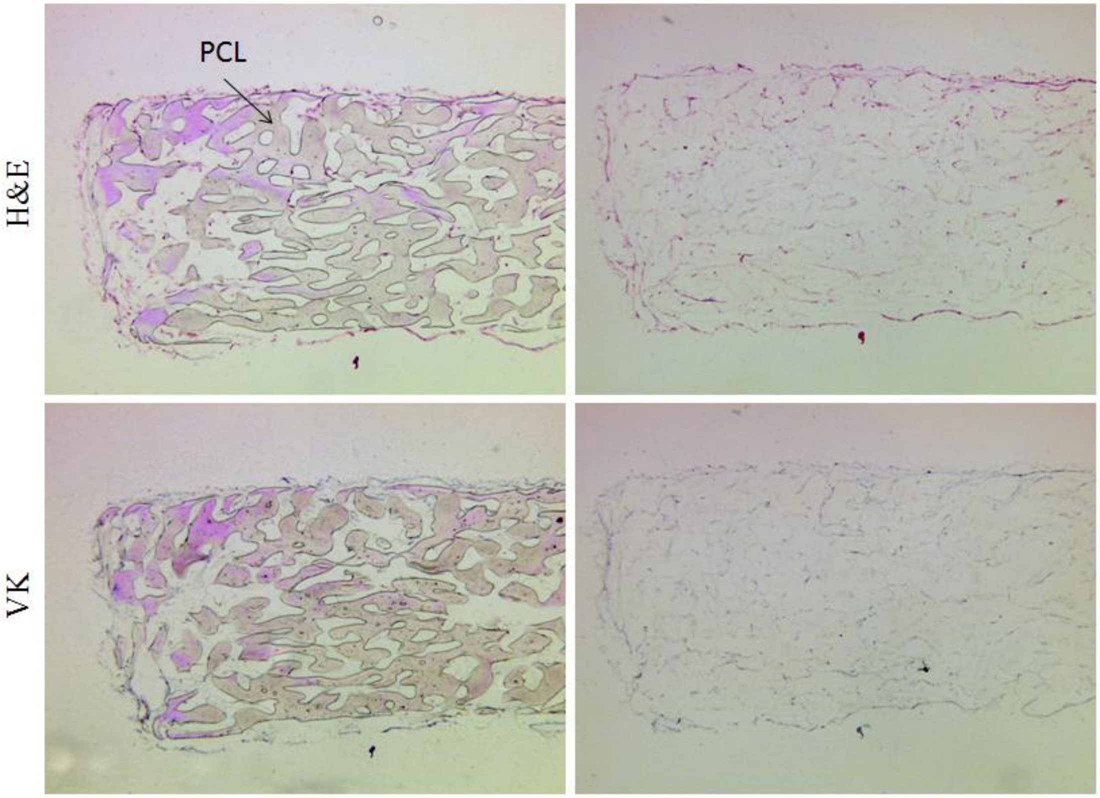

Figure A4.1: Effect of toluene on the information obtained by H&E and VK staining

Thus, it is clear that for histomorphometric measurements in Chapter 6, the scaffolds had to be extracted for us to obtain reasonable results which are not affected by the scaffolds on the slides.

Effect of pore size and seeding at 37 °C

In Chapter 4, we determined a minimum pore size requirement for having the optimal cell escape/retention in PCL scaffolds. However, for our osteogenic assay two distinct pore sizes needed to be investigated: PCL1 with pore size < 100 µm and PCL2 with pore size> 100 µm. In this pilot study (osteogenic assay 1), PCL1 scaffolds with 41 µm and PCL2 with 141 µm (unchanged) average pore diameter were selected. Following a classic seeding at 37°C, 5 day culture period in CCM, the osteogenic assay of BMSCs was carried out for three weeks, after which the samples were harvested, cryosectioned and stained for histology and other experiments like those discussed in Chapter 6.

H&E staining images shown in Figure A4.2 demonstrates the effect of pore size on the formation of matrix inside the toluene extracted scaffolds after 21 days of osteogenic assay in the presence or absence of chitosan coating.

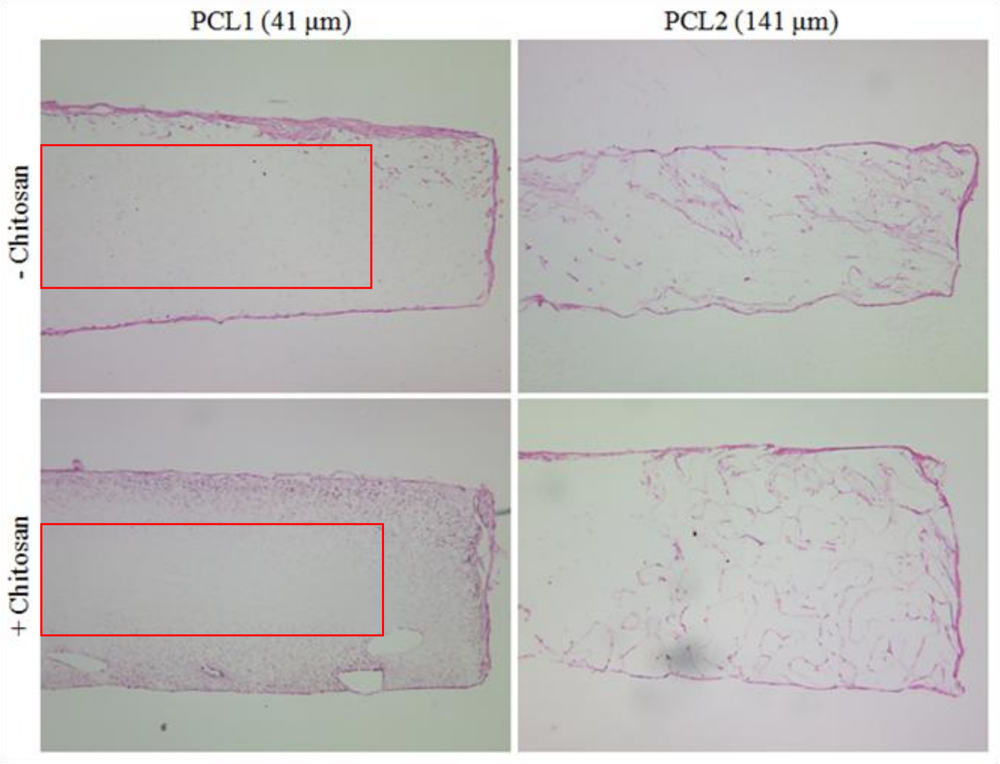

Figure A4.2: Effect of pore size on the infiltration and tissue formation within PCL scaffolds. Red squares represent areas where ECM is missing

It is clear that PCL1 scaffolds with 41 μm pore size pre-seeded at 37°C do not allow proper scaffold infiltration, and therefore the cell penetration is hindered near the structure edges. However, the addition of chitosan appears to be improving the cell penetration and ECM deposition. PCL2 scaffolds, on the other hand, are fully infiltrated by cells and hence show high levels of ECM formation. This is in accordance with our infiltration results in Chapter 4. Therefore, due to infiltration limitations imposed by such small pore size, we decided to increase the pore size of PCL1 samples to a higher value of 84 μm as well as reduce the seeding temperature down to 4°C (to decrease the metabolic activity of the cells) for the osteogenic assay used in Chapter 6.

Effect of chitosan surface modification

Furthermore, it is evident that the chitosan surface treatment in this pilot study also leads to the formation of more matrix on the surface of the pores after 21 days of culture, as shown in Figure A4.3. These observations are also in agreement with our results in Chapter 6.

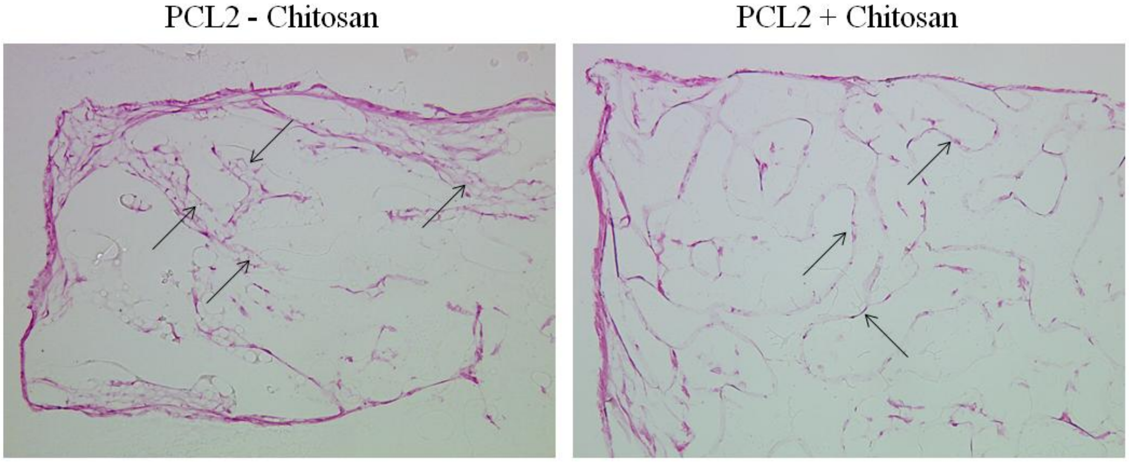

Figure A4.3: Effect of chitosan surface treatment on the deposition of ECM

Efficiency of VK (toluidine blue) staining

Having selected a higher pore size for PCL1 for our osteogenic assay, BMSCs were cultured inside the scaffolds for 10 days in a proliferation medium (CCM), after which the osteogenic assay was performed for three weeks. VK staining involves the reaction of silver ions with phosphates to produce silver phosphate which is reduced to silver through photochemical degradation by the UV light and can later be visualized as dark brown-black silver deposits. Figure A4.4 describes the efficiency of the VK (Tol Blue) staining.

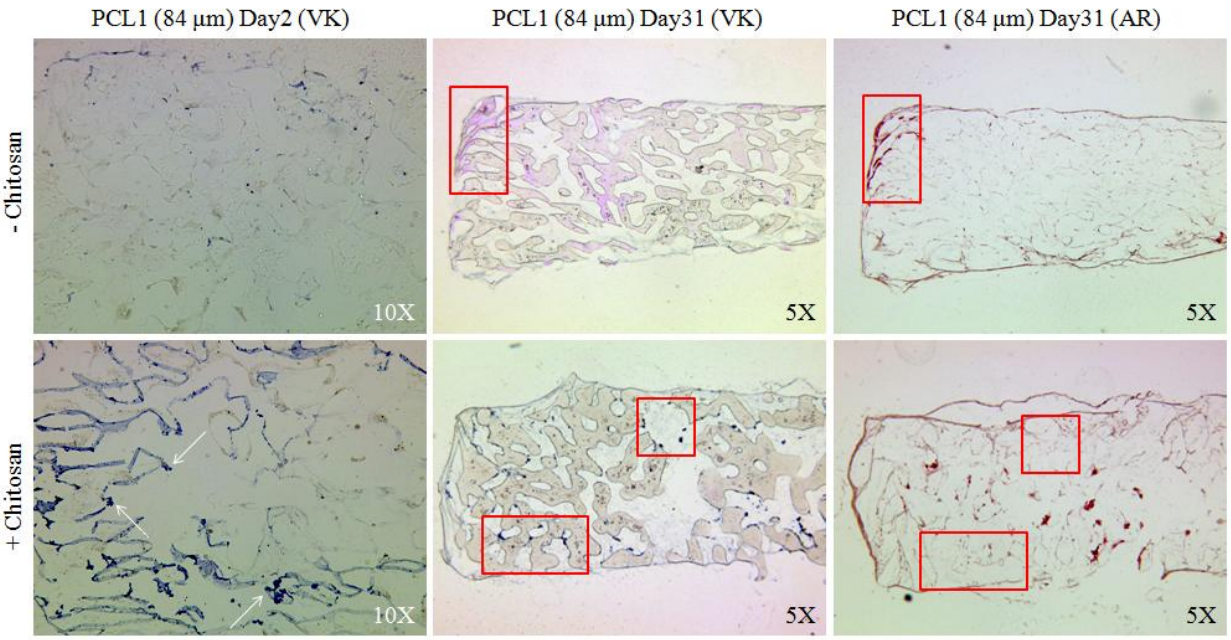

Figure A4.4: Efficiency of VK (Tol Blue) as compared to AR staining

Our results at Day2 demonstrate that the chitosan layer deposited on the PCL1 surface are visibly affected by the Toluidine Blue (Tol Blue) counterstain used in the VK staining. It is yet unclear whether the Tol Blue is reacting with chitosan or the LbL polyelectrolytes underneath. Also, surprisingly, some dark deposits (represented by white arrows) are observed inside chitosan coated scaffolds at Day2 which could not be due to any minerals, knowing that the osteogenesis assay started at Day10. Furthermore, such artifacts due to the VK staining does not match the mineral deposits observed in the AR stained sections (depicted by red squares); VK staining led to unreliable results. It should be also noted that another study has shown that VK staining might be insufficient to confirm biomineralization *in vitro* (Bonewald et al., 2003).

In order to check whether the patches of minerals detected by the AR staining correspond to the pores with highly colonized cells, we performed a side-by-side analysis of AR and H&E (non-eluted PCL) staining images (5x) at Day31 for uncoated (Figure A4.5) and chitosan coated

(Figure A4.6) PCL scaffolds. According to Figure A4.5, the occurrence of mineral deposits overlaps with highly colonized areas on the top and on the edges of the scaffolds. Figure A4.6 shows that the minerals in the LbL-chitosan coated scaffolds are deposited mostly on the surface and some in the interspace between the pores, where cells also exist but are not necessarily dense.

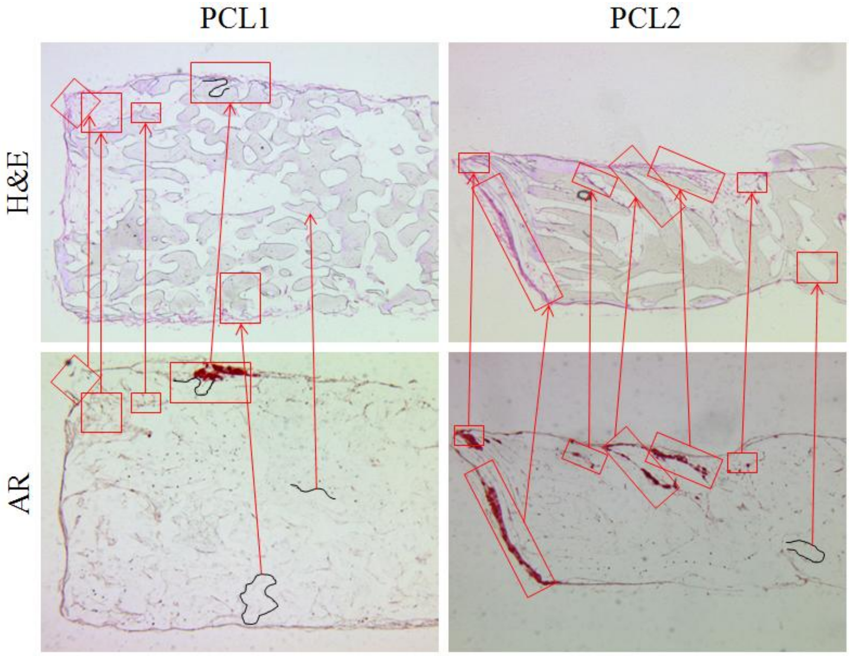

Figure A4.5: Side-by-side H&E and AR 5x images of PCL-only scaffolds at Day31

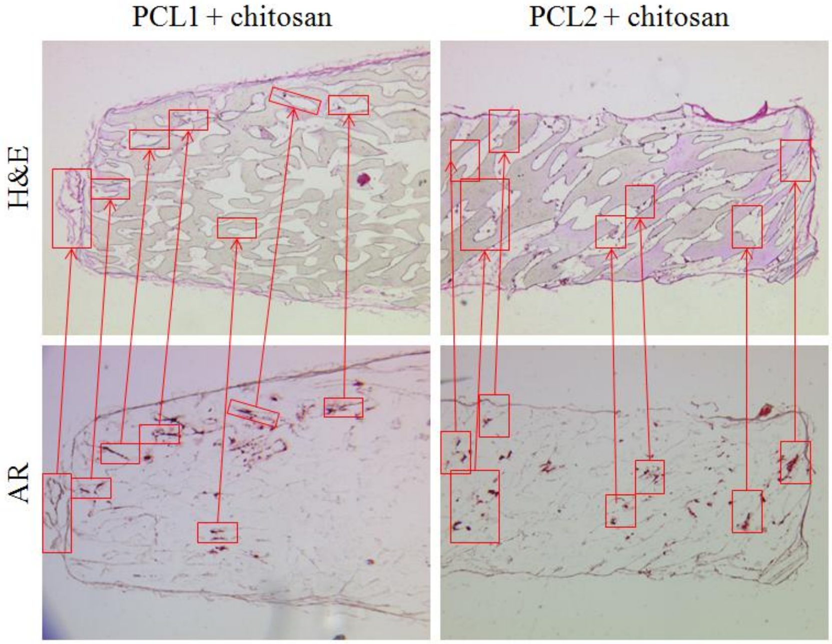

Figure A4.6: Side-by-side H&E and AR 5x images of PCL-chitosan scaffolds at Day31

APPENDIX 5 – MICRO-COMPUTED TOMOGRAPHY

Micro-CT was initially selected as a method for confirming biomineralization inside PCL scaffolds at Day31. To achieve this goal, binary image thresholding has been done in order to be able to distinguish between the PCL scaffold and mineral deposits. Table A5.1 summarizes the preliminary selected thresholds for different samples.

Table A5.1 : Thresholds for detection of scaffolds and/or minerals in CT-Analyser (CTAn)

Sample	**Threshold**
Cell-seeded scaffolds : Scaffold + Mineral	70-255
Cell-seeded scaffolds : Mineral only	160-255
Non-seeded PCL1	Failed
Non-seeded PCL2	40-110

However, the thresholds above led to positive signals which were located inside the bulk of PCL rather than on the pore surface, as illustrated in u-CT images generated by the CTAn software (Figure A5.1). In this figure, green, black and pink sections respectively represent the scaffold, pores and positive mineral signals. We speculate that these positive signals originate from the segments inside the PCL bulk which are probably under tension and whose radio-opacity is comparable to that of the minerals. These false-positive signals are much less observed for PCL2 samples. Real mineral signals are probably those detected at the edges of the pores.

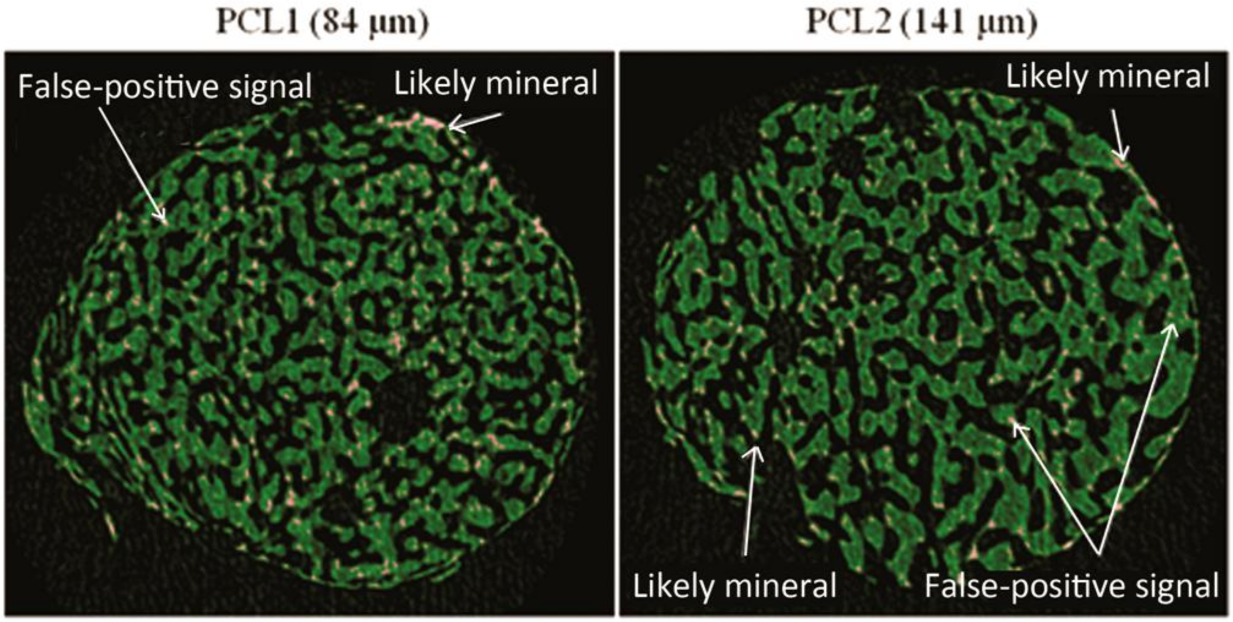

Figure A5.1: Real and false-positive signals for minerals at Day 31 (scaffolds cross-section)

Considering the successful formation of minerals in the form of a "skin" at the perimeter of the scaffolds (Figure 6.7(i, k)) using the same thresholds mentioned above), we conclude that the extent of mineralization is not sufficient for the mineral particles to be quantified separately from PCL.

APPENDIX 6 – ENERGY-DISPERSIVE X-RAY SPECTROSCOPY

Energy-dispersive X-ray spectroscopy (EDS or EDX) is an analytical surface characterization technique which is based on the principle that each element has its unique atomic structure which is represented by the X-ray peaks emitted off that specific atom at the surface of a substrate. In order to obtain elemental surface information, therefore, the emission of characteristic X-rays should be stimulated. This can be done by bombarding the surface with X-ray, protons and electron beams. Electron beam excitation is used in scanning electron microscopes (SEM). This electron bombardment ejects an electron from the inner shells of an atom at its ground state, creating an “electron hole” which is filled by another high energy electron from an outer shell hence releasing an X-ray beam. Like in the case of XPS, the level of this energy along with the number of ejected X-rays is measured using a detector called energy-dispersive spectrometer. The detected energy is attributed to the difference in the energies of the two shells and is specific to a unique atomic structure from which the X-rays were emitted.

As a pilot study, we used the EDX functionality of the ESEM apparatus (ESEM, Quanta 200 FEG, FEI Company, Czech Republic) to detect mineral deposits inside the pores of the PCL scaffolds. Figure A6.1 illustrates the EDX analysis of the regions of interest (white rectangles) in the chitosan-coated PCL scaffolds after the osteogenic assay (Day31). The negative control corresponding to the bulk of PCL does not show a calcium peak, whereas the area between the pores exhibits up to 4.3% calcium. The samples used for this study, unfortunately, were gold-coated for the sake of ESEM visualization, and therefore a considerable gold peak is present which overlaps with that of the phosphate. Future works could potentially look into EDX analysis in further detail with PCL samples without chitosan coating and before gold-sputtering in order to reveal more information including the phosphate peak.

In conclusion, the EDX analysis also proves the occurrence of biomineralization inside chitosan coated PCL scaffolds, which is in agreement with our AR calcium staining results.

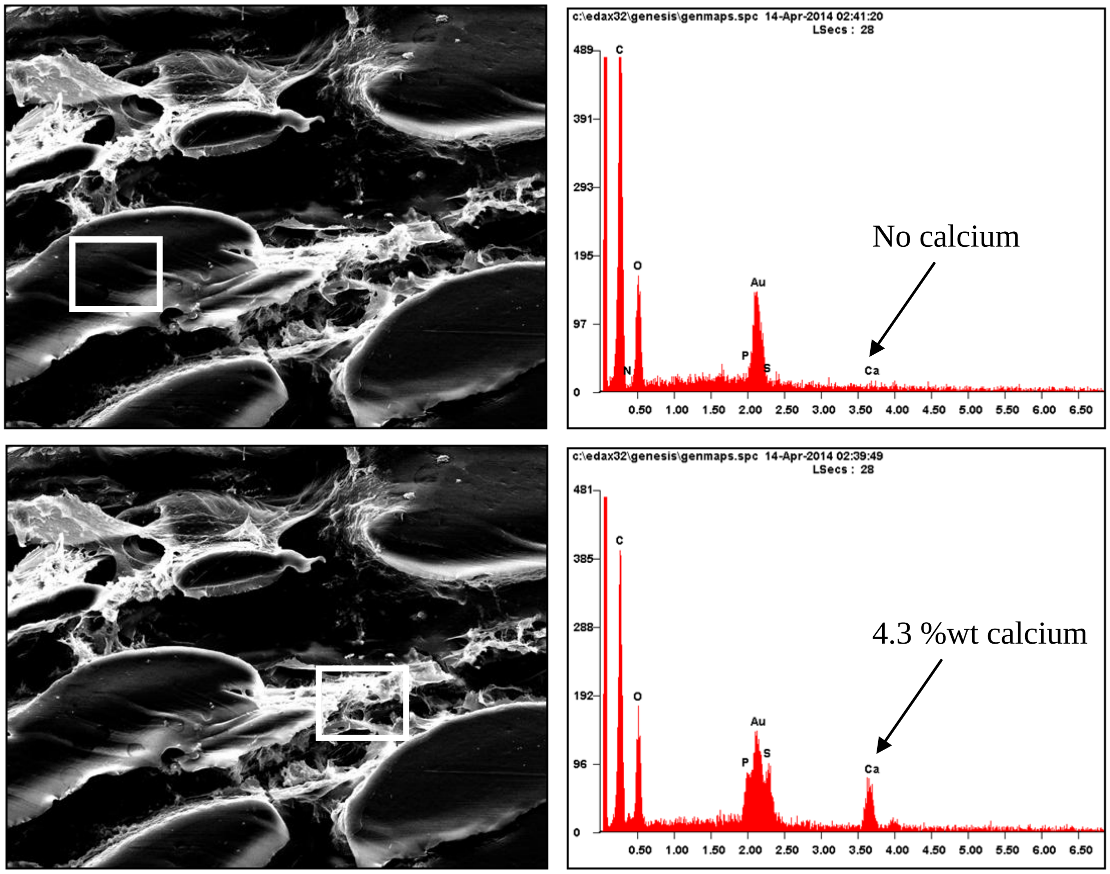

Figure A6.1: EDX analysis of chitosan-coated PCL scaffolds at Day31 points to successful biomineralization